Geodätisch-geophysikalische Arbeiten in der Schweiz

(Fortsetzung der Publikationsreihe
«Astronomisch-geodätische Arbeiten in der Schweiz»)

herausgegeben von der

Schweizerischen Geodätischen Kommission
(Organ der Schweizerischen Akademie der Naturwissenschaften)

Sechsundvierzigster Band
Volume 46

ORBITS OF SATELLITE SYSTEMS IN SPACE GEODESY

Markus Rothacher

1992

Geodätisch-geophysikalische Arbeiten in der Schweiz

(Fortsetzung der Publikationsreihe
«Astronomisch-geodätische Arbeiten in der Schweiz»)

herausgegeben von der

Schweizerischen Geodätischen Kommission
(Organ der Schweizerischen Akademie der Naturwissenschaften)

Sechsundvierzigster Band
Volume 46

ORBITS OF SATELLITE SYSTEMS IN SPACE GEODESY

Markus Rothacher

1992

Adresse der Schweizerischen Geodätischen Kommission:

Institut für Geodäsie und Photogrammetrie
Eidg. Technische Hochschule Zürich
ETH-Hönggerberg
CH-8093 Zürich

Redaktion des 46. Bandes:
Dr. M. Rothacher
Dr. B. Bürki

Druck: OWADRUCK, 3173 Oberwangen

VORWORT

Die Anwendungen des amerikanischen satellitengestützten Navigationssystems GPS erreichen in zunehmendem Ausmass viele aktuelle Bereiche, wie z.B. die Navigation, Geodynamik oder Landesvermessung. Bei diesen Anwendungen wächst immer mehr das Bedürfnis nach einem zivilen Bahndienst, der den Nutzern auf operationeller Basis möglichst speditiv Parameter der GPS-Bahnen zur Verfügung stellt.

Setzte sich ein Literaturkritiker zum Ziel, die Dissertationen systematisch einer wissenschaftlichen Disziplin zuzuordnen, er würde bestimmt als Eckpfeiler die Klassen der Uebersichtsarbeiten und der reinen Spezialuntersuchungen einführen. Die Arbeit von Herrn Dr. Markus Rothacher ist in die erste Kategorie einzuordnen: Während der letzten zehn Jahre hat er sich die nötigen theoretischen Werkzeuge erarbeitet und diese in der Praxis vielfach erprobt. Nur dank diesem reichen Erfahrungsschatz war sein Thema "Orbits of Satellite Systems in Space Geodesy" überhaupt zu bewältigen. Nach einer Uebersicht über die im Moment interessierenden Satellitensysteme wird in Teil 1 die Bahnbestimmung für das amerikanische "Global Positioning System (GPS)" kritisch durchleuchtet. Im Teil 2 werden die theoretischen Entwicklungen durch umfangreiche Auswertungen illustriert. Diese Untersuchungen bildeten für das Astronomische Institut der Universität Bern das theoretische Fundament für die Beteiligung am "International GPS Geodynamics Service (IGS)". Die Anwendungen (Kap. 8 GIG' 91 sowie Kap. ESA' 91) waren erste praktische Schritte in dieser Richtung.

Zusätzlich sind in dieser Dissertation aber auch Spezialprobleme angeschnitten, welche in Zukunft zu grösseren Arbeiten Anlass geben könnten. Es sei insbesondere auf die Behandlung der Troposphäre hingewiesen (Kapitel 5): Herr Rothacher präsentiert hier eine valable und einfach in die Praxis umzusetzende Alternative zur stochastischen Troposphärenmodellierung, welche sich bis jetzt sehr gut bewährt hat.

Die Schweizerische Geodätische Kommission (SGK) anerkennt die grosse Leistung von Herrn Rothacher und dankt ihm für den hochstehenden Beitrag zur schweizerischen Satellitengeodäsie und Landesvermessung. Die Schweiz. Akademie für Naturwissenschaften (SANW) unterstützt die SGK seit vielen Jahren. Wie auch in vorangegangenen Fällen übernahm die SANW die Druckkosten für diese Publikation, wofür wir im Namen der SGK unseren Dank aussprechen.

Prof Dr. G. Beutler
Direktor des Astronomischen Instituts der Universität Bern

Direktor F. Jeanrichard
Bundesamt für Landestopographie
Vizepräsident der SGK

Prof. Dr. H.-G.Kahle
ETH Zürich
Präsident der SGK

PRÉFACE

Les applications du système américain GPS de navigation par satellites touchent de plus en plus de nombreux domaines d'actualité, tels que la navigation, la géodynamique ou la mensuration nationale. Pour ces applications, le besoin d'un service civil capable de mettre à disposition des utilisateurs les paramètres des orbites GPS aussi rapidement que possible va croissant.

Si un critique littéraire s'avisait de classer systématiquement les thèses de doctorat d'une discipline scientifique donnée, les deux piliers de ce classement seraient certainement les travaux à caractère synoptique d'une part et les recherches spécifiques d'autre part. Le travail de Monsieur Markus Rothacher, dr ès sc., est à classer dans la première de ces catégories: durant les dix dernières années, il a acquis les outils théoriques nécessaires et les a testés maintes fois dans la pratique. Cette vaste expérience lui a permis de maîtriser totalement son thème "Orbits of Satellite Systems in Space Geodesy". Après une vue d'ensemble des systèmes de satellites qui nous intéressent pour le moment, la détermination des orbites du système américain "Global Positioning System (GPS)" est examinée de facon critique dans la première partie. Dans la seconde partie, les développements théoriques sont illustrés par d'amples analyses. Ces recherches ont formé la base théorique de la participation de l'Institut d'astronomie de l'Université de Berne au projet "International GPS Geodynamics Service (IGS)". Les applications (chapitre 8 GIG' 91 ainsi que le chapitre ESA' 91) constituaient les premiers pas pratiques dans cette direction.

En outre, dans ce travail de doctorat, des problèmes spécifiques sont évoqués qui pourraient faire l'objet de travaux plus fouillés. Ainsi, par exemple, le problème de la troposphère (chapitre 5): M. Rothacher présente ici une alternative valable et simple à réaliser dans la pratique en vue de l'élaboration de modèles stochastiques de la troposphère et qui a fait ses preuves jusqu'ici.

La Commission géodésique suisse reconnaît le grand mérite de M. Rothacher et le remercie de sa précieuse contribution à la géodésie suisse par satellites et à la mensuration nationale. L'Académie suisse des sciences naturelles (ASSN) soutient la Commission géodésique suisse (CGS) depuis de nombreuses années. Comme elle l'a fait en d'autres occasions, l'ASSN a pris à sa charge les frais d'impression de cette publication et, au nom de la CGS, nous lui exprimons notre gratitude.

Prof. Dr. G. Beutler
Directeur de l'Institut
d'astronomie de
l'Université de Berne

F. Jeanrichard, directeur
Office fédéral de topographie
Vice-président de la CGS

Prof. Dr. H.-G. Kahle
EPF- Zurich
Pésident de la CGS

PREFACE

The application of the new U.S. satellite-based navigation system GPS is increasingly important for many current fields of work, such as navigation, geodynamics or land surveying. Emerging with these applications, there is a growing need for a civil orbit service, which should make parameters of the GPS-orbits available to users on an operational basis as efficiently as possible.

Would it be the goal of a literature critic to class dissertations systematically with scientific disciplines, he would surely introduce the category of broad review-type theses and the category of theses with special topics. The work of Dr. Markus Rothacher belongs to the first kind. In the last ten years he has acquired the theoretical means and put them to test many times. Only with this rich experience could his subject "Orbits of Satellite Systems in Space Geodesy" be managed. After a general view on the currently interesting satellite systems part one takes a critical look at the orbital determination for the American "Global Positioning System (GPS)". Part two then illustrates these theoretical developments with thorough evaluation. This research work constitutes for the Astronomical Institute of the University of Berne (AIUB) the theoretical background of its participation in the "International GPS Geodynamics Service (IGS)". The applications (chapter 8 GIG' 91 and chapter ESA' 91) were the first practical steps in this direction.

In addition to this the dissertation also deals with many special problems, which will give rise to future research work. A special reference should be made to the handling of the troposphere (chapter 5): Markus Rothacher presents a highly valuable alternative to the stochastic modelling of the troposphere which has proven to be very reliable.

The Swiss Geodetic Commission (SGK) acknowledges the great achievement of Dr. Rothacher and appreciates his high-standing contribution to Swiss satellite geodesy and land surveying. The Swiss Academy for Natural Sciences (SANW) has been supporting the SGK for many years. As in previous cases the SANW has taken over the cost of print of this publication, for which the SGK is very grateful.

Prof. Dr. G. Beutler
Director of the Astronomical Institute, University of Berne

Director F. Jeanrichard
Federal Office of Topography
Vice president SGK

Prof. Dr. H.-G. Kahle
ETH Zurich
President SGK

TABLE OF CONTENTS

1. INTRODUCTION

The Navy Navigation Satellite System TRANSIT, the first satellite system that has become available for geodetic positioning, is in use for civilian purposes since 1967. Although it is mainly used for navigation, geocentric point positions with an accuracy of a few decimeters could be obtained with several days worth of doppler measurements.

The first launch of a satellite of the NAVSTAR Global Positioning System (GPS) in 1978 initiated the building up of a new satellite system for navigation and geodetic positioning that will reach its full constellation in a few years. At this time the older TRANSIT system will be switched off. A few other navigation satellite systems that already exist in a test configuration, like the Soviet GLONASS [Anodina, 1988], or that are being planned, like e.g. the European system NAVSAT [Carnebianca et al., 1985], together with new satellite tracking systems (e.g. DORIS in France [Willis et al., 1989] and PRARE in Germany [Hartl et al., 1985]) will also be available in future for high precision geodetic positioning. With these developments space geodesy has become more and more important for geodetic and geodynamic applications.

Although only two thirds of the Navstar GPS satellites have been put into orbit until now, the system has already demonstrated its tremendous potential in many different fields of geodesy:

- In local networks methods have been developed that allow the determination of relative site coordinates with an accuracy of about 1 cm within a few minutes [Frei & Beutler, 1990]. If longer observation periods are analysed the quality of results for short baselines (< 100 km) is likely to be below one centimeter making GPS attractive for monitoring crustal deformation [Prescott et al., 1989].

- In regional networks (500 to 2000 km) comparisons with results obtained from Very Long Baseline Interferometry (VLBI) or Satellite Laser Ranging (SLR) show an agreement of the order of

few parts in 10^8 of these independent methods (see e.g. [Lichten & Bertiger, 1989]).

- Recently it has been demonstrated that GPS may also successfully be used on a global scale to estimate site coordinates with an accuracy of $1 \cdot 10^{-8}$ or below and even to determine earth rotation parameters with a yet unseen temporal resolution [Blewitt & King, 1991].

Much of the strength of the GPS solutions lies in the fact that GPS is a satellite system, where, in contrast to conventional SLR, several satellites may be observed at the same time (the launch of Lageos II and the observation of the Etalon Satellites may change this situation). The geometrical rigidity resulting from simultaneous measurements is amazing.

It is clear that in the case of regional and global baselines such results are not achievable using the satellite ephemerides of an accuracy of 3-10 meters publicly available today. The satellite orbits have to be carefully modeled and estimated.

Modeling the orbits of a satellite system is the central aspect to be analyzed in this thesis.

The situation is complicated by the presence of biases. The most important error source (apart from the satellite orbits) is tropospheric refraction. The tropospheric delays of the radio signals have to be modeled and/or estimated, therefore, with the same care as the satellite orbits. In most cases satellite orbit and tropospheric zenith delay parameters will even have to be determined simultaneously from the observation material available.

Thus modeling the troposphere and estimation of troposphere model parameters is the second focus of this thesis.

Whereas the results of troposheric delay estimations are not very useful for a larger community, most of the users of a satellite system are highly interested in getting high-accuracy orbits as a prerequisite to obtain the best possible solutions for their own

baseline estimations, without having at hand complex algorithms needed for orbits determination of an entire satellite system.

In the near future the IGS (International GPS and Geodynamic Service) will be the responsible international organization to control the production and distribution of high-accuracy orbits of the NAVSTAR GPS bitterly needed by the geodetic community.

With this thesis we hope to contribute to this topic of interest to most geodesists and geophysicists dealing with the GPS.

This thesis is divided into two major parts. In the first part the theoretical background will be developed, in the second part the quality of the theoretical models will be tested using real and simulated data of the GPS.

In Chapter 2 we give an overview over some of the new satellite systems in space geodesy, including GPS and GLONASS. The satellite orbit characteristics are described and the different observation types used in satellite geodesy are introduced.

Chapter 3 deals with the modeling of the observables of GPS and GLONASS (observation equations for code and phase measurements). The forming of linear combinations of the original carriers and the differencing techniques are introduced for later use. The influence of the two most important error sources (the satellite orbits and the tropospheric refraction) on the estimation of site coordinates is then motivating the study and modeling of these effects.

The theoretical aspects of the satellite orbit modeling and estimation are covered in Chapter 4. Models for the various forces acting on the satellite are given and the principles of orbit determination (including a short description of numerical integration) are presented.

Chapter 5 lists the modeling and estimation methods available tc

reduce the effects of the tropospheric refraction. Deterministic as well as stochastic approaches are looked at.

In Chapter 6 we deal with the problem of orbit precision and accuracy. Different possibilities to assess the quality of satellite orbits are outlined and methods to compare individual satellite orbits as well as systems of satellite orbits are presented.

Chapter 7 is devoted to the models used in the simulation of GPS observations and the generation of different bias types. Simulated data will be used in Part II to study some aspects of orbit and troposphere modeling and estimation.

In the second, the application part of this thesis we present results obtained from four different campaigns.

Simulated data for a subset of the sites occupied during the First Global IERS and Geodynamic GPS Campaign (GIG'91) are used in Chapter 8 to study the influence of different bias types on global orbit determination. The qualities of regional and global orbits are compared.

Some results of the European ESA GPS Campaign are given in Chapter 9 to show the potential of continuous satellite tracking. Free network solutions and solutions using the fiducial point concept are presented.

Chapter 10, finally, deals with a very small network in Switzerland measured using GPS in 1989. The large height differences in this mountainous region and the availability of a high precision terrestrial solution qualifies this network as an ideal test field for troposphere model studies.

PART 1:

THEORY

2. MODERN SATELLITE SYSTEMS

In the last decade the huge potential of systems of satellites for navigation and positioning has become more and more evident. The geometrical strength resulting from the possibility to track several satellites at the same time is only now beginning to be fully realized. The idea of real time navigation with 4-7 satellites on one hand and geodetic applications with 24 hour sessions and 24 satellites on the other hand opens up a new dimension. In view of this trend it is not astonishing, that new satellite systems have been planned and even developed in the last few years.

In this chapter we give a short description of some of these new satellite systems developed in the field of satellite geodesy, namely DORIS, PRARE, GPS, and GLONASS. Each system uses its own measurement philosophy (doppler, ranges, phases, one-way or two-way observations, ...) depending on the application type, the accuracies to be obtained, and the potential users.

Since we are going to use data of NAVSTAR GPS to study the orbital aspects of a satellite system, and since the NAVSTAR GPS has already been partly operational for geodetic purposes for 6-7 years and much experience has been gathered during this time interval, a more detailed description will be given for NAVSTAR GPS than for the other systems.

It should be pointed out that the four satellite systems presented in the next paragraphs are only an important but not a representative selection out of the many satellite systems under planning or construction today. Not described here is e.g. the NAVSAT, a European satellite navigation system under study by the European Space Agency (ESA) [Carnebianca et al., 1985] that combines geostationary satellites, such as communication satellites, with high earth-orbiting satellites, such as those used in the Navstar GPS program, a combination called GEO/HIO mix [Rosetti et al., 1988], or the GRANAS, another satellite positioning initative [Euler et al., 1983].

2.1 DORIS

In France a satellite tracking system is currently developed with the acronym

DORIS: Doppler Orbitography and Radiopositioning Integrated by Satellite.

Whereas its main purpose is the precise orbit determination, the DORIS system will also have remarkable positioning capabilities for geodesy and geophysics. It is built to be used for orbit determination in the joint US-French oceanographic project TOPEX/ POSEIDON planned for 1992 [Lefebvre, 1989; Willis et al., 1990].

The three French groups involved in the design and realization of the DORIS system are the CNES (Centre National d'Etude Spatiale), the GRGS (Groupe de Recherche en Géodésie Spatiale), and the IGN (Institut Géographique National).

The different parts of the DORIS system are shown in Figure 2.1.

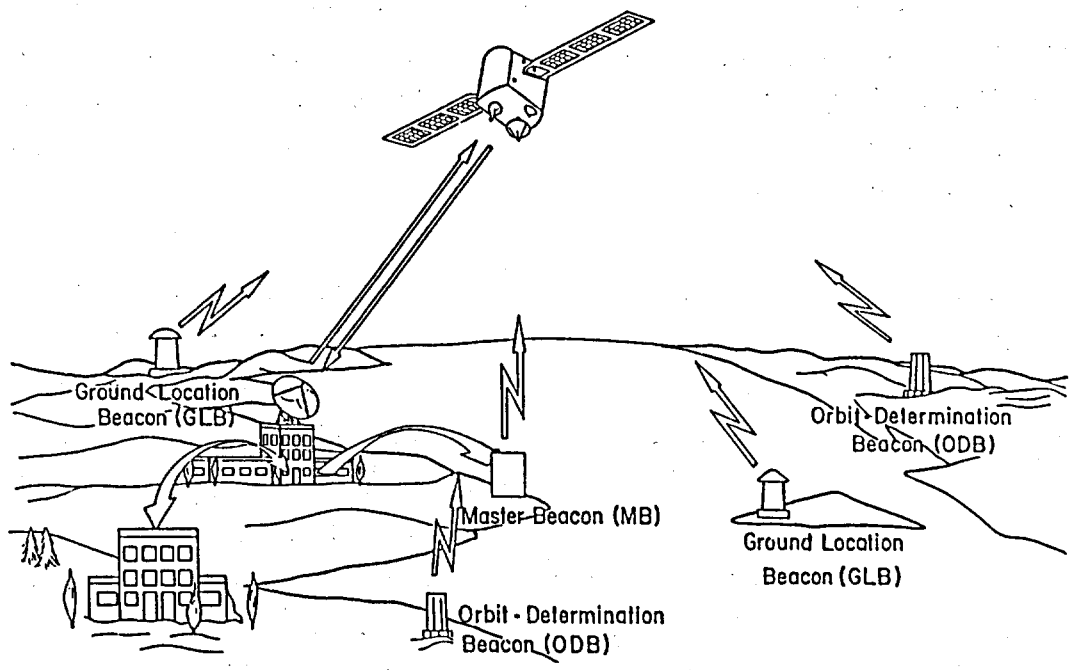

Figure 2.1
The DORIS System

DORIS will fly on low altitude orbiting satellites as SPOT2 (for test purposes), SPOT3, and, as mentioned above, TOPEX/POSEIDON. DORIS is a dual frequency uplink doppler system, the two nominal frequencies being 2.03625 GHz and 0.40125 GHz. The on-board instrument consists of a doppler receiver, an omnidirectional antenna to receive the two frequencies, and an ultra stable oscillator (stability of $5 \cdot 10^{-13}$ over periods of 10 to 100 seconds). All the doppler data are collected by the electronics on-board the satellite and then retransmitted to the control station in Toulouse. DORIS may therefore be called a centralized system (no data collection in the field). All the data are directly archived and processed in Toulouse.

In order to determine precisely the orbit of the satellite carrying DORIS a dense network of about 50 permanent beacons (Orbit Determination Beacons) is being installed (see Figure 2.2) whenever possible near VLBI or SLR sites to have precise geocentric coordinates. The orbit accuarcy is estimated to be about 10 cm in the radial component [La Brune et al., 1986].

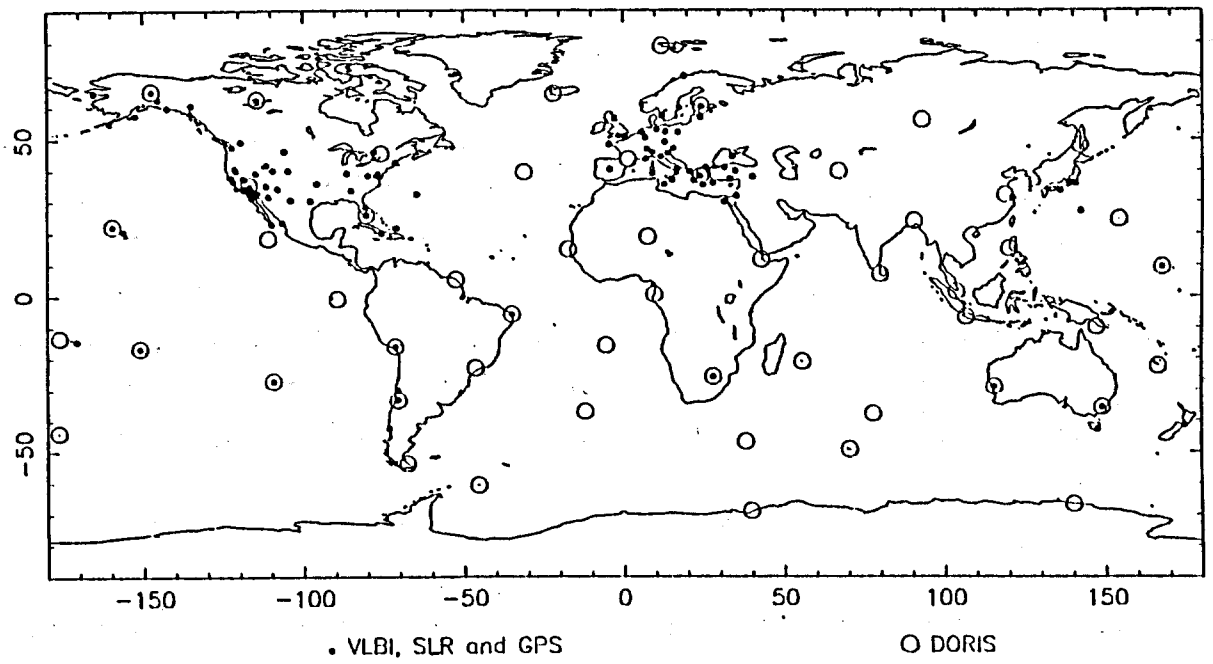

Figure 2.2
The DORIS Tracking Network

In addition to the beacons mentioned above mobile units (Ground Location Beacons) will be available to be placed at locations of geodetic or geophysical interest. The designers expect an absolute positioning accuracy within a global reference frame of 8 cm using 40 satellite passes, and a relative accuracy of 2 cm + 0.1 ppm using 30 passes [Willis et al., 1989].

2.2 PRARE

The satellite tracking system

PRARE: Precise Range And Range Rate Equipment

was proposed in 1982 as an additional experiment on ESA's (European Space Agency) First Remote Sensing Satellite ERS-1 (to be launched in July 1991) [Hartl et al., 1985]. The development of the PRARE system is a national German project of the following institutions and companies: the INS (Institut für Navigation, Universität Stuttgart), Kayser Threde GmbH (München), Dornier GmbH (Friedrichshafen), and the DGFI (Deutsches Geodätisches Forschungsinstitut, Abt. 1, München).

The space segment of the PRARE system is a small compact unit to be placed on a satellite (the first is ERS-1). Two continuous signals are emitted from the space segment to the earth with the frequencies 2.2 GHz (S-band) and 8.5 GHz (X-band). Both signals are modulated with a pseudo-random noise code (PN-code) used for the distance measurements and containing broadcast information for the ground station operation (see also Figure 2.3) [Flechtner et al., 1990].
In the ground station the time delay in the reception of the two simultaneously emitted signals is measured and the result is retransmitted and stored on-board the satellite. The X-band signal is transposed to 7.2 GHz at the ground station, coherently modulated with the regenerated PN-code including the two-frequency delay data, and is returned to the space segment. There the PN-code is fed into a correlator to determine the two-way signal de-

lay. In addition the received carrier frequency is evaluated in a doppler counter. The two-way tracking allows highest measurement precision because the signal generation and the measurement are based on the same ultra-stable quartz oscillator. Four independent correlators and doppler counters allow the simultaneous measurements of up to four ground stations.

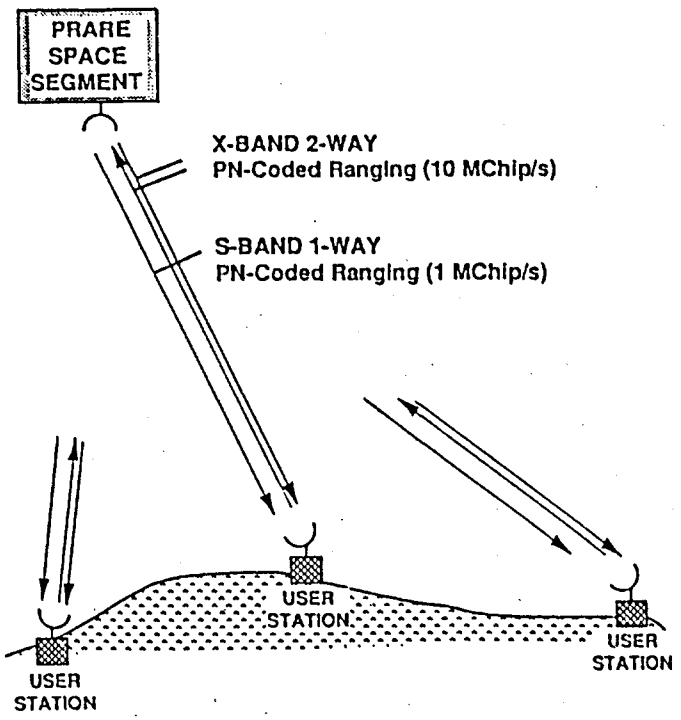

Figure 2.3
The PRARE Measurement Principle

The information collected in the space segment will be transmitted to the master control station during every suitable pass. In the control station the incoming data are processed, archived, and finally disseminated to the users.

The planned network of PRARE ground stations is shown in Figure 2.4.

The measurement accuracy is thought to be 0.1 mm/s for the X-band doppler and 3-7 cm for X-band ranging, the main error being th tropospheric refraction.

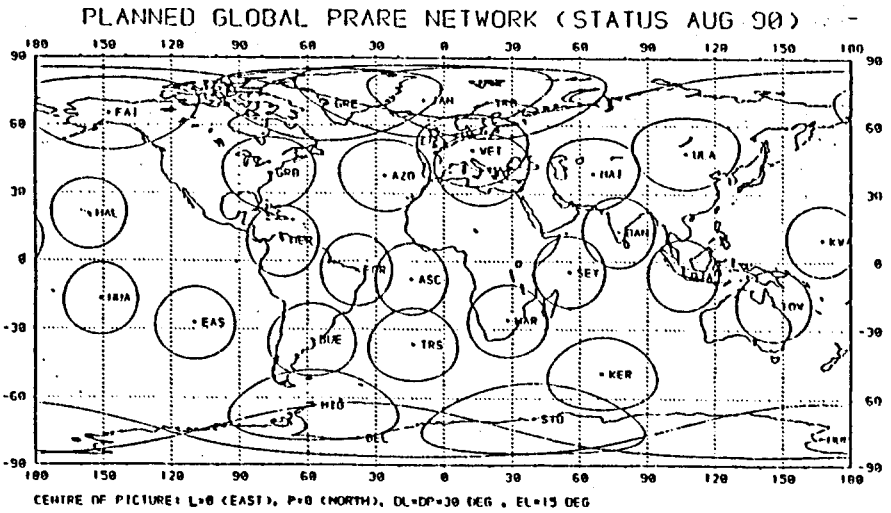

Figure 2.4.
Planned Global PRARE Tracking Network

An extended PRARE system, PRAREE, is proposed to be flown on the first European Polar Platform. With additional signals (for instance a two colour laser in the ground station) a direct measurement of the atmospheric refraction will be made possible leading to estimated range errors in the few mm range [Reigber et al., 1988].

2.3 NAVSTAR GPS and GLONASS

Two satellite systems for global positioning and navigation as well as time transfer (one developed in the United States by the Department of Defence (DoD) and one designed in the USSR), are already used in a test configuration and will soon become fully operational. These systems, the

NAVSTAR GPS: **Navigation Satellite Timing And Ranging Global Positioning System**

and the

GLONASS : Global Navigation Satellite System

are going to replace the older Navy Navigation Satellite System, known as TRANSIT, and the equivalent Russian doppler system TSICADA. In 1995 it is planned to switch off the TRANSIT system.

Both systems, NAVSTAR GPS (or simply GPS) and GLONASS, have a very similar overall system design indeed (for NAVSTAR see [Milliken et al., 1980], for GLONASS [Anodina, 1988]), and will be presented together here. They are composed of three integral design parts: the space segment, the ground or control segment, and the user segment.

2.3.1 The Space Segment

The space segment consists of 21 to 24 active satellites to be operational in the final satellite configuration.

NAVSTAR GPS:

The full constellation of the Navstar satellites (see Figure 2.5) has been subject to several changes, mainly due to budgetary problems. The current plan calls for a uniform 24 satellite configuration (21 production satellites and 3 active spares) [Green et al., 1989]. The satellites will be located in six planes in almost circular orbits approximately 20'200 km above the earth's surface resulting in an orbital period of approximately 11 hours 58 minutes or half a sidereal day. Thus almost the same satellite scenario will recur 4 minutes earlier every day. The six orbital planes will be separated by 60 degrees in longitude and will have an inclination of 55 degrees relative to the equatorial plane. Four satellites will be located in each plane. With this constellation at least 4 satellites will always be in view from every point on the earth's surface 24 hours a day. In some instances as

many as 8 or more satellites will be visible to a ground user. It is expected that the system will be fully operational in 1993.

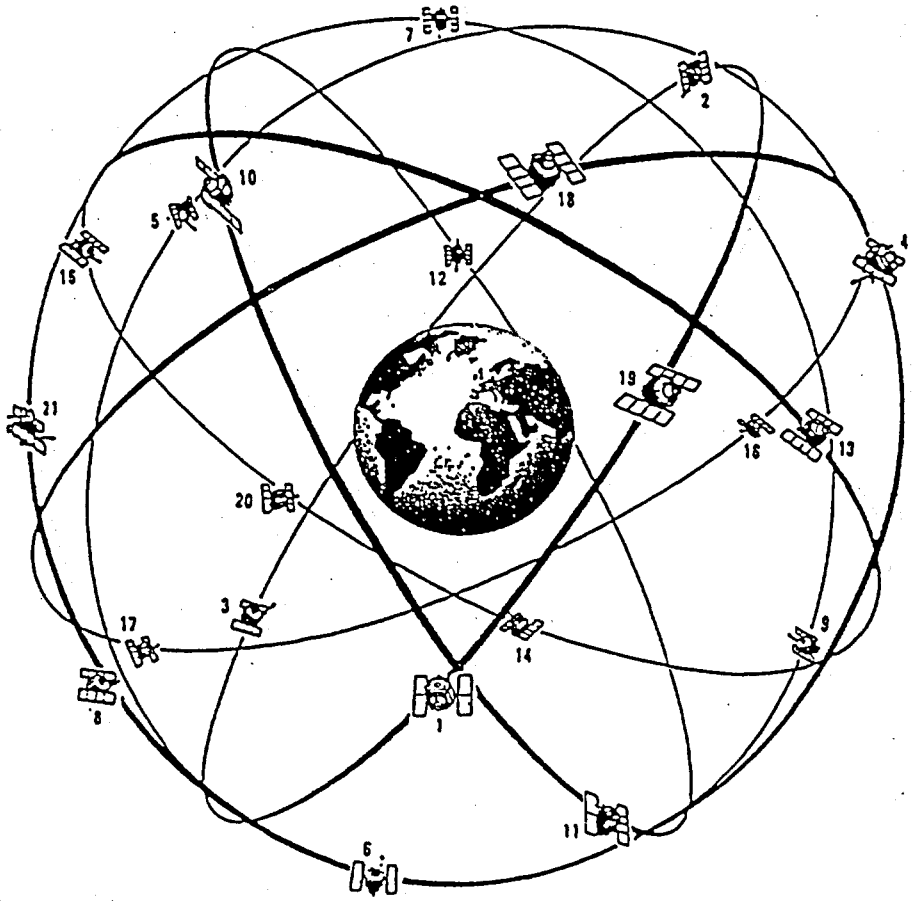

Figure 2.5
Navstar GPS Satellite Constellation

The satellites used in the Navstar program (see Figure 2.6) are large, multi-purpose platforms utilized for a series of other (military) projects (e.g. atomic flash detection) beside the positioning requirements. The first satellites launched (in 1978) were Block I satellites for the test phase of the project. Of the ten launched satellites 5 are still operating today. Table 2.1 summarizes the current status of Block I satellites.

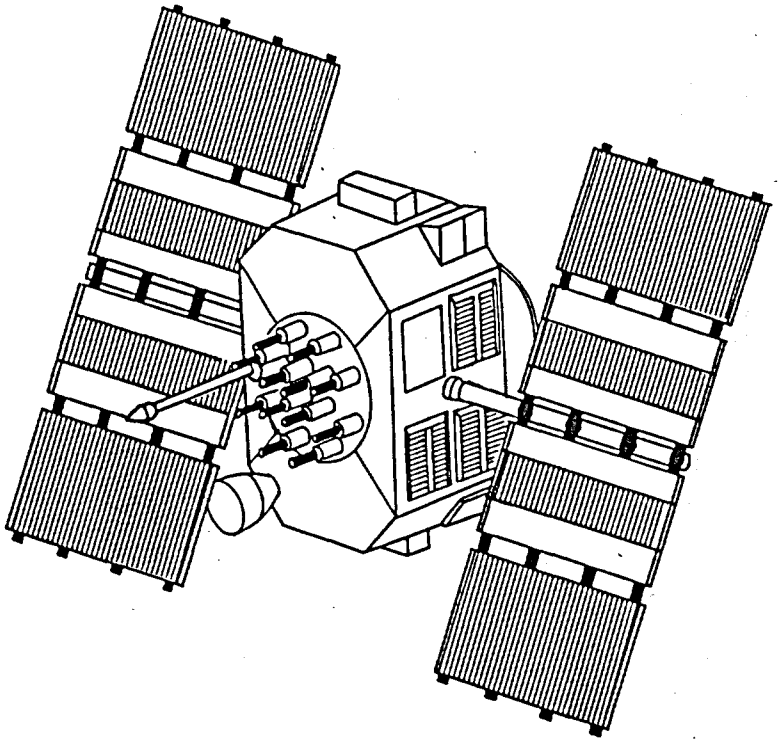

Figure 2.6
GPS Block I Satellite

Satellite SVN	Satellite PRN	Launch Date	Current Status (September 1991)
01	04	22-FEB-78	Turned off 17-JUL-85
02	07	13-MAY-78	Turned off FEB-88
03	06	7-OCT-78	Still operating, batteries low
04	08	10-DEC-78	Turned off 14-OCT-89
05	05	9-FEB-80	Reaction wheel fail. 11-MAY-84
06	09	26-APR-80	Operation terminated 6-MAR-91
07	-	Failure	---
08	11	14-JUL-83	Fully operational
09	13	13-JUN-84	Fully operational
10	12	8-SEP-84	Fully operational
11	03	9-OCT-85	Fully operational

SVN = Space Vehicle Number, PRN = Pseudo-Random-Noise Code Number

Table 2.1
Current Status of Block I NAVSTAR GPS Satellites

In February 1989 the first of the Block II or production satel-

lites was launched (PRN 14). Since then 10 further Block II satellites have been deployed in orbit. Accordingly the present constellation consists of 16 active satellites (5 Block I, 11 Block II) and the so-called two-dimensional coverage has been reached: at every instant from every point on the earth's surface at least three satellites can be observed. This allows the determination of the horizontal position (assuming the height to be known) of the antenna in real-time. Figure 2.7 shows the present satellite constellation and Table 2.2 gives the launch dates of Block II satellites.

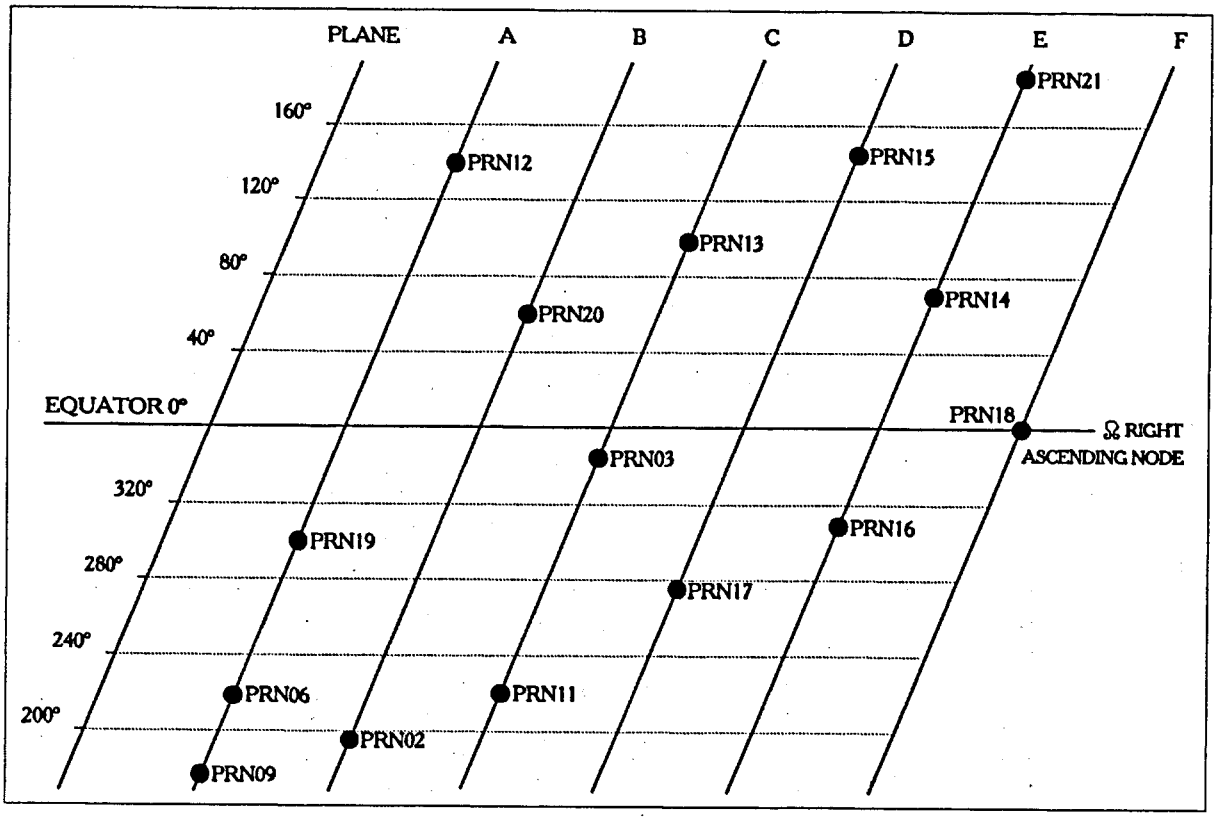

Figure 2.7
Navstar GPS Satellite Constellation of May 1991

In the Block II family 28 production satellites are planned. In addition, plans have already been made for a further 20 replenishment satellites to be known as Block IIR. These will replace the Block II satellites as necessary and introduce some new design features (e.g. inter-satellite communications and ranging).

Satellite SVN	Satellite PRN	Launch Date	Current Status (September 1991)
14	14	14-FEB-89	Successfully launched
13	2	10-JUN-89	Successfully launched
16	16	18-AUG-89	Successfully launched
19	19	21-OCT-89	Successfully launched
17	17	11-DEC-89	Successfully launched
18	18	24-JAN-90	Successfully launched
20	20	26-MAR-90	Successfully launched
21	21	2-AUG-90	Successfully launched
15	15	1-OCT-90	Successfully launched
23	23	26-NOV-90	Successfully launched
24	24	4-JUL-91	Successfully launched

Table 2.2
Launch dates and Status of Block II NAVSTAR GPS Satellites

Block I and II satellites only have a limited supply of propellant to allow orbit manoeuvres. Therefore the re-positioning process tends to be long (see section 4.1.7).

GLONASS:

The GLONASS satellites are located at 19'100 km, a slightly lower altitude than that of NAVSTAR satellites, but the orbit planes have a similar inclination of 64.8 degrees to the equator and a plane separation of 120 degrees in longitude. The satellites themselves are located in the orbital planes at 45 degree intervals. GLONASS is also expected to achieve eventually a 24 satellite constellation (including 3 spares), but arranged in only three orbit planes [Anodina et al., 1989].

The GLONASS satellites currently have an orbital period of 11 hours and 16 minutes and will show a ground track repetition after nearly 8 days. Unlike NAVSTAR GPS individual GLONASS satellites, therefore, do not appear at the same point in space daily (minus 4 minutes). However, as the satellites are 45 degrees out of phase another satellite in the same plane will meet this re-

quirement, making geometry repeatable and predictable as in NAVSTAR.

Much less information is available about GLONASS than about GPS, especially with respect to the launch schedule. GLONASS has been partly operational since 1982. The full constellation could have been completely installed within a two year period due to multiple payload launches [Daly, 1988]. Unfortunately the USSR were not too successful in maintaining the stability of their test constellation. At present there appear to be 12 healthy GLONASS satellites (see Figure 2.8) from a total of more than 27. (See Table 2.3 for launch dates of the GLONASS satellites from 1982 to 1989.)

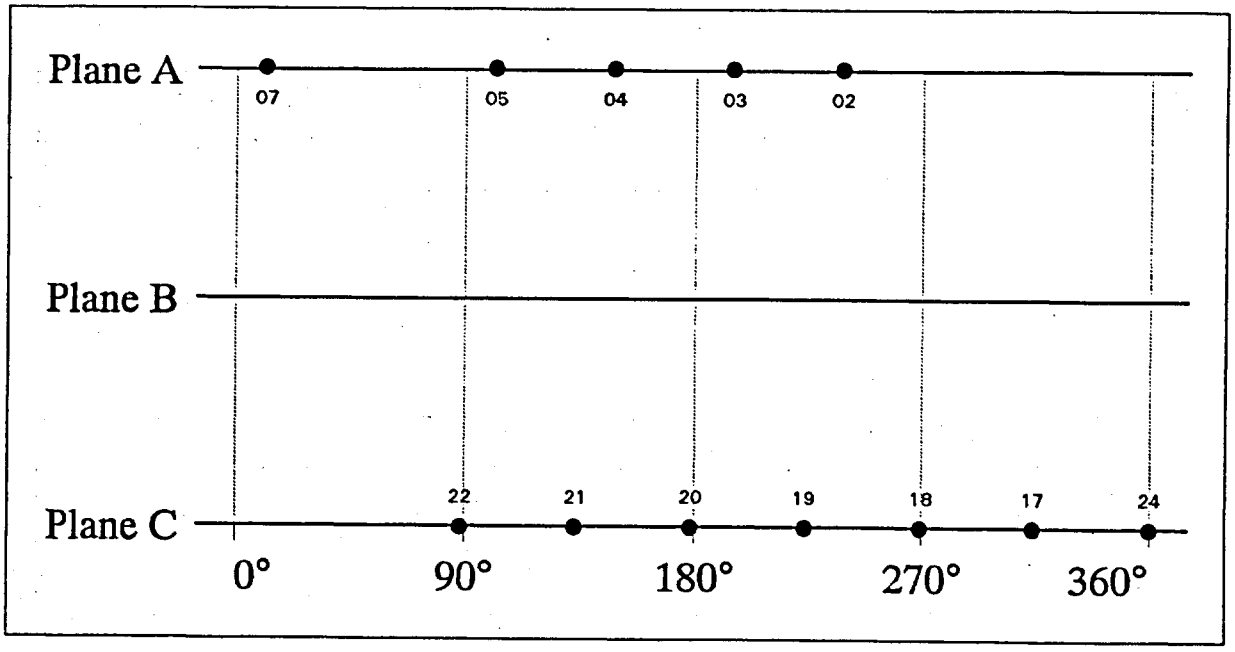

Figure 2.8
GLONASS Satellite Constellation of July 1991

GLONASS satellites apparently do not fully rely on solar or battery power but contain an alternative power source. This gives them significant manoeuvring capabilities. Orbit changes will only take a few days as opposed to months in the case of the NAVSTAR system. The satellites also have the ability to communicate, and possibly range, between each other [Ackroyd et al., 1990].

Satellite No. Internat./USSR		Launch Date	Orbit Plane	Frequencies L_1 (MHz)	L_2 (MHz)
COS 1413	--	12-OCT-82	B	---	---
1414	--	"	B	---	---
1415	--	"	B	---	---
COS 1490	03	10-AUG-83	B	1603.6875	1247.3125
1491	--	"	B	---	---
1492	--	"	B	---	---
COS 1519	24	29-DEC-83	A	1615.5000	1256.5000
1520	02	"	A	1603.1250	1246.8750
1521	--	"	A	---	---
COS 1554	09	19-MAY-84	A	1607.0625	1249.9375
1555	18	"	A	1612.1250	1253.8750
1556	--	"	A	---	---
COS 1593	--	4-SEP-84	B	---	---
1594	--	"	B	---	---
1595	17	"	B	1611.5625	1253.4375
COS 1650	07	17-MAY-85	B	1605.9375	1249.0625
1651	10	"	B	1607.6250	1250.3750
1652	--	"	B	---	---
COS 1710	04	24-DEC-85	A	1604.2500	1247.7500
1711	19	"	A	1612.6875	1254.3125
1712	--	"	A	---	---
COS 1778	11	16-SEP-86	B	1608.1875	1250.8125
1779	20	"	B	1613.2500	1254.7500
1780	22	"	B	1614.3750	1255.6250
COS 1838	--	24-APR-87	-	Launch failure	
1839	--	"	-	Launch failure	
1840	--	"	-	Launch failure	
COS 1883	14	16-SEP-87	A	1609.8750	1252.1250
1884	21	"	A	1613.8125	1255.1875
1885	05	"	A	1604.8125	1248.1875
COS 1917	--	17-FEB-88	-	Launch failure	
1918	--	"	-	Launch failure	
1919	--	"	-	Launch failure	
COS 1946		21-MAY-88	B		
1947		"	B		
1948		"	B		
COS 1970		16-SEP-88	A		
1971		"	A		
1972		"	A		

Table 2.3 (First Part)

COS 1987	10-JAN-89	B	
1988	"	B	
1989 ETALON 1	"	-	
COS 2022	31-MAY-89	A	
2023	"	A	
2024 ETALON 2	"	-	

Table 2.3 (Second Part)
GLONASS Satellite Launch Dates 1982-1989
(Table incomplete due to missing information)

Table 2.4 summarizes the characteristics of both the NAVSTAR GPS and GLONASS.

Characteristics	NAVSTAR GPS	GLONASS
Inclination of Orbital Planes	63° (Block 1) 55° (Block 2)	64.8°
Orbital Period	11 h 58 min	11 h 16 min
# of Orbit Planes	6	3
# of Satellites	24 (3 spares)	24 (3 spares)
Mass	815 kg	700 kg
Data Rate	50 bit/sec	50 bit/sec
Code	Satellite dependent	Satellite independ.
Carr. Frequencies	Satellite independ.	Satellite dependent
Frequency L_1	1575.42 MHz	$\nu_j=\nu_1+j\cdot d\nu_1$ $\nu_1=1602.0000$ MHz $d\nu_1=0.5625$ MHz
Frequency L_2	1227.60 MHz	$\nu_j=\nu_2+j\cdot d\nu_2$ $\nu_2=1246.0000$ MHz $d\nu_2=0.4375$ MHz

Table 2.4
NAVSTAR GPS and GLONASS Constellation and Satellite Characteristics

2.3.2 The Ground/Control Segment

The ground or control segment refers to the ground based element of the satellite system which controls the performance of the satellites through orbital tracking, clock monitoring, etc.

NAVSTAR GPS:

The Operational Control System (OCS) (see Figure 2.9) for the NAVSTAR GPS became operational in September 1985. The Master Control Station situated at Colorado Springs is responsible for the overall satellite control, the determination of satellite ephemeris and clock state predictions for each satellite. Four additional sites at Hawaii, Ascension Islands, Diego Garcia, and Kwajalein are operated as monitor stations for tracking the satellites and collecting range data to produce satellite ephemerides. Ascension, Diego Garcia, and Kwajalein also have uplink antennas to transmit satellite orbit and clock information, and commands to the satellites.

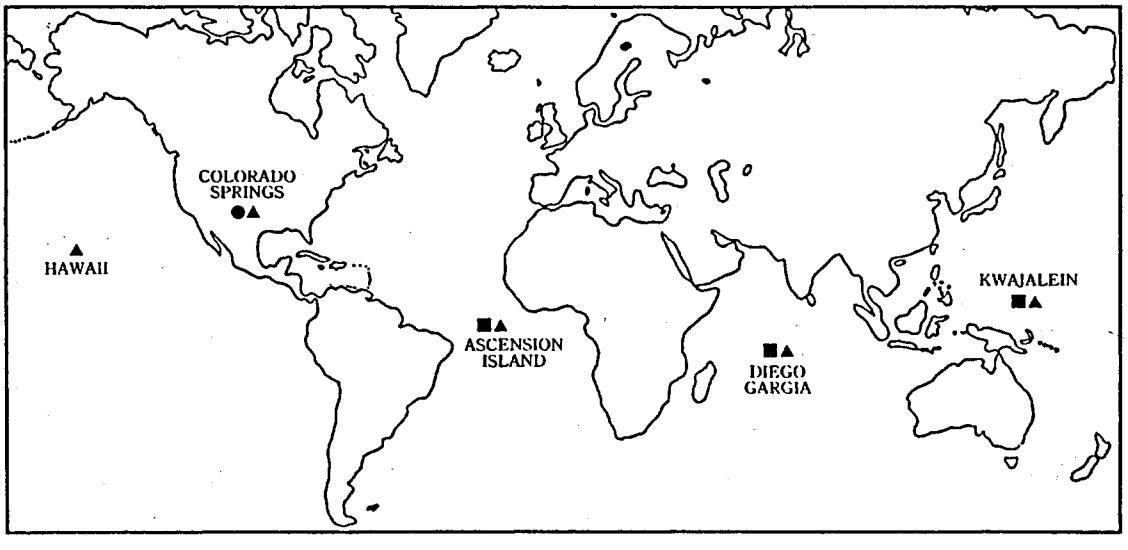

Figure 2.9
Operational Control System for NAVSTAR GPS

The overall policy-making body is the Joint Program Office (JPO), represented by the US Army, the US Navy, the US Air Force, the Department of Transportation (DOT), the Defence Mapping Agency (DMA), and the NATO.

GLONASS:

Little information is available about the details behind the organization of the GLONASS system. The ground-based tracking stations appear to be located in the Soviet Union only. This limits the overall control of the system resulting in less reliable health monitoring and a degraded ephemeris. It is important to realize, however, that the GLONASS satellites can also monitor each other which will allow monitoring during times, when satellites are out of direct view by the ground stations.

2.3.3 The User Segment

The user segment of the satellite system(s) includes all the elements required to receive the signals being broadcast from the satellites. In essence this means the GPS or GLONASS receiver(s). Different receiver types are commercially available by now. We will not go into any detail concerning receiver design and operation, however.

There also exist GLONASS receivers (e.g. the ASN-16 receiver) and attempts are made to construct hybrid NAVSTAR-GLONASS receivers being able to track both, NAVSTAR GPS and GLONASS satellites.

The setting up of national or international user groups for distribution of information could also be considered part of the user segment. In this context we should mention the Civil GPS Information Centre (CGIC) and the International GPS and Geodynamics Service (IGS). The IGS represents a permanent international service to be established under the auspices of the International Association of Geodesy (IAG). The primary objective is to provide

IGS users with GPS information and data products developed under strict standards. Among these products are high accuracy GPS ephemerides, satellite clock information, earth rotation parameters, and ionospheric data. For these services the IGS depends on a permanent global tracking network.

2.3.4 The Signal Structure

Both global positioning systems derive the different signals (codes and carrier phases) they emit from the basic frequency of the oscillator(s) on-board each satellite: 10.23 MHz for the NAVSTAR GPS, and 10 MHz for GLONASS. (Due to effects of special and general relativity, these standard frequencies are set to a marginally lower value prior to launch). Since both systems are also used for precise time transfer the NAVSTAR GPS time is referenced to UTC (Universal Time Coordinated) and controlled by the United States Naval Observatory, whereas GLONASS time appears to be connected with a time frame called Moscow Time [Ackroyd et al., 1990].

NAVSTAR GPS:

NAVSTAR GPS has two main carrier frequencies known as L_1 and L_2, used for positioning purposes. L_1 is centered on 1575.42 MHz (154 times the clock frequency of 10.23 MHz) and L_2 on 1227.60 MHz (120 times 10.23 MHz). (For uplinking and downlinking of data the satellites also operate at two other frequencies (1783.74 and 2227.5 MHz), and a third emitted frequency (1381.05 MHz) is reserved for atomic flash monitoring). Two pseudo-random noise codes (PN-codes) are transmitted by the satellites by modulating the carrier frequencies. The C/A-code (clear or coarse acquisition code, for civilian use) is available only on the L_1 carrier, whereas the more precise P-code (precise or protected code, for military use) is available on both carriers [Spilker, 1978; Bauersima, 1983] (see Figure 2.10).

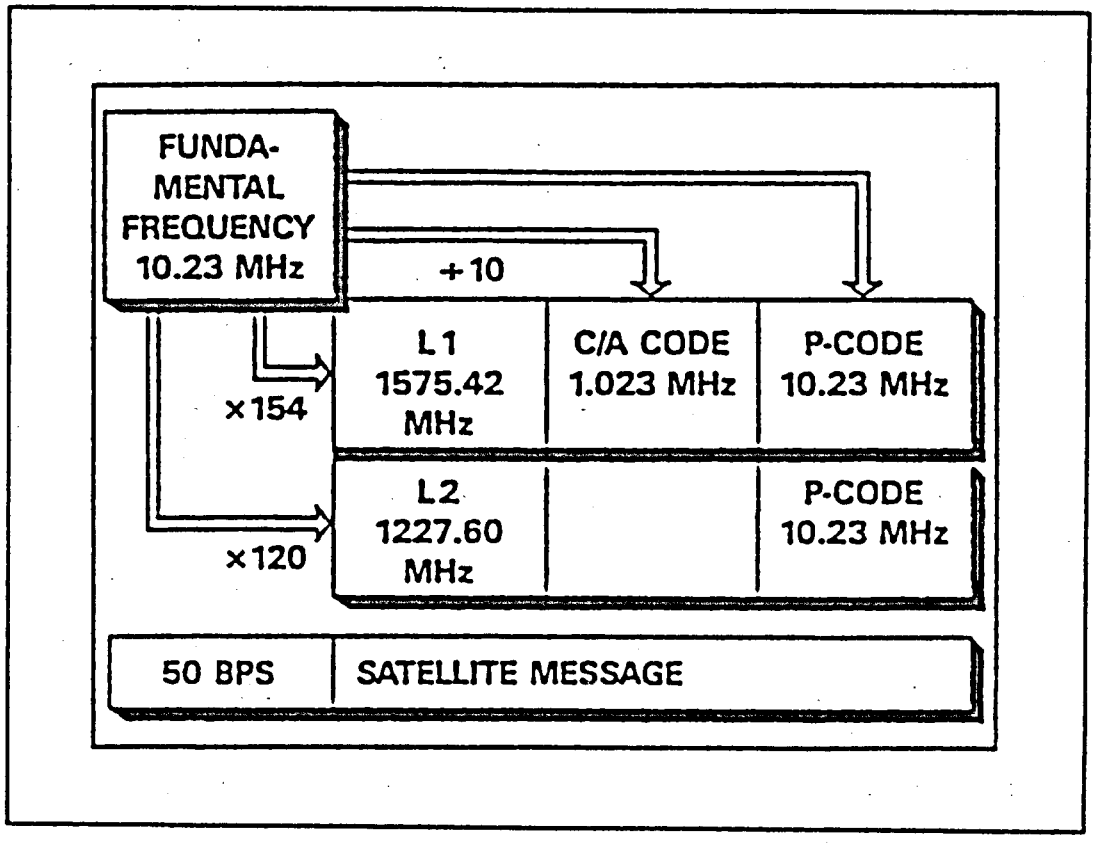

Figure 2.10
Signal and Frequency Generation of a GPS Satellite

The C/A-code is made up of a sequence of binary zeroes and ones (realized by phase changes of 180 degrees) with a frequency of 1.023 MHz (a tenth of the basic clock frequency) corresponding to a "wavelength" of about 300 meters. For the P-code generation the original frequency of 10.23 MHz is used corresponding to about 30 meters. As an additional coded modulation the so-called broadcast navigation message is transmitted by each satellite at a rate of 50 bits/sec containing information on the satellite ephemeris, the satellite clock corrections, the satellite health and status, and others [Van Dierendonck et al., 1978].

When completing the Block II constellation, the US intend to change the P-code to a new encrypted code called Y-code. The details of this code will not be available and only a special code key will enable its use. Already at present signals transmitted by Block II satellites are degraded to limit the highest accuracy

of the system to authorized users. This mode of degraded operation is called **Selective Availability** (SA) and involves the degradation of the quality of broadcast ephemerides and the dithering of the satellite clocks (see [Feigl et al., 1991]).

There are two different types of measurements performed by a geodetic NAVSTAR GPS receiver:

- Pseudorange Measurements: The range (distance satellite - receiver) is measured as the time difference between the emission of a specific code (C/A or P) sequence and its reception at the receiver. Since the instant of emission is defined by the satellite clock, whereas reception time is measured in receiver time the derived ranges are called "pseudoranges", biased by the synchronization errors of the two clocks with respect to GPS time. The receiver identifies the code sequence emitted by a specific satellite by generating an exact replica of the code and then correlating the incoming signal against slightly advanced and delayed versions of this local replica, a technique known as auto-correlation. The continuity in tracking of the code is achieved through a delay lock loop, which adjusts the code replica in time to maintain a perfect match. The resolution of the correlation is a few percent of the "wavelength" in consideration, thus leading to a measurement accuracy of about 1 meter for P-code, 3-5 meters for C/A-code pseudoranges.

- Carrier Phase Measurements: First the carriers have to be reconstructed using the known codes. (If the P-code is not known, the L_2 carrier can e.g. be reconstructed by squaring the signal, thus loosing the information of the phase sign). The carriers are then differenced with a reference carrier generated by the receiver and the resulting signal (the carrier beat phase) is tracked using a similar technique to tracking the code, except that a frequency lock loop is used to maintain lock on the phase. The accuracy of these phase measurements is about 1-3 mm. They would represent very accurate ranges, if, at the time of the first measurement, the exact number of integer wavelengths between the satellite and the receiver was known and not only the fractional part. The unknown integer number of

cycles to be added to the phase measurement to get a range is called the initial phase ambiguity. This phase ambiguity remains the same as long as the receiver keeps lock on the phase transmitted by the satellite.

GLONASS:

GLONASS has a frequency design different from NAVSTAR GPS. In NAVSTAR GPS all satellites transmit on the same two carrier frequencies (L_1 and L_2). The individual satellites are identified by having a unique code sequences, a technique known as code division multiple access. In GLONASS the individual satellites are identifiable as each actually transmits a slightly different carrier frequency (frequency division multiple access). The L_1 frequency of GLONASS is centered on 1602.0 MHz, the L_2 on 1246.0 MHz. Each satellite transmits at an offset of 0.5625 MHz from its neighbour, e.g. satellite 1 would transmit at 1602.5625 MHz, satellite 2 at 1603.1250 MHz, etc. The frequency spacing on the L_2 band is 0.4375 MHz (see Table 2.4).

As in the case of the NAVSTAR system there are two codes transmitted, one for civilian and one for military purposes. In contrast to the NAVSTAR system, however, the same codes can be used for all the satellites.

GLONASS and GPS receivers collect essentially the same measurement types.

3. MODELING OF THE OBSERVABLE

The measurement types of the NAVSTAR GPS and GLONASS have been introduced in section 2.3.4: P-code on L_1 and L_2, C/A-code, carrier phases L_1 and L_2. These are also the basic observables used for the estimation of relevant geodetic parameters like site coordinates and orbital elements. GPS and GLONASS receivers registrate, depending on the receiver type and application, a subset or all of these different measurement types with an observation interval of typically 30 seconds for geodetic purposes. (The sampling rate may be much higher in the case of navigation.)

In the following we will discuss the observation equations for both, pseudorange and carrier phase observations, introduce the most important linear combinations of the above measurement types and the various levels of observation differences used, and characterize the most important biases affecting the observations.

3.1 The Observation Equations

Many observation equations for both, carrier phase and pseudorange measurements, have been published. Among the first such publications we may refer to [Davidson et al., 1983], [Goad & Remondi, 1983], and [Bauersima, 1983]. Details and numerous references may also be found in [Landau, 1988], and [Sovers & Border, 1987]. Therefore the outline given here will be limited to the topics of interest in the course of this work.

3.1.1 Pseudorange Observation Equation

The pseudorange observation provides a measure of the absolute range between satellite and receiver, offset by the receiver and satellite clock errors.

Let us define the following terms:

t_i^S : Emission time of signal i from satellite S in GPS time
$\tilde{t}_i^S$: Reading of the satellite clock at time t_i^S
t_{Ri} : Reception time of signal i at receiver R in GPS time
$\tilde{t}_{Ri}$: Reading of the receiver clock at reception of signal i
τ_{Ri}^S : Travel time of signal i between satellite S and receiver R

With these definitions the satellite clock synchronization error Δt_i^S and receiver clock synchronization error Δt_{Ri} with respect to GPS time at times t_i^S resp. t_{Ri} can be written as:

$$\Delta t_i^S = \tilde{t}_i^S - t_i^S \tag{3.1}$$

$$\Delta t_{Ri} = \tilde{t}_{Ri} - t_{Ri} \tag{3.2}$$

Obviously we also have

$$\tau_{Ri}^S = t_{Ri} - t_i^S \tag{3.3}$$

In this nomenclature the observed quantity, the **pseudorange** O_{Ri}^S, between satellite S and receiver R, is given (in length units) by:

$$O_{Ri}^S = c\cdot(\tilde{t}_{Ri}-\tilde{t}_i^S) \tag{3.4}$$

where c denotes the speed of light.
Using equations (3.1) to (3.3) we may rewrite eqn. (3.4) in the following way:

$$O_{Ri}^S = c\cdot\tau_{Ri}^S + c\cdot\Delta t_{Ri} - c\cdot\Delta t_i^S \tag{3.5}$$

The term $c\cdot\tau_{Ri}^S$ contains the information relevant for geodesy:

$$c\cdot\tau_{Ri}^S = \rho_{Ri}^S + \Delta\rho_{Ri,ion}^S + \Delta\rho_{Ri,trop}^S - \Delta\rho_{Ri,rel}^S \tag{3.6}$$

with $$\rho_{Ri}^S = \left| \mathbf{r}^S(t_{Ri}-\tau_{Ri}^S) - \mathbf{r}_R(t_{Ri}) \right| \tag{3.7}$$

and

ρ^S_{Ri} : Distance between satellite S at time t^S_i and receiver R at time t_{Ri}

$\mathbf{r}^S(t)$: Geocentric position vector of satellite S at GPS time t in an inertial reference frame

$\mathbf{r}_R(t)$: Geocentric position vector of receiver R at GPS time t in the same inertial frame

$\Delta\rho^S_{Ri,ion}$: Ionospheric refraction correction

$\Delta\rho^S_{Ri,trop}$: Tropospheric refraction correction

$\Delta\rho^S_{Ri,rel}$: Periodic relativistic correction

The observation equation of the pseudorange measurements is then given by

$$O^S_{Ri} - O^{S\,\prime}_{Ri} = v^S_{Ri} \tag{3.8}$$

where

$O^{S\,\prime}_{Ri}$: Pseudorange observation between satellite S and receiver R.

v^S_{Ri} : Residual (measurement noise and remaining unmodelled effects)

or substituting (3.5) and (3.6):

$$\boxed{\rho^S_{Ri} + \Delta\rho^S_{Ri,ion} + \Delta\rho^S_{Ri,trop} - \Delta\rho^S_{Ri,rel} + c\cdot\Delta t_{Ri} - c\cdot\Delta t^S_i - O^{S\,\prime}_{Ri} = v^S_{Ri}} \tag{3.9}$$

Since τ^S_{Ri} appears in eqn. (3.6) on the left hand side and also implicitly on the right hand side in ρ^S_{Ri} (see eqn. (3.7)), ρ^S_{Ri} has to be determined either iteratively or by developing the satellite position into a Taylor series around the time t_{Ri} (neglecting terms of order 2) and solving for the resulting quadratic equations in ρ^S_{Ri}. (For more details see [Schildknecht, 1986].)

According to [Weiffenbach, 1967] the ionospheric refraction correction for code observations may be approximated by

$$\Delta\rho^{s}_{Ri,ion} = \frac{k}{\nu^2} \cdot E \qquad (3.10)$$

with ν : Frequency of the carrier being processed.

E : Total number of electrons seen by the signal travelling from satellite to receiver in the cyclinder with the signal path as axis and a unit area ground surface.

$$k \approx 41 \frac{m^3}{sec^2} \qquad (3.11)$$

The frequency dependency of the ionospheric refraction (proportional to $1/\nu^2$) as well as the numerical value for k are only approximations. [Prilepin, 1986] has shown, however, that for frequencies in the range of 1 to 2 GHz considered here the terms neglected in (3.10) are of the order of 0.1 % .

The tropospheric refraction corrections $\Delta\rho^{s}_{Ri,trop}$ will be discussed in more details in section 5.1.

The periodic relativistic correction $\Delta\rho^{s}_{Ri,rel}$ for the satellite clock caused by the eccentricity of the satellite orbit is given by

$$\Delta\rho^{s}_{Ri,rel} = \frac{2}{c^2} \cdot \mathbf{r}^{s}(t^{s}_{i}) \cdot \dot{\mathbf{r}}^{s}(t^{s}_{i}) \qquad (3.12)$$

The relativistic delay due to the gravitational field of the earth (see [Bernstein, 1987]) is of the order of 10^{-9} [Zhu and Groten, 1988]. So far it has not been accounted for in our software.

Exactly the same observation equation may be used to process GLONASS data.

3.1.2 Carrier Phase Observation Equation

The carrier phase observation equation is very similar to the pseudorange observation equation. If we assume that the receiver R generates a reference signal of the same frequency ν (wavelength λ) as the satellite S, the basic zero difference phase observable ψ^S_{Ri} may be written (in length units) as:

$$\psi^S_{Ri} = \lambda^S \cdot (\phi_R(\tilde{t}_{Ri}) - \phi^S(\tilde{t}^S_i)) \qquad (3.13)$$

with λ^S : Nominal wavelength of the satellite oscillator
$\phi_R(\tilde{t}_{Ri})$: Reference phase generated by the receiver R at time $\tilde{t}_{Ri}$
$\phi^S(\tilde{t}^S_i)$: Phase generated by the satellite S and emitted at time $\tilde{t}^S_i$
$\tilde{t}_{Ri}, \tilde{t}^S_i$: Explained in section 3.1.1

Taking into account the satellite and receiver clock synchronization errors Δt^S_i and Δt_{Ri} (see eqn. (3.1) and (3.2)) we find an equation similar to eqn. (3.5):

$$\psi^S_{Ri} = c\cdot\tau^S_{Ri} + c\cdot\Delta t_{Ri} - c\cdot\Delta t^S_i + \lambda^S\cdot N^S_R \qquad (3.14)$$

where c : Speed of light
τ^S_{Ri} : Travel time of carrier phase between satellite S and receiver R
N^S_R : Initial carrier phase ambiguity being an unknown, but integer number

Apart from the fact that the phase measurement is ambiguous by an integer number of cycles N^S_R, there is also a difference in the computation of the light travel time:

$$c\cdot\tau^S_{Ri} = \rho^S_{Ri} - \Delta\rho^S_{Ri,ion} + \Delta\rho^S_{Ri,trop} - \Delta\rho^S_{Ri,rel} \qquad (3.15)$$

with ρ^S_{Ri}, $\Delta\rho_{Ri,ion}$, $\Delta\rho^S_{Ri,trop}$, and $\Delta\rho^S_{Ri,rel}$ explained in section 3.1.1. Comparing eqn. (3.15) to eqn. (3.6) for pseudoranges, the only difference is the sign of the ionospheric refraction correc-

tion: a delay in the case of pseudorange (group velocity), an acceleration for carrier phase (phase velocity).

The observation equation of the carrier phase measurements may finally be written (substituting eqn. (3.15) into (3.14)):

$$\rho^{S}_{Ri} - \Delta\rho^{S}_{Ri,ion} + \Delta\rho^{S}_{Ri,trop} - \Delta\rho^{S}_{Ri,rel} + c\cdot\Delta t_{Ri} - c\cdot\Delta t^{S}_{i} + \lambda^{S} N^{S}_{R} - \psi^{S\,\prime}_{Ri} = v^{S}_{Ri} \qquad (3.16)$$

where

$\psi^{S\,\prime}_{Ri}$: Carrier phase observation between satellite S and receiver R

v^{S}_{Ri} : Residual

To be able to use the same equation for GLONASS carrier phase observations, we have written the wavelength λ^{S} of the carrier phase with a superscript S to indicate that in GLONASS different satellites use different wavelengths (see section 2.3.4 and Table 2.4).

3.1.3 Linear Combinations

In many situations during the processing of GPS (or GLONASS) data it is very useful or even mandatory to form linear combinations of the original L_1 and L_2 carrier phase and/or code measurements.

The general form of such a linear combination L_ℓ of the L_1 and L_2 carrier phase observables (the same equation holds for the code) is given by:

$$\tilde{L}_\ell = \alpha_{\ell,1}\cdot\tilde{L}_1 + \alpha_{\ell,2}\cdot\tilde{L}_2 \qquad (3.17)$$

where $\alpha_{\ell,1}$, $\alpha_{\ell,2}$: Coefficients of the linear combination

$\tilde{L}_1$, $\tilde{L}_2$: Original carrier phase observables L_1 and L_2 in cycles of the respective carriers

$\tilde{L}_\ell$: Linear combination L_ℓ in units of cycles

The frequency ν_ℓ and wavelength λ_ℓ of the resulting linear combination L_ℓ is then easily derived to be

$$\nu_\ell = \alpha_{\ell,1} \cdot \nu_1 + \alpha_{\ell,2} \cdot \nu_2 \qquad (3.18)$$

and

$$\lambda_\ell = \frac{c}{\nu_\ell} = \frac{\lambda_1 \cdot \lambda_2}{\alpha_{\ell,1} \cdot \lambda_2 + \alpha_{\ell,2} \cdot \lambda_1} \qquad (3.19)$$

where ν_1 and ν_2 are the frequencies, λ_1 and λ_2 the wavelengths of the original carriers L_1 and L_2, and c the speed of light.

Denoting the observables expressed in units of length by

$$L_\ell = \lambda_\ell \cdot \tilde{L}_\ell \quad , \quad (\ell=1,2,\ldots) \qquad (3.20)$$

we may write instead of (3.17):

$$L_\ell = x_{\ell,1} \cdot L_1 + x_{\ell,2} \cdot L_2 \qquad (3.21)$$

where

$$x_{\ell,1} = \alpha_{\ell,1} \cdot \frac{\lambda_\ell}{\lambda_1} \qquad (i=1,2) \quad . \qquad (3.22)$$

The most important linear combinations together with some of their characteristics are summarized in Table 3.1. We include some comments:

L_1, L_2: Original carriers. They have a very small measurement noise (the noise of an L_3, L_4, and L_5 observation (see below) is roughly 3 times, 1.4 times, and 5 times the noise of a L_1 or L_2 observation respecitvely).

L_3 : Ionosphere-free linear combination. The advantage of L_3 is the elimination (or essential reduction) of the ionospheric path delay. The assumption thereby is that the distance correction due to the ionosphere is inversely proportional to the frequency squared (see eqn. (3.10)).

LC	λ	LC-Factors		Tropospheric/Orbit Biases		Ionospheric Biases		Observation Noise	
	[m]	$x_{\ell,1}$	$x_{\ell,2}$	[length]	[cycles]	[length]	[cycles]	[length]	[cycles]
L_1	c/ν_1 0.19	1	0	1	1	1	1	1	1
L_2	c/ν_2 0.24	0	1	1	$\frac{\nu_2}{\nu_1}$ 0.78	$\frac{\nu_1^2}{\nu_2^2}$ 1.6	$\frac{\nu_1}{\nu_2}$ 1.3	$\frac{\nu_1}{\nu_2}$ 1.3	1
L_3	0	$\frac{\nu_1^2}{\nu_1^2-\nu_2^2}$ 2.5	$\frac{-\nu_2^2}{\nu_1^2-\nu_2^2}$ -1.5	1	-	0	-	$\frac{\nu_1\sqrt{\nu_1^2+\nu_2^2}}{\nu_1^2-\nu_2^2}$ 3.1	-
L_4	∞	1	-1	0	-	$-\frac{\nu_1^2-\nu_2^2}{\nu_2^2}$ -0.6	-	$\sqrt{1+\frac{\nu_1^2}{\nu_2^2}}$ 1.6	-
L_5	$\frac{c}{\nu_1-\nu_2}$ 0.86	$\frac{\nu_1}{\nu_1-\nu_2}$ 4.5	$\frac{-\nu_2}{\nu_1-\nu_2}$ -3.5	1	$\frac{\nu_1-\nu_2}{\nu_1}$ 0.22	$-\frac{\nu_1}{\nu_2}$ -1.3	$\frac{\nu_2-\nu_1}{\nu_2}$ -0.28	$\frac{\nu_1}{\nu_1-\nu_2}\sqrt{2}$ 6.4	$\sqrt{2}$ 1.4

Table 3.1

Linear Combinations of the L_1 and L_2 Carrier Phase Observations

There also exists a third frequency emitted by the GPS satellites reserved for atomic flash monitoring sometimes called L_3. In this thesis L_3 will always be used for the ionosphere-free linear combination.

L_4 : Geometry-free linear combination. L_4 is independent of receiver clocks and of geometry (orbits, coordinates). It only contains the ionospheric delays and (for phase observations) the initial phase ambiguities.

L_5 : Wide-lane. Whereas systematic, unmodeled errors (like e.g. orbit errors) are of the same order of magnitude (expressed in meters) in L_5 as in the original carriers L_1 and L_2, the wavelength of L_5 ($\lambda_5 \approx 86$ cm) is roughly 4 times longer. This means that ambiguity resolution is usually much simpler in L_5 than in L_1 or L_2.
The L_5 initial phase ambiguity N_5 is equal to the difference N_1-N_2, where N_1 and N_2 are the ambiguities of the L_1 and L_2 observable.

Besides these phase (or code) linear combinations, we should make a remark concerning a special linear combination of both, carrier phase (L_1 and L_2) and P-code (P_1 and P_2) observables first described by [Wübbena, 1985] and [Melbourne, 1985]:

$$L_{W+M} = \beta_1 \cdot L_1 + \beta_2 \cdot L_2 + \beta_3 \cdot P_1 + \beta_4 \cdot P_2 \qquad (3.23)$$

with the coefficients:

$$\beta_1 = \frac{\nu_1}{\nu_1-\nu_2} = 4.529 \qquad \beta_3 = \frac{-\nu_1}{\nu_1+\nu_2} = -0.562$$

$$\beta_2 = \frac{-\nu_2}{\nu_1-\nu_2} = -3.529 \qquad \beta_4 = \frac{-\nu_2}{\nu_1+\nu_2} = -0.438$$

Starting from the observation equations (3.9) and (3.16) it is easy to show that in the case of GPS the following simple observation equation results:

$$(N_1-N_2)\cdot\lambda_5 - L'_{W+M} = v_{W+M} \qquad (3.24)$$

Eqn. (3.24) shows that the observable L_{W+M} is unbiased by coordinates, orbits, and ionosphere. What may be a problem is multipath.
With good P-code data this linear combination may successfully be used for the resolution of the wide-lane ambiguities N_5 independent of the baseline length.

All the linear combinations discussed here can be processed with the "Bernese GPS Software Version 3.3" (see [Rothacher et al., 1991]).

3.1.4 Differences of the Original Observables

Starting from the original carrier phase or code measurements differences may be formed to eliminate (or reduce) common error sources. These differencing techniques have been described in extenso in the literature (e.g. [King et al., 1985], [Wells et al., 1986]. Here we will just define the single and double difference phase observables and point out the differences between NAVSTAR GPS and GLONASS.

Let us assume that receivers R_1 and R_2 are observing almost simultaneously. The **single difference phase observable** $\Delta\psi^S_{R_1R_2i}$ is then defined as:

$$\Delta\psi^S_{R_1R_2i} = \psi^S_{R_1i} - \psi^S_{R_2i} \qquad (3.25)$$

or substituting eqn. (3.14), we get

$$\boxed{\Delta\psi^S_{R_1R_2i} = c\cdot\Delta\tau^S_{R_1R_2i} + c\cdot\Delta t_{R_1R_2i} + \lambda^S\cdot N^S_{R_1R_2}} \qquad (3.26)$$

where
$$\Delta\tau^S_{R_1R_2i} = \tau^S_{R_1i} - \tau^S_{R_2i}$$
$$\Delta t_{R_1R_2i} = \Delta t_{R_1i} - \Delta t_{R_2i}$$
$$N^S_{R_1R_2} = N^S_{R_1} - N^S_{R_2}$$

and where the drift of the satellite clock between epoch $t_{R_1 i} - c \cdot \tau^{S}_{R_1 i}$ and epoch $t_{R_2 i} - c \cdot \tau^{S}_{R_2 i}$ has been neglected.

Assuming a satellite clock drift of the order of 10^{-11} (e.g. of a Block I satellite) and a receiver mis-synchronization of 0.1 sec, the neglected term is about 0.3 mm. This shows that the satellite clock behaviour is eliminated in the single difference observation, when selective availability (SA) is turned off (see section 2.3.4). In the presence of SA the satellite clock has to be carefully modeled, if the two receivers are sampling data asynchronously.

The **double difference phase observable** is obtained by forming the difference between two single differences to the satellites S_1 and S_2 at epoch i:

$$\nabla\Delta\psi^{S_1 S_2}_{R_1 R_2 i} = \Delta\psi^{S_1}_{R_1 R_2 i} - \Delta\psi^{S_2}_{R_1 R_2 i} \tag{3.27}$$

or, substituting eqn. (3.26) for satellites S_1 and S_2, we get:

$$\boxed{\nabla\Delta\psi^{S_1 S_2}_{R_1 R_2 i} = c \cdot \nabla\Delta\tau^{S_1 S_2}_{R_1 R_2 i} + \lambda^{S_1} \cdot N^{S_1 S_2}_{R_1 R_2} + \Delta\lambda^{S_1 S_2} \cdot N^{S_2}_{R_1 R_2}} \tag{3.28}$$

with
$$\nabla\Delta\tau^{S_1 S_2}_{R_1 R_2 i} = \Delta\tau^{S_1}_{R_1 R_2 i} - \Delta\tau^{S_2}_{R_1 R_2 i}$$
$$N^{S_1 S_2}_{R_1 R_2} = N^{S_1}_{R_1 R_2} - N^{S_2}_{R_1 R_2}$$
$$\Delta\lambda^{S_1 S_2} = \lambda^{S_1} - \lambda^{S_2}$$

By forming the double difference observations the relative receiver clock correction $\Delta t_{R_1 R_2 i}$ is eliminated. To compute the satellite positions (contained in $\nabla\Delta\tau^{S_1 S_2}_{R_1 R_2 i}$) accurately enough, however, the GPS times (see eqns. (3.1) and (3.2))

$$\begin{aligned} t_{R_1 i} &= \tilde{t}_{R_1 i} - \Delta t_{R_1 i} \\ t_{R_2 i} &= \tilde{t}_{R_2 i} - \Delta t_{R_2 i} \end{aligned} \tag{3.29}$$

and therefore the receiver clock errors $\Delta t_{R_1 i}$, $\Delta t_{R_2 i}$ have to be known on the 1 μsec level (remaining receiver clock error times relative satellite velocity ≈ 1 μsec·1 km/sec = 1 mm).

For NAVSTAR GPS, where every satellite emits its signals at almost the same frequency, we may immediately write

$$\Delta\lambda^{S_1 S_2} \approx 0 \tag{3.30}$$

For GLONASS, however, we have to take into account that the satellites transmit on different frequencies (see section 2.3.4 and Table 2.4). In the case of L_1 the frequency ν_1^i of satellite i is given by

$$\nu_1^i = \nu_1^0 + i\cdot\Delta\nu_1 \qquad (i=1,2,\ldots,24) \tag{3.31}$$

where $\nu_1^0 = 1602.0$ MHz
$\Delta\nu_1 = 0.5625$ MHz

The maximum wavelength difference in L_1 between two GLONASS satellites (satellite 1 and satellite 24) is therefore

$$\Delta\lambda_{1,max}^{S_1 S_2} = \lambda^1 - \lambda^{24} = \frac{c}{\nu_1^1} - \frac{c}{\nu_1^{24}} = 1.5 \text{ mm} \tag{3.32}$$

For L_2 a similar calculation gives

$$\Delta\lambda_{2,max}^{S_1 S_2} = 1.9 \text{ mm} \tag{3.33}$$

The term $\Delta\lambda^{S_1 S_2}\cdot N_{R_1 R_2}^{S_2}$ in eqn. (3.28) causes problems when resolving ambiguities with observations of the GLONASS.

The "Bernese GPS Software Version 3.3", with which the data processing described in this work has been done, uses, as many other GPS software packages, the double difference as main observable.

3.2 Biases

If we look at the observation equations (3.9) and (3.16) we see that there are many possible error sources:

- Satellite orbits
- Tropospheric refraction
- Ionospheric refraction
- Receiver and satellite clocks
- Multipath

All these biases (except multipath) are considerably reduced, especially for short baselines, by forming **double difference observations.**

In the next two sections we will have a closer look at the biases introduced by satellite orbit errors and tropospheric refraction errors. The influence of the ionosphere is almost eliminated by forming the ionosphere-free linear combination of the L_1 and L_2 observations (see section 3.1.3). Due to forming double differences, the satellite clock term is eliminated (assumption: no asynchronous sampling of the receivers) and the receiver clock synchronization has only to be known within 1 μs (see 3.1.4, double differences) which is easily achieved by using the code observations. Multipath, finally, will not be considered in this thesis.

3.2.1 Orbit Biases

3.2.1.1 Impact of Orbit Biases on Site Coordinates

A very simple formula to estimate the effect of orbit biases on the determination of site coordinates when processing carrier phase difference observations has been given by [Bauersima, 1983; eqn. 84]:

$$\frac{|\Delta b|}{|b|} \approx \frac{|\Delta r|}{|r|} \tag{3.34}$$

where Δr : Orbit error of the satellite
r : Geocentric satellite position vector
Δb : Resulting error in the baseline vector b
b : Baseline vector between two sites

According to formula (3.34) the baseline errors increase linearly with increasing baseline length, a fact we will see confirmed in all our results. Table 3.2 compiles the results obtained with formula (3.34) for different baseline lengths and orbit errors, assuming a mean value of $|r| = 25'000$ km for GPS satellites.

Orbit Error $\lvert\Delta r\rvert$	Baseline Error $\lvert\Delta b\rvert$ for Baseline Length 1 km	10 km	100 km	1'000 km	10'000 km	$\frac{\lvert\Delta b\rvert}{\lvert b\rvert}$
10 cm	0.004 mm	0.04 mm	0.4 mm	4 mm	4 cm	$4\cdot10^{-9}$
1 m	0.04 mm	0.4 mm	4 mm	4 cm	40 cm	$4\cdot10^{-8}$
10 m	0.4 mm	4 mm	4 cm	40 cm	4 m	$4\cdot10^{-7}$
100 m	4 mm	4 cm	40 cm	4 m	40 m	$4\cdot10^{-6}$

Table 3.2
Approximate Errors in the Baseline Vector for Different Orbit Errors and Baseline Lengths According to Eqn. (3.34)

A more detailed analysis of orbital biases has been performed by [Zielinski, 1988]. Studying the covariance matrix he came to the conclusion that a more realistic estimation would be

$$\frac{|\Delta r|}{10\cdot|r|} < \frac{\Delta b}{|b|} < \frac{|\Delta r|}{4\cdot|r|} \tag{3.35}$$

Here Δb is the error in the **baseline length**, whereas in eqn. (3.34) the error $|\Delta \mathbf{b}|$ of the **baseline vector** is used. This important difference, together with the fact that along track orbit errors mainly propagate into the station height (see below), explains the smaller biases expected by Zielinski.

It is clear that in reality all the satellites will have somewhat different errors in size and in direction and thinking of a 24-satellite constellation and long sessions (e.g. 24 hours), a considerable part of the orbit errors may be averaged out in the coordinate results. To get an idea of the size of the remaining baseline errors simulation techniques (see [Geiger, 1987] and Chapter 7) are more promising tools than analytical approaches.

There are also errors in the satellite orbits, however, that are a consequence of a wrong orientation of or a scale in the satellite orbit system. Such errors concerning the satellite orbit system as a whole are produced, if fiducial sites used in the orbit estimation are kept fixed at wrong geocentric positions. This effect is particularly important if only a few fiducial sites are used for orbit improvements.

A scale in the satellite orbits (radial orbit error common to all satellites) has been discussed in [Beutler et al., 1988]: the result is a scale in the network which is by a factor 4 smaller than the scale in the orbits (ratio of Earth radius to geocentric satellite distance). A rotation in the satellite orbit system will cause a rotation of comparable size and direction in the network to be adjusted, affecting the station heights. This is confirmed by [Beutler et al., 1988] when analyzing the effect of along track orbit biases.

It is worth-wile to emphasize two points:

1) Errors in the orientation of the satellite orbit system (e.g. along track errors) propagate into GPS baseline results in a much less favourable way than errors in the scale of the system (radial errors).

2) Along track orbit biases mainly affect the verticals of a network. The same is true for troposphere biases (see section 3.2.2) letting us expect a strong correlation between the two main error sources in GPS.

3.2.1.2 Quality of Broadcast and Precise Orbits

Today the geodetic user of GPS has, if he does not improve orbits with his own software, mainly the choice of using the broadcast orbits or the precise orbits.

Broadcast Orbits:

In the case of the broadcast orbits (see also section 2.3.2 and [Wells et al., 1986]) the most recent tracking data (e.g. 12 to 24 hours of code data) are used for an orbit improvement starting from a reference orbit generated with the data of one week. The orbits thus obtained are then extrapolated for the next day and for each hour orbital elements are computed and uploaded to the GPS satellites.

The quality of the baseline results when using broadcast orbits (see e.g. [Beutler et al., 1987b] or [Landau, 1988]) is of the order of

$$\left(\frac{\Delta b}{b} \right)_{BC} \approx 1 \cdot 10^{-7} \text{ to } 4 \cdot 10^{-7} \qquad (3.36)$$

According to eqn. (3.34) the mean errors in the broadcast orbits may then be estimated as

$$\boxed{| \Delta r_{BC} | \approx 2.5 \text{ to } 10 \text{ m}} \qquad (3.37)$$

Precise Orbits:

The Naval Surface Warfare Center (NSWC) together with the Defence Mapping Agency (DMA) generates the so-called precise orbits approximately 4-8 weeks after the collection of the tracking data. In addition to the five Air Force stations (see section 2.3.2) used for the broadcast ephemerides, data are collected at five more stations, namely Quito (Ecuador), Buenos Aires (Argentina), Smithfield (Australia), Hermitage (England), and Bahrain. With an orbit determination program [Swift, 1985] approximately 8 days of data are fitted in a least squares estimation of orbit parameters.

The precise orbits are of about the same quality as the broadcast orbits:

$$| \Delta r_{PR} | \approx | \Delta r_{BC} | \qquad (3.38)$$

This can be concluded from the comparisons done by [Remondi et al., 1989] between broadcast and precise orbits, where the mean differences between the two orbit types are found to be about 3-4 meters. Results of [Landau, 1988] even show slightly worse baseline repeatabilities when using precise instead of broadcast orbits.

Today the only way to reduce the orbit errors of the broadcast or precise ephemerides is the improvement of the orbital parameters using phase (plus code) observations from global or regional tracking data. This procedure will be discussed in Chapter 4.2 .

In the near future regional and global GPS orbits will be produced by dedicated ephemeris computation centers using the data of permanent tracking sites. Such activities will be coordinated by the IGS, the International GPS and Geodynamics Service (see section 2.3.3), having as principle goal the production of high precision GPS orbits (~ 10^{-8} or better). These orbits will then be distributed to the various users of the GPS.

3.2.2 Troposphere Biases

Many studies have been performed in the last few years in the field of tropospheric refraction and, more specifically, on the influence of troposphere biases on the estimation of site coordinates. Here we will review some of the recent results that are of importance for the interpretation of results in Part II of this thesis. Tropospheric refraction errors may be reduced by appropriate troposphere models and/or the estimation of troposphere parameters. These possibilities will be dealt with in Chapter 5.

3.2.2.1 Relative Tropospheric Refraction Error

A detailed analysis of the effect of a **relative tropospheric zenith delay error**, the difference of tropospheric zenith delay errors on both sides of a baseline, has been performed by [Santerre, 1991]. He has shown that

1) A tropospheric zenith delay error mainly affects the station height, whereas the effects on the horizontal position are negligible.

2) The magnification factor (error in station height divided by the tropospheric zenith delay error) depends on the satellite visibility and therefore changes with geographical latitude of the site between 2.6 for an equatorial and 3.9 for a polar site, assuming a maximum zenith distance of 70°.

Additional errors are introduced when the zenith delay is mapped to the zenith distance z due to errors in the mapping function (see eqn. (5.10)) and due to azimuthal variations and horizontal gradients (see [Gardner, 1976] and [Tralli et al., 1988]). Details on azimuthal variations of the tropospheric delays measured with water vapour radiometers may be found in [Elgered et al., 1990].

3.2.2.2 Absolute Tropospheric Refraction Error

An **absolute tropospheric zenith delay error** is the arithmetic mean of tropospheric zenith delay errors on both sides of a baseline. The impact of such an absolute delay error is much smaller than the effect of a relative troposphere error discussed in the previous section. An absolute troposphere zenith delay error has the same consequence as an absolute ionosphere error (although with the opposite sign), namely a scale factor in the baseline length (see [Santerre, 1991] for absolute ionospheric delay errors).

Neglecting tropospheric refraction makes the GPS derived baselines longer. The entire tropospheric zenith delay is of the order of 2.3 meters giving a maximum scale factor of about 1 ppm, if we neglect tropospheric refraction completely. A more realistic assumption is, that remaining unmodeled errors of the order of a few centimeters, due to the wet component of the tropospheric refraction, lead to scale factors of several parts in 10^{-8}.

3.2.2.3 Impact of Biases in Surface Met Data

Biases may also be introduced into the GPS results by using incorrect or inappropriate surface met data in the data analysis. Computing the partial derivatives of the tropospheric zenith delay $\Delta\rho^0_{trop}$ with respect to temperature T, pressure P, and relative humidity H using a simplified version of the Saastamoinen formula (see [Bauersima, 1983]) gives the values compiled in Table 3.3 (see also [Beutler et al., 1988]).

Table 3.3 shows that even small inconsistencies in the measured surface met data may lead to considerable biases in the tropospheric refraction correction which will, according to section 3.2.2.1, propagate into the station heights amplified by a factor of about 3. Especially for small networks, therefore, the use of surface met data may be quite destructive (see [Gurtner et al., 1987]). The inconsistencies in the met measurements may be due to instrument errors (calibration) or due to the fact that the met

values measured at the surface are not representative for the atmosphere above the site (inversion situations, local anomalies, ...).

T °C	P mbar	H %	$\frac{\partial \Delta\rho^0_{trop}}{\partial T}$ mm/°C	$\frac{\partial \Delta\rho^0_{trop}}{\partial P}$ mm/mbar	$\frac{\partial \Delta\rho^0_{trop}}{\partial H}$ mm/(1%)
0°	1000	100	5	2	0.6
30°	1000	100	27	2	4
0°	1000	50	3	2	0.6
30°	1000	50	14	2	4

Table 3.3
Dependence of the Tropospheric Zenith Refraction Correction $\Delta\rho^0_{trop}$ on Surface Met Data (Temperature T, Pressure P, and Humidity H)

4. MODELING OF A SATELLITE ORBIT SYSTEM

We have seen in section 3.2.1 that the accuracy of GPS orbits publicly available today are of the order of 3-10 meters. Table 3.2 has also shown that the biases introduced into the estimated baseline vectors by such orbit errors are of the order of a few parts in 10^7. We know, therefore, that for baselines longer than 50-100 km the orbit quality is the limiting factor for the estimation of site coordinates (together with the troposphere). All the high-precision results for regional and global site coordinates obtained by various groups could only be achieved with orbit improvement techniques. Orbit estimation and the underlying force model are therefore of utmost importance.

The orbit characteristics of GPS and GLONASS satellites have already been described in section 2.3.1 .

4.1 The Force Model

4.1.1 The Equations of Motion

The equations of motion of a satellite in its orbit around the earth can be written as a system of second order differential equations:

$$\ddot{\mathbf{r}}(t) = \mathbf{f}(t,\mathbf{r}(t),\dot{\mathbf{r}}(t),p_1,\ldots,p_n) \qquad (4.1)$$

where

- $\mathbf{r}(t)$: Column matrix of Cartesian coordinates of position vector of the satellite at time t in an inertial, geocentric coordinate system.
- $\dot{\mathbf{r}}(t)$, $\ddot{\mathbf{r}}(t)$: First and second time derivatives of $\mathbf{r}(t)$.
- $\mathbf{f}(\ldots)$: Column matrix of force vector in the same system as $\mathbf{r}$.

p_i (i=1,2,...,n): Force model parameters defining the forces acting on the satellite (e.g. describing solar radiation pressure, drag, or the earth potential field).

A particular (unique) solution of the differential equation system (4.1) may e.g. be defined in the following two ways:

(1) by supplying initial values (position and velocity) at epoch t_0:

$$\begin{aligned} \mathbf{r}(t_0) &= \mathbf{r}_0(q_1,q_2,\ldots,q_6) \\ \dot{\mathbf{r}}(t_0) &= \dot{\mathbf{r}}_0(q_1,q_2,\ldots,q_6) \end{aligned} \tag{4.2}$$

or

(2) by supplying boundary values at epochs t_1 and t_2:

$$\begin{aligned} \mathbf{r}(t_1) &= \mathbf{r}_1(q_1,q_2,\ldots,q_6) \\ \mathbf{r}(t_2) &= \mathbf{r}_2(q_1,q_2,\ldots,q_6) \end{aligned} \tag{4.3}$$

where the q_i (i=1,2,...,6) are six parameters that uniquely define the vectors $\mathbf{r}_0$ and $\dot{\mathbf{r}}_0$, or $\mathbf{r}_1$ and $\mathbf{r}_2$ respectively.

Possible choices for these parameters are:

a) $(q_1,q_2,q_3) = \mathbf{r}_0^T \qquad (q_4,q_5,q_6) = \dot{\mathbf{r}}_0^T$ (4.4)

b) $(q_1,q_2,q_3) = \mathbf{r}_1^T \qquad (q_4,q_5,q_6) = \mathbf{r}_2^T$ (4.5)

c) $(q_1,q_2,\ldots,q_6) = (a,e,i,\Omega,\omega,t_p)$ (4.6)

where $\mathbf{r}^T$ is the transpose of matrix $\mathbf{r}$ and where a,e,i,Ω,ω,t_p are the osculating Keplerian elements at epoch t_0 (see Figure 4.1):

a : Semi-major axis
e : Eccentricity
i : Inclination

Ω : Right ascension of ascending node

ω : Argument of perigee

t_p : Perigee passing time

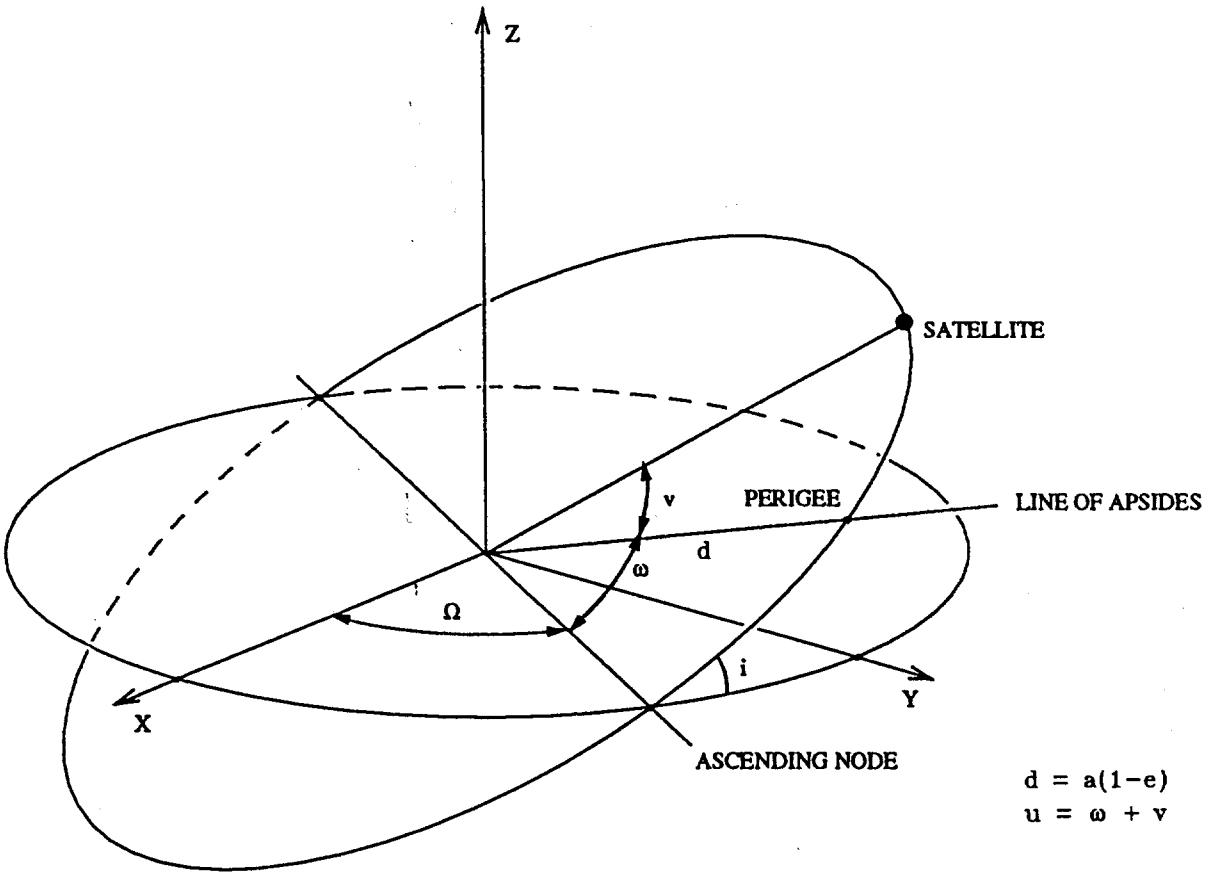

Figure 4.1
The Keplerian Elements

The formulae to compute the initial values $\mathbf{r}_0$ and $\dot{\mathbf{r}}_0$ from the osculating elements and vice versa are listed in Appendices A.1 and A.2.

If we know the parameters q_i (i=1,2,...,6), and thus the right-hand side of (4.2) or (4.3), and all force model parameters p_i (i=1,2,...,n) the satellite orbit is uniquely defined and can be computed using numerical integration techniques.

Coming back to the equation of motion (4.1) we can write

$$\ddot{\mathbf{r}} = - \frac{G \cdot M_E}{|\mathbf{r}|^3} \cdot \mathbf{r} + \mathbf{a} \qquad (4.7)$$

where the first term represents the central force and

- G : Gravity constant
- M_E : Mass of the earth
- $\mathbf{a}$: Acceleration vector due to perturbations

The perturbing acceleration a is composed of

$$\mathbf{a} = \mathbf{a}_{NS} + \mathbf{a}_{MS} + \mathbf{a}_{ET} + \mathbf{a}_{RP} + \mathbf{a}_1 \qquad (4.8)$$

Perturbing Force	Acceleration (m/sec^2)	Orbit Error (m) After 1 Day
Central term of the earth's gravity field	0.59	∞
Earth's oblateness (C_{20})	$5 \cdot 10^{-5}$	10'000
Non-sphericity of the earth (excluding C_{20})	$3 \cdot 10^{-7}$	200
Attraction by the moon	$5 \cdot 10^{-6}$	3'000
Attraction by the sun	$2 \cdot 10^{-6}$	800
Earth's tidal potential	$1 \cdot 10^{-9}$	0.3
Ocean tides	$5 \cdot 10^{-10}$	0.04
Direct solar radiation pressure	$6 \cdot 10^{-8}$	200
Y-bias effect	$5 \cdot 10^{-10}$	1.4
Albedo	$4 \cdot 10^{-10}$	0.03
Relativistic effects	$3 \cdot 10^{-10}$	?

Table 4.1
Effect of Perturbing Forces on GPS Satellites
(from [Landau, 1988])

where the various accelerations are due to:

NS : Non-sphericity of the earth potential
MS : Third body effects of the moon and the sun
ET : Earth's tidal potential
RP : Solar radiation pressure

and a_1 denotes the sum of all the small accelerations ($< 10^{-9}$ m/sec^2) listed in section 4.1.6 that are not taken into account in our orbit model. The other terms will be discussed in the next sections. Table 4.1 summarizes the order of magnitude of the various perturbing forces.

4.1.2 Non-Central Part of the Earth Gravitational Potential

The most important perturbation of the elliptic motion of a satellite is caused by the non-sphericity of the earth's gravity field.
The non-spherical part, V_{NS}, of the earth gravity potential is usually represented by a spherical harmonic expansion in a geocentric earth-fixed system:

$$V_{NS} = \frac{G \cdot M_E}{r} \sum_{n=2}^{\infty} \left(\frac{a_E}{r} \right)^n \sum_{m=0}^{n} P_{nm}(\sin\phi) \cdot [S_{nm} \cdot \sin(m\lambda) + C_{nm} \cdot \cos(m\lambda)] \qquad (4.9)$$

where

G : Gravity constant
M_E : Mass of the earth
r : Geocentric satellite distance
ϕ : Geocentric latitude of the satellite
λ : Geocentric longitude of the satellite
a_E : Mean equatorial radius of the earth
P_{nm} : Associated Legendre function of degree n and order m
n : Degree of the geopotential term
m : Order of the geopotential term

C_{nm}, S_{nm} : Denormalized geopotential coefficients
(Zonal coefficients : $m = 0$
Sectorial coefficients : $m = n$
Tesseral coefficients : $n > m \neq 0$)

Terms with $n < 2$ are zero, since the origin of the earth-fixed system is defined to coincide with the earth's center of mass.

The acceleration a_{NS} in the inertial frame is then given by:

$$a_{NS} = R \cdot D \cdot VV_{NS} \tag{4.10}$$

where

VV_{NS} : Gradient of the non-spherical geopotential
D : Matrix containing the partial derivatives of the earth-fixed coordinates r, ϕ, λ with respect to geocentric x, y, z in the earth-fixed frame. The exact form of the matrix may be found in [Landau, 1988].

R is the transformation matrix from the earth-fixed into the inertial coordinate system:

$$R = P \cdot N \cdot U \cdot X \cdot Y \tag{4.11}$$

with

P : Precession matrix
N : Nutation matrix
U : UT1 transformation matrix (earth rotation)
X,Y: Polar coordinate matrices

The details of the transformation from an earth-fixed into an inertial frame will not be presented here. The transformation matrices may be found in e.g. [IAU Resolution, 1981], [IERS, 1989], or [Sovers & Border, 1987].

The largest contribution to the acceleration a_{NS} comes from the earth potential coefficient C_{20} representing the oblateness of the earth. It is e.g. responsible for the precession of the line of nodes of a satellite orbit.

Because GPS and GLONASS satellites are in high altitude orbits, they are much less affected by the short wavelength terms of the geopotential than low orbiting satellites. It is sufficient, therefore, to use an earth potential model up to degree and order 8 (81 coefficients) (see [Beutler et al., 1985], or [Swift & Gouldman, 1987]).

Due to the revolution period of almost exactly half a sidereal day (~ 11 hours 58 minutes), the GPS satellites (but not the GLONASS satellites) repeat their ground tracks daily. As a consequence there will be resonance effects, caused by tesseral and sectorial terms (see eqn. (4.9)) of the earth's gravity field. As an example Figure 4.2 shows the perturbations of the semi-major axis of a GPS satellite over 10 years [Beutler, 1992] using an earth potential model up to degree and order 4. The period is about 12 years with an amplitude of about 4 km. A drastic reduction of the long term perturbations is obtained by changing the revolution period by only 2 minutes to 12 hours (see Figure 4.3 which shows the perturbations over one year only).

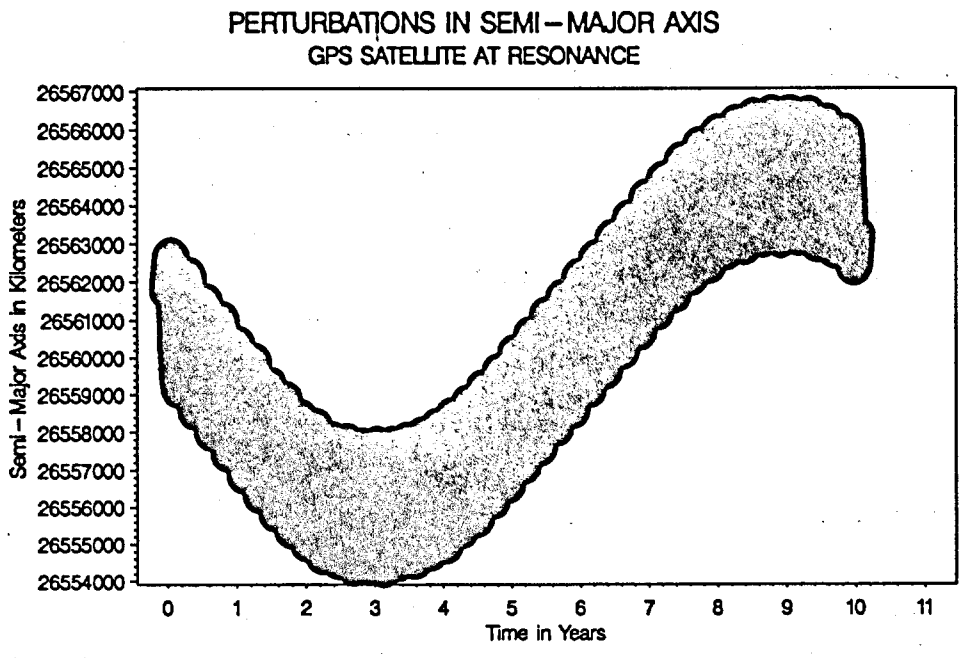

Figure 4.2
Perturbations in the Semi-Major Axis
of a GPS Satellite at Resonance Over 10 Years

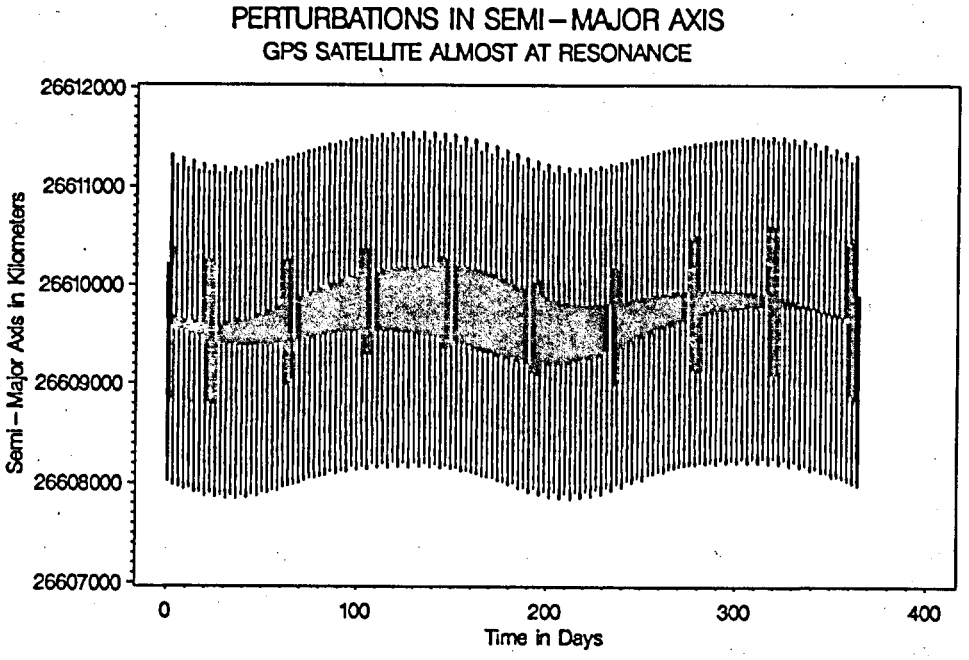

Figure 4.3
Perturbations in the Semi-Major Axis of a GPS Satellite Over one Year with a Revolution Period Changed by 2 Minutes

Today there are many different sets of earth potential coefficients available (e.g. WGS84 [White, 1986], GEM-L2 [Lerch et al., 1983], and others). The differences between these models are small, since the low order coefficients of the potential are very well known from SLR observations of low orbiting satellites. Maximum discrepancies are of the order of 2 meters after an integration over one week (see [Landau, 1988]). The models we use at present in the Bernese GPS software are the older models GEM-10 or GRIM-3L1.

4.1.3 Gravitational Effects of Sun and Moon

The gravitational perturbations due to the moon or the sun are not caused by the full gravitational attraction of these objects but only by the corresponding 'tidal' term, i.e. by the difference between the force on the satellite and that on the earth. The acceleration vector a_{MS} is given by (see [Beutler, 1982])

$$\mathbf{a}_{MS} = -G\cdot M_M\cdot\left(\frac{\mathbf{r}-\mathbf{r}_M}{|\mathbf{r}-\mathbf{r}_M|^3}+\frac{\mathbf{r}_M}{|\mathbf{r}_M|^3}\right) - G\cdot M_S\cdot\left(\frac{\mathbf{r}-\mathbf{r}_S}{|\mathbf{r}-\mathbf{r}_S|^3}+\frac{\mathbf{r}_S}{|\mathbf{r}_S|^3}\right) \tag{4.12}$$

where

$\mathbf{r}, \mathbf{r}_M, \mathbf{r}_S$: Geocentric position vectors of the satellite, the moon, and the sun respectively in the inertial frame

G : Gravity constant

M_M, M_S : Masses of the moon and the sun

For the perturbation due to the planets see section 4.1.6.

4.1.4 Solid Earth Tidal Effects

The gravitational attraction of the moon and sun also has an indirect effect on the satellite orbit due to the solid earth tides and ocean tides it causes: the tidal deformations change the earth's gravity potential which in turn has a perturbing effect on the satellite orbit.

A derivation of the acceleration $\mathbf{a}_{ET}$ due to the potential caused by the solid earth tides may be found in [Lambeck, 1974] or [Melchior, 1983] and gives the following result:

$$\mathbf{a}_{ET} = k_2\cdot\frac{G\cdot M_M}{|\mathbf{r}_M|^3}\cdot\frac{a_E^5}{|\mathbf{r}|^4}\cdot\left(P_2'(\cos z_M)\cdot\frac{\mathbf{r}}{|\mathbf{r}|}-P_3'(\cos z_M)\cdot\frac{\mathbf{r}_M}{|\mathbf{r}_M|}\right) + k_2\cdot\frac{G\cdot M_S}{|\mathbf{r}_S|^3}\cdot\frac{a_E^5}{|\mathbf{r}|^4}\cdot\left(P_2'(\cos z_S)\cdot\frac{\mathbf{r}}{|\mathbf{r}|}-P_3'(\cos z_S)\cdot\frac{\mathbf{r}_S}{|\mathbf{r}_S|}\right) \tag{4.13}$$

where

k_2 : Love number of degree 2
a_E : Mean equatorial radius of the earth

$$\cos z_M = \frac{\mathbf{r}\cdot\mathbf{r}_M}{|\mathbf{r}||\mathbf{r}_M|} \quad , \qquad \cos z_S = \frac{\mathbf{r}\cdot\mathbf{r}_S}{|\mathbf{r}||\mathbf{r}_S|} \tag{4.14}$$

and

$$P_2'(\cos z) = 3\cdot\cos z, \; P_3'(\cos z) = 3\cdot(5\cdot\cos^2 z - 1)/2 \tag{4.15}$$

The remaining quantities have been defined in eqn. (4.12).

The effect of the ocean tides on the satellite is very small (see section 4.1.6).

4.1.5 Solar Radiation Pressure

The acceleration of the satellite caused by the radiation pressure from the sun is quite large (see Table 4.1). The neglection of this effect will result in orbit errors of the order of 200 m after one day for the GPS satellites. Due to the complicated shape of active satellites (like the GPS or GLONASS satellites) the modeling of the effects of solar radiation pressure is the most difficult part in the force model. Studies of [Rizos & Stolz, 1985] show, that the GPS satellite orbits are very sensitive to the solar radiation pressure model. Since the orientation of the orbits with respect to the sun changes slowly, solar radiation also causes considerable resonance effects.

Very important is also the modeling of eclipses by the earth (or the moon) (see 4.1.5.3), whereas the indirect effects of solar radiation pressure, earth-reflected radiation pressure (albedo pressure) or thermal radiation of the satellite (see 4.1.6), are very small.

All these difficulties make it clear, that the estimation of parameters of the solar radiation pressure model (see section 4.2.1.3) is indispensable for satellite arcs longer than a day, even if detailed models are used like the ROCK4 and ROCK42 (see section 4.1.5.2).

4.1.5.1 Standard Radiation Pressure Model

The perturbating acceleration a_{RP} due to direct solar radiation pressure may be expressed as follows (see [Cappellari et al., 1976]):

$$a_{RP} = \nu \cdot \left\{ P_S \cdot C_r \cdot \frac{A}{m} \cdot a_S^2 \cdot \frac{(r-r_S)}{|r-r_S|^3} + a_Y \right\} \qquad (4.16)$$

where

- ν : Eclipse factor:
  $\nu = 0$ if the satellite is in the shadow
  $\nu = 1$ if the satellite is in the sunlight
  $0<\nu<1$ if the satellite is in the penumbra
- P_S : Radiation pressure of the sun in a distance of 1 AU (Astronomical Unit)
- C_r : Reflection coefficient depending on the reflective properties of the satellite
- A : Effective cross-section area of the satellite experiencing solar radiation pressure
- m : Mass of the satellite
- a_S : Astronomical Unit (semi-major axis of the earth's orbit around the Sun)
- r : Geocentric position vector of the satellite in the inertial frame
- r_S : Geocentric position of the sun in the inertial frame
- a_Y : Acceleration perpendicular to the incident radiation, an effect called Y-bias in the literature (see [Fliegel et al., 1985]).

Numerical values for the quantities C_r, A, and m for GPS Block I satellites may be found in [Fliegel et al., 1985]. For details on the solar radiation pressure P_s see [Willson, 1978] or [Wakker et al., 1983].

The Y-bias is an acceleration component in the direction of the y-axis in a satellite fixed coordinate system (see Figure 4.4) caused probably by the misalignment of the solar panels and the asymmetric thermal radiation (preferably in the direction of the y-axis = axes of the solar panels) [Fliegel et al., 1985]. It is usually introduced as a constant or estimated (as a constant or stochastically, see [Swift et al., 1988]).

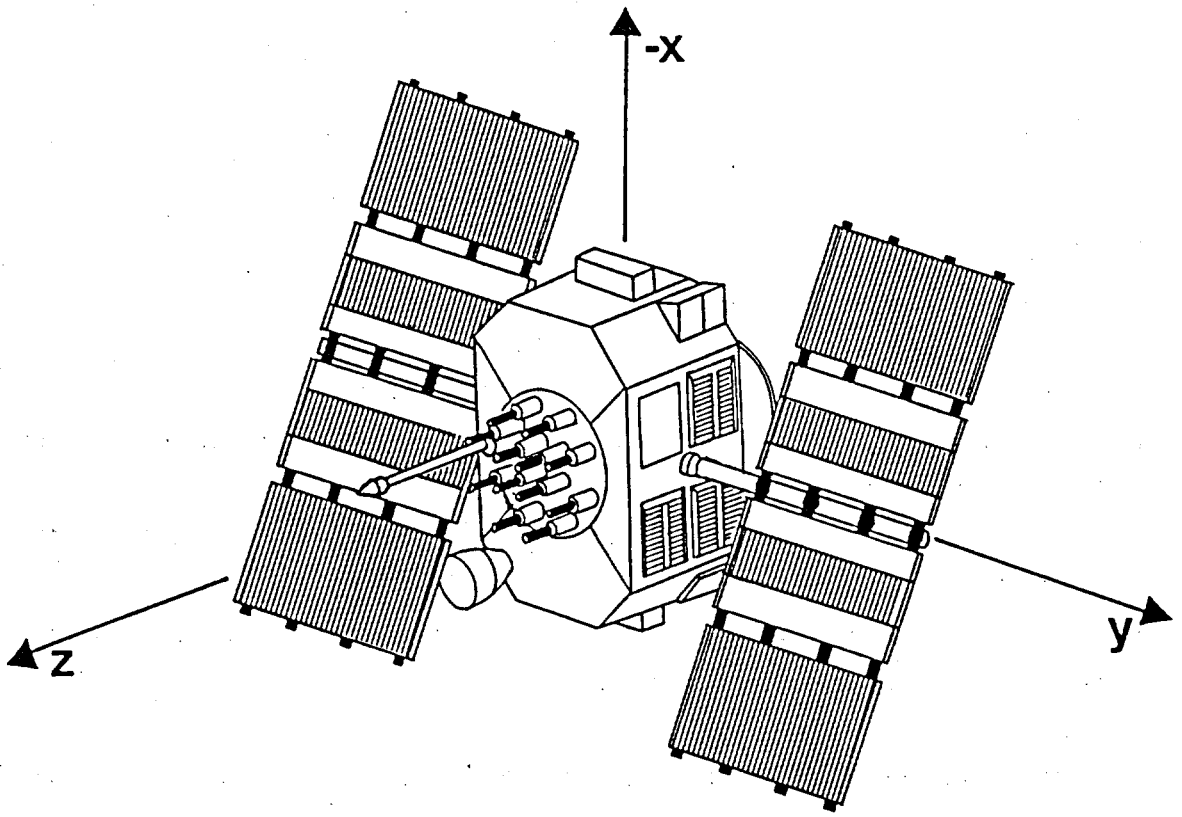

Figur 4.4
The Satellite Fixed Coordinate System

Apart from the Y-bias there are a few other uncertainties in the model given by eqn. (4.16):

- The solar radiation pressure is not constant (variations of about 7 % over a year)

- the surface of a GPS or GLONASS satellite consists of many different parts with different reflective properties. It is therefore a coarse simplification to use a single value for the quantities C_r and A.

- shadowing due to the antennas and the satellite body are ignored.

The solar radiation pressure model we use in our software has the same form as equation (4.16):

$$a_{RP} = \nu \cdot \{-p_0 \cdot e_0 + p_2 \cdot e_2\} \tag{4.17}$$

where

$$e_0 = \frac{r_S - r}{|r_S - r|} \quad , \qquad e_2 = \frac{r \times e_0}{|r \times e_0|} \tag{4.18}$$

Comparing eqn. (4.17) with eqn. (4.16) we see that the direct radiation pressure parameter p_0 is given by (neglecting the intensity variation due to the motion of the earth (and the satellite)):

$$p_0 = P_S \cdot C_r \cdot \frac{A}{m} \tag{4.19}$$

and the Y-bias radiation pressure parameter p_2 by

$$p_2 = |a_Y| \tag{4.20}$$

4.1.5.2 ROCK4 and ROCK42 Models

The ROCK4 and ROCK42 models, for GPS Block I and Block II satellites respectively, have originally been developed by Rockwell International (see [Porter, 1976] and [Fliegel et al., 1985] for Block I, [Abramson, 1982] and [Fliegel & Gallini, 1989] for Block II satellites) and have become the standard radiation pressure models for the GPS satellites. They depict the satellites as a

number of flat or cylindrical surfaces, each having its own reflectivity and specularity characteristics. Shadowing is taken into account. The original ROCK4 and ROCK42 models are rather complex. Simpler models may be found in [Fliegel & Gallini, 1989] or [Feltens, 1988].

4.1.5.3 Eclipses

The GPS satellites are, due to their high altitude, almost permanently in the sunlight. Eclipses by the earth happen about twice per year. During these eclipse periods of a few days the satellite is periodically eclipsed by the earth [Colombo, 1986]. [Swift et al., 1990] have shown that the orbit estimation of satellites being eclipsed are considerably degraded, because of the difficulties to model the eclipses, especially the penumbra.

The shadow factor ν in eqns. (4.16) and (4.17) is computed in our software using a simple cylinder model for the shadow of the earth (see Figure 4.5):

$$\nu = \begin{cases} 0 \quad \text{if} \quad \cos\gamma = \dfrac{\mathbf{r}\cdot\mathbf{r}_S}{|\mathbf{r}||\mathbf{r}_S|} < 0 \text{ and} \\ \qquad\qquad h = |\mathbf{r}|\sqrt{1-\cos^2\gamma} < a_E \\ 1 \quad \text{else} \end{cases} \tag{4.21}$$

where

$\mathbf{r}$: Geocentric position vector of the satellite
$\mathbf{r}_S$: Geocentric position vector of the sun
a_E : Equatorial radius of the earth

A more elaborate shadow model has been described by [Landau, 1988].

To avoid numerical problems attention has to be paid to the step size of the numerical integration, when a satellite enters and exits the earth's shadow.

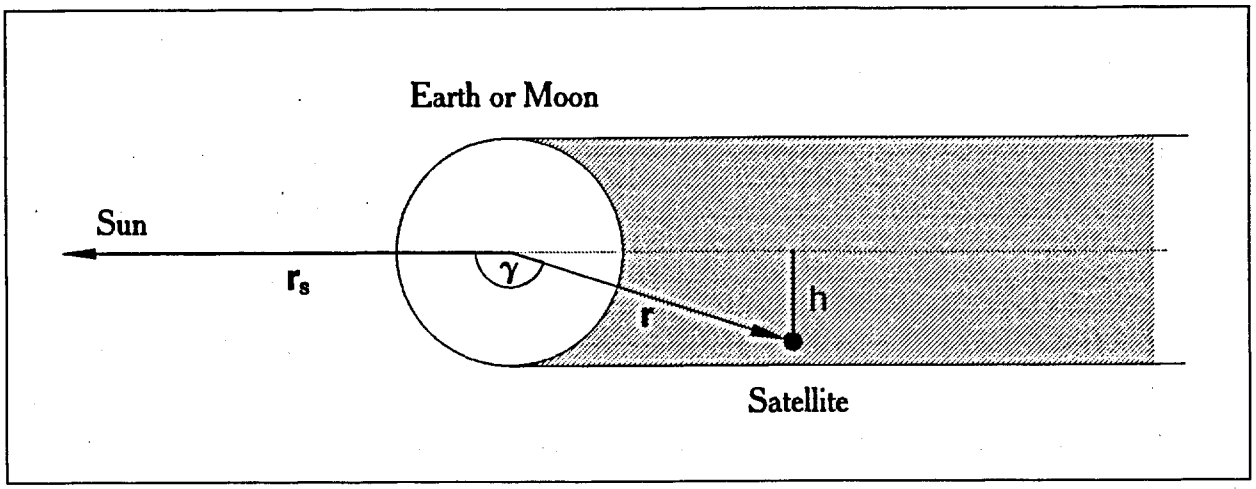

Figure 4.5
Simple Cylinder Model for the Shadow of the Earth

With an increasing number of satellites in orbit the probability that one of the satellites goes through a series of eclipses increases, too. Because of the difficulties to model the eclipses systematical effects will remain in the orbit of a satellite being eclipsed by the earth. A way out of this problem might be the estimation of "eclipse" parameters as e.g. the estimation of one constant acceleration (in the direction to the sun) for the duration of the eclipse.

4.1.6 Other Perturbations

There are a few small effects that are not modeled in the present version of our software. They result in accelerations of about 10^{-9} m/sec^2 or below (see also Table 4.1):

(1) Albedo radiation pressure
(2) Gravitational effects of ocean tides

(3) Gravitational effects of the planets
(4) Relativistic corrections
(5) Thermal emission of the satellite
(6) Drag

Albedo radiation pressure:

The earth and its atmosphere reflect a large portion of the received solar radiation back into space. The radiation pressure on the satellite due to the albedo of the earth is very difficult to model (distribution of land, ocean, and clouds) and is about 1-2 % of the direct solar radiation pressure at the altitude of GPS satellites (see [Rizos & Stolz, 1985]). The magnitude of the perturbing acceleration is approximately $4 \cdot 10^{-10}$ (see [Landau, 1988]).

Gravitational effects of ocean tides:

The gravitational effects of the ocean tides, too, are difficult to model (see [Milani et al., 1987]), since the ocean waves caused by the moon and the sun cannot propagate frictionless and also interact with the sea floor (shallow waters). The resulting acceleration of a GPS satellite is of the order of $5 \cdot 10^{-10}$ [Landau, 1988].

Gravitational effects of the planets:

The forces acting on the satellite due to the gravitational attraction of the planets may in principle be computed in the same way as the forces due to the Moon and the Sun. Venus provides the largest contribution, but the total effect of all planets is only about 30 cm for an orbit arc of one week (see [Landau & Hagmaier, 1986]).

Relativistic corrections:

The general relativistic perturbation due to the gravity field of the earth may be found in [Zhu et al., 1987]. The resulting acceleration amounts to about $3 \cdot 10^{-10}$ m/sec^2 for satellites at the altitude of GPS satellites and is well below the size of other remaining unmodeled effects.

Thermal emission of the satellite:

A part of the energy absorbed by the satellite is re-radiated as heat. This thermal re-radiation is not taken into account in the standard versions of the ROCK4 and ROCK42 models of solar radiation pressure (see section 4.1.5.2). [Fliegel & Gallini, 1989] have given corrections to the ROCK42 model (for Block II satellites) that include the effect of re-radiated heat.

Drag:

A satellite not too far from the earth's surface experiences a drag due to the interaction with the particles of the atmosphere. Since the GPS and GLONASS satellites are orbiting at a high altitude the effects of drag can be neglected. In the near future, however, low orbiting satellites will carry GPS receivers and for these satellites orbit determination will have to be done including atmospheric drag modeling. For a detailed presentation of this subject see e.g. [King-Hele, 1964].

4.1.7 Attitude Control and Orbital Manoeuvres

The GPS satellites are oriented in space so that the antennas transmitting the GPS signals always point towards the center of the earth. The satellites are therefore rotating about an axis perpendicular to the orbital plane once per revolution. Due to disturbing forces exerting torques on the satellite, however, the antennas will not remain correctly oriented towards the earth

without active control mechanisms. Each satellite is therefore equipped with four momentum wheels and with small hydrazine thrusters. By expelling mass the thrusters produce torques on the satellite that are compensated by the acceleration of the momentum wheels. At some time these wheels will reach their maximum speed and they must be unloaded by firing the thrusters. This operation is called a **momentum dump** and can occur as frequently as once a week. The time of the most recent momentum dump is given in the satellite broadcast messages (in the TLM word).

Due to the action of perturbative forces on the individual satellite orbits the constellation of the GPS satellites is not stable. Especially the fact that GPS satellites have a revolution period of almost exactly half a sidereal day, leads to resonance phenomena caused by the tesseral and sectorial terms of the earth's gravity field (see section 4.1.2) and by solar radiation pressure.

It is clear, therefore, that in order to maintain a certain satellite configuration, satellite manoeuvres (so-called station keeping) have to be performed from time to time by firing the thrusters. Such manoeuvres are announced by the U.S. Coast Guard.

Large changes in the relative positions of satellites within a particular orbital plane are known as **delta-V** manoeuvres. Such a manoeuvre took place in 1986/1987 to move satellite PRN 3 from a position ahead of satellite PRN 8 to a position behind satellite PRN 13 (all in the same orbital plane). The thrusters were fired on October 29, 1986, to increase the semi-major axis of the orbit from about 26'560 km to 26'584 km. On May 13, 1987, the thrusters were fired a second time to change the semi-major axis back to its previous value. Figure 4.6 shows the changes in the mean motion of satellite PRN 3 during the manoeuvre. The entire repositioning process took more than six months.

It is obvious that all these adjustments of the orientation and position of a satellite (apart from the problems of modeling radiation pressure) make it more or less impossible to model GPS orbits accurately (10 cm or better) over a period longer than a

few days. Although [Lichten et al., 1989b] were able to model a manoeuvre of satellite 4 (November 1985) by estimating the three components of an instantaneous velocity change and a time of burn interval (the solution converged after three iterations), the strength of the future satellite constellation and the degree of automation needed in the production of GPS satellite ephemeris will rather call for a very flexible definition of satellite arcs by automatically setting up a new set of orbital parameters whenever a change in a satellite orbit occurs that is difficult to model. The loss of mass during a manoeuvre changes the area to mass ratio of the satellite and thus the radiation pressure coefficients (see section 4.1.5.1). New radiation pressure parameters should therefore be estimated after such an event (not only new initial values).

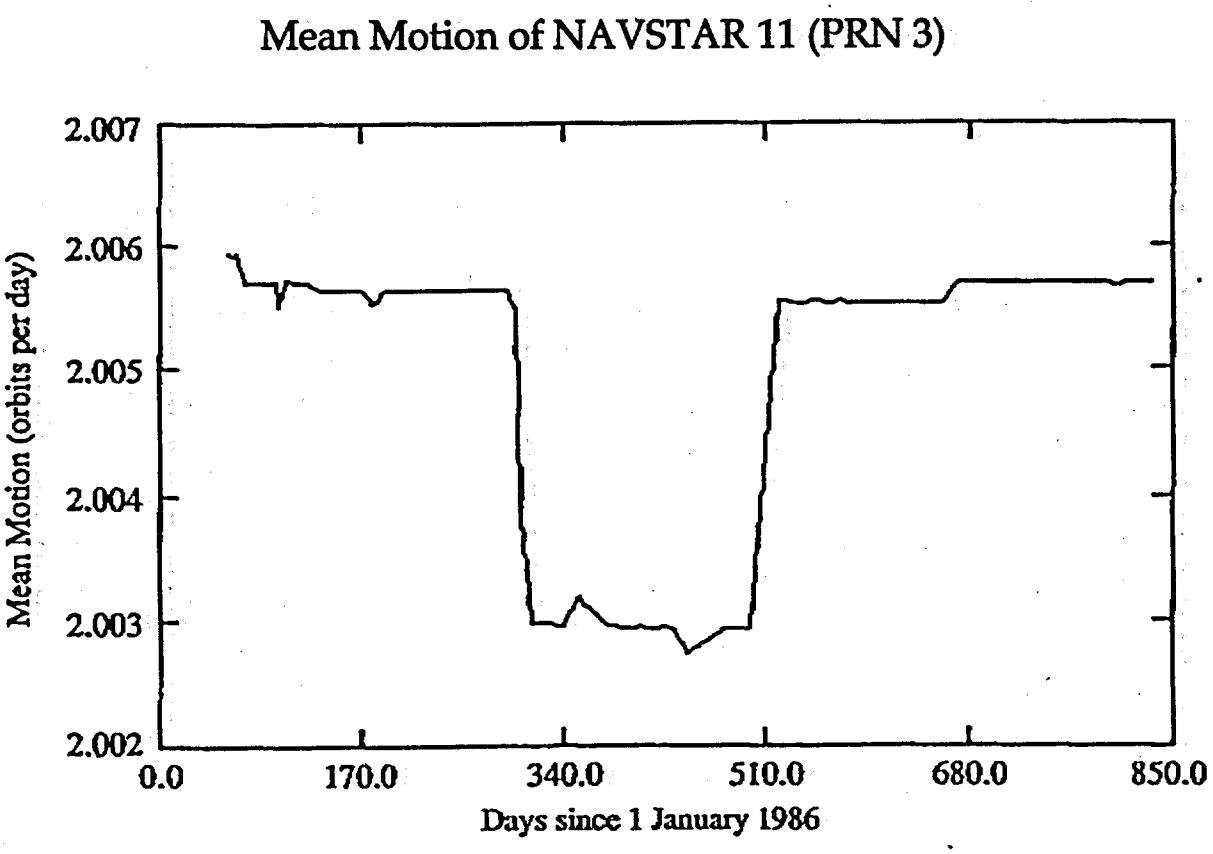

Figure 4.6
Delta-V Manoeuvre of Satellite PRN 3
Lasting From October 29, 1986 to May 13, 1987

Leakages of the thrusters' valves may slightly change the satellite velocity even in the absence of manoeuvres (see [Milani et al., 1987]).

4.2 Estimation of Satellite Orbits

4.2.1 Orbit Determination

4.2.1.1 Statement of the Problem

In section 4.1.1 the equations of motion (eqn. (4.1)) of the satellite have been given together with the parameters p_i (i=1,...,n) and q_i (i=1,...,6) needed to define a unique (particular) solution of the differential equation system (4.1). In the previous sections following section 4.1.1 the details of the force model have been discussed giving us the right-hand side of eqn. (4.1).

The problem of orbit determination may now be stated as follows:

(1) Orbit determination in its usual, more restricted, sense is defined as the problem of determining the six parameters q_i (i=1,2,...,6) defining the initial or boundary values on the right-hand side of eqns. (4.2) or (4.3).

(2) Orbit determination in its most general sense is the problem of determining the six parameters q_i (i=1,2,...,6) defining the initial or boundary values and the dynamical parameters p_i (i=1,2,...,n).

In the case of GPS or GLONASS orbits most of the dynamical parameters p_i in eqn. (4.1) may be assumed known (earth potential coefficients, Love numbers for solid earth tides ...). The dynamical parameters describing the solar radiation pressure model will have to be estimated, however, to obtain high accuracy orbits.

4.2.1.2 Observations

For actual orbit determination we need **observations.** Although in principle any type of measurement containing information about the satellite orbit could be used for orbit determination, we will only deal with two types of observations:

(1) Geocentric satellite positions (computed e.g. from osculating elements given in the satellite messages) as fictitious observations to obtain a solution of the equation of motion to be used later as an a priori orbit for orbit improvement.

(2) Double difference GPS carrier phase and, optionally, code observations in the real data processing.

The GPS measurements have been introduced in section 2.3.4, the observation equations, relating the observation to the parameters of interest, and the definition of double differences have been stated in section 3.1.

4.2.1.3 Principles of Orbit Determination

In our case orbit determination is always an **orbit improvement process** using observations of the kind mentioned in the last section. These observations are non-linear functions of the satellite position $\mathbf{r}(t)$, the satellite velocity $\dot{\mathbf{r}}(t)$, and possibly some dynamical parameters p_i $(i=1,2,\ldots,n)$. The satellite position $\mathbf{r}(t)$ in turn is a non-linear function of the parameters q_i $(i=1,2,\ldots,6)$ and also the dynamical parameters p_i $(i=1,2,\ldots,n)$. The (necessary) linearization of the observation equations may therefore be done in two steps:

(1) Approximation of the observation as a linear function of the satellite position $\mathbf{r}$ and possibly the dynamical parameters p_i.

(2) Representation of the satellite position $\mathbf{r}(t)$ as a linear function of the parameters q_i $(i=1,2,\ldots,6)$ defining the

initial or boundary values and the dynamical parameters p_i $(i=1,2,\ldots,n)$.

Due to these linearizations we have to determine our orbit iteratively, where in each iteration step we have to assume that we have a known approximate orbit $\mathbf{r}^a(t)$ at our disposal. This approximate orbit may be obtained by numerical integration (or with analytical methods) starting with approximate values for q_i^a $(i=1,2,\ldots,6)$ and for p_i^a $(i=1,\ldots,n)$:

$$\ddot{\mathbf{r}}^a(t) = \mathbf{f}(t;\mathbf{r}^a,\dot{\mathbf{r}}^a;p_1^a,\ldots,p_n^a) \tag{4.22}$$

and

$$\begin{aligned} \mathbf{r}^a(t_0) &= \mathbf{r}_0(q_1^a,q_2^a,\ldots,q_6^a) \\ \dot{\mathbf{r}}^a(t_0) &= \dot{\mathbf{r}}_0(q_1^a,q_2^a,\ldots,q_6^a) \end{aligned} \tag{4.23}$$

The linearization step (1) above takes on the following form for an observation O (where we assume that O does not depend on satellite velocities):

$$O(t;\mathbf{r}(t),p_1,\ldots,p_n) := O(t,\mathbf{r}^a(t),p_1^a,p_2^a,\ldots,p_n^a) + \sum_{j=1}^{3} \frac{\partial O}{\partial r_j}\Big|_{r=r^a} \cdot \Delta r_j + \sum_{i=1}^{n} \frac{\partial O}{\partial p_i}\Big|_{p=p^a} \cdot \Delta p_i \tag{4.24}$$

where $\mathbf{r}^T = (r_1,r_2,r_3)$, $\mathbf{r}^{aT} = (r_1^a,r_2^a,r_3^a)$

and

$$\begin{aligned} \Delta r_j &= (r_j - r_j^a) \qquad (j=1,2,3) \\ \Delta p_i &= (p_i - p_i^a) \qquad (i=1,2,\ldots,n) \end{aligned} \tag{4.25}$$

The second linearization (2) results in

$$\mathbf{r}(t) = \mathbf{r}^a(t) + \sum_{i=1}^{6} \mathbf{z}_{q_i}(t)\cdot\Delta q_i + \sum_{i=1}^{n} \mathbf{z}_{p_i}(t)\cdot\Delta p_i \tag{4.26}$$

where

$$\mathbf{z}_{q_i}(t) = \left.\frac{\partial \mathbf{r}}{\partial q_i}\right|_{q=q^a,\,p=p^a} \qquad (i=1,2,3) \tag{4.27}$$

$$\mathbf{z}_{p_i}(t) = \left.\frac{\partial \mathbf{r}}{\partial p_i}\right|_{q=q^a,\,p=p^a} \qquad (i=1,2,3\ldots,n) \tag{4.28}$$

The functions $\mathbf{z}_{q_i}(t)$ and $\mathbf{z}_{p_i}(t)$ are solutions of the initial (or boundary) value problems we obtain from the primary problem (defined by eqns. (4.22) and (4.23)) by taking the total derivative of the equations (4.22) and (4.23) with respect to the parameters q_i (i=1,2,...,6) and p_i (i=1,2,...,n) respectively. The resulting set of differential equations are usually called the **variational equations:**

$$\ddot{\mathbf{z}}_{q_i} = \mathbf{A}_0\cdot\mathbf{z}_{q_i} + \mathbf{A}_1\cdot\dot{\mathbf{z}}_{q_i} \tag{4.29}$$

with the initial values:

$$\mathbf{z}_{q_i}(t_0) = \frac{\partial \mathbf{r}_0^a}{\partial q_i}\,, \qquad \dot{\mathbf{z}}_{q_i}(t_0) = \frac{\partial \dot{\mathbf{r}}_0^a}{\partial q_i} \tag{4.30}$$

and

$$\ddot{\mathbf{z}}_{p_i} = \mathbf{A}_0\cdot\mathbf{z}_{p_i} + \mathbf{A}_1\cdot\dot{\mathbf{z}}_{p_i} + \frac{\partial \mathbf{f}}{\partial p_i} \tag{4.31}$$

$$\mathbf{z}_{p_i}(t_0) = \mathbf{0}\,, \qquad \dot{\mathbf{z}}_{p_i}(t_0) = \mathbf{0} \tag{4.32}$$

The elements $A_{0,ik}$ and $A_{1,ik}$ of the 3×3 matrices A_0 and A_1 respectively are defined by:

$$A_{0,ik} = \frac{\partial f_i}{\partial r_k}\bigg|_{q=q^a,\,p=p^a}, \qquad A_{1,ik} = \frac{\partial f_i}{\partial \dot{r}_k}\bigg|_{q=q^a,\,p=p^a} \tag{4.33}$$

where $f^T = (f_1, f_2, f_3)$.

For GPS or GLONASS satellites, where no significant velocity-dependent accelerations are present (like e.g. atmospheric drag), we have

$$A_{1,ik} = 0 \quad (i=1,2,3;k=1,2,3) \tag{4.34}$$

Formulae for the elements $A_{0,ik}$ are given in e.g. [Beutler, 1982] or [Landau, 1988].

The differential equation systems (4.29) and (4.31) are linear and the systems (4.29) are even homogeneous.

All this means, that in each iteration step of the orbit improvement process we have to solve one system of nonlinear differential equations (the primary system given by eqns. (4.22) and (4.23)), six linear systems of type (4.29), plus n systems of type (4.31).

The rest of the orbit improvement process is given by the well-known formulae of the least squares adjustment, or by stochastic filter algorithms (see e.g. [Lichten et al., 1989b]).

4.2.1.4 Choice of Parameters

Let us start with the parameters q_i (i=1,2,...,6) defining the initial (or boundary) value problem given by eqns. (4.1) and (4.2) or (4.3). Possible choices of these parameters have been listed in section 4.1.1, eqns. (4.4) to (4.6). The most commom choice is certainly the selection of the initial values r_0 and $\dot{r}_0$ as parameters q_i (i=1,...,6) according to eqn. (4.4). In this case

the computation of the partial derivatives (4.27) is straight forward (usually with numerical integration).

In the orbit improvement process we use the osculation Keplerian elements (4.6) as parameters q_i (i=1,2,...,6). Because for almost circular orbits the perigee passing time t_p is highly correlated with the argument of perigee ω, the argument of latitude $u_0 = \omega + v_0$ (v_0 = true anomaly at epoch t_0) (see Figure 4.1 and Appendix A.1) was chosen as sixth parameter instead of t_p. With this selection of parameters the partials in eqn. (4.27) are the partials of the satellite position with respect to the orbital elements. These partials have the advantage that they can be computed **analytically** by using the Keplerian approximation:

$$\begin{aligned} a(t) &= a(t_0) = a_0 \\ e(t) &= e(t_0) = e_0 \\ i(t) &= i(t_0) = i_0 \\ \Omega(t) &= \Omega(t_0) = \Omega_0 \\ \omega(t) &= \omega(t_0) = \omega_0 \\ u(t) &= u(t;a_0,e_0,\omega_0) \end{aligned} \qquad (4.35)$$

The formulae to compute the partials are listed in Appendix A.3.

Some advantages of using osculating elements as parameters should be recalled:

a) Since the Keplerian approximation is good enough to compute the partials in (4.27) for satellite arcs of a few days, we can save the time-consumptive numerical integration of the six variational equations of type (4.29) and no tables are needed containing the solutions of these differential equation systems.

b) We have the possibility to estimate a subset of the six osculating elements. This is useful when processing the GPS data of regional networks (100 to 500 km), where no fiducial sites are available. Orbit improvement in a limited way is then still possible to reduce the influence of orbit errors (orbit relaxation, see e.g. [Beutler et al., 1987b]).

c) More realistic a priori constraints may be introduced than in the case of the initial values as parameters. A smaller constraint may e.g. be put on the argument of latitude u_0 knowing that in general the along track component of an orbit is the most uncertain to predict.

More details on the topic "numerical versus analytical methods" are given in [Beutler et al., 1984].

We thus combine numerical and analytical methods, trying to make use of the advantages of both methods:

(1) We solve the primary problem given by eqns. (4.1) and (4.2) or (4.3) by rigorous numerical integration starting with initial values defined by the osculating elements at epoch t_0 (see eqn. (4.6)) and using a force model as complex as necessary.

(2) Approximate partials of the satellite orbit with respect to the osculating elements are computed using a very simple analytical approximation of the orbit, the Keplerian approximation (4.35) in our case. Although this procedure may reduce the convergence speed of the orbit improvement process, it does not affect the final results.

(3) The partials of the orbit with respect to the dynamical parameters p_i (i=1,2,...,n) are, at present, computed by numerical integration together with (1).

The most important dynamical parameters for GPS or GLONASS orbits are those concerning the radiation pressure model. The two radiation pressure coefficients p_0 and p_2 used in our software are defined by the model given in 4.1.5.1, eqn. (4.17). They are estimated as constants over one satellite arc. (Other groups e.g. [Lichten et al., 1989b] use stochastic processes to model radiation pressure.)

Although the differential equation systems of type (4.31) for the partials with respect to dynamical parameters are solved by numerical integration, these systems could in principle be solved analytically using appropriate formulae of perturbation theory.

Other dynamical parameters that might be determined using GPS (or GLONASS) observations are parameters concerning satellite eclipses (see 4.1.5.3).

4.2.2 Numerical Integration

Since numerical integration is an important part in the orbit determination process a short introduction into the principles of numerical integration is given here.

It is our understanding that numerical integration is a part of approximation theory, where the "true" solution r(t) of the eqns. (4.1) and (4.2) or (4.3) is approximated in a certain time interval Δt by a polynomial $r^*(t)$ of degree q (other sets of base functions might also be used):

$$r^*(t) = \sum_{i=0}^{q} a_i \cdot (t - t_0)^i \qquad (4.36)$$

where

a_i : Column matrices of polynomial fit
t_0 : Origin of development

t_0 may be chosen arbitrarily. In the case of an initial value problem, it will be chosen to coincide with the epoch of the initial values.

The problem of numerical integration now consists of the determination of the polynomial coefficients a_i (i=0,1,...,q). This is done by setting up the following conditions:

(1) The approximating function $\mathbf{r}^*(t)$ has to satisfy the initial conditions (4.2) or the boundary conditions (4.3). From this we get two linear (vectorial) condition equations for the unknowns $\mathbf{a}_i$ $(i=0,1,\ldots,q)$.

(2) The approximating function $\mathbf{r}^*(t)$ is then asked to satisfy eqn. (4.1) at q-1 different time arguments t_j $(j=1,2,\ldots,q-1)$ in the integration interval Δt. This gives us together with (1) a total of (q+1) independent algebraic equations for the (q+1) unknowns $\mathbf{a}_i$ $(i=0,1,\ldots,q)$.

The solution of a system of differential equations has thus been reduced to the solution of a system of nonlinear algebraic equations. It can be shown that most of the classical methods are actually special approaches to solve this nonlinear algebraic system. In our case this system is solved by an iterative process, starting with approximate values for the coefficients $\mathbf{a}_i$ that are then successively improved.

If a satellite orbit has to be integrated over a long time period, the entire time interval is subdivided into smaller intervals. A set of coefficients $\mathbf{a}_i$ $(i=0,1,\ldots,q)$ is then determined for each subinterval where at the interval boundaries the satellite position and velocity are required to be continuous functions in time.

The result of this procedure is **not** an ephemeris table of satellite coordinates, but one or more sets of coefficients $\mathbf{a}_i$ $(i=0,1,\ldots,q)$, which enable us to compute $\mathbf{r}^*(t)$ or any of its derivatives for any time in the integration interval Δt.

More details on the numerical integration method outlined here may be found in [Beutler, 1990].

In practice we normally use a polynomial degree of q=10 and an integration interval of 1 hour for the numerical integration of GPS satellite orbits. An orbit piece of one hour is then represented by one set of polynomial coefficients $(3\cdot(q+1) = 33$ numbers per satellite and hour for q=10).

4.3 The Orbits in the Bernese GPS Software

For the understanding of the following chapters it is important to give a short overview of the orbit part of the Bernese GPS Software, more information may be found in [Rothacher et al., 1991].

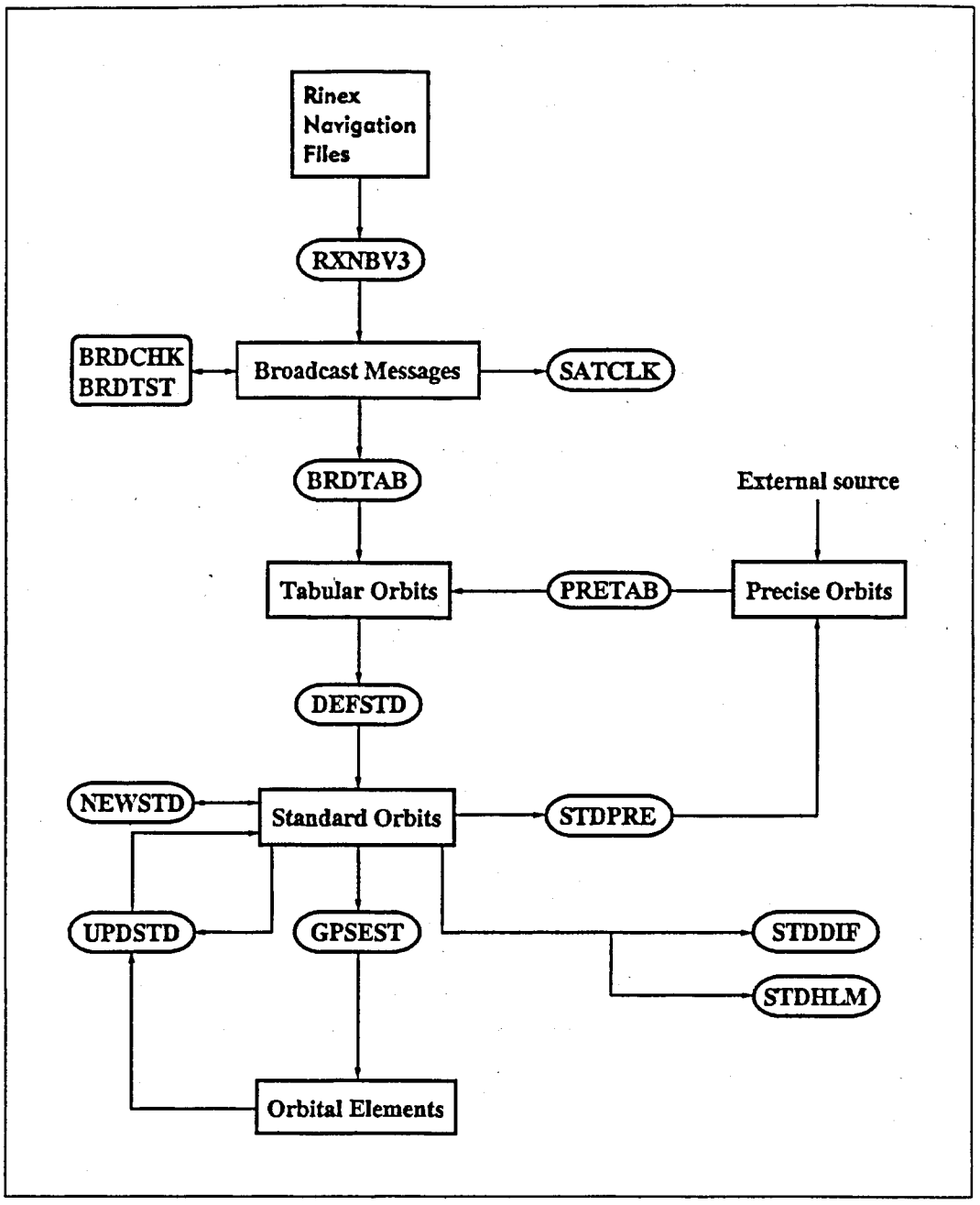

Figure 4.7
Functional Flow Diagram of the Orbit Part of the Bernese GPS Software

The functional flow diagram of the orbit part of the software is given in Figure 4.7 and shows the interactions between the different orbit programs and orbit data files.

Orbit information may be imported into the software either in the form of RINEX Navigation Files (RINEX: Receiver Independent Exchange format, see [Gurtner & Mader, 1990a]) containing the broadcast elements and satellite clock coefficients (see section 2.3.4) or in the form of precise orbit files (tabulated satellite positions) as defined by [Remondi, 1985] or [Remondi, 1989].

RXNBV3, BRDCHK, BRDTST, and SATCLK:

As a first step the RINEX navigation files are transferred into Bernese broadcast files using the program RXNBV3. The broadcast messages of all the satellites are then checked for consistency (BRDCHK or BRDTST). Scrambled messages are removed and satellite manoeuvres are detected (drastic changes in the orbital elements). The satellite clock information may be extracted from the broadcast message files with the program SATCLK for later use (of importance in the case of asynchronously sampling receiver types).

BRDTAB and PRETAB:

The programs BRDTAB and PRETAB both generate tabular orbit files containing tabulated satellite positions in the inertial frame 1950.0. BRDTAB computes these satellite positions from the orbital elements given in the broadcast message files. PRETAB obtains them transforming the precise orbit positions into the inertial frame 1950.0.

DEFSTD:

The program DEFSTD (definition of Bernese standard orbits) is, apart from the main parameter estimation program GPSEST, the most important program dealing with satellite orbits.

In DEFSTD an orbit improvement process is performed exactly as described in section 4.2.1.3. The observations (pseudo-observations in this case) are the tabulated satellite positions in the inertial frame 1950.0 obtained from the broadcast elements or the precise orbit positions. Using the methods of least squares orbital parameters are estimated fitting the tabulated positions as accurately as possible (in the least squares sense).

At the beginning of the program two satellite positions $\mathbf{r}_1$ and $\mathbf{r}_2$ at times t_1 and t_2 (about 20-60 minutes apart) are used to solve the boundary value problem defined by eqns. (4.1) and (4.3). This is done with the integration method outlined in section 4.2.2. With the resulting initial values a first approximate orbit $\mathbf{r}^a(t)$ is then computed by numerical integration to be used as a priori orbit in the improvement process (see 4.2.1.3).

The parameters to be improved are the osculating Keplerian elements (see Figure 4.1) and, depending on the length of the satellite arc, zero, one, or two radiation pressure parameters (p_0 and p_2) as defined by eqn. (4.17). In each iteration step the satellite positions and the partials with respect to the radiation pressure parameters are obtained by the numerical integration technique outlined in 4.2.2 using the force model presented in section 4.1. The result of the last iteration (integration) is stored in a Bernese standard orbit file (satellite position coefficients) and a radiation pressure coefficient file (radiation pressure partials). The partials with respect to the osculating Keplerian elements are computed later in GPSEST, using analytical formulae (see section 4.2.1.4).

Several arcs per satellite may be computed and stored in one standard orbit file.

When processing GPS data of a small network no further orbit computations have to be done after running program DEFSTD. The standard orbit resulting from the orbit determination is accurate enough (of the quality of broadcast or precise orbits respectively (see 3.2.1.2), but more consistent) and may be used in other programs to compute the satellite positions.

For a regional network, however, the satellite orbits have to be improved using the GPS data. This actual improvement is done with the program GPSEST.

GPSEST:

GPSEST is the main data processing program of the Bernese GPS Software. It may estimate a variety of parameters:

- Initial carrier phase ambiguities (see 3.1.2)
- Site coordinates
- Orbit parameters
- Troposphere zenith delays
- Parameters of a local troposphere model
- Ionosphere model parameters

  and others.

The estimation of these parameters is done by the method of least squares using phase and/or code double difference observations (see 3.1.4). For dual frequency receivers all the linear combinations given in section 3.1.3 may be processed, even in the same program run. In the estimation process observations may be used from one baseline, one session, one campaign, or even several campaigns.

Let us focus on the estimation of orbit parameters:
As in DEFSTD (see above) the osculating Keplerian elements, the direct radiation pressure scaling, and the y-bias may be estimated. Any combination of these parameters may be determined and a priori constraints may be introduced for each parameter. Some of

the advantages of the osculating elements as unknowns have been put forward in 4.2.1.4.

The orbital parameters resulting from the orbit improvement porcess in GPSEST are saved in an orbital element file.

UPDSTD:

GPSEST "only" computes the improvements to the orbital parameters, but does not produce any new, improved standard orbit file. (There is no iteration process, including the numerical integration of the orbit and the partials, in GPSEST.) The actual orbit update, the generation of an improved standard orbit file, has to be done with the program UPDSTD. This program takes as input the improved orbital parameters (osculating Keplerian elements plus radiation pressure parameters stored in a orbital element file by GPSEST) and the standard orbit file that was used in GPSEST as a priori orbit information, and generates a new standard orbit file with exactly the same arc definitions as in the input standard orbit file. The updated orbit representation is obtained by a numerical integration of the equation of motion (see eqns. (4.1) and (4.2)) using the improved orbital parameters. This is done together with the integration of the partials with respect to the radiation pressure parameters (see eqns. (4.31) and (4.32)). These partials (or better the polynomial coefficients representing the partials) are stored in an updated radiation pressure coefficient file. The updated standard orbit file (and the updated radiation pressure coefficient file) may then be used in further GPSEST runs or distributed to other users in the form of precise orbits (see program STDPRE below).

NEWSTD:

We use the program NEWSTD to extrapolate orbits. This is of importance for orbit comparison (see section 6.2).

STDPRE:

To export orbital information (see section 6.4) the program STDPRE creates an ephemeris file in the precise orbit format (see program PRETAB above) starting from a Bernese standard orbit file.

STDPLT and STDHLM:

Auxiliary programs are used to compare standard orbit files. One such program is STDPLT. It computes the differences between standard orbit files in radial, along track, and out of plane directions (see section 6.1.2, Figure 6.1) and optionally the formal errors of the satellite positions, if the full variance-covariance matrix of the orbit improvement in GPSEST is available (see section 6.1.2 for more details). To compare satellite orbits given in different reference frames the program STDHLM may be used. This program is described in detail in section 6.2.4 .

5. MODELING OF THE TROPOSPHERIC REFRACTION

Tropospheric refraction, as stated in section 3.2.2, is the main accuracy limiting factor in the determination of station heights using the GPS. To get better verticals we may proceed along two different lines:

(a) Model tropospheric refraction without making use of the GPS observations.

(b) Use the GPS observations to estimate troposphere model parameters together with all the other relevant parameters.

It is clear that approach (a), if successful, will strengthen the GPS solution for the other parameters (e.g. site coordinates), since the knowledge of the troposphere is provided independently of the GPS observations. The tropospheric delays may be derived from standard troposphere models, from surface met measurements (SM) (pressure, temperature, and relative humidity at the sites), or from more complex techniques like water vapour radiometers (WVR) measuring the water vapour of the atmosphere, or meteo sondes, supplying a profile of the atmosphere.

Approach (b) is, in its uncompromising form, totally independent of any, (perhaps unreliable) meteorological data (see e.g. section 3.2.2.3). However, the estimation of troposphere parameters has its price as well: it is only reasonable, if it is possible to separate the contributions of the different parameter types (station heights, ambiguities, orbits, and troposphere) with the GPS data available. The number of satellites tracked and the session length are of great importance, therefore.

Combinations of the two approaches making use of the advantages of both, are likely to give the best results.

5.1 Troposphere Refraction Models

It is not the goal of this chapter to present a detailed analysis of all the different models of tropospheric refraction in use today. Many papers have recently been published on this subject. After a general introduction in 5.1.1 we will concentrate on one special topic: the computation of a local troposphere model from SM data.

5.1.1 General Introduction

The refraction of radio waves in the neutral (non-ionized) atmosphere produces a non-dispersive delay in the time of reception relative to free space propagation. The path delay is governed by the distribution of the refraction index along the propagation path. For mid-latitude stations at sea level typical values of the delay of a radio wave travelling from space to the earth surface range from 2.3 m at zenith to about 25 m at a zenith angle of 85°.

The apparent electrical path lengths L_E of a radio wave which propagates along a path L through the atmosphere is given according to Fermat's principle by:

$$L_E = \int_L n(s)ds \tag{5.1}$$

where n(s) is the refractive index as a function of the position s along the path. The **tropospheric delay** or **excess path length** $\Delta\rho_{trop}$ is the difference between L_E and the straight-line geometrical distance L_G (see e.g. [Hopfield, 1977] or [Tralli et al., 1988]):

$$\Delta\rho_{trop} = L_E - L_G = \int_L (n(s)-1)ds + (L_S - L_G) \tag{5.2}$$

where L_S is the path length along L. The term $L_S - L_G$ due to re-

fractive bending is insignificant, namely less than 1 cm at elevation angles greater than 15° (see [Resch, 1984]). Clearly, the effect of ray bending is more important for larger zenith distances whereas at zenith L_S is equal to L_G.

Neglecting the ray bending and introducing the **refractivity** N as

$$N = (n-1)\cdot 10^6 \tag{5.3}$$

we get

$$\boxed{\Delta\rho_{trop} = 10^{-6}\cdot\int_L N(s)ds} \tag{5.4}$$

According to [Thayer, 1974], for frequencies up to 20 GHz, the refractivity N of moist air may be written as

$$\boxed{N = k_1\cdot\frac{P_d}{T}\cdot Z_d^{-1} + k_2\cdot\frac{e}{T}\cdot Z_w^{-1} + k_3\cdot\frac{e}{T^2}\cdot Z_w^{-1}} \tag{5.5}$$

with P_d : Partial pressure of dry air (mbar)
e : Partial pressure of water vapour (mbar)
T : Temperature (K)
k_1, k_2, k_3 : Empirically determined constants (K/mbar, K/mbar, K/mbar^2)
Z_d^{-1}: Inverse compressibility of dry air
Z_w^{-1}: Inverse compressibility of water vapour

The first term on the right hand side of eqn. (5.5) is the so called dry refractivity N_d, whereas the last two terms form the wet refractivity N_w:

$$N = N_d + N_w \tag{5.6}$$

The physical meaning of the terms in eqn. (5.5) may be found in [Smith & Weintraub, 1953]. The inverse compressibilities account for the fact that dry air and water vapour do not exactly behave

like ideal gases. Assuming that the atmosphere and its constituents behave like ideal gases, we have

$$Z_d^{-1} = Z_w^{-1} = 1 \tag{5.7}$$

and

$$P_d = P - e \tag{5.8}$$

where P is the total pressure of moist air. Substituting (5.7) and (5.8) into (5.5) yields in this case

$$N = k_1 \cdot \frac{P}{T} + (k_2 - k_1) \cdot \frac{e}{T} + k_3 \cdot \frac{e}{T^2} \tag{5.9}$$

Detailed expressions for the dry as well as the wet component of the refractivity may be found in [de Jong, 1991].

About 90 % of the zenith delay arises from the dry component of the refractivity and changes slowly with time (about 2 cm/12 h, [Mueller & Zerbini, 1989]). The wet zenith delay is less than 0.40 m, but is less uniform both spatially and temporally. It is also more likely to be mismodelled, since the distribution of liquid water and vapour is much less predictable than that of temperature and pressure (see eqn. (5.5) and [Chao, 1973]). Its variations are about three times as large as those in the dry zenith delay [Treuhaft & Lanyi, 1987].

The trospospheric delay depends on the distance travelled by the radio wave through the neutral atmosphere and is therefore also a function of the satellite elevation angle. To show this elevation-dependence the tropospheric delay is often written as the product of the delay at zenith and a mapping function f(z) relating the zenith delay $\Delta\rho^0_{trop}$ to the delay $\Delta\rho^z_{trop}$ at zenith distance z

$$\Delta\rho^z_{trop} = f(z) \cdot \Delta\rho^0_{trop} \tag{5.10}$$

Since the water vapour content of the atmosphere becomes zero at a height of about 10 km, whereas the dry atmosphere extends to approximately 40-50 km above the earth's surface, it is prefer-

able to use different mapping functions for the dry and wet part of the tropospheric delay:

$$\Delta\rho^{z}_{trop} = f_{dry}(z)\cdot\Delta\rho^{0}_{dry} + f_{wet}(z)\cdot\Delta\rho^{0}_{wet} \qquad (5.11)$$

where $f_{dry}(z)$: Mapping function of the dry component
$f_{wet}(z)$: Mapping function of the wet component
$\Delta\rho^{0}_{dry}$: Dry tropospheric delay at zenith
$\Delta\rho^{0}_{wet}$: Wet tropospheric delay at zenith

Analytical elevation angle mapping functions have been derived by [Saastamoinen, 1972], [Chao, 1973], [Lanyi, 1984], [Davis et al., 1985], and others. When using only GPS observations above 20 degrees satellite elevation, the choice of the mapping function to be used is rather irrelevant, since the differences between different mapping functions are very small (see [de Jong, 1991]).

5.1.2 Local Troposphere Models Derived From Surface Met Data

As we have seen in section 3.2.2.3 the SM data are usually not good enough to give reliable estimates for the vertical, especially in small networks. When using values for pressure, temperature, and humidity extrapolated from sea level values on the other hand, we obviously have a consistent set of met values to compute tropospheric delays, but it is quite clear that these values will not represent the vertical gradients of the real troposphere. These are very important, however, if large height difference exist in the network.

The SM data actually stemming from the sites of the network (located at different heights) or stemming from special meteo sites (chosen to avoid local effects and well distributed in height) contain, in contrast to a standard atmosphere, the information on the gradients present in the real atmosphere. We therefore use the SM data to compute the vertical gradients of a local model of the troposphere. The method discussed here has been outlined in [Rothacher et al., 1990] and starts from the following assumptions:

- The GPS network to be processed is small (< 100 km) but contains large height differences.

- The entire network is dominated by the same micro-climate (e.g. no high mountain ranges between different parts of the net).

- **No horizontal gradients** are present in the troposphere above the area we are interested in.

In agreement with these assumptions the refractivity N (see 5.1.1, eqn. (5.3)) is now modeled as a function of height h and time in the layer between the lowest and the highest site of the survey:

$$N(h,t_i) = N^m(h) + \sum_{k=0}^{q} \Delta N_k(t_i) \cdot (h-h_0)^k \qquad (5.12)$$

where
- $N(h,t_i)$: Refractivity at height h and epoch t_i
- $N^m(h)$: Smooth time-independent a priori model of the refractiviy
- $\Delta N_k(t_i)$: Coefficients of a low degree polynomial in height at epoch t_i to be estimated using SM data
- q : Polynomial degree
- h_0 : Arbitrarily chosen reference height of the polynomial

As we have seen in section 5.1.1 the refractivity may be computed from pressure P, temperature T, and the partial pressure of water vapour e by eqn. (5.9). The International Association of Geodesy (IAG) recommended to use the values derived by Essen & Froome (see [IAG Resolution, 1963]) for the constants k_1, k_2 and k_3 in (5.9):

$$\begin{aligned} k_1 &= 77.64 \quad K/mbar \\ k_2 &= 64.70 \quad K/mbar \\ k_3 &= 371780 \quad K/mbar^2 \end{aligned} \qquad (5.13)$$

The partial pressure of water vapour e, finally, is given by (see [Kahmen, 1978]):

$$e = \frac{H}{100} \cdot e^{c_1 + c_2 \cdot T + c_3 \cdot T^2} \tag{5.14}$$

with the relative humidity H in percent and

$$\begin{aligned} c_1 &= -37.2465 \\ c_2 &= 0.213166\ K^{-1} \\ c_3 &= -0.000256908\ K^{-2} \quad . \end{aligned} \tag{5.15}$$

To compute the a priori model $N^m(h)$ of the refractivity N we use pressure P, temperature T, and humidity H derived from the following **standard atmosphere** (see [Berg, 1948]):

$$P = P_r \cdot (1 - 0.000226 \cdot (h - h_r))^{5.225} \tag{5.16}$$

$$T = T_r - 0.0065 \cdot (h - h_r) \tag{5.17}$$

$$H = H_r \cdot e^{-0.0006396 \cdot (h - h_r)} \tag{5.18}$$

where h_r : Reference height of the standard atmosphere model (e.g. sea level)

h : Station height

p_r, T_r, H_r : Pressure, temperature, and humidity at the reference height h_r

p, T, H : Pressure, temperature, and humidity at height h.

Pressure is thereby measured in millibar, temperature in degrees Celsius, the humidity in percent, and the heights in meters.

The reference values h_r, p_r, T_r, and H_r are defined as:

$$h_r = 0\ m \tag{5.19}$$

$$p_r = 1013.25\ mbar \tag{5.20}$$

$$T_r = 18^\circ\ Celsius \tag{5.21}$$

$$H_r = 50\ \% \tag{5.22}$$

Using actually measured SM data a set of "observed" refractivity values can be computed for all the sites of the net using the same eqns. (5.9), (5.13), (5.14), and (5.15) as in the case of the standard atmosphere. The differences between the refractivity values derived from a standard atmosphere and the values obtained

from SM data are then fitted by a low degree polynomial in height as stated in eqn. (5.12).

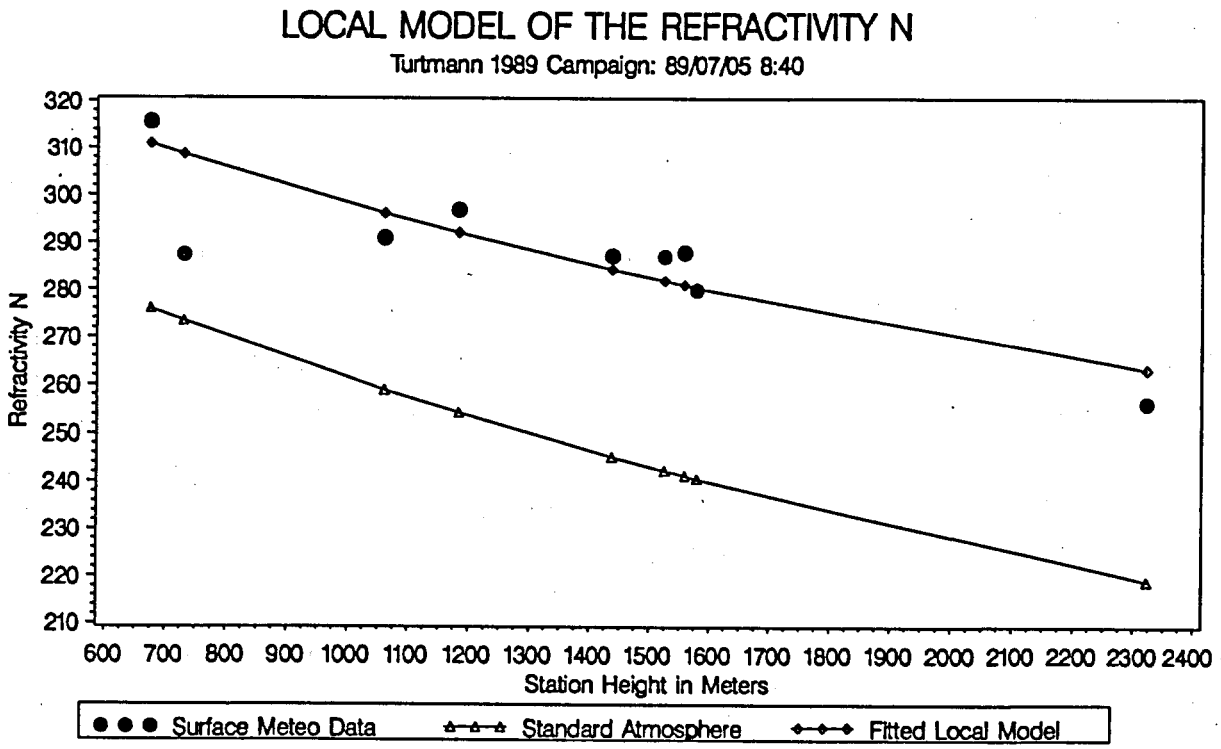

Figure 5.1
Local Model of the Refractivity Obtained by Fitting a Low Degree Polynomial in Height Through Refractivity Values Computed from SM Data

As an example the refractivity values computed from a standard atmosphere, those computed from SM data, as well as the values obtained by the polynomial fit have been plotted in Figure 5.1 for the sites of the Turtmann 1989 GPS Campaign (see section 10.1 for a description of this campaign). A polynomial degree q=2 was used in this example.

An a priori model of the refractivity has to be subtracted before the fit to remove the major height-dependence of the refractivity so that a polynomial of degree q=2 or 3 is sufficient to model the remaining trends in the refractivity. Refractivity values from (obviously) bad SM measurements (as the one shown in Figure 5.1 at the height of 720 meters) should not be used for the poly-

nomial fit. Typically refractivity polynomials are estimated in intervals of 15-30 minutes during the observation sessions depending on the rate of SM measurements available. The tropospheric zenith correction $\Delta\rho^0_{Ri,trop}$ at station R is then computed by integration using eqn. (5.4) with $N(h,t_i)$ according to (5.12):

$$\Delta\rho^0_{Ri,trop} = 10^{-6} \cdot \int_{h_R}^{h_{max}} N(h,t_i)\,dh + \Delta\rho^0_{h_{max}i,trop} \qquad (5.23)$$

where $\Delta\rho^0_{Ri,trop}$: Tropospheric zenith delay for station R at time t_i

$N(h,t_i)$: Refractivity at height h at time t_i according to eqn. (5.12)

h_R : Height of station R

h_{max} : Height of the highest station of the network

$\Delta\rho^0_{h_{max}i,trop}$: Tropospheric zenith delay due to the atmosphere above the highest station

The delay due to the atmosphere above the highest station is accounted for by the Saastamoinen model [Saastamoinen, 1972].

Figure 5.2 shows the tropospheric zenith delays for the sites of the Turtmann 1989 GPS Campaign computed

(1) with the Saastamoinen model using pressure, temperature, and humidity from the standard atmosphere defined by eqns. (5.16) to (5.22),
(2) with the Saastamoinen model using SM data, and
(3) with eqn. (5.23) according to the local refractivity model discussed in this section.

For the highest station of the survey (at height h_{max}) the tropospheric zenith delays computed according to (2) and (3) (see above) are the same as can be seen from Figure 5.2 and eqn. (5.23).

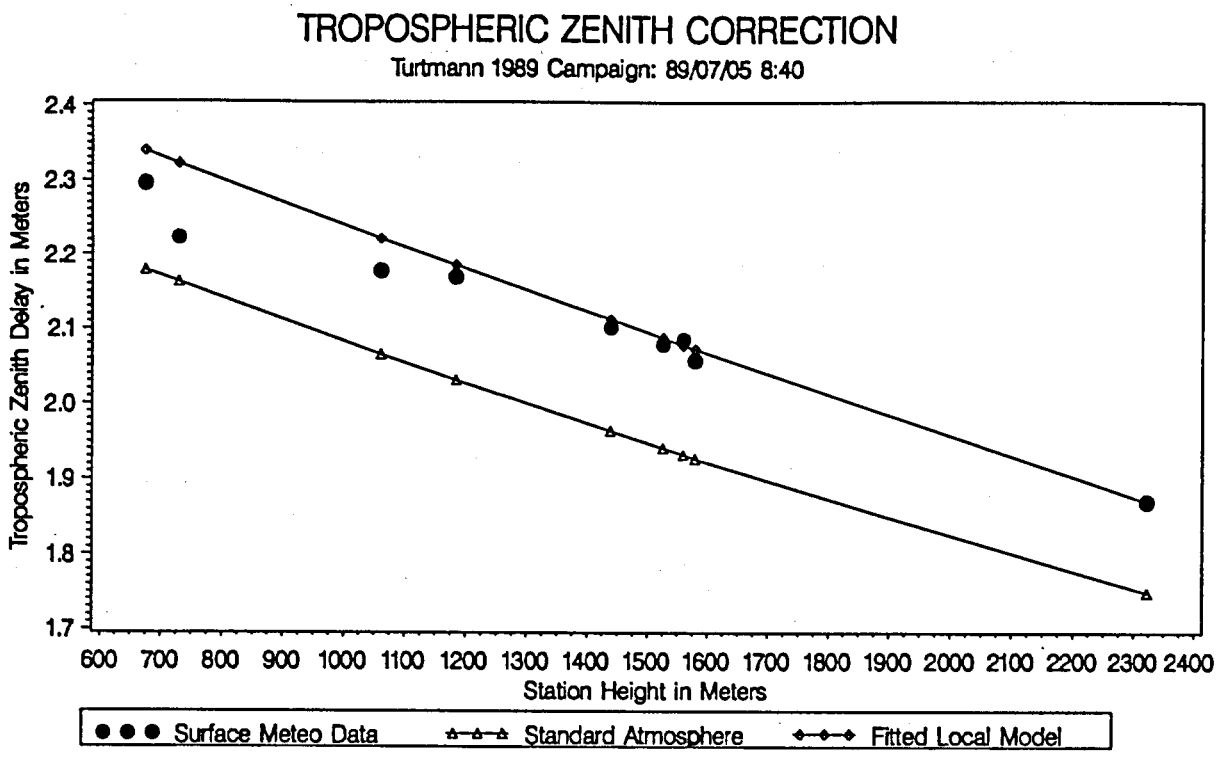

Figure 5.2
The Tropospheric Zenith Corrections Obtained by Saastamoinen (SM Data and Standard Atmosphere) and From the Local Refractivity Model of Figure 5.1

The simple mapping function (see eqn. (5.10))

$$f(z) = \frac{1}{\cos(z)} \tag{5.24}$$

is good enough to compute the tropospheric delay $\Delta\rho^{z}_{Ri,trop}$ for a zenith distance z:

$$\Delta\rho^{z}_{Ri,trop} = \frac{\Delta\rho^{0}_{Ri,trop}}{\cos(z)} \tag{5.25}$$

as long as observation data above a satellite elevation of 20 degrees are used.

5.2 Estimation of Troposphere Parameters

There are two major methods of troposphere parameter estimation that have been implemented into the most important GPS software systems of today:

1) the deterministic estimation of tropospheric zenith corrections (typically one parameter per session and station) using standard least squares procedures and

2) the estimation of the tropospheric zenith delays as a stochastic process using filter algorithms.

In addition to these two standard procedures there exist intermediate approaches like the deterministic estimation of the troposphere as a low order polynomial in time, the deterministic estimation of several troposphere parameters per session (e.g. one parameter for every half hour). Finally there are special methods available with limited applicability like e.g. the estimation of a height-dependent troposphere model for small networks outlined in [Gurtner et al., 1989b].

5.2.1 Deterministic Troposphere Estimation

5.2.1.1 Troposphere Zenith Delay Parameters

Most scientific programs used to process GPS data allow the estimation of one constant troposphere zenith correction per station and session.

Obviously the estimation of one parameter per session is reasonable under the assumption that most of the effect of the short-time changes in the tropospheric refraction averages out over a few hours.

The procedure of estimating one troposphere zenith delay per session and station can be refined by

(a) increasing the number of parameters to be estimated per session. We may want to estimate e.g. one troposphere parameter per hour.

(b) introducing a priori constraints between successive troposphere parameters of the same station.

It is easy to realize option (a). It is only necessary to relate each observation to the proper parameter (which is done using the epoch). If data of many stations have to be processed, the number of parameters in the normal equation system may turn out to be very large, when many troposphere parameters are introduced. The combined processing of 10 stations having observed during 10 sessions of 10 hours each, for instance, will result in 1000 troposphere parameters, if one troposphere zenith correction/hour is introduced. To avoid problems with available computer memory the troposphere parameters can be pre-eliminated. The troposphere parameters for the next time interval are then taking the place of the eliminated parameters. Like this the normal equation matrix will just have to contain one troposphere parameter per station at any one time.

Let us assume now that n_t troposphere zenith delay parameters p_i ($i=1,2,\ldots,n_t$) are set up for a specific station.

Constraints of type (b) may be introduced into the normal equation system as "pseudo-observations" in two ways:

1) We add the following observation equation for parameter p_i to the normal equation system using the weight w_i:

$$p_i^0 - o_i' = v_i \qquad (i=1,2,\ldots,n_t) \tag{5.27}$$

$$w_i = \frac{\sigma_0^2}{\sigma_i^2} \qquad (i=1,2,\ldots,n_t) \tag{5.28}$$

where

p_i^0 : A priori value of the parameter p_i. Since the tropospheric zenith delay is corrected for by a

standard model (e.g. Saastamoinen) p_i is estimated as the improvement to this a priori model and we set: $p_i^0 = 0$ $(i=1,2,\ldots,n_t)$.

O_i' : Pseudo-observation of parameter p_i with $O_i' = p_i$.

v_i : Residual

w_i : A priori weight of observation O_i'

σ_0^2 : A priori variance of the observations of unit weight

σ_i^2 : A priori variance for paramter p_i

These a priori weights will constrain the estimates of the tropospheric delay parameters, not allowing them to deviate too much from the standard model values.

2) We add the following observation equation for the difference between subsequent troposphere parameters of the same station to the normal equation system using the weight $w_{i,i+1}$:

$$(p_i^0 - p_{i+1}^0) - O_{i,i+1}' = v_{i,i+1} \qquad (i=1,\ldots,n_t-1) \tag{5.29}$$

$$w_{i,i+1} = \frac{\sigma_0^2}{\sigma_{i,i+1}^2} \tag{5.30}$$

where

$p_i^0 - p_{i+1}^0$: A priori value for the difference between the subsequent parameters p_i and p_{i+1}.
We set $p_i^0 - p_{i+1}^0 = 0$ $(i=1,2,\ldots,n_t-1)$ as a priori model.

$O_{i,i+1}'$: Pseudo-observation of the difference between subsequent troposphere parameters of the same station with $O_{i,i+1}' = p_i - p_{i+1}$.

$v_{i,i+1}$: Residual

$w_{i,i+1}$: A priori weight of observation $O_{i,i+1}'$

σ_0^2 : See eqn. (5.28) above

$\sigma_{i,i+1}^2$: A priori variance of the difference between parameters p_i and p_{i+1}

These a priori weights will ensure that the differences between

subsequent estimates of the tropospheric delay will not be much larger than $\sigma_{i,i+1}$.

The variances $\sigma^2_{i,i+1}$ have a similar meaning as the power spectral density PSD Φ_t of a stochastic process (see section 5.2.2). They both limit the change of the tropospheric delay allowed from parameter to parameter in the deterministic, from epoch to epoch in the stochastic estimation procedure. It is difficult, however, to find a simple correspondence between the variances $\sigma^2_{i,i+1}$ and the power spectral density Φ_t, because in the Kalman filter (see section 5.2.2) the variance at time t+1 (one epoch after epoch t) is given by the variance at time t **plus** the increase in the variance due to the PSD during the time interval from t to t+1 (see eqn. 5.59). Assuming a random walk as stochastic process we may write as an approximation:

$$\sigma^2_{i,i+1} \approx \Phi_t \cdot \Delta t_{i,i+1} \tag{5.31}$$

where $\Delta t_{i,i+1}$ is the time interval between the subsequent troposphere parameters. When estimating for example one troposphere zenith delay every hour a PSD of 10^{-8} m^2/s would then be comparable to a $\sigma_{i,i+1}$ of 6 mm.

Initializing the normal equation matrix **N** with the pseudo-observations and a priori weights given in eqns. (5.27) to (5.30) we get the following structure for the submatrix $\mathbf{N}_{trop}$ of the normal equation matrix **N** just containing the subsequent troposphere parameters of one station:

$$N_{trop} = \begin{pmatrix} w_1+w_{1,2} & -w_{1,2} & 0 & & & \\ -w_{1,2} & w_2+w_{1,2}+w_{2,3} & -w_{2,3} & & 0 & \\ 0 & -w_{2,3} & \ddots & \ddots & & \\ & \ddots & \ddots & \ddots & -w_{n_t-2,n_t-1} & 0 \\ & 0 & & -w_{n_t-2,n_t-1} & w_{n_t-1}+w_{n_t-2,n_t-1}+w_{n_t-1,n_t} & -w_{n_t-1,n_t} \\ & & & 0 & -w_{n_t-1,n_t} & w_{n_t}+w_{n_t-1,n_t} \end{pmatrix} \tag{5.32}$$

The matrix $\mathbf{N}_{trop}$ can be simplified by assuming the same a priori variances σ_{abs} and σ_{rel} for all the troposphere parameters and parameter differences respectively:

$$\sigma_i = \sigma_{abs} \qquad (i=1,2,\ldots,n_t) \tag{5.33}$$

$$\sigma_{i,i+1} = \sigma_{rel} \qquad (i=1,2,\ldots,n_t-1) \tag{5.34}$$

and

$$w_{abs} = \frac{\sigma_0^2}{\sigma_{abs}^2} \tag{5.35}$$

$$w_{rel} = \frac{\sigma_0^2}{\sigma_{rel}^2} \tag{5.36}$$

We then have:

$$N_{trop} = \begin{pmatrix} w_{abs}+w_{rel} & -w_{rel} & 0 & & & \\ -w_{rel} & w_{abs}+2w_{rel} & -w_{rel} & & 0 & \\ 0 & -w_{rel} & \ddots & \ddots & & \\ & & \ddots & \ddots & -w_{rel} & 0 \\ & 0 & & -w_{rel} & w_{abs}+2w_{rel} & -w_{rel} \\ & & & 0 & -w_{rel} & w_{abs}+w_{rel} \end{pmatrix} \tag{5.37}$$

When estimating troposphere parameters (independently of whether the estimation is a deterministic or stochastic one) attention has to be paid to the fact that in small networks the tropospheric delays of nearby stations are totally correlated because these stations see a satellite at almost the same zenith angle. The use of single (or double) differences then makes it impossible to distinguish between the delays of the two stations involved. In this case only the relative (differential) tropospheric delays with respect to one reference station may be reliably determined, else it may happen that all the stations are systematically shifted in height due to the badly determined absolute troposphere zenith delay and, according to section 3.2.2.2, a slightly wrong scale of the network will result.

Troposphere parameters are estimated after removal of a standard model for the dry (or dry and wet) components of the tropospheric refraction.

5.2.1.2 Height-Dependent Troposphere Parameters for Small Networks

The motivation for this method comes from small networks in areas with large height differences (like in the Swiss mountains). When processing such networks the most important errors in the verticals stem from the atmospheric layer between the lowest and highest station of the network. Assuming that horizontal gradients are small the vertical variations of the troposphere within the layer of interest (e.g. situations with temperature inversion, that occur frequently in alpine valleys) may be taken into account by estimating the tropospheric zenith delay as a low degree polynomial in height [Gurtner et al., 1989b]:

$$\Delta\rho^0_{trop}(h) = \sum_{j=1}^{n_t} c_j \cdot (h-h_0)^j \qquad (5.39)$$

where

$\Delta\rho^0_{trop}(h)$: Tropospheric zenith delay at height h

n_t : Number of parameters in this model, typically one or two

c_j : Parameters to be estimated using the GPS data of all stations in the network

h_0 : Reference height of the model (e.g. the height of the lowest station in the network).

Term c_0 was left out in eqn. (5.39), since it corresponds to an absolute tropospheric zenith delay for all sites. It does not make sense to solve for absolute tropospheric delays in small networks. The term c_0 is accounted for, however, by a standard model of tropospheric refraction.

The tropospheric zenith delay $\Delta\rho^0_{R,trop}$ for station R at height h_R is then given by:

$$\Delta\rho^0_{R,trop} = \Delta\rho^0_{trop}(h_R) \tag{5.40}$$

The advantage of this model is definitely the much smaller number of parameters to be estimated (one or two per session) compared to the estimation of one troposphere parameter per baseline as described in section 5.2.1.1. There are no horizontal gradients taken into account in model (5.39).

5.2.2 Stochastic Troposphere Estimation

The stochastic troposphere estimation in the Bernese GPS Software is based on a Kalman filter estimator. Although the formulae may be found in many textbooks (e.g. [Liebelt, 1967] or [Gelb, 1974]), we give a short overview following the one by [Herring et al., 1990].

Let us start with the linear version of the observation equation (3.9) or (3.16) with respect to the parameters to be estimated:

$$\mathbf{A}_t \cdot \mathbf{x}_t - \mathbf{y}_t = \mathbf{v}_t \tag{5.41}$$

All these quantities refer to epoch t with

- $\mathbf{y}_t$: Vector of terms "observed - computed" (differences between the observations ψ'_t at epoch t and their theoretical values ψ_t computed from a priori values of the parameters)
- $\mathbf{x}_t$: Parameter vector
- $\mathbf{A}_t$: Matrix of partial derivatives $\frac{\partial \psi_t}{\partial \mathbf{x}_t}$ of the observables with respect to the parameters $\mathbf{x}_t$ (first design matrix)
- $\mathbf{v}_t$: Vector of residuals representing the noise of the observations

The state transition equation describes the dynamics of the parameters:

$$\mathbf{x}_{t+1} = \mathbf{S}_t \cdot \mathbf{x}_t + \mathbf{w}_t \tag{5.42}$$

where $\mathbf{x}_{t+1}$: Vector of parameter values at epoch t+1 (t+1 denoting the next observation epoch after t).

$\mathbf{S}_t$: State transition matrix at epoch t defining the transition from the state at epoch t to the expected state at epoch t+1.

$\mathbf{w}_t$: Vector of random perturbations affecting the state during the interval between epoch t and t+1. For nonstochastic parameters $\mathbf{w}_t$ is zero.

To obtain a Kalman filter estimator the following statistical assumptions are made, where angle brackets denote expectation values, the superscript T the transpose of the vector:

$$\langle \mathbf{v}_t \rangle = 0 \quad \text{for all t} \tag{5.43}$$
$$\langle \mathbf{v}_t \ \mathbf{v}_{t+j}^T \rangle = 0 \quad \text{for all } j \neq 0 \tag{5.44}$$
$$\langle \mathbf{v}_t \ \mathbf{w}_{t+j}^T \rangle = 0 \quad \text{for all t and j} \tag{5.45}$$
$$\langle \mathbf{v}_t \ \mathbf{x}_{t+j}^T \rangle = 0 \quad \text{for all t and j} \tag{5.46}$$
$$\langle \mathbf{w}_t \rangle = 0 \quad \text{for all t} \tag{5.47}$$
$$\langle \mathbf{w}_t \ \mathbf{w}_{t+j}^T \rangle = 0 \quad \text{for all } j \neq 0 \tag{5.48}$$
$$\langle \mathbf{x}_t \ \mathbf{w}_{t+j}^T \rangle = 0 \quad \text{for all } j > 0 \tag{5.49}$$

and we define the correlation matrices $\mathbf{V}_t$ and $\mathbf{W}_t$ as

$$\mathbf{V}_t = \langle \mathbf{v}_t \ \mathbf{v}_t^T \rangle \tag{5.50}$$
$$\mathbf{W}_t = \langle \mathbf{w}_t \ \mathbf{w}_t^T \rangle \tag{5.51}$$

The assumptions (5.45) and (5.46) require that the measurement process and the random motion of the system are uncorrelated. Assumption (5.48) says that the random perturbations at any epoch are uncorrelated with those of any other epoch, and (5.49) requires that the current state of the system does not affect the random perturbations in the system at later epochs.

The Kalman filter estimation is carried out sequentially, epoch by epoch. The following steps have to be performed to add the ob-

servations of epoch t+1 to the estimation, if the state vector $\hat{\mathbf{x}}_t^t$ (subscript t indicating the epoch, superscript t denoting the epoch of the last data included in the estimate) and its covariance matrix $\mathbf{C}_t^t$ are given:

$$\hat{\mathbf{x}}_{t+1}^t = \mathbf{S}_t \cdot \hat{\mathbf{x}}_t^t \tag{5.52}$$

$$\mathbf{C}_{t+1}^t = \mathbf{S}_t \cdot \mathbf{C}_t^t \cdot \mathbf{S}_t^T + \mathbf{W}_t \tag{5.53}$$

$$\hat{\mathbf{x}}_{t+1}^{t+1} = \hat{\mathbf{x}}_{t+1}^t + \mathbf{K} \cdot (\mathbf{y}_{t+1} - \mathbf{A}_{t+1} \cdot \hat{\mathbf{x}}_{t+1}^t) \tag{5.54}$$

$$\mathbf{C}_{t+1}^{t+1} = \mathbf{C}_{t+1}^t - \mathbf{K} \cdot \mathbf{A}_{t+1} \cdot \mathbf{C}_{t+1}^t \tag{5.55}$$

where **K** is the Kalman gain given by

$$\mathbf{K} = \mathbf{C}_{t+1}^t \cdot \mathbf{A}_{t+1}^T \cdot (\mathbf{V}_{t+1} + \mathbf{A}_{t+1} \cdot \mathbf{C}_{t+1}^t \cdot \mathbf{A}_{t+1}^T) \tag{5.56}$$

Equations (5.52) and (5.53) form the filter prediction step, equations (5.54) and (5.55) the filter update step. Together the equations (5.52)-(5.56) form a complete sequence for the processing of observations with the filter. When the computations at epoch t+1 are completed, the sequence is repeated with quantities at epoch t+2 (substitution of t+2 for t+1, t+1 for t in the filter equations) and so forth until all observations have been included. We refer to this sequence as the forward Kalman filter. To start the forward Kalman filter a priori values for the parameters and their covariance matrix have to be specified.

After having processed all observations with the forward Kalman filter, the resultant state yields the final estimates of the nonstochastic parameters. To determine full time history of the estimates of stochastic parameters, however, a backward or smoothing Kalman filter solution must be performed. This smoothing is necessary because the estimates of stochastic parameters at epoch t do not contain the information about the parameters supplied by observations of later epochs t+1, t+2, ... For more information on the backward Kalman filter see [Herring et al., 1990].

Only the forward Kalman filter has been implemented so far into the parameter estimation program of the Bernese GPS Software. Thus the exact values of the tropospheric delays cannot be determined. However, if many satellites are visible simultaneously the

forward Kalman filter provides quite reasonable estimates of the tropospheric zenith delays.

The stochastic process model used in our Kalman filter is a random walk, which is well suited to model the stochastic behaviour of the troposphere. In this case the state transition matrix $\mathbf{S}_t$ (see eqn. (5.42) is equal to the identity matrix I:

$$\mathbf{S}_t = \mathbf{I} \tag{5.57}$$

The prediction step (eqns. (5.52), (5.53)) is simply

$$\hat{\mathbf{x}}^t_{t+1} = \hat{\mathbf{x}}^t_t \tag{5.58}$$

$$\mathbf{C}^t_{t+1} = \mathbf{C}^t_t + \mathbf{W}_t \tag{5.59}$$

where $\mathbf{W}_t$ gives the noise to be added to the covariance matrix $\mathbf{C}^t_t$ due to the time interval between epoch t and t+1.

The elements $w_{t,ij}$ of the covariance matrix $\mathbf{W}_t$ are given by:

$$\begin{aligned} w_{t,ij} &= 0 && \text{for } i \neq j \\ w_{t,ii} &= 0 && \text{for nonstochastic parameter i} \\ w_{t,jj} &= \Phi_{t,j} \cdot \Delta t && \text{for stochastic parameter j} \end{aligned} \tag{5.60}$$

where $\Phi_{t,j}$: Power spectral density (PSD) of parameter j. It fully characterizes the random walk process.

Δt : Time interval between epoch t and t+1.

The PSD $\Phi_{t,j}$ has to be specified for all stochastic parameters j to be estimated with the Kalman filter. In principle it could be time-dependent as indicated by the subscript t. A typical value of the PSD for troposphere zenith delay parameters is given by [Lichten et al., 1989b] or [Herring et al., 1990]:

$$\Phi_{t,trop} = 4 \cdot 10^{-8} \text{ to } 1 \cdot 10^{-7} \text{ m}^2/\text{s} \quad . \tag{5.61}$$

Many details on the real temporal and spatial variations of the tropospheric delay may be found in [Elgered et al., 1990].

As in the case of deterministic troposphere estimation usually the troposphere parameters of all stations but one are determined and the estimation is done on top of an a priori model for the delays.

5.3 Tropospheric Refraction in the Bernese GPS Software

A detailed description of the programs of the Bernese GPS Software and their options to model tropospheric refraction and of the file types containing troposphere information may be found in [Rothacher et al., 1991]. Some of the programs used to obtain the results discussed in this thesis have only recently been developed, however, and can not be found in the description. A few remarks may therefore be necessary.

The models to account for the tropospheric refraction implemented in the Bernese GPS Software are

- The Saastamoinen model [Saastamoinen, 1972]
- The modified Hopfield model [Goad & Goodman, 1974]
- The simplified Hopfield model [Wells, 1974]
- A differential refraction model based on formulae by Essen and Froome [Rothacher et al., 1986]

In all these models either measured SM data or pressure, temperature, and humidity derived from a standard atmosphere model (see eqns. (5.16) to (5.18)) starting with appropriate values at an arbitrary reference height may be introduced.

There exist three troposphere file types containing information on the troposphere in our software system. Apart from header information such as the file type, the station name, and the difference between local time and UTC (it is assumed that SM data is recorded in local time), the following quantities are available:

File type 1: Date and time, air pressure, temperature, and relative humidity

File type 2: Date and time, air pressure, dry and wet temperature
File type 3: Date and time, and troposphere zenith delays

An example of file type 1 is given in Figure 5.3. All the data of one station are stored in one file. File type 3 may be used for many different purposes: to introduce WVR data, to store the delays of a local troposphere model derived from SM data (see section 5.1.2), etc.

```
TURTMANN CAMPAIGN 1989
STATION : BRAE 2                UTC-LOCAL TIME(HOURS) =  0 TYP= 1
  JJ MM DD HH MM SS  PPP.PP  TT.TT  HH.HH
  89  7  5  8 15  0  860.8   16.6   73.4
  89  7  5  8 30  0  859.8   16.6   71.7
  89  7  5  8 45  0  859.8   16.8   67.0
  89  7  5  9  0  0  859.8   17.4   62.8
  89  7  5  9 15  0  859.8   18.5   60.8
  89  7  5  9 30  0  859.8   18.6   60.9
  89  7  5  9 45  0  859.8   18.8   51.0
  89  7  5 10  0  0  859.8   19.0   51.2
  89  7  5 10 15  0  859.8   19.8   53.5
  89  7  5 10 30  0  858.8   21.0   53.5
  89  7  5 10 45  0  858.8   20.4   50.8
  89  7  5 11  0  0  859.3   20.6   55.1
  89  7  5 11 15  0  859.3   21.0   50.2
  89  7  5 11 30  0  859.3   21.2   50.4
-1 0 0 0 0 0 0 0 0 (=LAST LINE)
```

Figure 5.3
Bernese Troposphere File of Type 1 Containing Surface Met Data

The flow of troposphere information in the Bernese GPS Software is summarized in Figure 5.4.

The SM data enters the software through RINEX meteo files [Gurtner et al., 1990a and 1990b]. The RINEX files are then converted into Bernese meteo files of type 1 by the program RXMBV3.

When simulating GPS observations with the program SIMULA (see section 7.2) the generated values for pressure, temperature, and relative humidity are stored in files of type 1, or, if stochastic troposphere zenith corrections are simulated, in files of type 3.

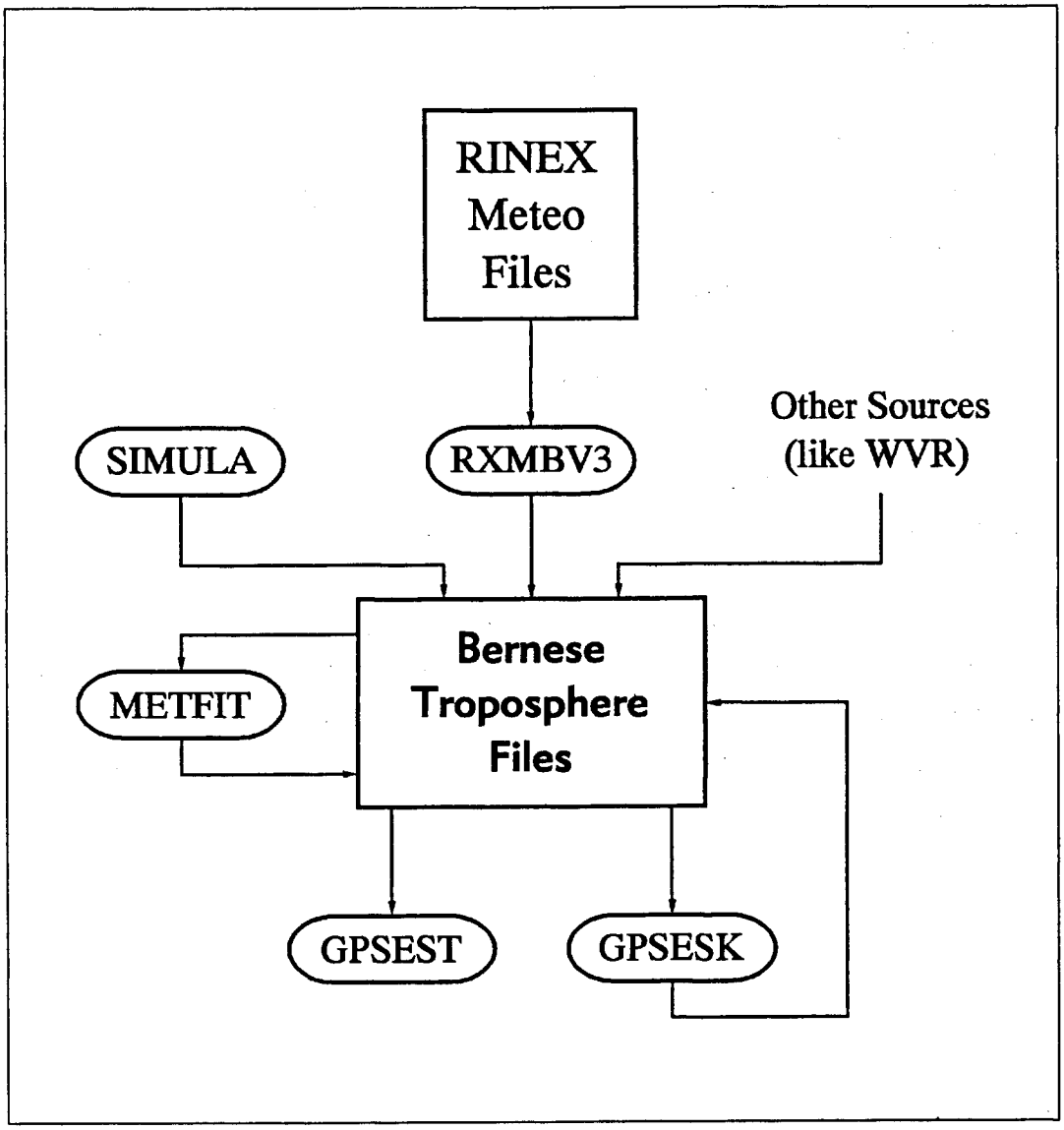

Figure 5.4
Flow Diagram of Troposphere Information
in the Bernese GPS Software

In GPSEST, the main parameter estimation program of the Bernese GPS Software [Rothacher et al., 1991], two different types of troposphere parameters may be estimated:

- One or more tropospheric zenith delays for individual stations imposing a priori constraints as discussed in section 5.2.1.1.

- The coefficients of a low degree polynomial in height of the

tropospheric zenith correction for small networks with large height differences (see section 5.2.1.2).

The program GSPEST (version 3.1) has been modified by Tom Herring at the Massachusetts Institute of Technology (MIT) for the U.S. Geological Survey to allow the stochastic estimation of parameters with a Kalman filter algorithm (see section 5.2.2). The new program was given the name GPSESK. It was updated to version 3.3 by the author in the course of this thesis.

GPSEST, as well as its counterpart GPSESK, will accept all the three troposphere file types to apply tropospheric delays.

The program METFIT, finally, is used to generate a local troposphere model starting from all the SM data files of a network (see 5.1.2): The resulting troposphere corrections are stored in troposphere files of type 3.

6. ASSESSMENT OF ORBIT ACCURACY

The groups developing GPS processing software to estimate site coordinates were in a very favourable position: VLBI and SLR on a global and regional scale, high precision terrestrial measurements on the local scale could be used as independent observation techniques to measure relative site coordinates. These comparisons helped to improve the models and techniques of the GPS data processing resulting in the fast progress made in the evaluation of GPS data. GPS has shown to have a tremendous potential and to be capable of obtaining results as good as or better than other techniques in most fields with a much smaller amount of work and money involved.

In the case of the satellite orbit modeling and estimation no such direct comparison with any independent technique is possible. This situation might change when some satellites carrying a GPS receiver plus retro-reflectors for SLR measurements will be in orbit. Today it is difficult to assess the accuracy of GPS orbits. We discuss three approaches to get a clearer picture of the orbit quality:

(1) Inspection of the formal orbit errors of the least squares estimation process.

(2) Comparison of satellite positions or orbital elements obtained with different data sets, processing strategies, or orbit models.

(3) Study of the influence of the orbit quality on non-orbital parameters like site coordinates or ambiguities.

These three methods will be discussed in more detail below.

A further difficulty lies in the circumstance that GPS orbits are tied to the reference system defined by fixing or constraining site coordinates in the estimation process. In the **fiducial point concept** the reference frame is defined by the coordinates of the

fixed fiducial sites. Using other fiducial site coordinates or other fiducial sites will change the orbits as well as the reference frame (see [Lichten et al., 1989a]). Even the estimation of tropospheric zenith delays may influence the stability of the reference frame. A reasonable comparison of orbits should be possible, however, even if the orbits are given in different reference frames. A method to do this type of orbit comparison will be given in section 6.2.4 .

6.1 Formal Errors of Satellite Orbits

A first indication of the quality of satellite orbit estimation is given by the formal errors of the estimated orbit parameters and the formal errors of the satellite positions. When interpreting these formal errors we should keep in mind that they are a measure of the internal consistency of the orbits only. Systematic effects not showing up in the formal errors may have introduced biases into the results.

6.1.1 Formal Errors of Orbital Parameters

One result of the least squares parameter estimation consists of the formal errors of the orbital parameters and even of the full variance-covariance matrix. The information that can be directly extracted from the formal errors depends very much on the type of orbital parameters. In our software the **osculating orbital elements at an epoch t_0** (see section 4.2.1.4) are the unknowns, and the interpretation is easier than in the case of an improvement of the initial conditions (position $\mathbf{r}_0$ and velocity $\dot{\mathbf{r}}_0$ at the epoch t_0). It is in principle always possible, however, to compute the osculating elements and their formal errors from the estimated initial conditions, their variance-covariance matrix, and the partials of the osculating elements with respect to the initial conditions (see eqn. (6.2) in the next section).

Equations (7.2) to (7.10) and Table 7.1 in section 7.2 are helpful to get an idea of the formal errors in the satellite posi-

tions to be expected as a function of the formal errors in the osculating orbital elements and the radiation pressure parameter p_0.

The variance-covariance matrix contains more information than just the diagonal elements (used to compute the formal errors of the orbital parameters): interesting information may be extracted from the variance-covariance matrix concerning the correlations between the orbit parameters of different satellites (e.g. the correlations between satellites revolving the earth in "the same" orbital plane) or even correlations between orbit parameters and other parameter types (e.g. site coordinates, troposphere zenith delays, or ambiguities).

6.1.2 Formal Errors of Satellite Positions

With the estimated parameters and the corresponding inverse normal equation matrix Q at our disposal we may compute the formal error m(x) of any analytical function

$$x = f\ (p_1, p_2, \ldots, p_{n_p}) \tag{6.1}$$

according to the general formula

$$m^2(x) = m_0^2 \cdot \sum_{i=1}^{n_p} \sum_{k=1}^{n_p} \frac{\partial f}{\partial p_i} \cdot \frac{\partial f}{\partial p_k} \cdot Q_{ik} \tag{6.2}$$

where

n_p	:	Number of estimated parameters
p_i	:	Estimated parameters ($i=1,2,\ldots,n_p$)
$m^2(x)$	:	A posteriori estimate of the variance of x
m_0^2	:	A posteriori estimate of the variance of the weight unit
$\frac{\partial f}{\partial p_i}$	:	Partial derivatives of the function f with respect to the estimated parameter p_i ($i=1,2,\ldots,n_p$)

Q_{ik} : Elements of the inverse normal equation matrix Q of the estimated parameters

$m_0^2 \cdot Q$: Variance-covariance matrix of the estimated parameters

Orbit errors are easily interpreted in the momentary coordinate system of the satellite defined by the **radial, the along track,** and **out of plane** directions (see Figure 6.1).

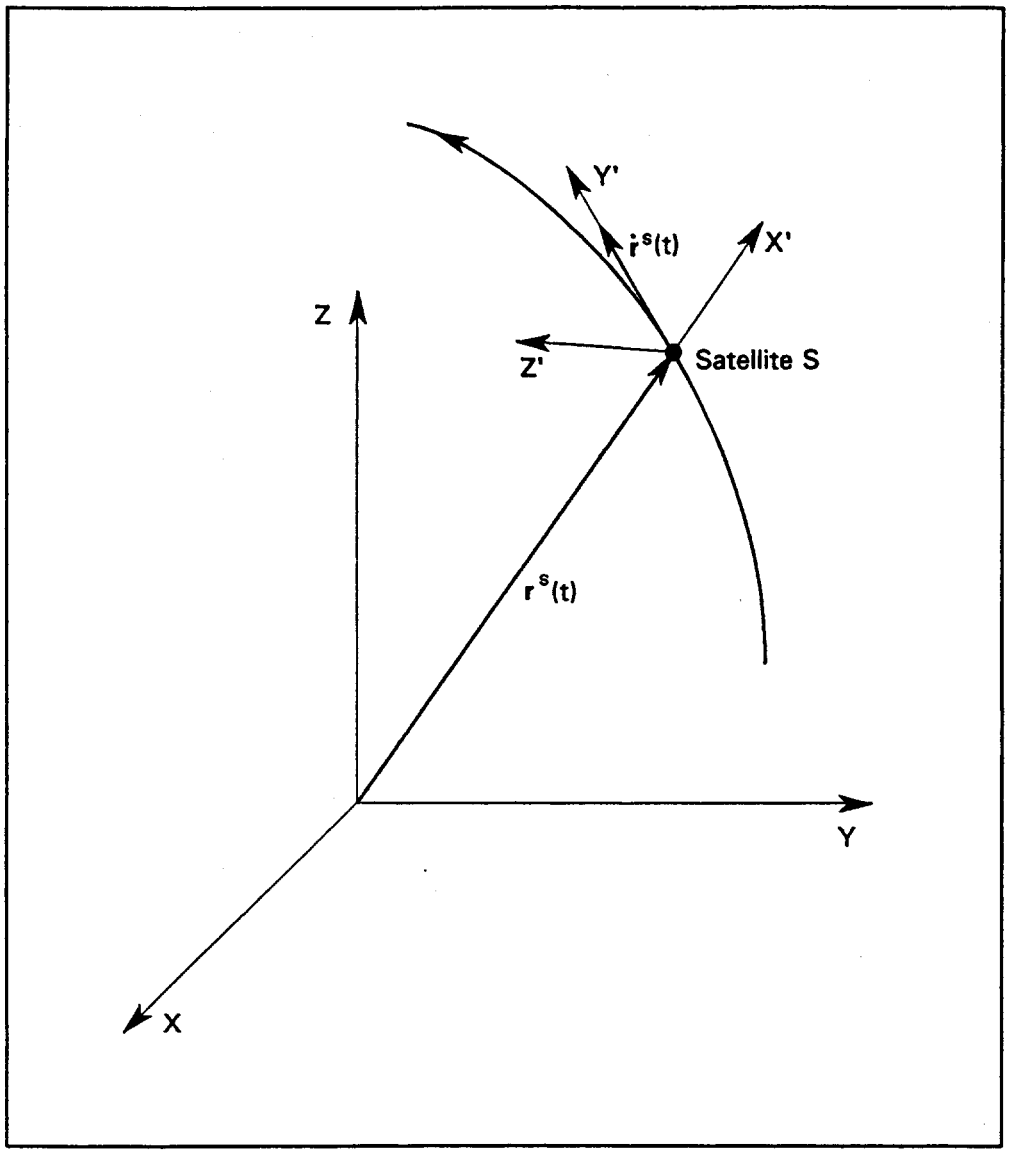

Figure 6.1
Momentary Satellite Coordinate System
(x,y,z: Axes of the Geocentric Inertial Frame;
x',y',z': Radial, Along Track, and Out of Plane Directions)

Due to the almost circular orbits of GPS satellites the transformation into this system may be approximated by a rotation matrix R depending on the geocentric position $\mathbf{r}^s(t)$ and velocity $\dot{\mathbf{r}}^s(t)$ of the satellite in the inertial frame:

$$\tilde{\mathbf{r}}^s(t) = \mathbf{R}(\mathbf{r}^s(t), \dot{\mathbf{r}}^s(t)) \cdot \mathbf{r}^s(t) \tag{6.3}$$

where $\tilde{\mathbf{r}}^s(t)$ is the satellite position in the momentary satellite coordinate system. The matrix R can also be written using the osculating elements Ω, i, and u (see section 4.1.1, Figure 4.1) at epoch t:

$$\mathbf{R} = \mathbf{R}_3(u)\mathbf{R}_1(i)\mathbf{R}_3(\Omega) \tag{6.4}$$

$\mathbf{R}_1$ and $\mathbf{R}_3$ denote rotations around the respective x- and z-axis:

$$\mathbf{R}_1(\alpha) = \begin{pmatrix} 1 & 0 & 0 \\ 0 & \cos\alpha & \sin\alpha \\ 0 & -\sin\alpha & \cos\alpha \end{pmatrix} \qquad \mathbf{R}_3(\alpha) = \begin{pmatrix} \cos\alpha & \sin\alpha & 0 \\ -\sin\alpha & \cos\alpha & 0 \\ 0 & 0 & 1 \end{pmatrix}$$

According to eqn. (6.2) the formal errors of the satellite position at time t in the momentary satellite coordinate system may therefore be computed as

$$m^2(\tilde{r}_j^s(t)) = m_0^2 \sum_{i=1}^{n_p} \sum_{k=1}^{n_p} \frac{\partial \tilde{r}_j^s}{\partial p_i}(t) \cdot \frac{\partial \tilde{r}_j^s}{\partial p_k}(t) \cdot Q_{ik} \qquad (j=1,2,3) \tag{6.4}$$

with $\tilde{\mathbf{r}}^{s\,T}(t) = (\tilde{r}_1^s(t), \tilde{r}_2^s(t), \tilde{r}_3^s(t))$

and

$$\frac{\partial \tilde{\mathbf{r}}^s}{\partial p_i}(t) = \mathbf{R}(\mathbf{r}^s(t), \dot{\mathbf{r}}^s(t)) \cdot \frac{\partial \mathbf{r}^s}{\partial p_i}(t) \qquad (i=1,2,\ldots,n_p) \tag{6.5}$$

neglecting the second order term containing the partials of the rotation matrix R.

In our case the parameters of the adjustment process are the os-

culating elements plus one or two radiation pressure parameters p_0 and p_2

$$p_i \in \{a, e, i, \Omega, \omega, u_0, p_0, p_2\}$$

The partials of the geocentric satellite positions $\mathbf{r}^S(t)$ with respect to the osculating orbital elements are listed in Appendix A.3 and may be computed analytically. The partials with respect to the radiation pressure parameters p_0 and p_2 are computed by numerical integration (see section 4.2.1.3 and 4.2.2).

The errors in the satellite positions are essential when comparing satellite orbits, because they show the time variation of the orbit precision.

6.1.3 Formal Errors of Relative Satellite Positions and Distances Between Satellites

Formal errors of relative satellite positions (differences between the positions of two satellites S_1 and S_2) and of the distance between two satellites may be obtained in the same way as the formal errors of the absolute satellite positions in section 6.1.2. Although the transformation into a satellite frame is not as essential in the case of two satellites as in the case of only one, we perform the analysis in the momentary system of satellite S_2:

$$\mathbf{R}_{S_2} = \mathbf{R}_{S_2}(\mathbf{r}^{S_2}, \dot{\mathbf{r}}^{S_2}) = \mathbf{R}_3(u_2) \cdot \mathbf{R}_1(i_2) \cdot \mathbf{R}_3(\Omega_2) \qquad (6.6)$$

and

$$\Delta\tilde{\mathbf{r}}^{S_1 S_2} = \mathbf{R}_{S_2} \cdot (\mathbf{r}^{S_1} - \mathbf{r}^{S_2}) \qquad (6.7)$$

where

Ω_2, i_2, u_2: Osculating elements of satellite S_2.

$\Delta\tilde{\mathbf{r}}^{S_1 S_2}$: Difference of the two satellite positions transformed into the satellite frame of satellite S_2.

We then have (denoting the component of the vector by the subscript j):

$$m^2(\Delta\tilde{r}_j^{S_1S_2}) = m_0^2 \cdot \sum_{i=1}^{n_p}\sum_{k=1}^{n_p} \frac{\partial\Delta\tilde{r}_j^{S_1S_2}}{\partial p_i} \cdot \frac{\partial\Delta\tilde{r}_j^{S_1S_2}}{\partial p_k} \cdot Q_{ik} \qquad (j=1,2,3) \qquad (6.7)$$

where

$$\frac{\partial\Delta\tilde{r}^{S_1S_2}}{\partial p_i} = R_{s_2}\left(\frac{\partial r^{S_1}}{\partial p_i} - \frac{\partial r^{S_2}}{\partial p_i}\right) \qquad (6.8)$$

The computation of the formal errors of the distances $d^{S_1S_2}$ between satellites S_1 and S_2 can easily be done by using eqn. (6.2) and

$$\frac{\partial d^{S_1S_2}}{\partial p_i} = \begin{cases} \dfrac{\Delta r^{S_1S_2}}{d^{S_1S_2}} \cdot \dfrac{\partial r^{S_1}}{\partial p_i} & \text{if } p_i \text{ is a parameter of satellite } S_1 \\ -\dfrac{\Delta r^{S_1S_2}}{d^{S_1S_2}} \cdot \dfrac{\partial r^{S_2}}{\partial p_i} & \text{if } p_i \text{ is a parameter of satellite } S_2 \end{cases} \qquad (6.9)$$

where $d^{S_1S_2} = |\, r^{S_1} - r^{S_2} \,|$.

There are two reasons why we want to look at the formal errors of relative satellite positions and the distance between satellites:

(1) All major GPS processing programs use (implicitly or explicitly) the double difference observable (see section 3.1.4) in their main parameter estimation program. Therefore only the **accuracy of the differences between satellite orbit positions is crucial** in the estimation procedure, whereas the absolute orbit quality is of secondary importance.

(2) In analogy to the fact, that the baseline length is the best determined quantity in relative positioning with GPS (for non-global baselines at least), we ask, whether the distances

between satellites not too far apart (visible from the same site) is the best determined orbit quantity.

It should be mentioned that with the increasing number of satellites in orbit and the use of global tracking networks for orbit determination the differences between the errors of absolute and relative satellite positions may become less important.

6.2 Comparison of Satellite Orbits

The comparison of satellite orbits estimated using different parts of a GPS data set (e.g. different sessions) is analogous to the well known repeatability studies for site coordinates. The orbit repeatabilities are a measure of the precision of the orbits, not of orbit accuracy, because the orbit sets compared could still contain common biases.

The comparison of satellite orbits may be done in different ways. Let us mention three:

(1) Direct comparison of the estimated initial conditions (position and velocity at a specific epoch) and the radiation pressure parameters.

(2) Comparison of the osculating elements and the radiation pressure parameters.

(3) Comparison of the satellite position vectors at different times.

Because the initial conditions do not give us directly the information on the time development of orbit differences, we will not discuss this type of comparison any further. It is easy, however, to compute the osculating elements of a satellite and their rms errors from the initial conditions and the associated variance-covariance matrix (see Appendix A.2 and A.3).

The comparison of osculating elements, radiation pressure parame-

ters, and satellite positions will be dealt with in the next sections.

In order to be able to compare satellite orbits directly the two sets of orbit parameters or satellite positions have to be given in the same reference frame. This will be the case if the estimated orbits are based on the same set of fiducial site coordinates or if the processing strategies are chosen to guarantee a common reference frame (e.g. several arcs per satellite estimated, but only one set of coordinates for the entire time period). If the two sets of satellite orbits are not refering to the same system, a comparison is still possible, as we will see in section 6.2.4, but only via the estimation of transformation parameters between the two systems.

Another basic requirement for orbit comparison is that the orbit quantities to be compared must be given at the same epoch(s). Osculating Keplerian elements must e.g. refer to the same epoch, and the orbits of two subsequent days can only be compared if the orbit of the first day is extrapolated to the second day or vice versa. It is clear that the accuracy of the estimated orbits will be degraded by the extrapolation necessary for comparison. The farther away from the time interval of the GPS observations used for the estimation of the orbital parameters we have to extrapolate the larger the errors of the orbits will become.

6.2.1 Comparison of Satellite Orbit Parameters

Osculating elements can only be compared if they refer to the same epoch, because the perturbations exerted on the satellite (see e.g. section 4.1.2) are permanently changing the shape and orientation of the orbit and thus the orbital elements. If the two sets of osculating elements have different reference epochs t_1 and t_2, one set of osculating elements (let us say the one at epoch t_1) has to be transformed to epoch t_2 according to Figure 6.2.

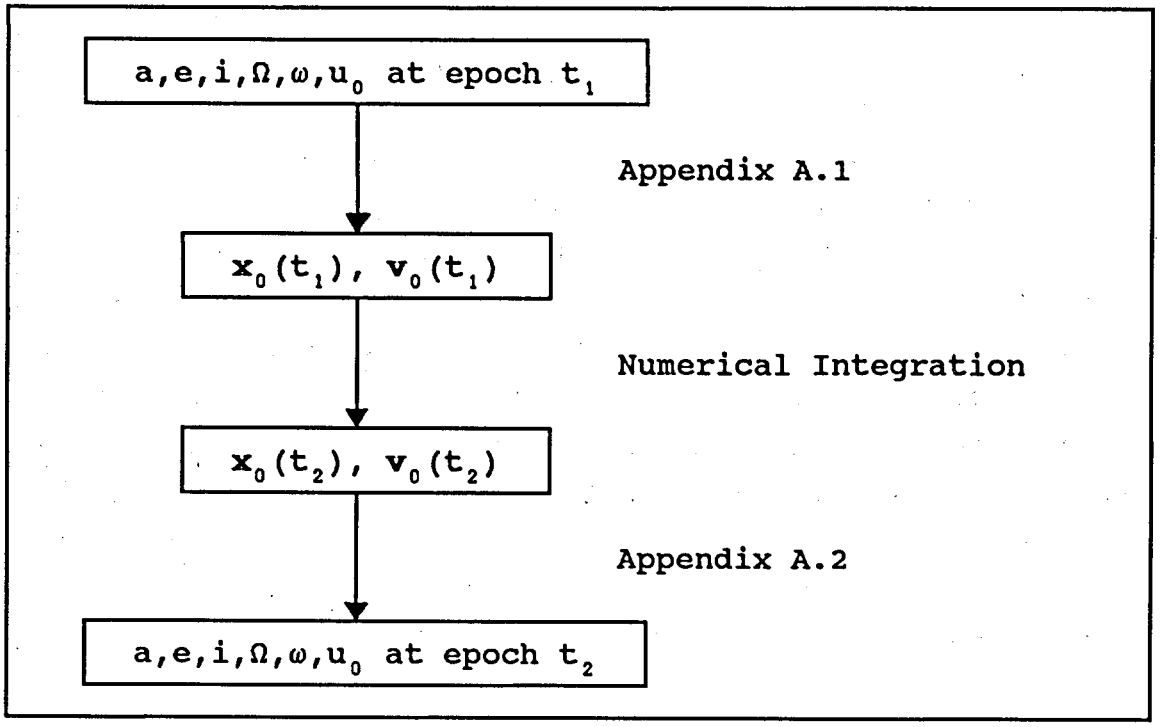

Figure 6.2
Transformation of Osculating Elements From Epoch t_1 to Epoch t_2

Using Table 7.1 or eqns. (7.2) to (7.10) in section 7.2 the order of magnitude of the orbit differences in meters and their direction may be approximately estimated from the differences in the osculating elements.

The physical meaning of the osculating elements as constants of integration of the two body problem helps to get a clearer picture of the type of differences between two orbit sets. The elements i, ω, and Ω will e.g. indicate rotations between the two sets etc.

Last but not least we would like to point out that all the comparisons should be done in consideration of the formal errors involved (see section 6.1.1). The argument of perigee may e.g. show large variations due to the fact that for almost circular orbits this element is very poorly determined. The associated formal error will confirm this fact.

6.2.2 Comparison of Satellite Positions

Differences in satellite positions are usually decomposed into the **along track, radial, and out-of-plane** components (see Figure 6.1). The along track component will show in most cases the biggest differences, since small errors in the mean motion of the satellite will result in errors in the along track component increasing linearly with time. The radial component usually shows the smallest differences due to the fact that differences in the semi-major axis (radial component) will lead to differences in the mean motion which in turn result in differences along the track growing with time as mentioned above. A difference of only 1 cm in the semi-major axis will give an along track difference of about 1 meter after 5 days for GPS satellites (see eqn. (7.4)).

For a specific experiment not all the satellite positions are of the same importance. Only the quality of the orbits above the region of interest will have an impact on the results obtained there, whereas that orbit part, when the satellites are below the horizon, will not contribute to the error budget. The situation is even more complex because of the use of double difference observations in the GPS data processing.

6.2.3 Comparison of Relative Satellite Positions and Distances Between Satellites

Due to the use of double differences in GPS data processing the absolute accuracy of the orbits used may not be the most important factor deciding on the quality of the baseline results. Orbit determination using the data from a regional tracking network may furnish very accurate relative satellite positions over the region of the tracking network, whereas in an absolute, global sense these orbits may very well be considerably rotated or distorted. Simulation results showing these effects may be found in Chapter 8.

6.2.4 Comparison of a System of Satellite Orbits

Differences between two sets of satellite orbits may be caused by two different reasons:

(1) They may be due to the fact that the two sets are given in different reference frames. In this case the orbits of all the satellites of one set will be translated, rotated, and/or scaled in the same way compared to the other set.

(2) They only show satellite specific trends and no translations, rotations, or scale factors common to all the satellites may be detected between the two sets, if the orbits are given in the same reference frame. The differences are due to remaining unmodeled orbit errors or the accuracy restrictions of the estimation.

Since we are dealing with a satellite system and not just with a single satellite the two types of orbit differences may be separated.

To determine possible differences in the reference frames of the two orbit sets we have to estimate transformation parameters (e.g. a 7 parameter similarity transformation) between the two sets using the positions of all the satellites in the system as pseudo-observations. This procedure is comparable to the estimation of a Helmert transformation between two coordinate sets that are given in different coordinate systems.

The program STDHLM was developed to allow exactly this type of orbit comparison. It starts with two Bernese standard orbit files (see section 4.3) each containing one set of satellite orbits to be compared. Satellite positions are then computed in specified time intervals and used as pseudo-observations to determine the transformation parameters. The option input file given in Figure 6.3 shows the program options available. (An arrow followed by a colon indicates an input field.)

```
STDHLM: OPTION INPUT FILE                                        91/03/10 14:52
------------------------------------------------------------------------------
(REMARK: YES=1,NO=0 ; 2 EMPTY LINES AFTER EVERY INPUT GROUP)

TITLE LINE:
----------
      ****************************************************************

--> : ORBIT COMPARISON OVER THE REGION OF GOLDSTONE                          (1)


PRINT OPTIONS:
-------------                                          *

PRINT RESIDUALS                                --> :  1                     (2)


PARAMETERS OF HELMERT TRANSFORMATION:
------------------------------------                   *

TRANSLATION IN X-DIRECTION                     --> :  0
TRANSLATION IN Y-DIRECTION                     --> :  0
TRANSLATION IN Z-DIRECTION                     --> :  0
ROTATION AROUND X-AXIS                         --> :  0                     (3)
ROTATION AROUND Y-AXIS                         --> :  0
ROTATION AROUND Z-AXIS                         --> :  0
SCALE FACTOR                                   --> :  0


GENERAL TIME INTERVAL:
---------------------

          START TIME            END TIME
      YYYY MM DD HH MM SS  YYYY MM DD HH MM SS

--> :  1990 12 11 00 00 00  1990 12 12 00 00 00                             (4)


OBSERVATION SELECTION:
---------------------                                  *****

SAMPLING INTERVAL                              --> :    600 SEC            (5)
MINIMUM ELEVATION FOR SATELLITES (IF ELEV. MASK)  --> :    20 DEGREES       (6)
MINIMUM # STATIONS WITH ELEV. > MIN. ELEV. REQUIRED --> :    1              (7)


STATION(S) FOR ELEVATION MASK (COMBINED WITH 'OR'):
--------------------------------------------------

      STATION NAME(S)
      ***************

--> :  GOLDSTONE                                                            (8)


SATELLITE SPECIFIC TIME INTERVALS: (SAT=99: ALL SATELLITES)
----------------------------------

      SAT     START TIME            END TIME
      **  YYYY MM DD HH MM SS  YYYY MM DD HH MM SS

--> :  16  1990 12 11 00 00 00  1990 12 12 00 00 00                         (9)


TYPE OF SATELLITE MARKING:
-------------------------

MARK POSITIONS WITHIN WINDOWS GIVEN BELOW  =  1
MARK POSITIONS OUTSIDE WINDOWS BELOW       =  2     --> :  2                (10)


TIME WINDOWS FOR MARKING: (SAT=99: ALL SATELLITES)
-------------------------

      SAT     START TIME            END TIME
      **  YYYY MM DD HH MM SS  YYYY MM DD HH MM SS

--> :  99  1990 12 11 00 00 00  1990 12 12 00 00 00                         (11)
```

Figure 6.3

Option Input File of the Program STDHLM Used to Compare Two Sets of Satellite Orbits Given in Different Reference Frames

Let us make some comments concerning the options of the program STDHLM:

(1) The title line is useful to document the program run

(2) The residuals of the satellite positions after the estimation of transformation parameters may be printed in the program output and/or written to a residual file that may be visualized later on. The residuals of the transformation may be interpreted as the differences between the orbits in the same reference frame.

(3) Selection of the transformation parameters to be estimated. If no parameter is determined, the residuals are equal to the plain differences between the two orbit sets. The selection of all parameters introduces a full 7 parameter similarity transformation between the two sets.

(4) A general time interval may be specified to define the boundaries within which satellite positions will be computed and used in the parameter estimation. Using this option the comparison of the two orbit sets may e.g. be confined to an observation session or to one arc per satellite. The time interval may also include more than one arc per satellite.

(5) The sampling interval defines the time interval between subsequent satellite positions.

(6) A minimum elevation angle may be given for the satellites. The elevation angles are computed as seen from the stations given in option (8). This option makes it possible to compare the orbits over a certain region (e.g. the region of the network used for orbit determination, or the region the orbits will be used for).

(7) If this option is set to 1 satellite positions will be used in the comparison only, if at least one of the stations specified in option (8) sees the satellite under an elevation angle larger than the minimum angle given in option (6). If

this option is set to 2, at least two of the stations given in option (8) must be able to observe the satellite above the minimum elevation angle corresponding to the use of single (or double) difference observations.

(8) List of stations used to define the elevation mask. The coordinates of the sites have to be given in a coordinate file.

(9) The satellite-specific time intervals are useful to exactly define the satellites that will be used for the comparison and in what time interval(s) they are going to be used.

(10) This and the next option (11) make it possible to mark satellite positions. Marked satellite positions are not used in the computation of the transformation parameters but the "residuals" with respect to the estimated transformation will be computed and listed in the residual table. With the setting of option (10) satellite positions will either be marked during the time intervals specified in option (11) (option (10) = 1) or satellite positions will be marked outside the regions specified in option (11) (option (10) = 2).

(11) Satellite specific windows to mark satellite positions according to option (10).

With all these options a very flexible and detailed comparison of two satellite orbit sets is possible.

To check the elevation angle of a satellite the satellite positions are transformed from the inertial system (1950.0 in our case) into an earth-fixed system.

Examples of orbit comparisons done with the program STDHLM may be found in Part II.

6.3 Non-Orbital Parameters as Indicators of Orbit Accuracy

The following procedure to assess the accuracy of GPS orbits was used again and again (e.g. [Beutler et al., 1986], [Lichten & Border, 1987], [Landau et al., 1988], [Lichten et al., 1989b] and many others):

(1) GPS observations of fiducial sites are used to improve the satellite orbits. The coordinates of the fiducial sites are kept fixed in this step.

(2) The improved orbits of step (1) are used to process baselines that were **not** included in step (1).

(3a) The repeatability of the baseline vectors and baseline lengths of step (2) are interpreted as a measure of the orbit accuracy according to eqn. (3.34) and Table 3.2 in section 3.2.1.1 .

(3b) If the baseline vectors have been determined by an independent method (VLBI or SLR) the comparison between two independent solutions can be made supplying again an indication of the orbit quality.

The assessment of orbit accuracy with repeatability studies (in most cases daily repeatabilities) of type (3a) has the drawback that effects showing up each day in the same way will not be detected and each single solution may be systematically biased. Repeatability studies will be the more realistic the more heterogeneous the conditions of the different solutions are.

When comparing baseline vectors with VLBI or SLR results much care has to be taken that both results are given in a consistent reference frame. This can only be achieved if either fiducial sites define the reference frame or if we allow for a system transformation, what is only possible if several sites of a network can be compared.

Apart from site coordinates any estimated parameter might in

principle be used as an indicator of orbit quality, if it can be compared to values obtained using an independent method.

As an example we may mention **ambiguity parameters**, where we do not know any independent "ground truth", but we know that the values should be integers. If the baselines are not too long the fractional parts of the real-valued estimates of the ambiguities may be used as indicators of the accuracy of the orbits. The interaction of ambiguities and orbit parameters has been clearly documented by [Counselman & Abbot, 1989] and [Dong & Bock, 1989] and has been embodied in the so-called bootstrapping method of ambiguity resolution, where the resolution of ambiguities on short baselines improves the orbit accuracy, which in turn enables the resolution of ambiguities on longer baselines etc.

In future the comparison of **earth rotation parameters** (pole coordinates and rate of UT1) obtained from GPS and from VLBI or SLR will give further evidence of orbit accuracies.

6.4 Exchange of Orbits

Within the problem area of orbit comparisons and the testing of orbit accuracies by dedicated institutions, as it will be the case in the framework of the IGS (International GPS Geodynamics Service, see 2.3.3), the exchange of orbit information and its use deserves a few remarks.

For groups using the same software the exchange of satellite orbits is easy and may even be done with binary files, if the same computer types are used. To be able to distribute orbits computed with the Bernese GPS Software to other users of the same program system using computers with a different binary number representation programs have been written to transform binary standard orbit files into ASCII files, that are easy to transfer, and vice versa.

The exchange of satellite orbit information is much more difficult between groups using different GPS software packages. A

software independent exchange format is needed. Such a format has been proposed by Remondi in 1985 (see [Remondi, 1985]), an updated version of the format has been defined in [Remondi et al., 1989]. This new format also includes satellite clock parameters.

So far, however, not many groups have exchanged GPS orbits. Certainly the satellite ephemerides should be made available in a well-defined earth-fixed system (like SV5 [Murray et al., 1990] or ITRF [Boucher & Altamini, 1989]), maybe even together with the coordinates of the fiducial sites used in the orbit improvement procedure, because the formulae used in the various software systems to do the transformation from an inertial system (e.g. 1950.0 or J2000.0) into the earth-fixed system may not be identical. Differences in this transformation will lead to inconsistencies between the reference frame of the satellite orbits and the reference frame of the site coordinates, if orbits are exchanged in an inertial frame.

Additional problems arise because most of the software systems available today will not allow the input of tabulated satellite ephemerides given in an earth-fixed system but will create their own orbit format by a numerical integration starting with a set of initial conditions taken from the ephemeris file obtained. The integration will be done, however, with constants (speed of light, gravity constant, ...) and a force model (earth potential, solar radiation pressure modeling, ...) that may not be identical with the ones used in the orbit estimation procedure. Even slight differences in the orbit modeling may then lead to large orbit differences compared to the original ephemeris. The satellite ephemerides obtained from another group should therefore be used as directly as possible (no system transformations and no numerical integration). An intermediate solution is the estimation of orbital parameters using the received satellite positions as pseudo-observations (as it is done in the Bernese GPS Software). Orbit differences may then be kept small by using short satellite arcs so that the force model used in the numerical integration is of secondary importance.

Figure 6.4 illustrates what happens, if satellite positions computed from the broadcast messages using a GM (gravity constant times mass of the earth) of $398.6005 \cdot 10^{12}$ m^3/sec^2 (WGS-84 value) are fitted in the least square sense (estimating orbital parameters) by an orbit obtained by the numerical integration of the equation of motion using a different GM value of $398.60044 \cdot 10^{12}$ m^3/sec^2. (See also section 4.3 for more details on the generation of Bernese standard orbits).

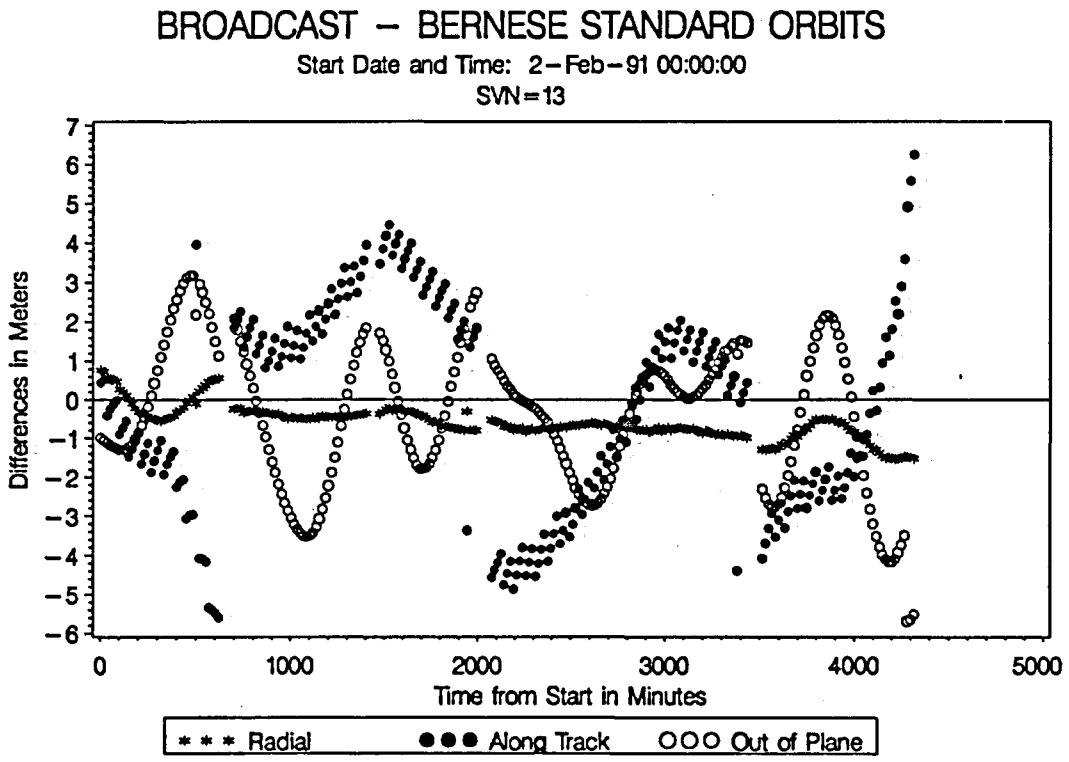

Figure 6.4
Differences Between the Broadcast Orbits and the Fitted Bernese Standard Orbits Using a Different GM Value

Finally, we should keep in mind that the groups interested in testing orbit accuracies by processing baselines will have to know the coordinates of the site(s) to be fixed in the baseline processing in exactly the same reference frame as the orbits, else the resulting network or baselines will be distorted (see [Beutler et al., 1988], [Santerre, 1991]: biases introduced due to errors in the height or horizontal position of the fixed site).

7. SIMULATIONS

Very early in the development of the Bernese GPS Software a simulation program was written. It has proven to be an essential tool to perform variance-covariance analyses, to study the effect of different biases on the estimated parameters, to test processing strategies, to carry out campaign preanaylses, and, last but not least, to check the results obtained by analytical methods. The program has since been modified and enlarged many times to keep track with the changes of the processing programs and to implement new or better models. For this thesis the simulation of tropospheric zenith delays using a stochastic process with correlations between sites has been added.

Using the simulation technique we will study the effect of the major biases present in GPS (orbit, troposphere, fiducial coordinates; see also section 3.2) on the parameters estimated. The possibility to include precisely the bias types in the data we are interested in (and nothing else) will make it much easier to identify the crucial biases (e.g. the limiting factor in ambiguity resolution or orbit determination). When analyzing real data only at rare occasions different bias types may be neatly separated.

We should not forget, however, that even sophisticated simulations will always fall short of reality: in many cases the models adopted for simulations are also used in the parameter estimation process (e.g. simulation of the tropospheric refraction by the same stochastic process used in the subsequent stochastic parameter estimation) and do not reflect the subtleties and complexity of the real data.

7.1 Simulation of GPS Observations

The simulation of GPS observations is based on the observation equations given in eqns. (3.9) and (3.16). Let us repeat the phase observation equation:

$$\rho^S_{Ri} - \Delta\rho^S_{Ri,ion} + \Delta\rho^S_{Ri,trop} - \Delta\rho^S_{Ri,rel} + c\cdot\Delta t_{Ri} - c\cdot\Delta t^S_i + \lambda^S N^S_R - \psi^{S\,\prime}_{Ri} = v^S_{Ri} \qquad (7.1)$$

where all the quantities have been defined in section 3.1.2.

To compute the distance ρ^S_{Ri} between satellite S and receiver R at time t_i appearing in eqn. (7.1), we have to start with a set of site coordinates and a set of satellite orbits (standard orbits, see section 4.3). These coordinates and orbits are by definition the **true values** which should eventually be recovered by a successful parameter estimation process using those simulated data.

Optionally receiver and satellite clock models may be specified as polynomials in time in special files to account for the terms $c\cdot\Delta t_{Ri}$ and $c\cdot\Delta t^S_i$ in eqn. (7.1).

An example of the option input file of the GPS simulation program SIMULA is given in Figure 7.1.

It shows the variety of parameters that define the generation of one session of GPS data (one session of data is produced in one run of SIMULA). Although the options are almost self-explanatory a few remarks seem appropriate:

- The receiver type in the third input field (input fields are always marked by an arrow and a colon "--> :") defines the type of measurements (carrier phase L_1, L_2 and/or code on L_1,L_2) to be generated and whether L_1 and L_2 have half cycle (squaring type receiver as e.g. the Minimac or Trimble SLD receiver) or integer cycle ambiguities (and cycle slips).

- The observations to be generated are selected by the session definition (start and end date and time), the sampling rate, and the minimum elevation angle of the satellites (cut-off angle).

```
SIMULA: OPTION INPUT FILE                                  21-APR-90 13:02
-------------------------------------------------------------------------
(REMARK: YES=1,NO=0 ; 2 EMPTY LINES AFTER EVERY INPUT GROUP)

CAMPAIGN NAME:
-------------
      ****************

--> : PGGA 1990 FULL


TITLE LINE:
----------
      ****************************************************

--> : SIMULATION: MARKOV TROP. (PSD 5.D-7,CD 1.D5,CT 3.6D3)


RECEIVER TYPE:
-------------
            *********

--> : SIMULA


SESSION DEFINITION:
------------------
            FROM                TO
       YYYY MM DD HH MM    YYYY MM DD HH MM

--> :  1990 07 12 00 00    1990 07 13 00 00

                                                        ****

SESSION NUMBER                                  --> :   193
FILE NUMBER (SAME SESSION, SAME STATION)        --> :     1
TIME BETWEEN SUBSEQUENT OBSERVATIONS (SEC)      --> :    30
MIN. ELEVATION (DEGREES)                        --> :    10


DETERMINISTIC TROPOSPHERIC MODEL:
--------------------------------                        *

NO METEO                          =  0
SAASTAMOINEN                      =  1
MODIFIED HOPFIELD (REMONDI)       =  2        --> :  0


STOCHASTIC TROPOSPHERE MODEL:
----------------------------                            *

NO STOCHASTICAL MODEL             =  0
SIMULATION OF SURFACE METEO DATA  =  1
SIMULATION OF STOCHASTIC PROCESS  =  2        --> :  2


PARAMETERS FOR SURFACE METEO DATA GENERATION:
--------------------------------------------            ******

RMS ERROR FOR PRESSURE MEASUREMENT              --> :   2.0    MBAR
RMS ERROR FOR TEMPERATURE MEASUREMENT           --> :   1.0    DEG C
RMS ERROR FOR HUMIDITY MEASUREMENT              --> :   5.0    %

MAXIMUM PRESSURE BIAS FOR ONE STATION           --> :   3.0    MBAR
MAXIMUM TEMPERATURE BIAS FOR ONE STATION        --> :   2.0    DEG C
MAXIMUM HUMIDITY BIAS FOR ONE STATION           --> :  10.0    %

                                                        *

SAME BIAS FOR ALL STATIONS                      --> :  0
MAX.BIASES = ACTUAL BIASES FOR ALL STAT.        --> :  0


PARAMETERS FOR STOCHASTIC TROPOSPHERE MODEL:
-------------------------------------------             *

WHITE NOISE                       =  1
RANDOM WALK                       =  2
FIRST ORDER GAUSS-MARKOV PROCESS  =  3        --> :  3

                                                        *********

RMS ERROR FOR CONSTANT TROPOS. BIAS IN TIME     --> :     0.030  M
CORRELATION DISTANCE FOR CONSTANT BIAS          --> :   1.D5     M

POWER SPECTRAL DENSITY FOR STOCHASTIC PROCESS   --> :     5.D-7  M**2/S
CORRELATION DISTANCE FOR STOCHASTIC BIAS        --> :   1.D5     M
CORRELATION LENGTH IN TIME (GAUSS-MARKOV ONLY)  --> :     3600.  S


IONOSPHERIC MODEL:
-----------------                                       ***

NIGHT TIME ELECTRON NUMBER (IN 10**16)          --> :   00 20
DAY   TIME ELECTRON NUMBER (IN 10**16)          --> :   00 30
VARIANCE OF IRREG. CHANGE OF IONOSPHERE CONTENT
  IN 1 MIN. AT 200 KM FROM REF.SITE (IN 10**15) --> :   1
                                                        ***************
REFERENCE SITE                                  --> :  MOJAVE


STATISTICAL INFORMATION:
-----------------------                                 **.***

A PRIORI SIGMA CODE L1                          --> :   1.000  M
A PRIORI SIGMA CODE L2                          --> :   1.000  M
A PRIORI SIGMA PHASE L1                         --> :    .003  M
A PRIORI SIGMA PHASE L2                         --> :    .003  M

                                                        ******

INITIAL INTEGER RANDOM NUMBER                   --> :  19576


INTRODUCE CYCLE SLIPS:
---------------------                                   ******

ONE SLIP PER SAT. AND FREQ. WITHIN (0: NO SLIPS) --> :      0 EPOCHS
MAXIMUM SIZE OF SLIP                            --> :   1000
L1 AND L2 SLIP AT SAME EPOCH (IN PERCENT TO ALL) --> :     20
```

Figure 7.1

Option Input File of the Simulation Program SIMULA

- The options to simulate the tropospheric refraction term $\Delta\rho^{S}_{Ri,trop}$ in eqn. (7.1) will be dealt with separately in section 7.3.

- The modeling of the ionospheric refraction (term $\Delta\rho^{S}_{Ri,ion}$ in eqn. (7.1)) is of no interest in our simulations since we will uniquely process the ionosphere-free linear combination of the L_1 and L_2 observations.

- The measurement noise may be defined separately for L_1 and L_2, phase and code observations. A random number generator produces the noise values v^{S}_{Ri} in eqn. (7.1) according to a normal distribution with a zero mean and a sigma equal to the noise value specified in the input option file.

- Even cycle slips might be generated!

There is no difference in the processing of simulated and real data. There are, however, many short cuts to speed up the procedure: usually all the preprocessing programs may be skipped and since the true phase ambiguity values are stored in the headers of the observation files they may either directly be introduced as known integer quantities or solved for as unknowns (and possibly resolved to integer numbers) as in the case of real data. In the latter case the obtained ambiguity values may be easily compared with the true values stored in the observation files.

7.2 Simulation of Orbit Biases

The simulation of orbit biases is not included in the simulation program SIMULA. This means that there are no orbit bias terms applied to the generated GPS observations. To simulate the effect of "bad" orbits the satellite orbits used for the simulation of the data (the "true" orbits) are changed to contain the required biases and these biased satellite orbits are then used instead of the "true" orbits in the parameter estimation.

The satellite positions for each arc contained in the standard orbit file have been computed by numerically integrating the equations of motion of the satellites starting with the appropriate initial conditions and radiation pressure coefficients (see 4.2.2 and 4.3). Each set of initial conditions (position and velocity vector $\mathbf{r}_0$ and $\dot{\mathbf{r}}_0$ of the satellite at epoch t_0), however, may be converted into a set of osculating Keplerian elements (a, e, i, Ω, ω, u_0, valid at the epoch t_0; see 4.1.1, Figure 4.1 and Appendix A.2). To create biased satellite positions these Keplerian elements (and the radiation pressure coefficients p_0 and p_2) may be slightly modified, converted back to initial conditions, and then used to generate a new, biased standard orbit.

The changes Δa, Δe, Δi, $\Delta\Omega$, $\Delta\omega$, and Δu_0 to be applied to the Keplerian elements and changes in the radiation pressure coefficients Δp_0 and Δp_2 are controlled by specifying a variance σ^2 for each element. Random biases in the elements are generated for the different satellite arcs assuming a normal distribution with mean zero and the variance σ^2.

The order of magnitude of the orbit errors Δr caused by orbit biases Δa, Δe, ... is given by the following formulae (examples are given in Table 7.1):

a :	Δr_{rad}	$\cong$	Δa	(radial)	(7.2)
	Δr_{along}	$\cong$	$-3\cdot\pi\cdot\Delta a$ per revolution	(along track)	(7.3)
e :	Δr_{rad}	$\cong$	$\pm\,\Delta e\cdot a$	(radial)	(7.4)
	Δr_{along}	$\cong$	$\pm\,\Delta e\cdot a$	(along track)	(7.5)
i :	Δr_{plane}	$\cong$	$\Delta i\cdot a$	(out of plane)	(7.6)
Ω :	Δr_{plane}	$\cong$	$\Delta\Omega\cdot a$	(out of plane)	(7.7)
u_0:	Δr_{plane}	$\cong$	$\Delta u_0\cdot a$	(out of plane)	(7.8)
ω :	Δr	$\cong$	0 (due to almost circular GPS orbits)		(7.9)
p_0:	Δr	$\cong$	$\Delta p_0\cdot\frac{\Delta t^2}{2}$ (after a time interval Δt, as a very coarse approximation)	(along track)	(7.10)

Orbital Element	Change in Element	Induced Orbit Errors in Meters Radial	Along Tr.	Out o.Plane
a	$\Delta a = 0.1$ m	0.1	1.8/day	0
e	$\Delta e = 10^{-7}$	2.6	2.6	0
i	$\Delta i = 0.01$ arcsec	0	0	1.3
Ω	$\Delta\Omega = 0.01$ arcsec	0	0	1.3
ω	$\Delta\omega = 0.01$ arcsec	0	0	0
u_0	$\Delta u_0 = 0.01$ arcsec	0	1.3	0
p_0	$\Delta p_0 = 10^{-9}$ m/s^2	0.6*	2.0*	0.06*
p_2	$\Delta p_2 = 10^{-10}$m/s^2	0.1*	0.8*	0.02*

* after one day, obtained by simulation

Table 7.1
Orbital Errors in Meters Caused by Changing the Keplerian Elements and the Radiation Pressure Coefficients (see eqns. (7.2) to (7.10))

The values listed in Table 7.1 for the orbit errors caused by biases Δp_0 and Δp_2 have been obtained by simulation. Illustrations are given in Figures 7.2 and 7.3.
Figure 8.5 in section 8.1.3.4 shows the differences between the "true" orbits and the derived biased orbit for satellite 2 with errors in the orbital elements of about $2 \cdot 10^{-8}$ or 0.5 meters.

7.3 Simulation of Troposphere Biases

As one can see from the option input file of the program SIMULA (Figure 7.1), there are two ways to simulate tropospheric effects:

1) Simulation of surface met data (measurements of temperature, pressure, and relative humidity) for the different stations involved.

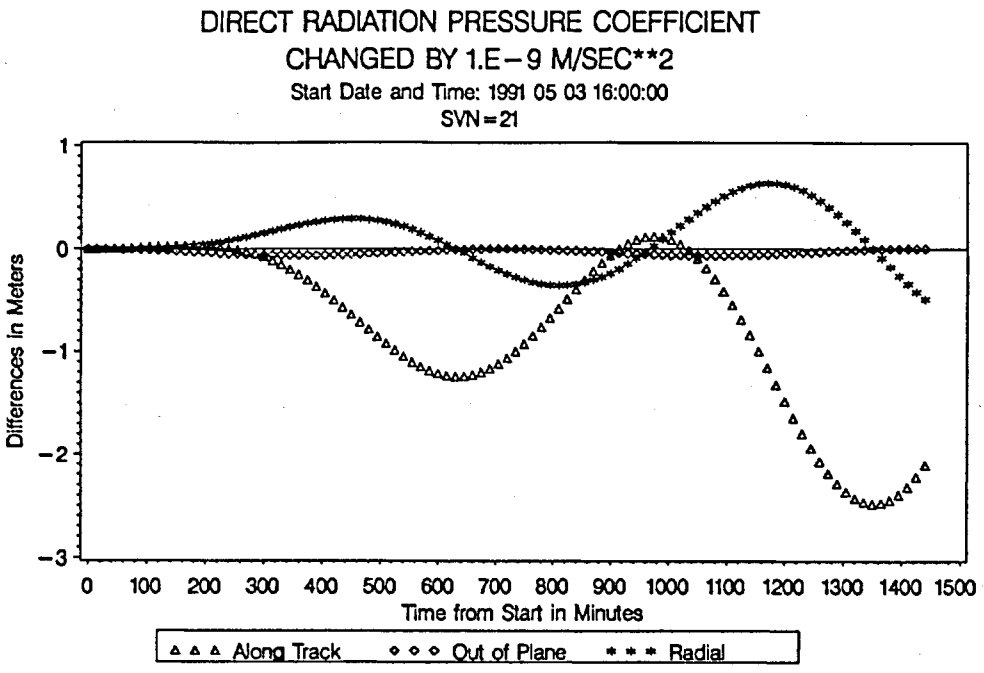

Figure 7.2

Biases Introduced Into the Orbit of Satellite 21 by Changing the Direct Radiation Pressure Coefficient

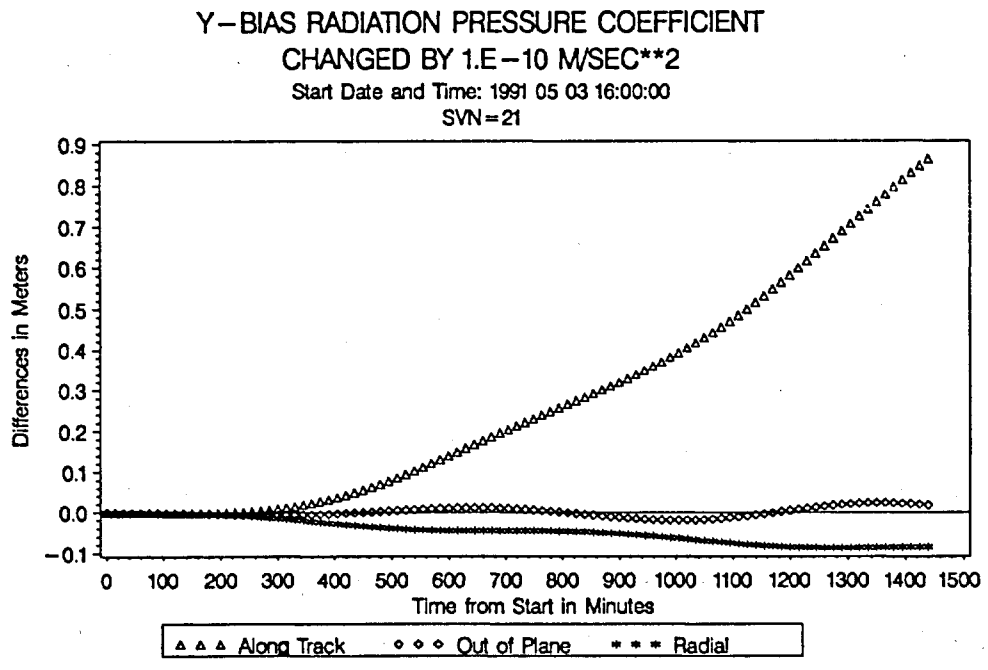

Figure 7.3

Biases Introduced Into the Orbit of Satellite 21 by Changing the Y-Bias Coefficient

2) Simulation of tropospheric zenith delays.

The first method, where the simulated met values are used to compute the tropospheric refraction delays, will not be used here.

In method 2) the troposphere zenith corrections $\Delta\rho_R^0$ (zero superscript to indicate zenith distance = 0) at time t_i for receiver R is modeled as

$$\Delta\rho_R^0(t_i) = \Delta\rho_R^m + \Delta\rho_R^c + \Delta\rho_R^s(t_i) \quad (R=1,\ldots,n_s,\ i=1,\ldots,n_e) \qquad (7.11)$$

where

n_s : Number of stations in the simulated session

n_e : Number of epochs of the session

$\Delta\rho_R^m$: Model part of the tropospheric zenith correction with formulae by Saastamoinen or Hopfield (see section 5.3) using a standard atmosphere model (see eqns. (5.16) to (5.22)) to obtain the needed values for pressure, temperature, and relative humidity at the height of station R

$\Delta\rho_R^c$: Constant bias in the troposphere zenith correction for station R

$\Delta\rho_R^s$: Time variation of the troposphere zenith correction modeled as a stochastic process (e.g. white noise, random walk, ...). This is the only time-dependent term in eqn. (7.11).

More details concerning the model part $\Delta\rho_R^m$ may be found in section 5.1.

For the second and third term on the right hand side of eqn. (7.11) we would like to generate values that are correlated with the distances between the stations involved: stations close to each other should have similar tropospheric corrections (similar meteorological conditions) whereas stations far apart should get tropospheric corrections that are more or less uncorrelated. We therefore write the correlation matrix for the constant corrections $\Delta\rho_R^c$ as follows (a similar matrix may be defined for the stochastic corrections $\Delta\rho_R^s$):

$$\mathbf{cov}\ (\Delta\rho^c) \;=\; E(\Delta\rho^c \cdot \Delta\rho^{cT}) \;=\; \sigma_c^2 \cdot \mathbf{C}^c \qquad (7.12)$$

where $\Delta\rho^{cT} = (\Delta\rho^c_1,\ \Delta\rho^c_2, \ldots, \Delta\rho^c_{n_s})$

and where σ_c^2 is the variance to be used for the generation of the random troposphere corrections.

Assuming an exponential decay of the correlations with distance the elements $C_{R_1R_2}$ of the matrix $\mathbf{C}^c$ are given by

$$C_{R_1R_2} = \exp\ (-\,|\,\mathbf{x}_{R_1} - \mathbf{x}_{R_2}\,|\,/\,d^c)\ \ (R_1=1,\ldots,n_S,\ R_2=1,\ldots,n_S) \qquad (7.13)$$

where

$\mathbf{x}_{R_1}$, $\mathbf{x}_{R_2}$: Coordinate vectors of station R_1 and R_2 respectively
d^c : Correlation distance for the constant tropospheric corrections $\Delta\rho^c_R$

To generate random values for the $\Delta\rho^c_R$ obeying the correlation matrix defined by eqns. (7.12) and (7.13) we start with a vector **a** containing n_S random numbers of the same normal distribution with variance σ_c^2:

$$\mathrm{cov}(\mathbf{a}) \;=\; E(\mathbf{a}\cdot\mathbf{a}^T) \;=\; \sigma_c^2\ \mathbf{I} \qquad (7.14)$$

where **I** is the identity matrix.

We now transform this vector **a** into $\Delta\rho^c$ with a matrix $\mathbf{A}^c$

$$\Delta\rho^c \;=\; \mathbf{A}^c \cdot \mathbf{a} \qquad (7.15)$$

with

$$\mathbf{A}^c \;=\; \mathbf{S}\cdot\sqrt{\mathbf{D}} \qquad (7.16)$$

S in (7.16) is the transformation matrix used to transform the correlation matrix $\mathbf{C}^c$ into a diagonal matrix **D**:

$$\mathbf{D} \;=\; \mathbf{S}^T\cdot\mathbf{C}\cdot\mathbf{S} \qquad (7.17)$$

The diagonal matrix **D** has the eigenvalues of $\mathbf{C}^c$ on its diagonal and the matrix **S** contains the eigenvectors of $\mathbf{C}^c$ as column-vec-

tors. $\sqrt{\mathbf{D}}$ in (7.16) stands for the matrix containing the square roots of the eigenvalues of **D** on its diagonal.

We can show now, that the constant tropospheric corrections $\Delta\rho^c$ given by eqn. (7.15) are indeed correlated with the correlation matrix defined by eqns. (7.12) and (7.13):

$$\begin{aligned} \mathrm{cov}(\Delta\rho^c) &= E(\Delta\rho^c \cdot \Delta\rho^{c\,T}) \\ &\overset{(7.15)}{=} E(\mathbf{A}^c \cdot \mathbf{a} \cdot \mathbf{a}^T \cdot \mathbf{A}^{c\,T}) \\ &= \mathbf{S} \cdot \sqrt{\mathbf{D}} \cdot E(\mathbf{a} \cdot \mathbf{a}^T) \cdot \sqrt{\mathbf{D}} \cdot \mathbf{S}^T \\ &\overset{(7.14)}{=} \sigma_c^2 \, \mathbf{S} \cdot \mathbf{D} \cdot \mathbf{S}^T \end{aligned} \tag{7.18}$$

or with (7.17) and the known identity $\mathbf{S}^{-1} = \mathbf{S}^T$ for orthogonal matrices we obtain

$$\mathrm{cov}(\Delta\rho^c) = \sigma_c^2 \cdot \mathbf{C}^c \tag{7.20}$$

which is identical with our assumption (7.12).

In summary we start with matrix $\mathbf{C}^c$, compute its eigenvalues (giving us **D**) and eigenvectors (giving us **S**), and finally transform the random numbers generated with mean zero and variance σ_c^2 with the matrix $\mathbf{A}^c$ (see (7.16)) to get the corrections $\Delta\rho^c$ (see (7.15)).

In the case of the stochastic corrections $\Delta\rho_R^S$ we have to define the stochastic process to be used to generate the time series of $\Delta\rho_R^s$ values.

Three types of processes are available in the simulation program:

a) White noise
b) Random walk
c) First order Gauss-Markov process

The computation of the values $\Delta\rho_R^s(t_i)$ is somewhat different for the three processes:

$$\Delta\rho_R^s(t_i) = \begin{cases} \Delta\rho_{Ri}^s & \text{for a)} \\ \Delta\rho_R^s(t_{i-1}) + \Delta\rho_{Ri}^s & \text{for b)} \\ \Delta\rho_R^s(t_{i-1}) \cdot e^{-\Delta t/\beta} + \Delta\rho_{Ri}^s & \text{for c)} \end{cases} \qquad (7.20)$$

To take into account the correlations in distance we can proceed as in the case of the constant tropospheric corrections (see above).

The variance σ_s^2 to generate the random numbers a (see eqn. (7.14)) has to be defined depending on the process type as:

$$\sigma_s^2 = \begin{cases} \Phi \cdot \Delta t & \text{for a) and b)} \qquad (7.21) \\ \Phi \cdot \beta \cdot (1 - e^{-\Delta t/\beta}) & \text{for c)} \qquad (7.22) \end{cases}$$

The quantities not yet defined are:

$\Delta t = t_i - t_{i-1}$: Time interval between subsequent epochs.
β : Correlation length in time used in the Gauss-Markov process (in sec).
Φ : Power spectral density (PSD) of the process (in m^2/sec) (see section 5.2.2).

The most realistic simulation of the tropospheric behaviour is no doubt obtained with the Gauss-Markov process. It has the advantage, that the exponential decay term in (7.22) prevents the values of $\Delta\rho_{Ri}^s$ from drifting too far away from the starting value ($\Delta\rho_R^s(t_0)=0$ in our case), which happens in the random walk with a probability increasing with time (see (7.21)). Another nice feature of the first order Gauss-Markov process is the possibility to define a correlation length in time. For these reasons we preferably used this process type.

All the troposphere zenith corrections are stored in station specific files (see 5.3) and may therefore easily be compared with estimated troposphere parameters later on.

A mapping function f(z) describing the dependence of the tropospheric correction on the zenith distance z is used to convert the corrections valid for zenith distance zero to the actual zenith distance z of the satellite (see eqn. (5.10)):

$$\Delta\rho_R^z(t_i) = f(z)\cdot\Delta\rho_R^0(t_i) \tag{7.24}$$

We use the simple mapping function

$$f(z) = \frac{1}{\cos(z)} \tag{7.25}$$

No azimuthal variations of the troposphere are considered here.

To complete this section we include Figures 7.4 and 7.5 as two examples of tropospheric zenith delays simulated for four sites in California, about 100 - 200 km apart, with a Gauss-Markov process defined by

$$\Phi = 5\cdot10^{-7}\ \ m^2/sec$$
$$\beta = 3600\ sec$$

and correlation distances for the constant and the stochastic part

$$d^c = d^s = 100\ km \quad \text{in Figure 7.4 and}$$
$$d^c = d^s = 1000\ km \quad \text{in Figure 7.5 .}$$

The stronger correlation in Figure 7.5 clearly shows up.

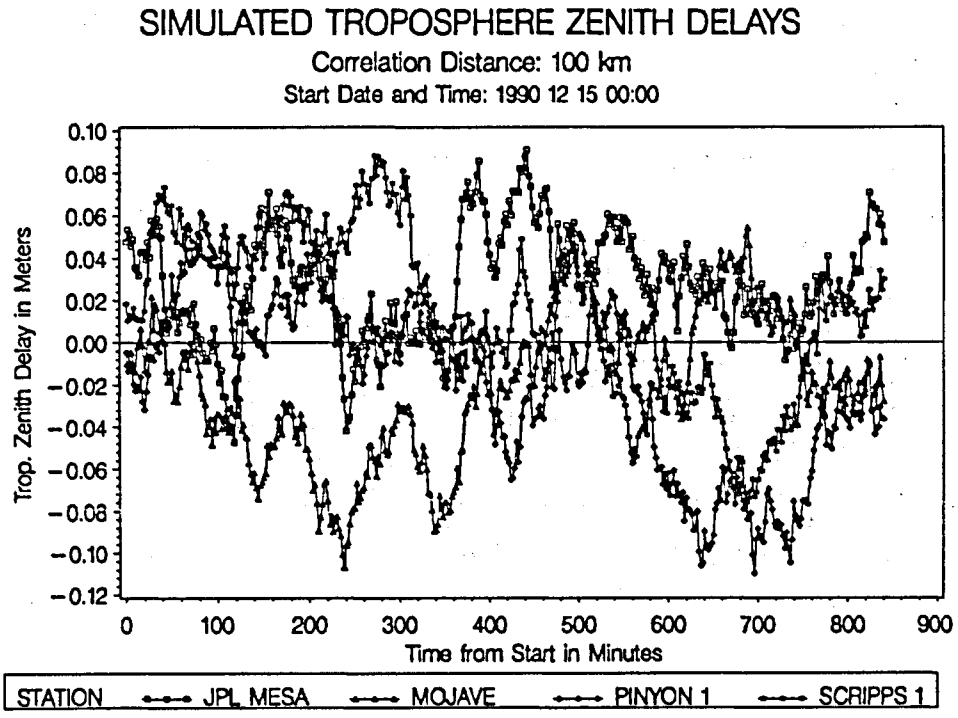

Figure 7.4

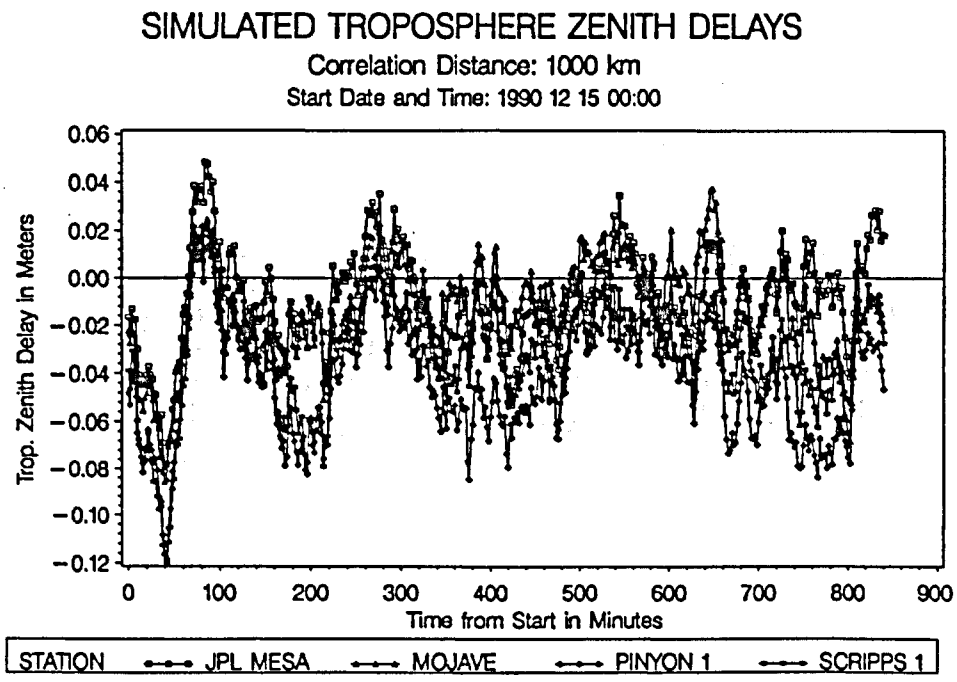

Figure 7.5

7.4 Simulation of Coordinate Biases

It is important to study the influence of coordinate biases (of fixed stations) on the estimated orbits.

The station coordinates are simply changed by adding random biases in height, north, and east direction according to a normal distribution with user specified characteristics.

An example of randomly generated coordinate biases is shown in Figure 8.4 .

Besides these random biases station coordinates may also be changed systematically (coordinates of all stations affected in the same way) to simulate common errors in a cluster of stations in a global network.

PART 2:

APPLICATIONS AND RESULTS

8. GIG'91 SIMULATIONS: GLOBAL GPS ORBITS

In this chapter we use simulated GPS data to study the effects of troposphere biases and biases in the fiducial site coordinates on the global orbit quality. Different baseline sets (regionally and globally distributed) are used in the orbit determination procedure. The resulting orbits are compared and the quality of coordinates estimated using these global orbits is discussed.

8.1 Global IERS and Geodynamic GPS Campaign (GIG'91)

8.1.1 Introductory Remarks

In December 1990 a project of the European Space Agency (ESA) was started at the Astronomical Institute, University of Berne, (in cooperation with the Institute of Physical Geodesy at the Technical University Darmstadt, Germany) to determine the locations of the globally distributed ESA tracking sites (see Figure 8.1) in a uniform, global reference frame using GPS [ESOC Contract, 1990]. The accuracy of the site coordinates aimed at was specified to be about 10 cm.

It is clear that up to now such a precise and uniform reference system could only be established by VLBI (Very Long Baseline Interferometry) or SLR (Satellite Laser Ranging). It was therefore decided, that VLBI and/or SLR sites with well known coordinates (so-called fiducial sites) should be occupied with GPS receivers during the same time as the ESA tracking sites to allow precise GPS satellite orbit determination within the reference system defined by VLBI and SLR and thus to realize the envisaged uniform reference frame for the ESA site estimation.

Because of the distribution of the ESA tracking sites (five in Europe, five outside Europe, see Figure 8.1) and in view of the limited number of GPS receivers available, the task was split up into two campaigns [ESA Proposal, 1990]:

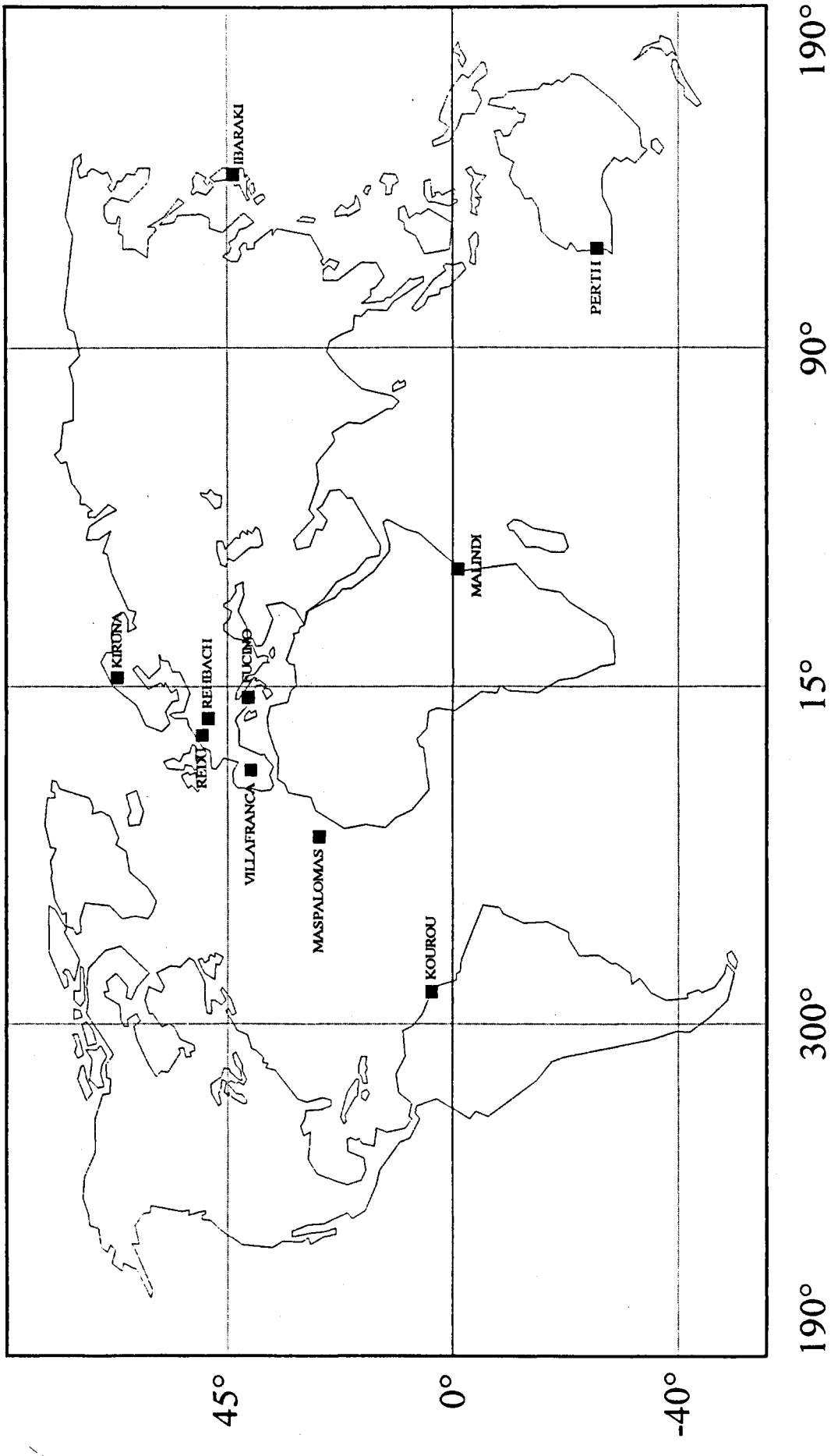

Figure 8.1
Location of the ESA Tracking Sites

(1) The **European ESA GPS Campaign** containing all the European ESA sites from Kiruna to Mas Palomas plus a limited number of fiducial sites in Europe. More details on this campaign may be found in Chapter 9.

(2) The **Global GPS Campaign:** A look at Figure 8.1 shows that it is necessary to determine the coordinates of the isolated points (Malindi, Ibaraki, Perth, and Kourou) using the data of a world-wide GPS campaign. These isolated points were therefore measured during the **First GPS IERS and Geodynamics Experiment GIG'91**, January 22 to February 13, when most of the VLBI and SLR sites were equipped with GPS receivers [IERS, 1990].

For this second campaign a preanalysis was performed as a part of the ESA project to answer the following two major questions:

- What are the sites that have to be included in the GPS campaign and the GPS data processing to ensure the site accuracy specified in the contract ?

- What quality of satellite orbits and site coordinates are attainable with such a global GPS campaign ?

Starting from these basic questions many problem areas showed up. In this chapter the results of this study will be presented.

The preanalysis contains the following steps:

(1) Selection of a reasonable set of sites (ESA tracking sites, fiducial sites, and auxiliary sites).

(2) Compilation of a set of orbital elements for all the satellites available during the GIG'91 Campaign.

(3) Computation of 4-day satellite arcs (December 10 to 13).

(4) Simulation of GPS data for these four days including data noise and troposphere biases.

(5) Definition of **clusters of sites** on different continents. Baselines were formed within each cluster and between clusters and common satellite visibilities were checked. Auxiliary sites were added to the network where necessary to get enough double difference observations.

(6) Processing of the simulated data to **estimate orbit parameters**, thereby fixing the fiducial sites on known coordinates and allowing for troposphere biases and/or biases in the fiducial site coordinates. Discussion of the orbit quality under different circumstances (biases, baselines used).

(7) Use of the orbits estimated in (6) to compute the **coordinates of the ESA tracking sites**, again allowing for different bias types. Discussion of the site coordinate accuracy for different orbit and processing types.

More details on the simulation and the processing strategies will be given below.

8.1.2 The GIG'91 Subnetwork Used in the Simulation

Due to the tremendous amount of data that was available from the GIG'91 Campaign we had to restrict ourselves to a manageable subset of fiducial sites to establish the reference frame. The following selection criteria were used:

- The site has to be a VLBI or SLR site with coordinates known in a global reference frame.

- The site should be located as closely as possible to an ESA site (the shorter the baseline length, the better the accuracy of the relative coordinates).

- 24 hour tracking of GPS satellites available during the entire GIG'91 experiment.

- Good geometry within the considered cluster: Baselines not too

long to ensure common satellite visibility, baselines not too short to allow for high precision orbit determination (single difference observations from short baselines contain almost no orbit information, see section 3.2.1).

- Receiver type used: sites occupied with P-code receivers are preferred.

The list of sites selected according to these criteria and used in the simulation study is given in Table 8.1 and Figure 8.2 shows a map containing these sites.

Station Name	State	Receiver Type	Co-Location	Type
Ibaraki	Japan	Trimble SST	---	ESA
Kiruna	Sweden	Ashtech LD-XII	---	ESA
Kourou	Fr. Guiana	Trimble STD	---	ESA
Malindi	Kenya	Ashtech LD-XII	---	ESA
Mas Palomas	Spain	Ashtech LD-XII	---	ESA
Perth	Australia	Trimble SLD	---	ESA
Canberra	Australia	Rogue	VLBI, SLR	FID
Hobart	Australia	Minimac 2816AT	VLBI	FID
Yarragadee	Australia	Rogue	SLR	FID
Goldstone	USA	Rogue	VLBI, SLR	FID
Kokee	USA (Hawaii)	Rogue	VLBI, SLR	FID
Richmond	USA	Rogue	VLBI, SLR	FID
Westford	USA	Rogue	VLBI, SLR	FID
Hartebeesthoek	South Africa	Rogue	VLBI	FID
La Silla	Chile	WM 102	SLR	FID
Santiago	Chile	Rogue	SLR	FID
Simosato	Japan	Trimble SST	SLR	FID
Tsukuba	Japan	Minimac 2816AT	VLBI (Mob.)	FID
Madrid	Spain	Rogue	VLBI	FID
Matera	Italy	Rogue	VLBI, SLR	FID
Onsala	Sweden	Ashtech LD-XII	VLBI	FID
Kaduna	Nigeria	Trimble SST	---	AUX
Quito	Ecuador	TI-4100, 7-Chan.	---	AUX

ESA: ESA Tracking Site FID: Fiducial Site AUX: Auxiliary Site

Table 8.1
List of Sites Selected from the GIG'91 Campaign for the Simulation Study

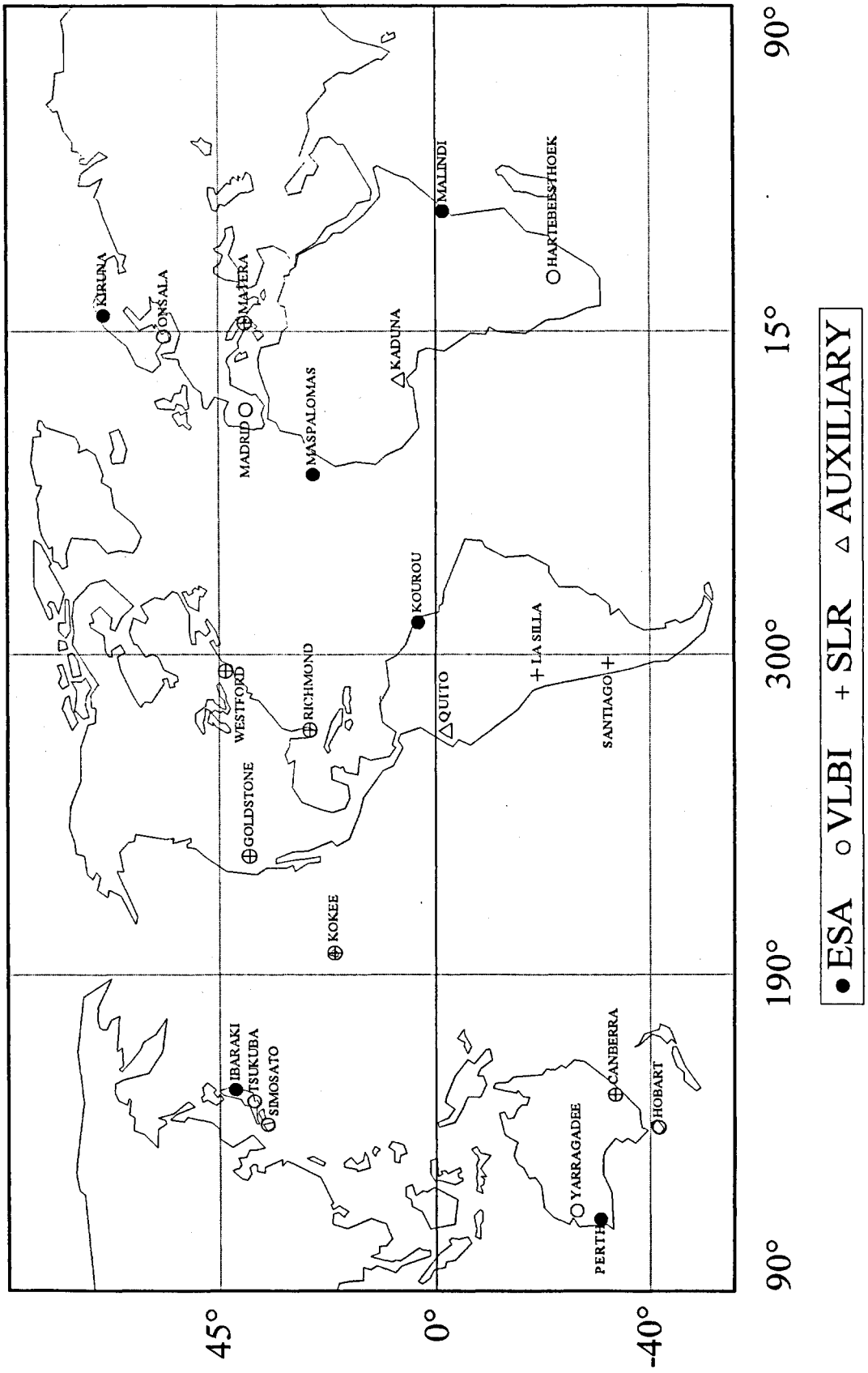

Figure 8.2
Map of Sites Selected from the GIG'91 Campaign for the Simulation Study

8.1.3 Simulated GIG'91 Data and Biases

8.1.3.1 Simulated GPS Observations

The simulation of GPS observations using the program SIMULA has been described in section 7.1. As a first step a list of coordinates for all the selected sites was compiled to be used in the simulation as **true** coordinate values.

Using an actual set of broadcast messages from December 10, 1990, a priori orbital elements were gathered for all the satellites. These orbital elements were the starting values for the generation of 4-day satellite arcs (December 10-13, 1990), the true orbits.

Using these true coordinates and orbits two sets of GPS phase and code observations were generated for the 4 days (December 10-13, day numbers 344-347, one day = one session): one set without, the other with troposphere biases.

The characteristics of the simulated data are listed in Table 8.2.

General Characteristics:		
Time span covered	:	December 10 - 13, 1990
Session definition	:	00:00 - 24:00
Number of sessions generated	:	4 sessions
Session length	:	24 hours
Number of Sites	:	23
Number of Satellites	:	15
Minimum satellite elevation	:	20 degrees
Data sampling rate	:	60 seconds
Observation Noise:		
Phase L_1 observation:		0.003 m
Phase L_2 observation:		0.003 m
Code L_1 observation:		1.000 m
Code L_2 observation:		1.000 m

Table 8.2
Characterization of the GIG'91 Data Simulation

The generation of the second set of simulated observations including troposphere biases was done using the same parameters as for the first set (data noise only). The type of tropospheric refraction errors generated for this second set will be discussed in section 8.1.3.2.

No ionosphere biases were introduced since in the coordinate and orbit estimation process the ionosphere-free linear combination L_3 (see 3.1.3) of the original L_1 and L_2 carrier phase measurements will be used.

Although for convenience the GPS data set was simulated for a time interval in December 1990, the results will be the same for January 1991 because the satellite constellation remains almost the same but shifted backward in time by 4 minutes per day.

8.1.3.2 Simulated Troposphere Biases

The tropospheric zenith delay biases were generated as described in section 7.3 using the parameter values given in Table 8.3.

Troposphere Modeling:		
Deterministic model	:	No deterministic model used
Stochastic process	:	First Order Gauss-Markov
RMS for constant tropo. bias	:	0.040 m (σ_c in 7.3)
Correlation distance	:	100 km (d^c, d^g in 7.3)
Power spectral density (PSD)	:	$1 \cdot 10^{-7}$ m^2/s (Φ in 7.3)
Correlation length in time	:	3600 s (β in 7.3)

Table 8.3
Parameters Used for the GIG'91 Simulation
of Troposphere Zenith Delay Biases

The constant zenith delays randomly generated with a variance σ_c^2 of 4 cm (see section 7.3) are compiled in Table 8.4 for all the sites used in the simulation study.

Station Name	Constant Troposphere Zenith Delay Biases (m)			
	Day 344	Day 345	Day 346	Day 347
Ibaraki	0.0287	-0.0342	-0.0576	0.0094
Kiruna	0.0045	0.0352	-0.0440	0.0499
Kourou	0.0566	-0.0296	-0.0115	0.0522
Malindi	0.0415	-0.0478	-0.0928	0.0778
Mas Palomas	0.0279	-0.0065	-0.0144	0.0283
Perth	-0.0093	-0.0148	-0.0129	-0.0492
Canberra	0.0246	-0.0585	0.0553	0.0129
Hobart	0.0067	0.0226	0.0550	-0.0049
Yarragadee	-0.0123	-0.0814	0.0425	0.0660
Goldstone	-0.0300	-0.0126	-0.0593	0.0078
Kokee	0.0063	0.0090	0.0560	-0.0591
Richmond	0.0157	-0.0559	0.0052	0.0115
Westford	-0.0270	0.0412	0.0082	-0.0043
Hartebeesthoek	-0.0814	-0.0390	0.0085	-0.0125
La Silla	0.0593	-0.0188	0.0195	0.0618
Santiago	0.0027	-0.0761	0.0698	-0.0112
Simosato	-0.0170	-0.0284	0.0330	0.0841
Tsukuba	0.0258	-0.0386	-0.0096	0.0125
Madrid	-0.0251	-0.0347	0.0241	-0.0244
Matera	-0.0365	0.0212	0.0012	-0.0849
Onsala	-0.0555	-0.0241	0.0678	-0.0411
Kaduna	-0.0265	0.0121	0.0273	0.0498
Quito	-0.0255	0.0209	0.0082	0.0234

Table 8.4
Constant Troposphere Zenith Delay Biases for Each Site and Session of the GIG'91 Simulation Study

An example for the variations in the delays because of the stochastic process is shown in Figure 8.3.

Due to the long distances in this global network spatial correlations of the tropospheric refraction between sites are negligible although they were taken into account.

The tropospheric zenith delays for the same site were computed independently for each day (session). This may not be very realistic since the weather conditions might as well be similar from one day to the next. With the formulae developed in section 7.3 it would easily be possible to generate tropospheric zenith delays not only correlated with distance but also from one day to

the next (same time of the day). From section 3.2.2.1, however, it is also clear that a mean tropospheric zenith bias over the four days of simulated data will have more or less the same effect on the orbits as a bias in the height of the site. Site coordinate biases (for fiducial sites) will be dealt with in the next section.

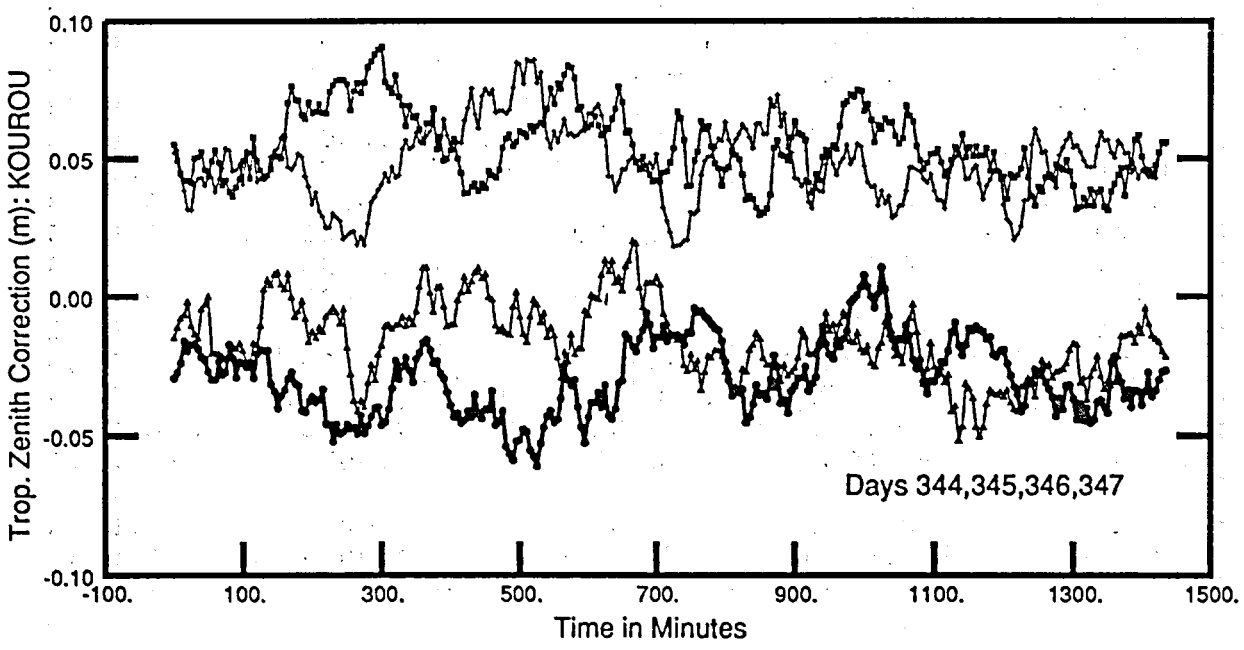

Figure 8.3
Tropospheric Zenith Delays for the Site Kourou Simulated Using a Stochastic Process

8.1.3.3 Simulated Fiducial Coordinate Biases

The simple procedure to simulate errors in the fiducial site coordinates has been outlined in section 7.4. The fiducial site coordinates were randomly changed by a few centimeters compared to the "true" set according to the following sigmas (assuming a normal distribution):

Sigma of coordinate changes in north direction:	0.030 m
Sigma of coordinate changes in east direction:	0.030 m
Sigma of coordinate changes in height :	0.050 m

Thus the coordinates of a fiducial site may be wrong by up to 9 cm in horizontal position and up to 15 cm in height. We will refer to this biased coordinate set as "AS". According to the institutes producing VLBI and SLR global solutions, the errors in the coordinates of the fiducial sites should be smaller.

The actual coordinate biases generated may be found in Table 8.5. For the fiducial sites closest to the ESA tracking sites the values are plotted in Figure 8.4.

Station Name	Coordinate Biases		
	Δ North (m)	Δ East (m)	Δ Up (m)
Canberra	0.026	0.016	0.133
Hobart	0.002	0.003	-0.064
Yarragadee	-0.019	0.004	-0.017
Goldstone	0.033	0.007	-0.049
Kokee	0.010	-0.063	0.090
Richmond	-0.044	-0.062	0.020
Westford	-0.022	0.034	0.107
Hartebeesthoek	-0.020	-0.035	0.039
La Silla	-0.040	-0.005	-0.075
Santiago	-0.022	-0.041	-0.056
Simosato	-0.031	-0.019	0.016
Tsukuba	-0.008	-0.033	0.099
Madrid	0.020	-0.023	0.014
Matera	0.000	0.084	0.054
Onsala	-0.030	0.021	-0.037

Table 8.5
Coordinate Biases for all the Fiducial Sites used in the GIG'91 Simulation Study

By fixing the fiducial sites at the "biased" locations in the orbit estimation step biases are introduced into the orbits. Biases are then introduced into the coordinates of the ESA sites, too, directly by the wrong fiducial coordinates fixed and indirectly by the "biased" orbits.

In addition to the coordinate set AS we created three different coordinate sets to study the influence of systematical errors in the fiducial site coordinates. In the first set all the Australian fiducial sites are shifted by the same considerable

amount of 50 cm in height, in the second by 50 cm in north direction, and in the third set by 50 cm in east direction (see Table 8.6).

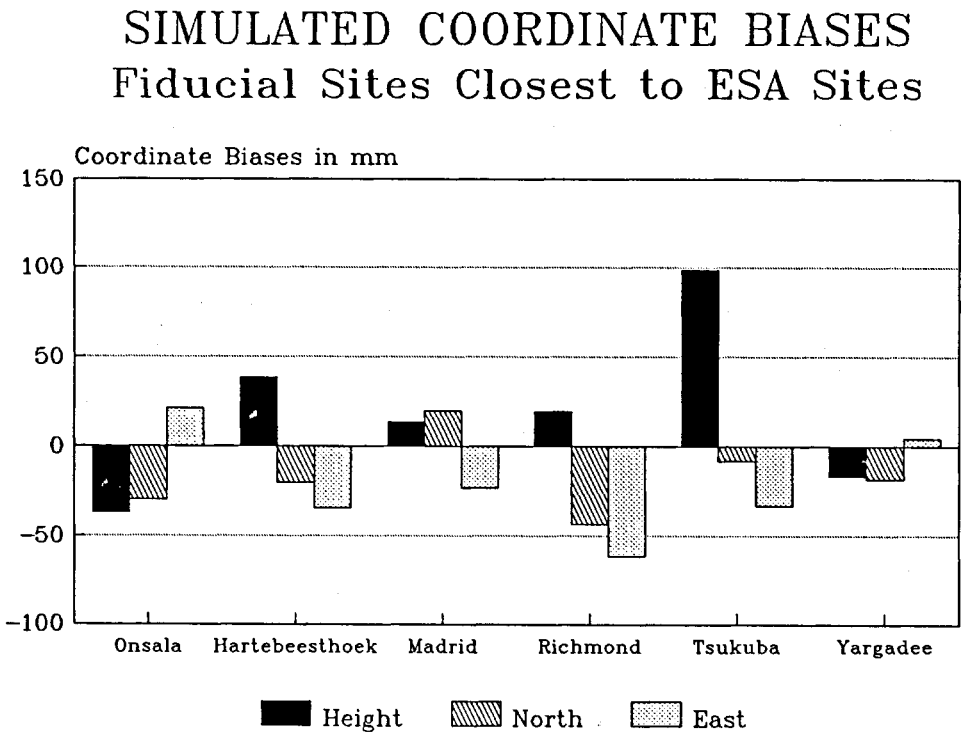

Figure 8.4

Coord. Set	Direction of Shift	Shift
AH	Height	50 cm
AN	North	50 cm
AE	East	50 cm

Table 8.6
Coordinate Sets with Systematic Shifts in the Australian Fiducial Site Coordinates

8.1.3.4 Simulated Orbit Biases

Two types of orbital errors were investigated in this study.

First, orbital biases are produced by introducing troposphere biases or by fixing the fiducial sites at wrong coordinates. In contrast to these indirect orbital biases we also produced orbit errors (see section 7.2) by randomly changing the "true" orbital elements in order to generate orbits with biases of the order of 0.5 to 1.0 m. The sigmas of the normal distributions used for the generation of the errors in the orbital elements are summarized in Table 8.7, a typical example for the differences between the true orbits and the biased orbits is given in Figure 8.5.

Orbital Element		Sigma used for Random Errors
a	Semi major axis	$\sigma_a = 0.002$ m
e	Eccentricity	$\sigma_e = 2 \cdot 10^{-8}$
i	Inclination	$\sigma_i = 0.001"$
Ω	Ascending Node	$\sigma_\Omega = 0.001"$
ω	Perigee	$\sigma_\omega = 0.001"$
u_0	Argument of Latitude	$\sigma_{u\,0} = 0.002"$
p_0	Direct Rad.Press.Coe.	$\sigma_{p\,0} = 10^{-10}$ m/s^2
p_2	Y-bias Coefficient	$\sigma_{p\,2} = 0$ m/s^2

Table 8.7
Sigmas for the Generation of Random Biases in the Orbital Elements for the GIG'91 Simulation Study

To see the influence of these "biased" orbits on the estimation of the ESA tracking site coordinates these "biased" orbits instead of the "true" orbits were used in the computations.

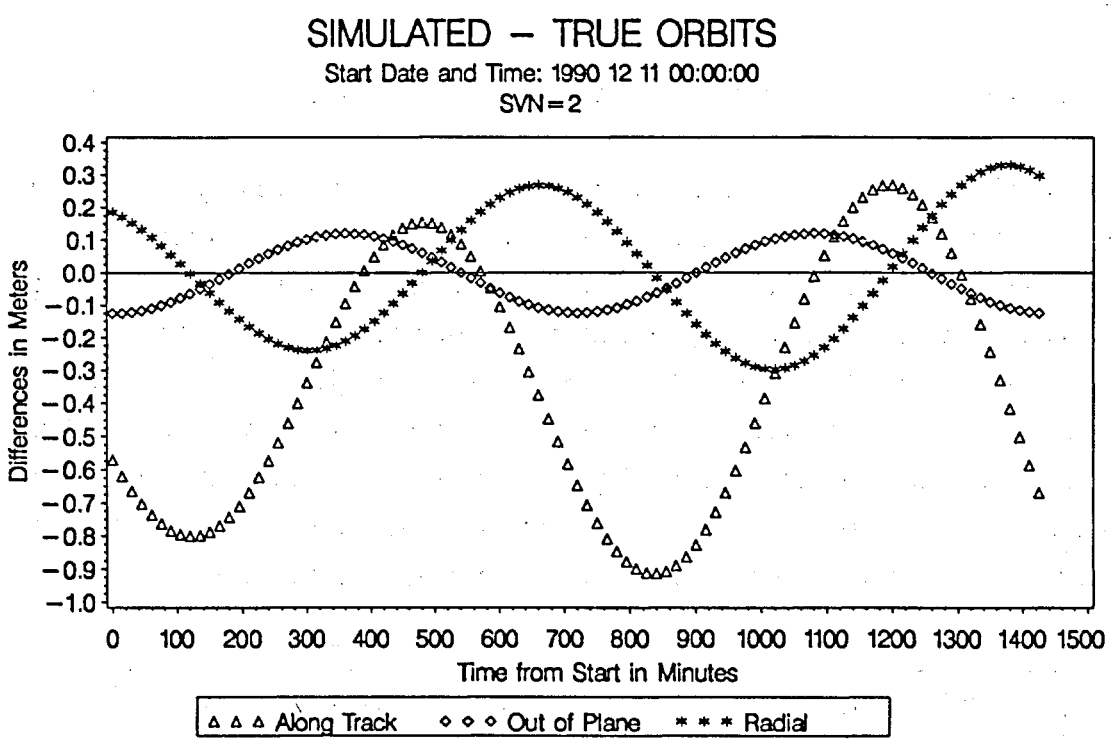

Figure 8.5

8.2 Processing Strategy and Solutions

8.2.1 Processing Strategy

Due to the distances between continents we decided to form clusters of sites on different continents (one cluster in Europe, one in the U.S.A., one in Australia, and one in Japan, see baseline set A defined in Figure 8.6). Each of these clusters must contain one or more fiducial sites. The different clusters are then linked to each another via the fiducial site coordinates given in a global reference frame and not via extremely long GPS baselines from cluster to cluster. For test purposes, however, we also formed the inter-cluster baselines to see the differences we get in the results when introducing these baselines, too (see baseline set B defined in Figure 8.7).

BASELINE SET A FOR ORBIT DETERMINATION

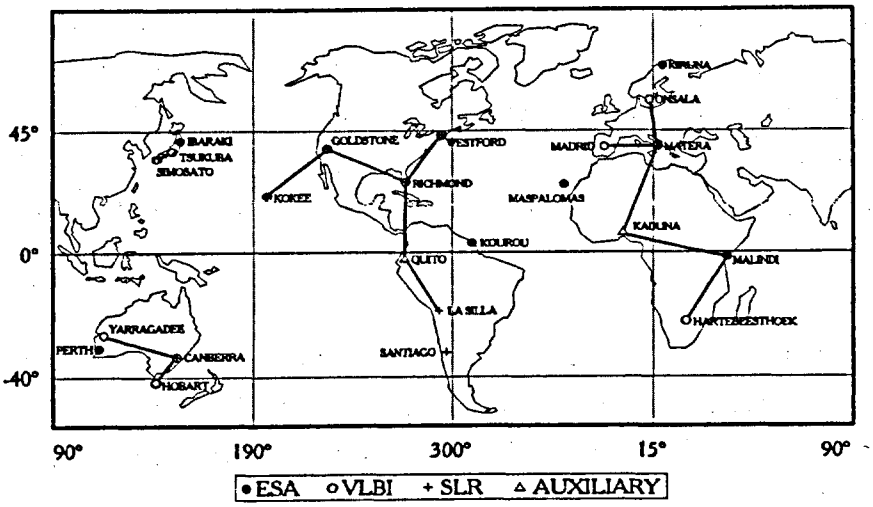

BASELINE SET B FOR ORBIT DETERMINATION

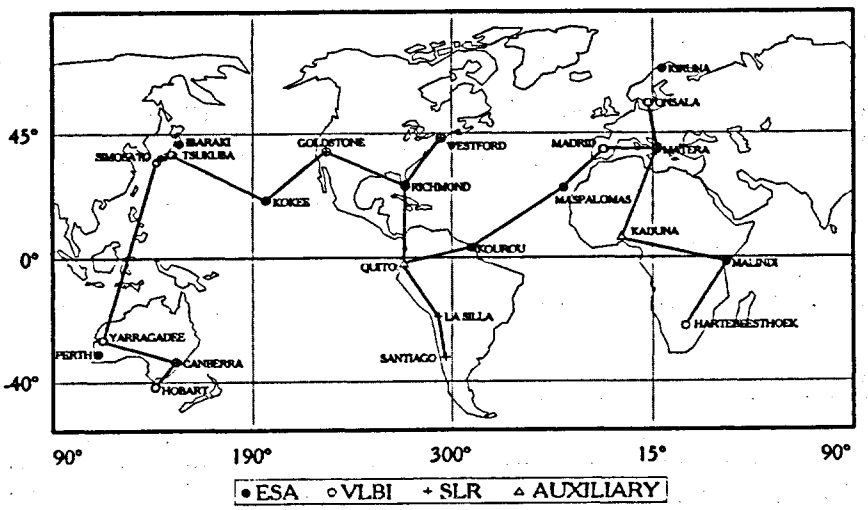

BASELINE SET C FOR ESA SITE DETERMINATION

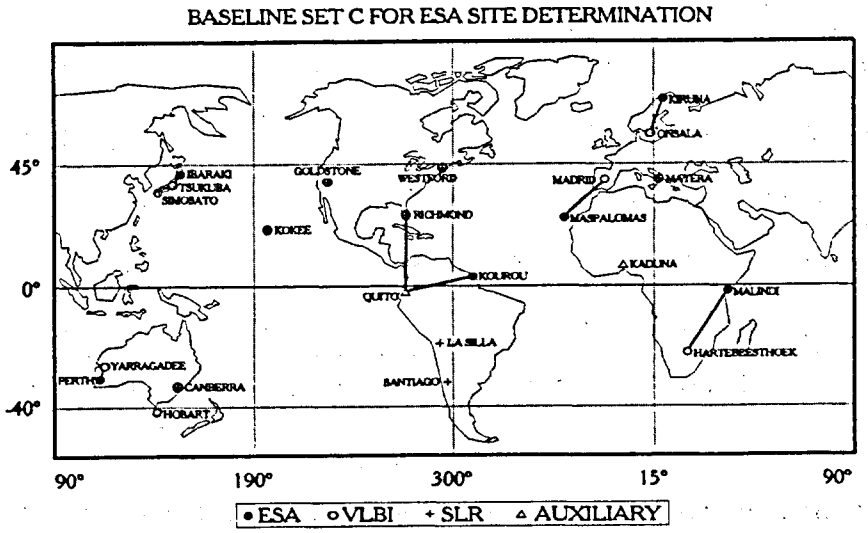

Figures 8.6, 8.7, 8.8

Data were processed in two steps:

Step 1: The baselines between the fiducial sites (and the necessary auxiliary sites) were used to estimate the satellite orbits. The coordinates of one or more fiducial sites per cluster were fixed. Due to the data noise and the different biases introduced the estimated orbits differed from the "true" orbits.

For this first step different baseline sets were used and the number of fiducial sites fixed was varied (see Table 8.8). The set **UE** contains the data of two clusters on the same hemisphere whereas set **UA** the data of one cluster on each hemisphere.

Step 2: The orbits estimated in step 1 were used together with the baselines connecting the ESA tracking sites with the fiducial sites (baseline set C, see Figure 8.8) to estimate the coordinates of the ESA sites. Due to the data noise, the different biases introduced, and the quality of the estimated orbits, the estimated ESA site coordinates differed from the "true" coordinates.

Set	Baselines Used	Fiducial Sites Fixed
A	All baselines within the clusters (see Figure 8.6)	All
B	All baselines (within and between clusters, see Figure 8.7)	All
1P	Baselines of set A	One per cluster *)
US	U.S. baselines only	U.S. Fiducials
UE	U.S. and European baselines	U.S. and Europe
UA	U.S. and Australian baselines	U.S. and Australia

*) Canberra, Goldstone, Hartebeesthoek, Madrid, La Silla, Tsukuba

Table 8.8
Baselines Used and Fiducial Sites Fixed for Different Orbit Estimation Runs

In all program runs uniquely the ionosphere-free linear combination L_3 was used (see section 3.1.3).

No attempt was made to estimate troposphere parameters in order to reduce the influence of troposphere biases, nor did we try to diminish the effect of the wrong fiducial site coordinates (e.g. by putting a priori constraints on the coordinates instead of fixing them).

8.2.2 Solution Types

According to the processing strategy outlined in the previous section and the different baseline sets listed in Table 8.8 solutions were produced with all the different combinations of biases. The list of the solutions computed in connection with set A is given in Table 8.9.

Solu. No.	Set used	Trop. Biases	Coor. Biases	Orbit Biases	Coo./Orb. Results
1	A *)	---	---	---	AA
2	A *)	yes	---	---	AATR
3	A *)	---	yes	---	AACO
4	A *)	yes	yes	---	AATRCO
5	C *)	---	---	AA	CCAA
6	C *)	yes	---	AATR	CCAATR
7	C *)	---	yes	AACO	CCAACO
8	C *)	yes	yes	AATRCO	CCAATRCO
9	A	---	AH	---	AAAH
10	A	---	AN	---	AAAN
11	A	---	AE	---	AAAE
12	C	---	AH	AAAH	CCAAAH
13	C	---	AN	AAAN	CCAAAN
14	C	---	AE	AAAE	CCAAAE
15	C	---	---	yes	CCOR
16	C	yes	---	yes	CCTROR
17	C	---	yes	yes	CCCOOR
18	C	yes	yes	yes	CCTRCOOR

*) The same solutions were produced for all the baseline sets given in Table 8.8.

Table 8.9

Solutions Computed for the ESA Preanalysis Study

The different solution types are:

1-4 : Orbit Determination with different error sources.
5-8 : Estimation of ESA site coordinates using the orbits estimated in 1-4.
9-11: Orbit determination with systematically biased Australian fiducial site coordinates.
12-14: Estimation of ESA site coordinates using the orbits estimated in 9-11.
15-18: Estimation of ESA site coordinates using randomly biased orbits according to section 8.1.3.4 .

8.3 Results

8.3.1 Global Orbit Quality

In this section we discuss the orbit results obtained in the orbit determination runs as defined by solutions 1-4 and 9-11 in Table 8.9.

8.3.1.1 The A Posteriori rms Error of the Phase Observation in Orbit Determination

Figure 8.9 shows the estimates of the a posteriori rms error m_0 for the different baseline sets (see Table 8.8, Figures 8.6 and 8.7) and the various error models used.

If the only error source is data noise, m_0 is identical with the noise σ_0 = 3 mm used in the simulation (see Table 8.2). If we add troposphere or coordinate biases to the error model, m_0 increases by about 60 %, if both effects are added m_0 is roughly doubled. It is worthwhile noting that coordinate biases obviously do not show up in m_0 if only data from one cluster are used (baseline set US) or if only one fiducial site per cluster is kept fixed. This means that in these cases coordinate biases may not be detected by comparing m_0 to the theoretical a priori value σ_0 and that the orbits may have undetectable systematic errors.

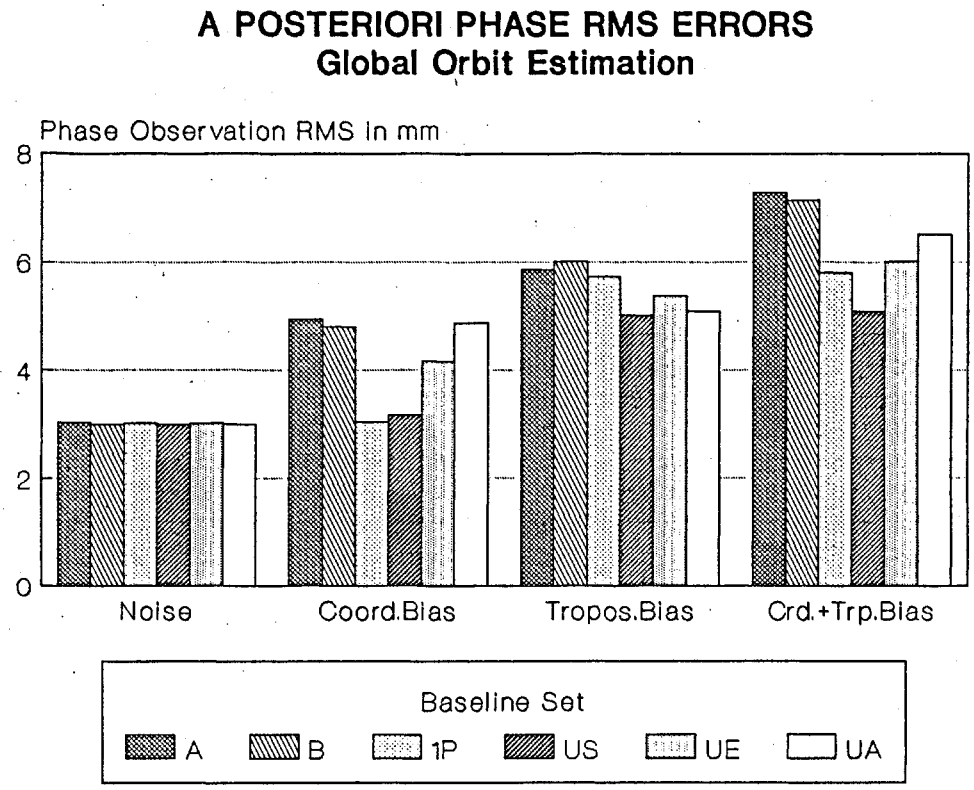

Figure 8.9

As soon as more than one cluster of fiducials is involved, the inconsistencies can no longer be absorbed by rotating or scaling the orbits, especially if we have clusters on both hemispheres (compare set UA to UE).

Below we will present the rms errors for the orbital parameters only for the case "data noise". The corresponding values for the cases "noise + troposphere biases", "noise + coordinate biases", and "noise + troposphere + coordinate biases" are easily obtained by multiplying the presented formal errors by

$$f = \frac{\text{rms of biased solution}}{\text{rms of unbiased solution}} \qquad (8.1)$$

where these values may be extracted from Figure 8.9 .

8.3.1.2 Formal Errors of Orbit Parameters

Figures 8.10(a)-8.10(h) contain for each orbit parameter the mean value of the associated formal error (mean over all satellites). Using formulae (7.2) to (7.10) we can deduce the corresponding formal errors of the satellite positions. The most important contributions come from the argument of latitude (about 2.5 m for set B), the ascending node (1.2 m), and the inclination (1 m). These numbers give, however, only a rough idea of the orbit precision.

For the set US the formal errors are by a factor of 2.5 (Y-bias) to 9 (inclination) larger as compared to those using set B. (We will see similar results in 8.3.1.3). By adding a second cluster to the set US the formal errors are considerably reduced, especially for the angular elements.

Formal Errors of the Satellite Positions:

In Figures 8.11 to 8.13 the formal errors in the satellite positions (using the six different baseline sets) are given for satellite 2 in radial, along track, and out of plane directions (see Figure 6.1) over a time interval of four days. They were computed using the formulae given in section 6.1.2 .

We see short period variations (with a period of one satellite revolution). Apart from this periodic behaviour the formal errors grow towards the boundaries of the arc (especially in along track direction, due to the error in the mean motion), showing that the orbital positions are best determined in the middle of the arc. If the satellite orbit has to be extrapolated, the formal errors (as well as the actual errors) will grow rapidly.

As expected there are significant differences in the strengths of the solutions: the orbits based on the US fiducial sites only are about 5-6 times less precisely determined than the orbits using the complete set of fiducial sites.

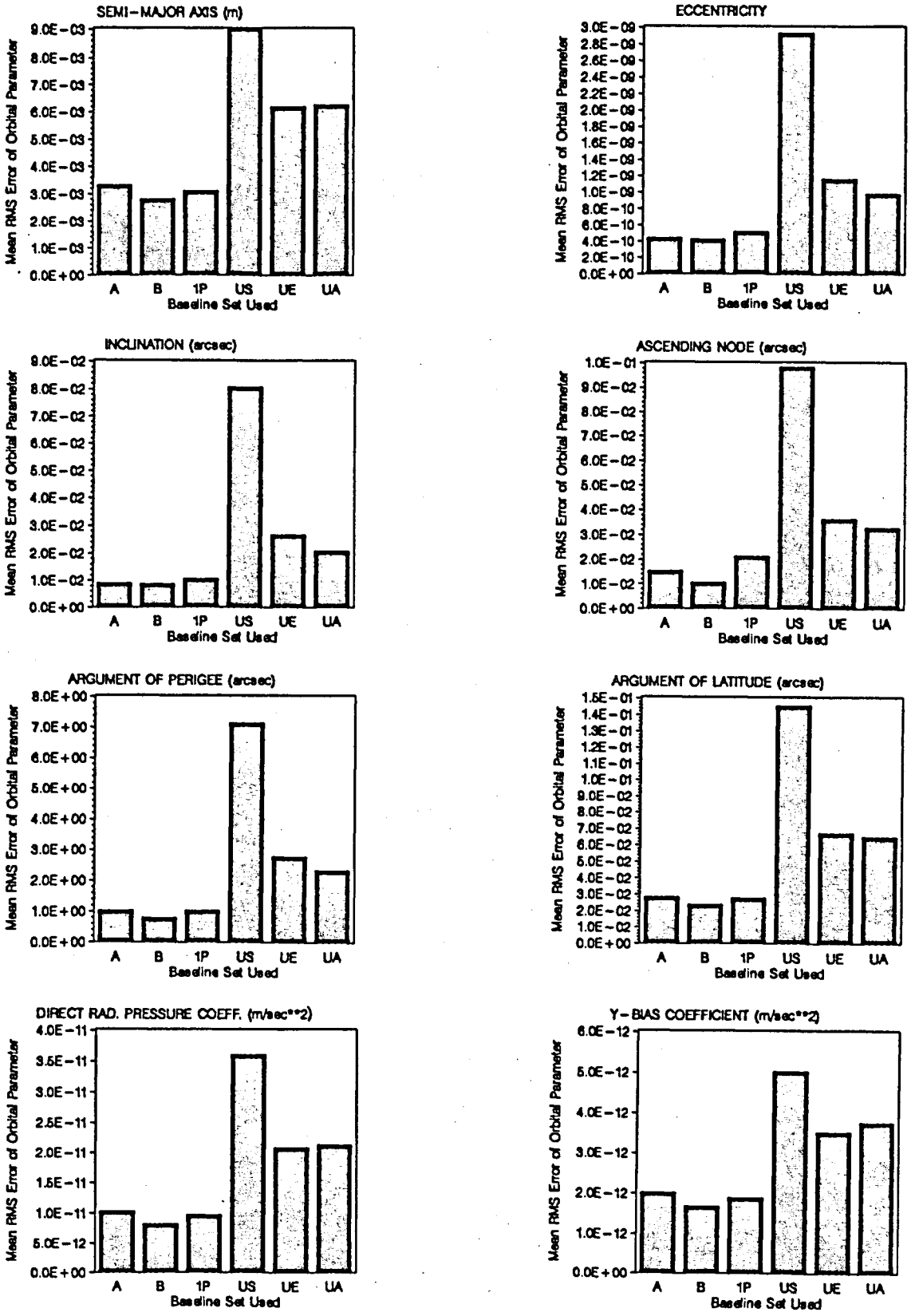

Figure 8.10

Mean Formal Errors of the Orbital Parameters for Solution 1 (Table 8.9) Using Different Baseline Sets (Table 8.8)

FORMAL ORBIT ERRORS: DATA NOISE ONLY
Start Date and Time: 1990 12 10 00:00:00

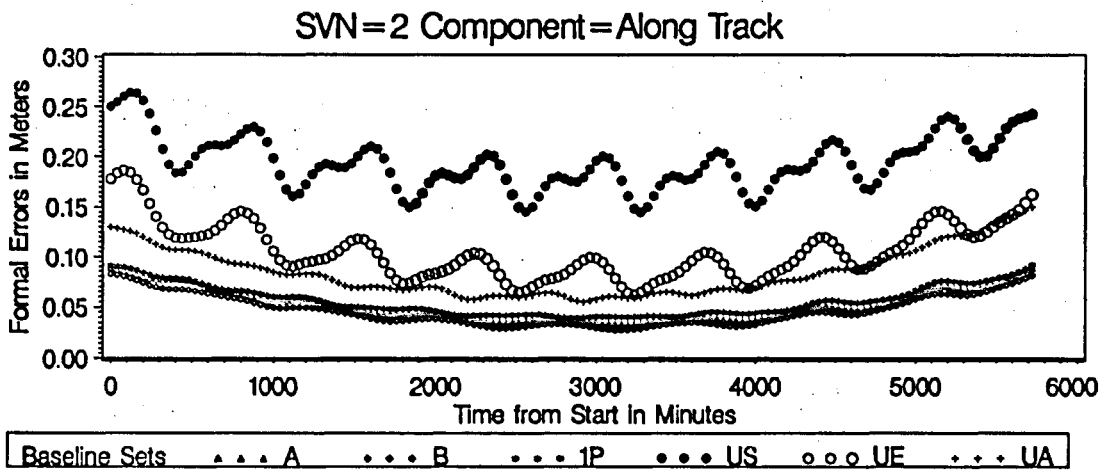

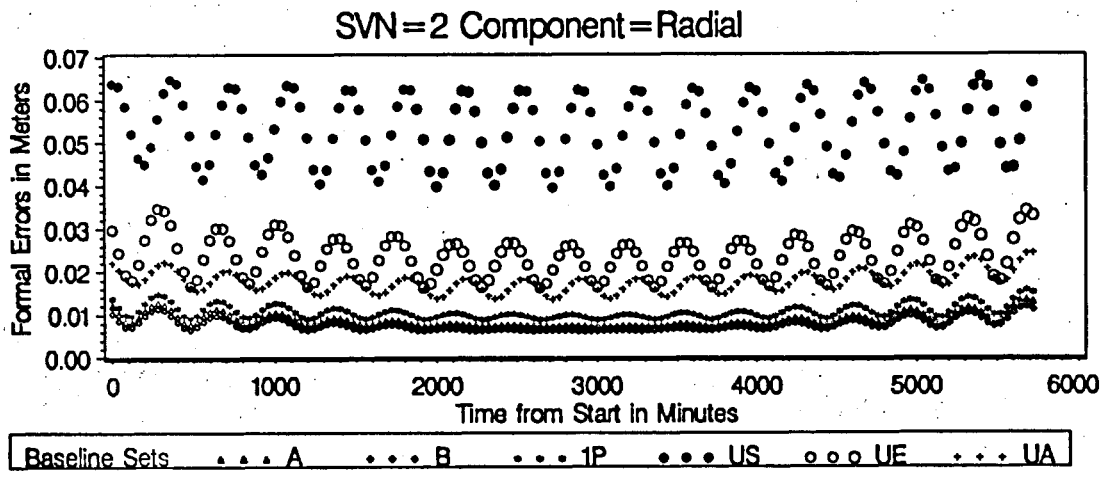

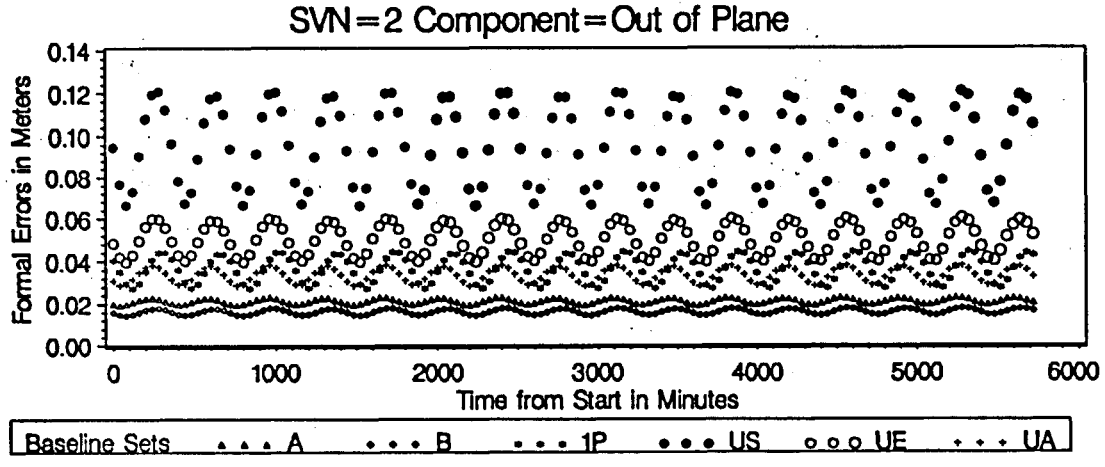

Figures 8.11, 8.12, 8.13

To have GPS data available from two clusters for orbit determination (set UE) already helps considerably, in particular if the two clusters are on different hemispheres (set UA). The differences between the sets A, B, and 1P, finally, are quite small and demonstrate, that global orbit improvements may be successful using only few clusters of fiducial sites.

We should point out that the formal errors of the satellite positions, even using the best case (set B), are already of the order of 10 to 30 cm without including biases (data noise only). The estimation of GPS satellite orbits with an accuracy of a few centimeters using double difference observations seems therefore unlikely in the near future.

Formal Errors of Relative Satellite Positions:

The motivation to study relative satellite positions was given in section 6.1.3. Let us select four satellites (SVN 2, 6, 9, and 13) visible from the US fiducial sites during the window in the frame of the satellite visibility plot in Figure 8.14.

In Figures 8.15 and 8.16 the formal along track errors of the four satellites are given for set A and set US on day 345. The visibility window is again indicated by the frame.

Within the window the formal along track errors of set A are about 1/3 those of set US.

Figures 8.17 and 8.18 correspond to Figures 8.15 and 8.16 but show the formal errors of the satellite positions relative to satellite 13 (formulae for the computations were given in section 6.1.3).

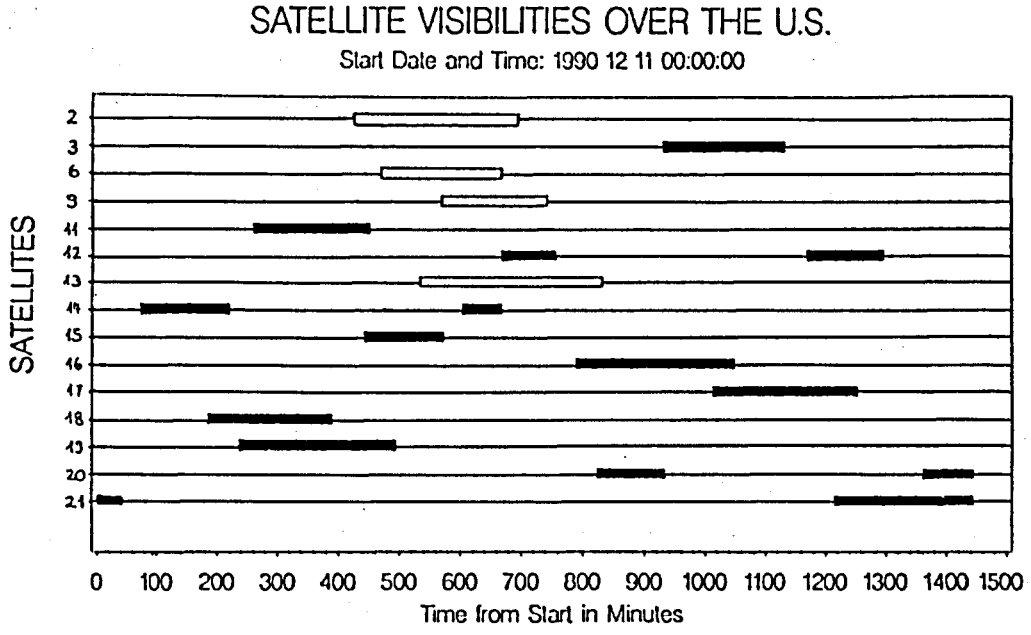

FORMAL ERRORS OF SAT. POSITIONS: DATA NOISE ONLY
Start Date and Time: 1990 12 11 00:00:00

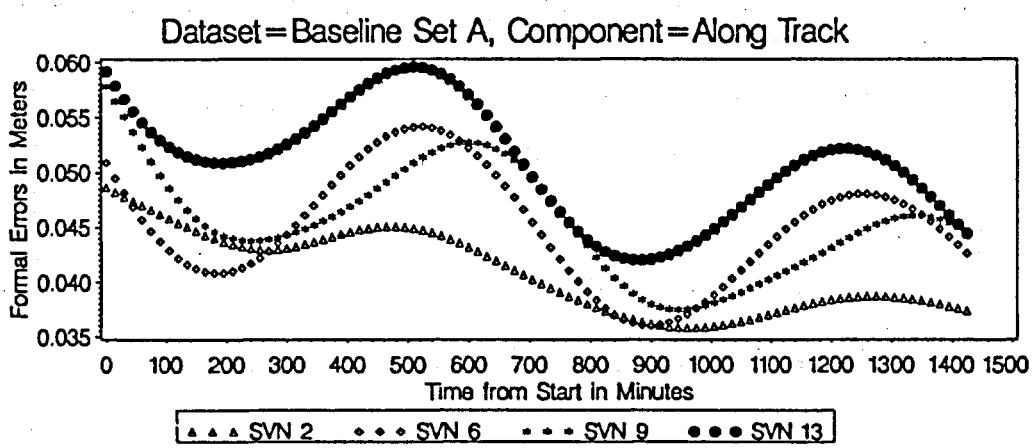

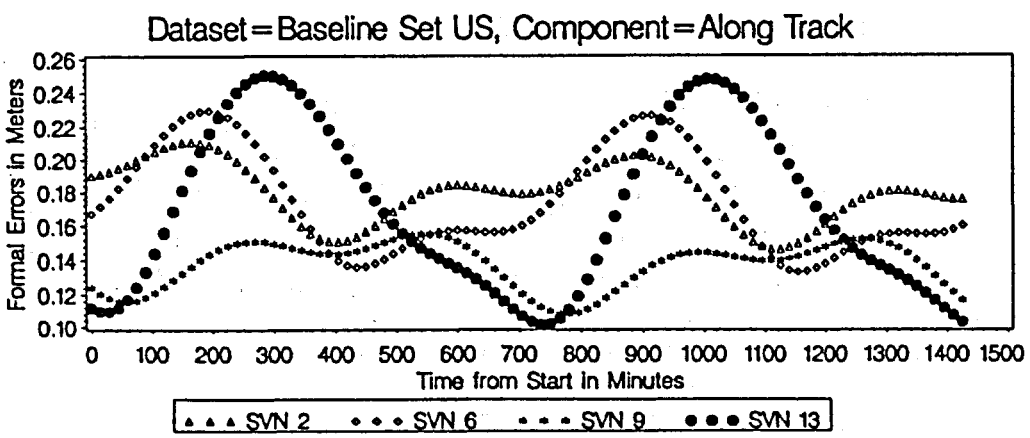

Figures 8.14, 8.15, 8.16

FORMAL ERRORS OF RELATIVE SAT. POSIT.: DATA NOISE ONLY
Start Date and Time: 1990 12 11 00:00:00

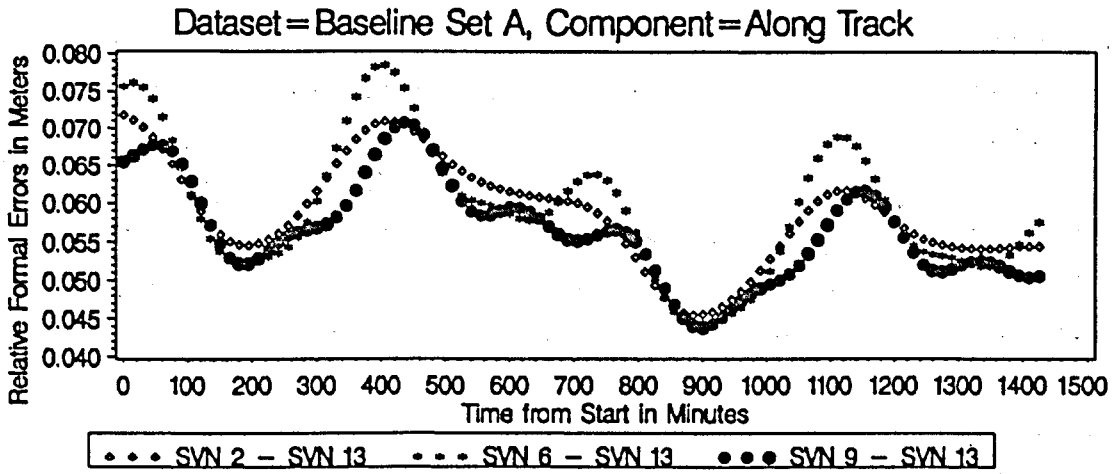

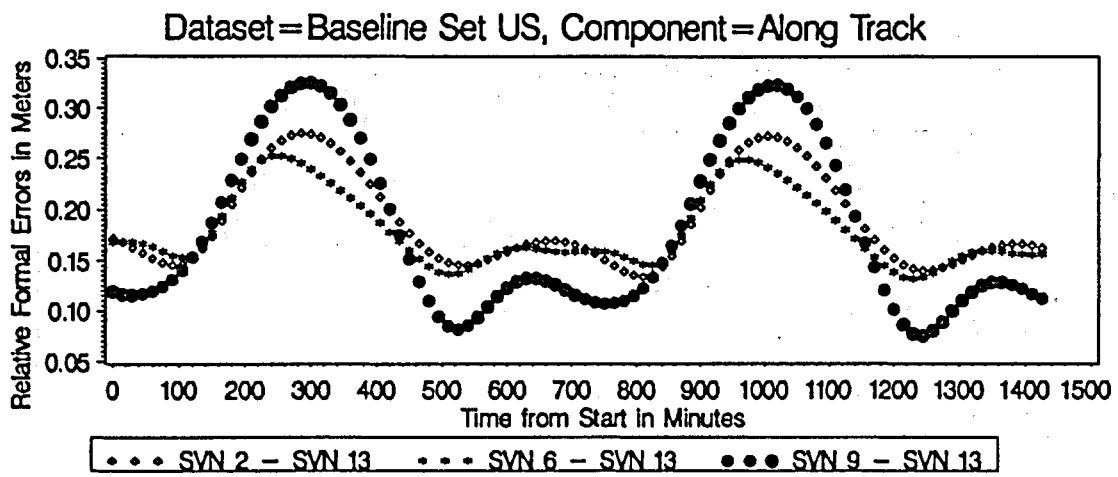

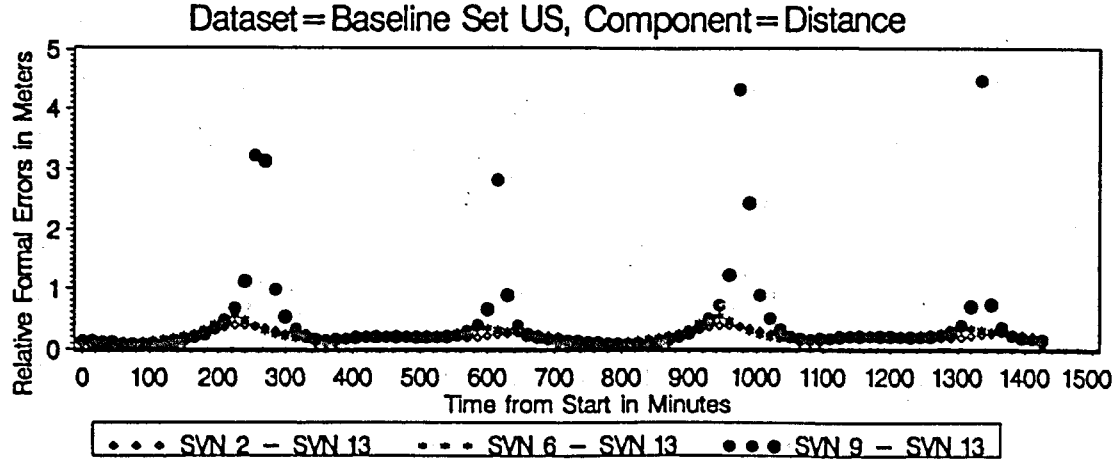

Figures 8.17, 8.18, 8.19

Whereas no big differences exist between the absolute and relative formal errors for set A (Figures 8.15 and 8.17), we see that for the set US the formal errors of the relative satellite positions over the US are much better than for the rest of the world.

When looking at the formal errors of distances between satellites (see Figure 8.19) we notice a strange effect in the satellite pair (9,13).

This effect is due to a relatively close encounter of the two satellites twice per revolution. Figure 8.20 shows the distances between satellite 9 and 13. SVN 9 revolves the earth in plane A, SVN 13 in plane C (see Figure 2.7) and both satellites arrive at the intersection of the two orbital planes at about the same time (see Figure 8.21).

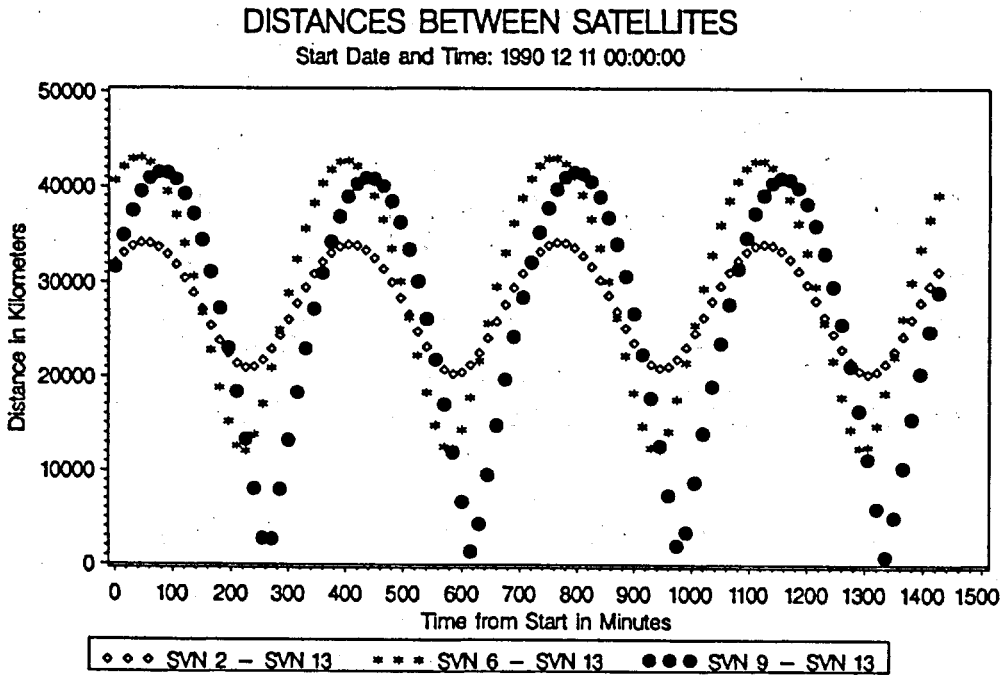

Figure 8.20

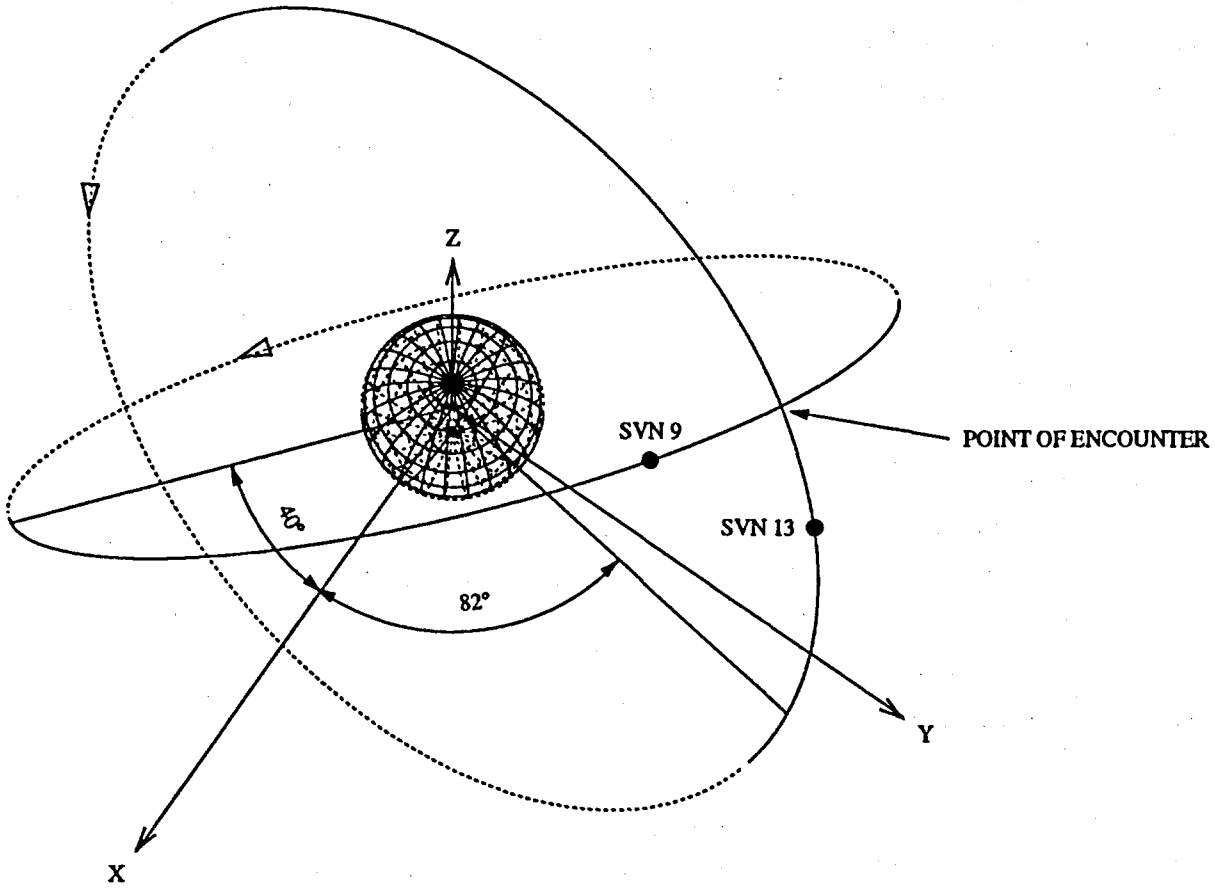

Figure 8.21
"Close" Encounters Between Satellites SVN 9 and SVN 13.
Satellite SVN 9 is located in Plane A, SVN 13 in Plane C.
December 11, 1990

8.3.1.3 Comparisons with the True Orbits

In this section we make use of the fact, that in the case of simulations we have the "true" orbits available for comparisons.

Comparison of Orbital Elements:

Figures 8.22(a)-(h) show the mean of the differences (absolute value) between the estimated and the "true" orbit parameters for the case "noise + troposphere + coordinate biases" (see Table 8.9). These differences do not show as strong a dependence on the baseline set used as the formal errors (see Figures 8.10(a)-(h)). They are also larger by almost an order of magnitude than the

corresponding formal errors. (The formal errors for solutions of type 4 (see Table 8.9) are given by the values in Figures 8.10(a)-(h) for solution type 1, multiplied by approximately a factor f=2 (see eqn. (8.1))). This makes it clear that large systematic errors have been introduced into the orbital parameters (due to the troposphere and coordinate biases) that are not reflected by the formal errors.

Comparison of Satellite Positions:

In the section on formal errors we have seen that already the data noise leads to formal errors in the satellite positions of 10 to 30 cm. This is confirmed by the differences between the orbits estimated using baseline set A and the true orbits for day 345 given in Figures 8.23 to 8.25 (radial, along track, and out of plane directions).

As usual the along track component shows the largest errors followed by the out of plane, and the radial component.

In Figures 8.23 to 8.25 we also see the effect of the troposphere and coordinate biases (see section 8.1.3.2 and 8.1.3.3) on the orbit quality: the troposphere biases do not degrade the orbit quality very much, whereas the effect of the wrong fiducial site coordinates is clearly visible. The maximum orbit errors due to the coordinate biases are of the order of 10 cm, 80 cm, and 20 cm for the radial, along track, and out of plane component respectively for satellite 9 shown here. For some satellites they are even larger (by up to a factor 4).

The dependence of the orbit quality on the baseline set used shows the same characteristics as in the case of the formal errors. Figure 8.26 is included as an illustration. The quality improvement from the weakest baseline set (US) to the strongest set (B) is about a factor of 5, when averaging over all satellites.

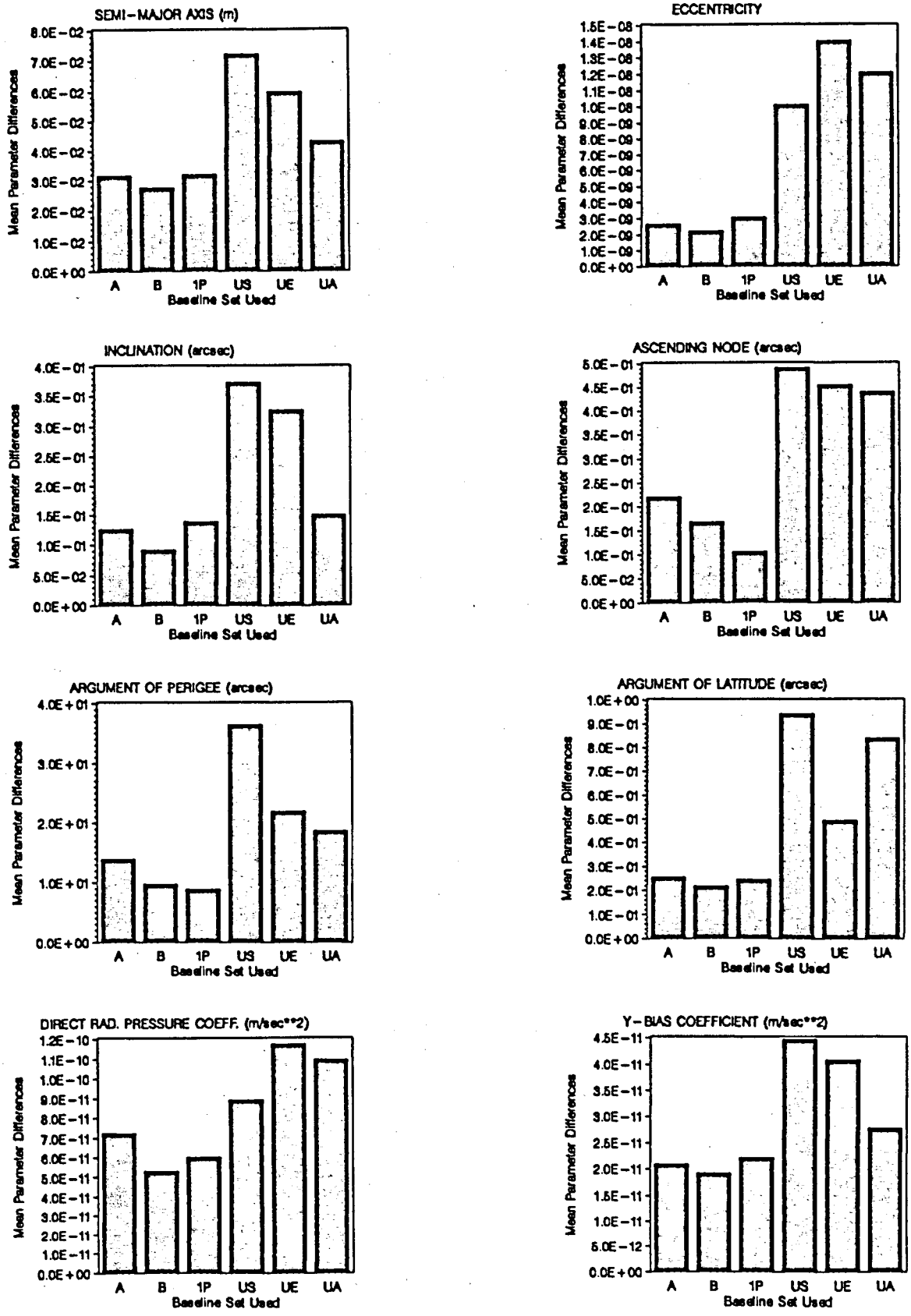

Figure 8.22

Differences Between Estimated And True Orbit Parameters, Mean Over All Satellites

ESTIMATED - TRUE ORBITS: BASELINE SET A
Start Date and Time: 1990 12 11 00:00:00

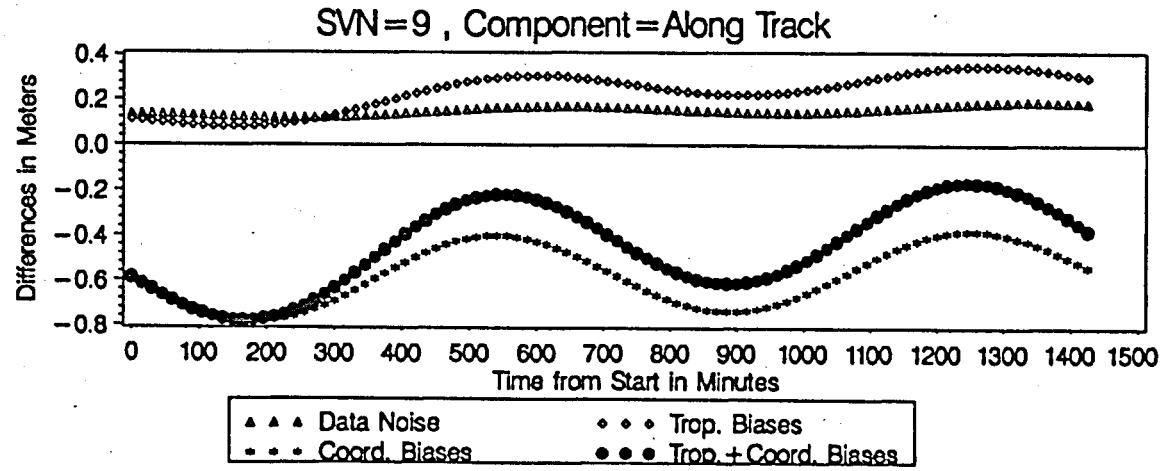

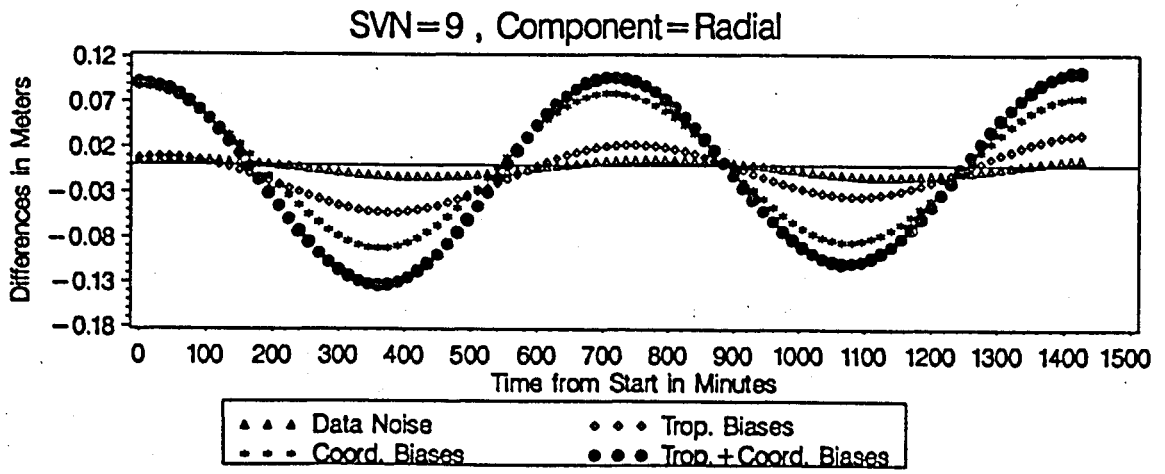

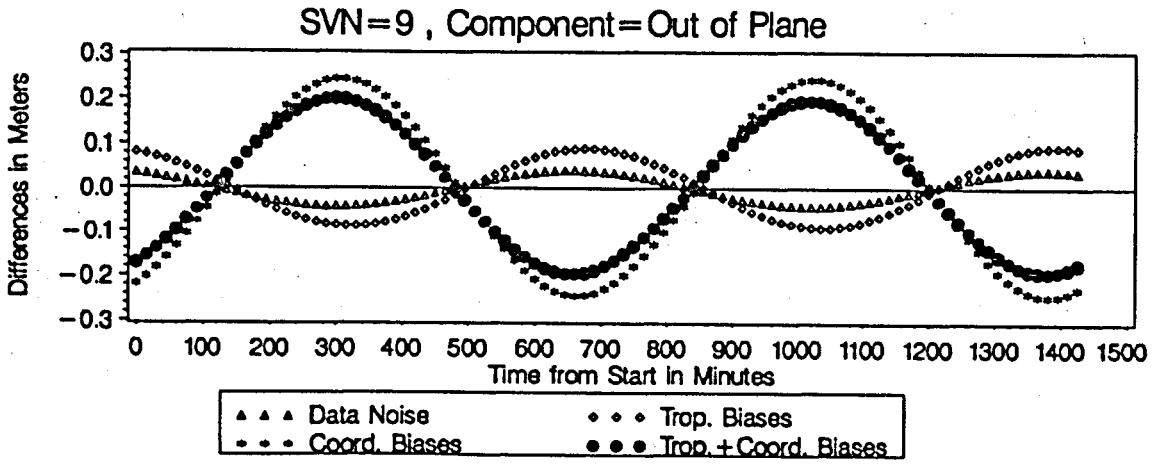

Figures 8.23, 8.24, 8.25

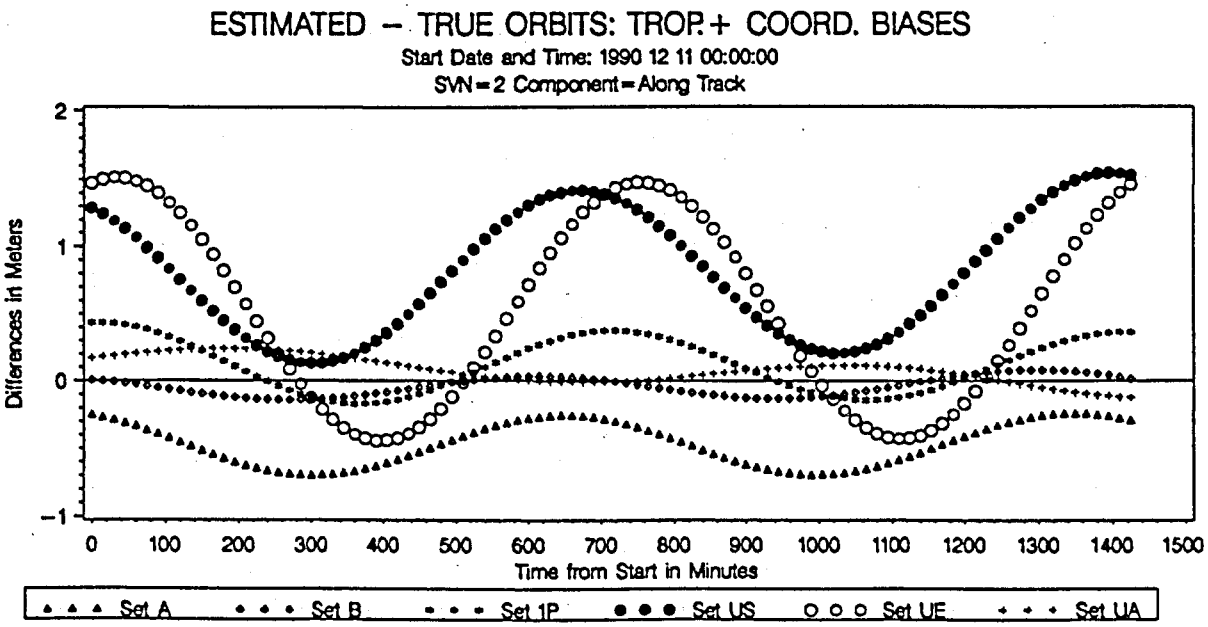

Figure 8.26

The best global (and regional) orbits that may be computed today show discrepancies of approximately 0.5 meters when compared in an overlapping time interval [Lichten & Bertiger, 1989b]. This is comparable to the differences between the estimated and "true" orbits given here.

Comparison of Relative Satellite Positions:

Let us have one more look at the relative positions of satellites 2,6,9, and 13, which are all above the US sites during the window defined in Figure 8.14. The picture we saw for the formal errors is even more pronounced in the differences between the estimated and the true relative positions (see Figures 8.27 and 8.28).

Assuming that the relative satellite positions are more important than the absolute positions when using double differences in the data processing (see section 6.1.3), these Figures seem to indicate, that using only the three US fiducial sites in the orbit determination gives orbit results as accurate over the region of the US as using the global baseline set A. Small errors or in-

consistencies in the coordinates of the fiducial sites outside the US could even degrade the orbit quality over the US.

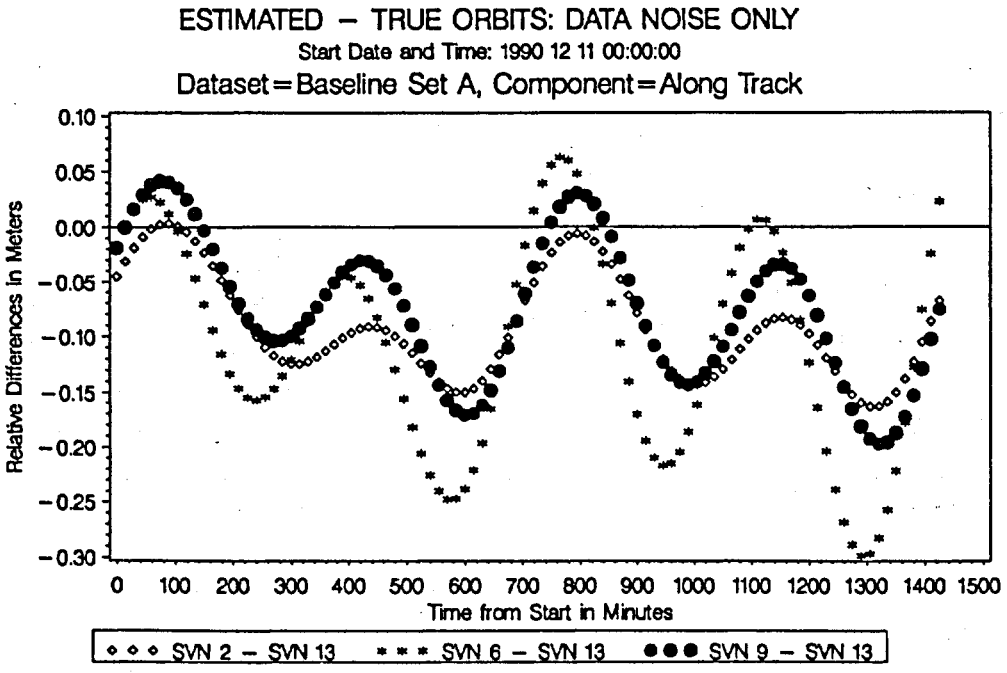

Figure 8.27

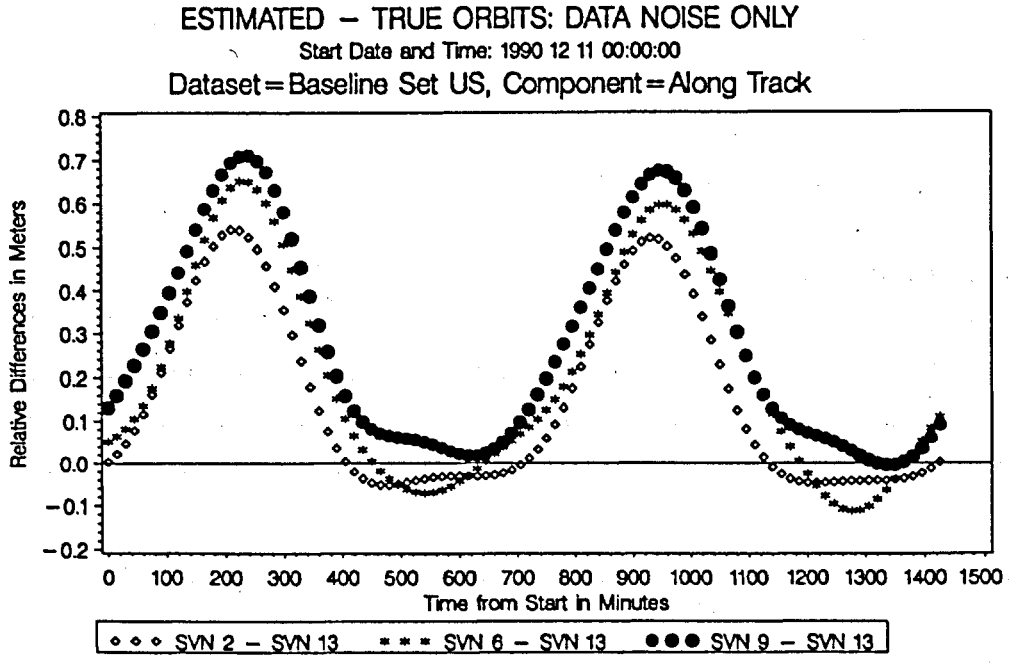

Figure 8.28

However, outside the US the quality of the orbits from set US decreases very rapidly (by a factor of 6 after half a revolution). The same holds when looking at the inter-satellite distances (see Figures 8.29 and 8.30 for orbits of set A and set US respectively).

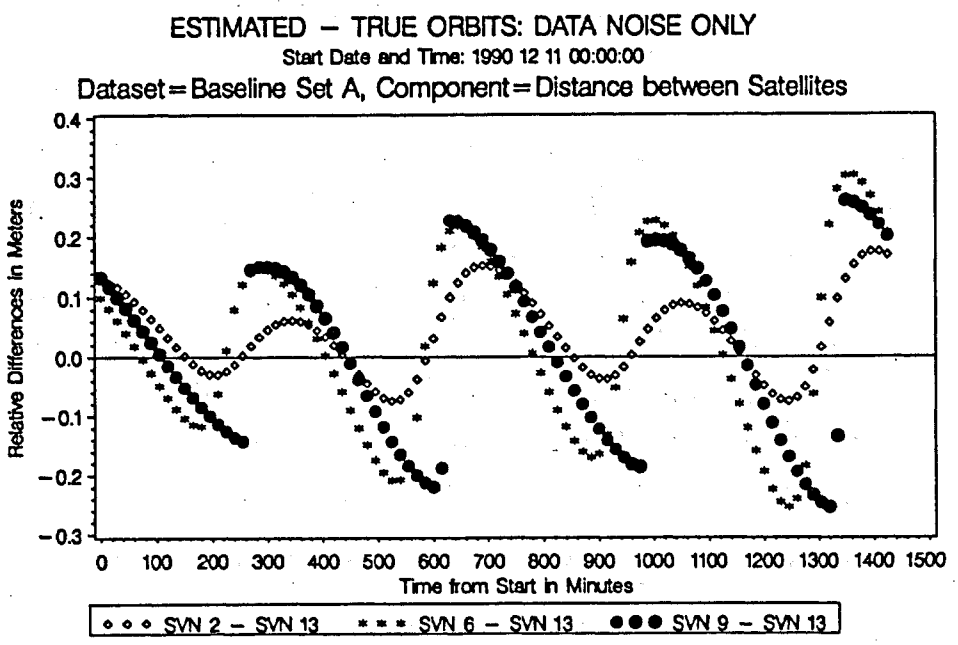

Figure 8.29

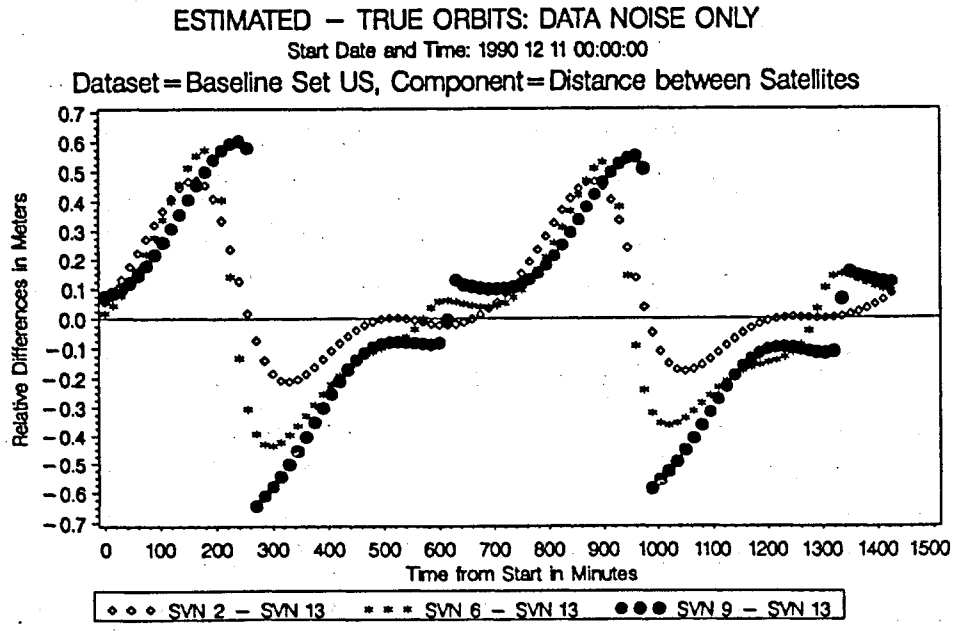

Figure 8.30

Comparison with a Coordinate System Transformation:

The reference system of the satellite orbits is primarily defined by the coordinates of the fiducial sites. In the presence of coordinate biases such systems may depend on the special selection of fiducial sites. In this case transformation parameters between the two frames may be estimated. The method was presented in section 6.2.4.

When comparing the "US orbits" (the orbits obtained with set US) with the true orbits using the program STDHLM (see 6.2.4), only very small rotations and small scale factors result between the two orbit sets (and orbit frames), showing that the orbits are given in almost the same system. That the "US orbits" are better determined above the US sites than elsewhere, may be seen by comparing the orbits over the region of the US and over e.g. South Africa (using the elevation mask option described in section 6.2.4): the rms of the estimated similarity transformation is larger by 50 % (30 cm instead of 21 cm) for the orbit comparison over South Africa.

More interesting is the case of the systematic fiducial site biases introduced in Australia (see Table 8.6). These systematic shifts of the fiducial coordinates on one continent change the individual satellite orbits and the reference frame of the orbit system. As an example the parameters of the similarity transformation (see program STDHLM, section 6.2.4) between the orbits obtained using the coordinate set AH (see Table 8.6) and the true orbits are given in Table 8.10 together with the residual rms errors in radial, along track, and out of plane directions.

The decrease of the residual rms errors in the radial and along track components shows that a considerable part of the orbital biases may be interpreted as a change in the orbit reference frame. From the estimated transformation parameters we see that no significant rotations and scale factors can be detected between the two frames. The main difference is a translation in z-direction. Shifting the fiducial sites in Australia by 50 cm causes the satellite orbits to move in the same direction by a com-

parable amount (the vertical in Australia is almost pointing in the direction of the geocentric z-axis). This also explains the remarkable decrease of the residual sum in the radial direction.

Residual RMS Errors:

Component	Without Transformation	With Transformation
Radial	0.203	0.097
Along Track	0.506	0.382
Out of Plane	0.398	0.437

Transformation Parameters:

Translation in x-direction:	0.019 ± 0.007 m
Translation in y-direction:	-0.004 ± 0.007 m
Translation in z-direction:	-0.326 ± 0.007 m
Rotation around x-axis:	0.000 ± 0.000 arcsec
Rotation around y-axis:	0.000 ± 0.000 arcsec
Rotation around z-axis:	0.000 ± 0.000 arcsec
Scale factor:	0.000 ± 0.000 ppm

Table 8.10
Comparison of Orbits Computed with the Australian Fiducial Site Coordinates Shifted in Height by 50 cm with the "True" Orbits Estimating a Similarity Transformation

At first sight a scale in the orbit system might look like a plausible consequence of the wrong station heights in Australia (see [Santerre, 1991]). A scaling of the orbits, i.e changing the semi-major axes, is not possible, however, because the resulting change in the mean motion of the satellites would lead to extremely large along track biases over 4 days. (Changing the semi-major axis by only 1 cm (see eqn. (7.1)) will introduce along track errors of about 40 cm after 4 days).

Orbits estimated using coordinate sets AN and AE (see Table 8.6) give similar results when compared with the STDHLM program.

8.3.2 Global Coordinate Quality

In the second step outlined in section 8.2.1 the ESA site coordinates were estimated (see solutions 5-8 and 12-14) using the orbits of step 1 (computed with different baseline sets and different biases). The isolated Kourou and Malindi sites (see Figure 8.1) were estimated together with the orbits in step 1 when the baseline sets A, B, or 1P were used and thus contributed to the estimation of the orbits.

Even for the short baselines ambiguities were not resolved to integer numbers in the solutions presented here.

8.3.2.1 The A Posteriori rms Error of the Phase Observation in Coordinate Estimation

Figure 8.31 gives the rms error of the phase observation when using orbits based on different baseline sets.

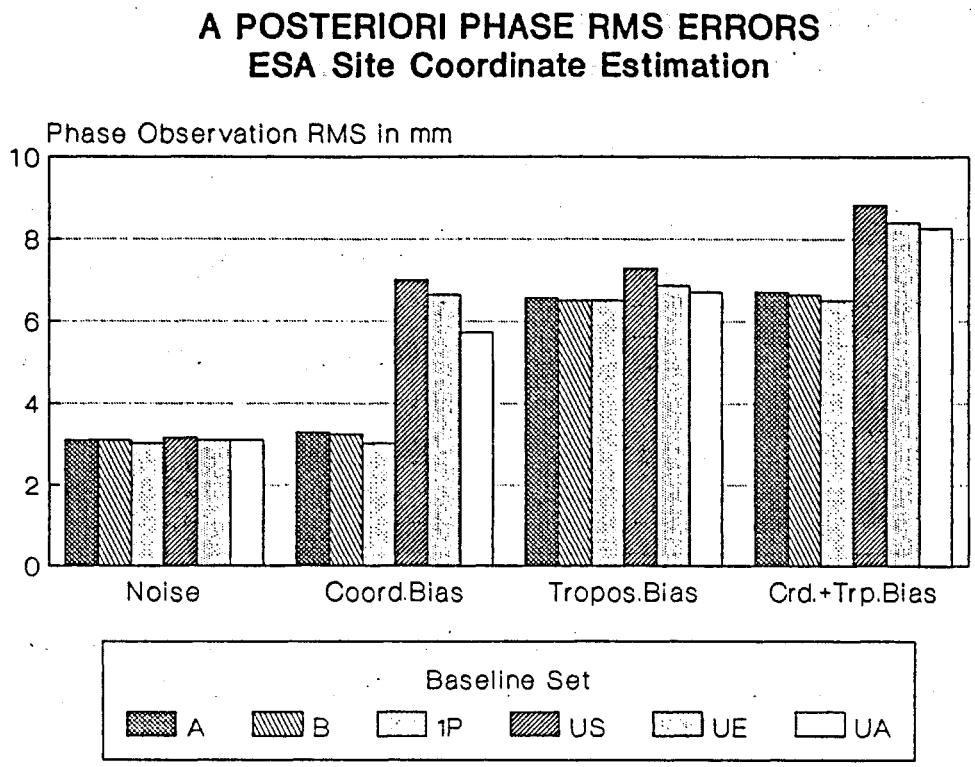

Figure 8.31

The solutions based on measurement noise only give an rms m_0 which is close to the 3 mm specified in data simulation. The rms error is slightly larger due to the orbit biases caused by the observation noise in the simulated data. With the exception of the solutions 7 (coordinate biases, see Table 8.9) using the orbits from baseline set A, B, and 1P (see Table 8.8), where no increase in the rms error can be detected, all the other solutions show an rms error about twice as large as the data noise. These larger observation rms errors are the result of the biases in the coordinates of the fiducial sites closest to the ESA sites, the troposphere biases, and the biases in the orbits estimated in step 1. In the case of the solutions with troposphere biases the rms errors are almost independent of the baseline set used. This means, that the main inconsistencies are due to the troposphere biases and not due to the errors in the satellite orbits.

8.3.2.2 Formal Coordinate Errors

The formal errors (see Figures 8.32 to 8.35) we obtain for the north, east, and height components as well as for the lengths of the baselines connecting the ESA sites to the closest fiducial site (see Figure 8.8), all are much smaller than the actual biases introduced into the estimated coordinates (see next section). A large portion of the biases is obviously absorbed by systematical deviations of the estimated ESA site coordinates from their true values and do not show up in the statistics.

In each of the four plots (Figures 8.32 to 8.35) we see a similar dependence of the formal errors on the baseline length. According to these formal errors the quality of the coordinates estimated does not change much depending on the baseline set used in the orbit estimation step. Solutions using orbits computed from set A, B (not plotted here), or 1P give almost identical formal errors.

Formal Coordinate Errors
Coord. and Trop. Biases involved

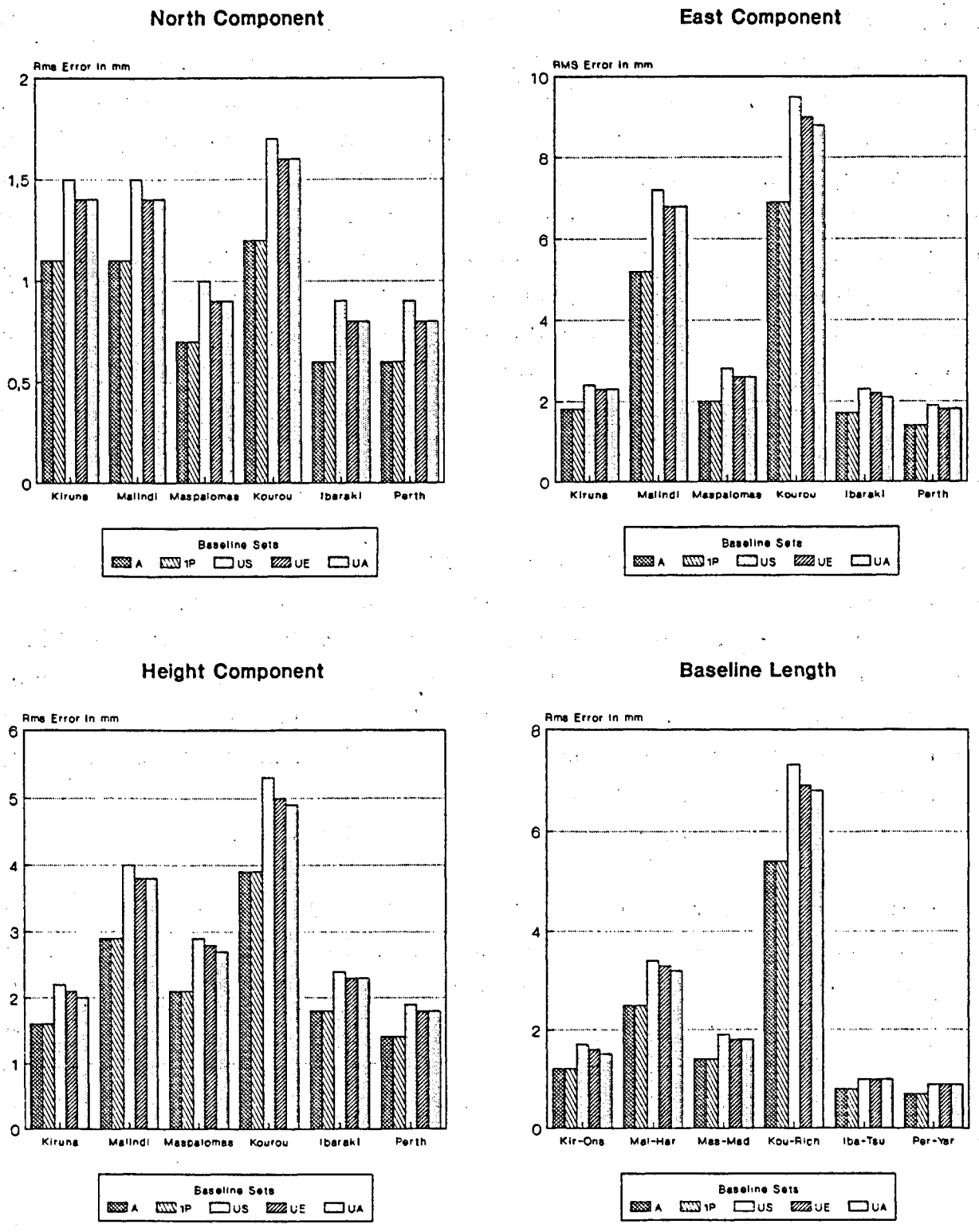

Figures 8.32, 8.33, 8.34, 8.35

The north component is, however, much better determined (by a factor of about 3 or 4) than the other quantities plotted. The reason for this asymmetry may be found in the satellite configuration as demonstrated by [Santerre et al., 1990]. What we see here is in good agreement with the ratio of the semi-axes of the error ellipsoid he gives for ambiguity-free solutions (ambiguities not resolved to integer numbers).

8.3.2.3 Comparison with the True Coordinates

The estimated ESA site coordinates differ from the "true" coordinates due to (depending on the biases introduced):

- data noise
- troposphere biases
- biases in the fiducial site coordinates and
- biases in the orbits estimated in step 1 .

The maximum differences between the estimated and the true coordinates, if data noise is considered only, are 7 mm in north, 28 mm in east, 13 mm in height direction, and 22 mm in the baseline length.

If in addition troposphere biases are included (see Figure 8.36), we get one more confirmation of the fact that troposphere biases are mainly influencing the station heights (see section 3.2.2.1). Figure 8.36 has been produced using the orbits of set A. It shows that the effect of the troposphere biases on the station heights is of the order 3-8 cm. We should remember, however, that troposphere biases were simulated assuming that the biases of a site were independent on different days. If there are not independent even larger height errors might result. In the case of very long baselines the troposphere will also affect the horizontal position (see Malindi in Figure 8.36).

The effect of biases in the fiducial site coordinates is demonstrated in Figure 8.37.

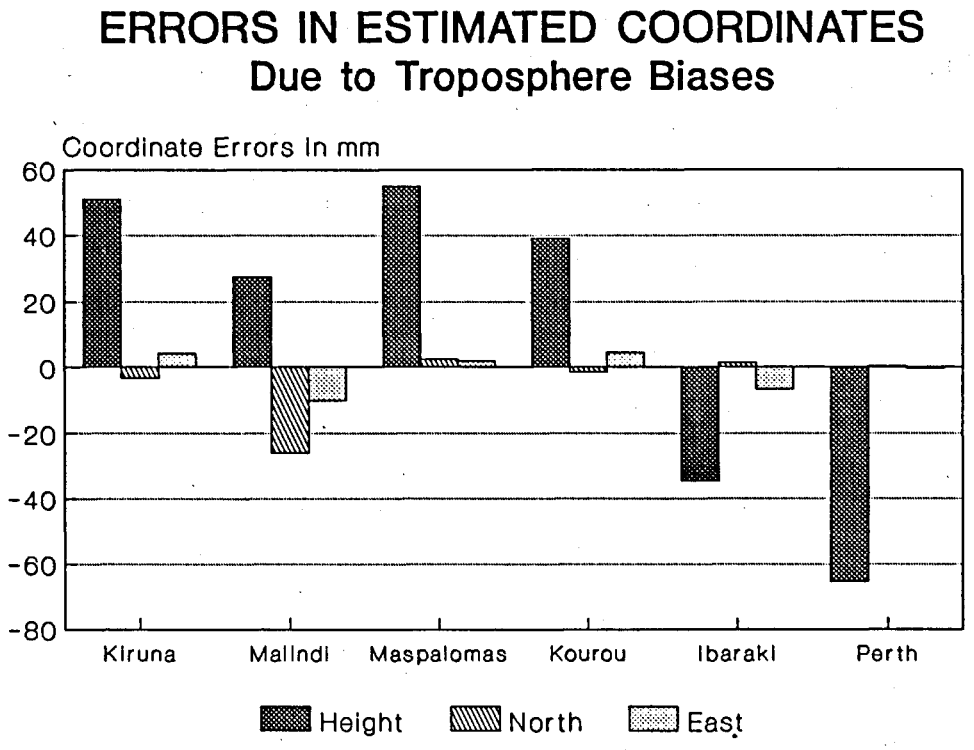

Figure 8.36

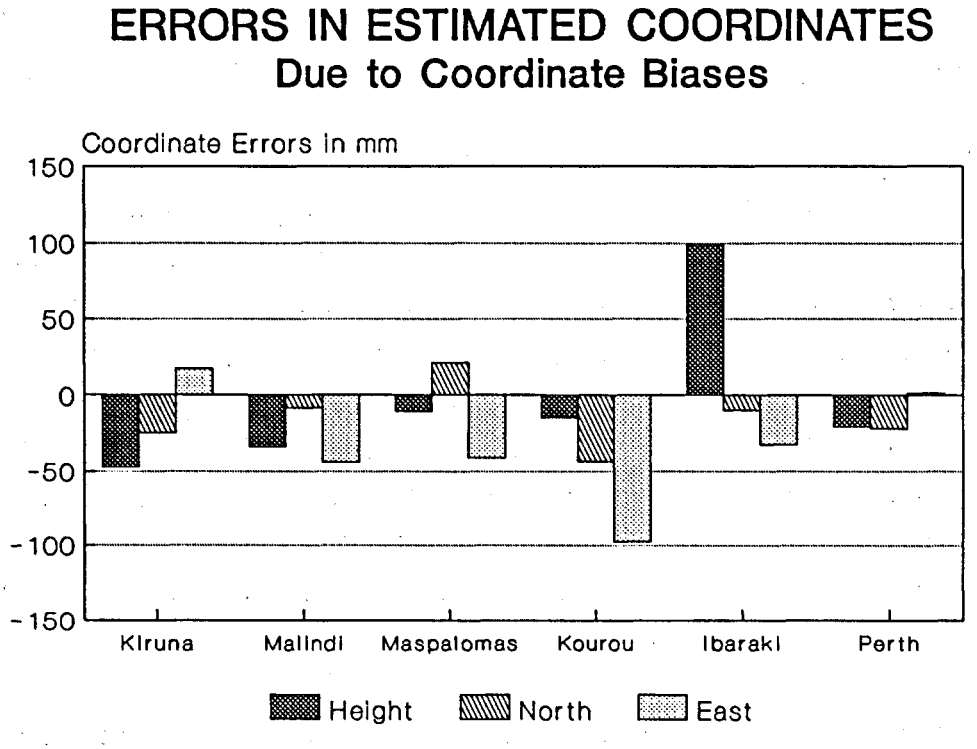

Figure 8.37

The comparison of Figures 8.37 and 8.4 makes it clear, that the major part of the errors in the estimated ESA site coordinates is caused by the errors in the fiducial sites closest to the ESA site considered (see also Figure 8.8). Since the errors in the estimated coordinates are of the same order of magnitude as the errors in the fiducial site coordinates (see Table 8.5), we may conclude that (at least for short baselines) the influence of the wrong fiducial coordinates on the ESA sites via orbit errors is small.

Figures 8.38 to 8.41 show the errors in the coordinates due to both, troposphere and coordinate biases. If only baselines from one or two clusters (US, UE, or UA) are used, errors of more than 20 cm in the east component and in height and more than 10 cm in the north component and baseline length may result. With the baseline sets A, B, or 1P, however, all the baseline errors are below 10 cm.

In a last study we wanted to check the approximate formula given by [Bauersima, 1983] (see eqn. (3.34)). We simulated orbits (see section 8.1.3.4) containing biases of about 0.5 to 1.0 meters or 2 to 4 parts in 10^8 (see Table 8.7 and Figure 8.5). The induced coordinate errors (when using these simulated orbits) are given in Figure 8.42. They are increasing with baseline length as postulated by eqn. (3.34). When taking the length of the coordinate error vector for the long baselines Richmond-Kourou (3713 km), Hartebeesthoek-Malindi (2838 km), and Madrid-Maspalomas (1772 km), we get an accuracy of $1.6 \cdot 10^{-8}$, $2.8 \cdot 10^{-8}$, and $2.0 \cdot 10^{-8}$, which is in good agreement with the worst case formula (3.34).

The east component is clearly the worst. This has to do with the fact, that the satellite ground tracks are in most cases running in a north-south direction due to the inclination of about 55 degrees and the rotation of the earth (see [Santerre, 1991]).

Estimated - True Coordinates
Coord. and Trop. Biases involved

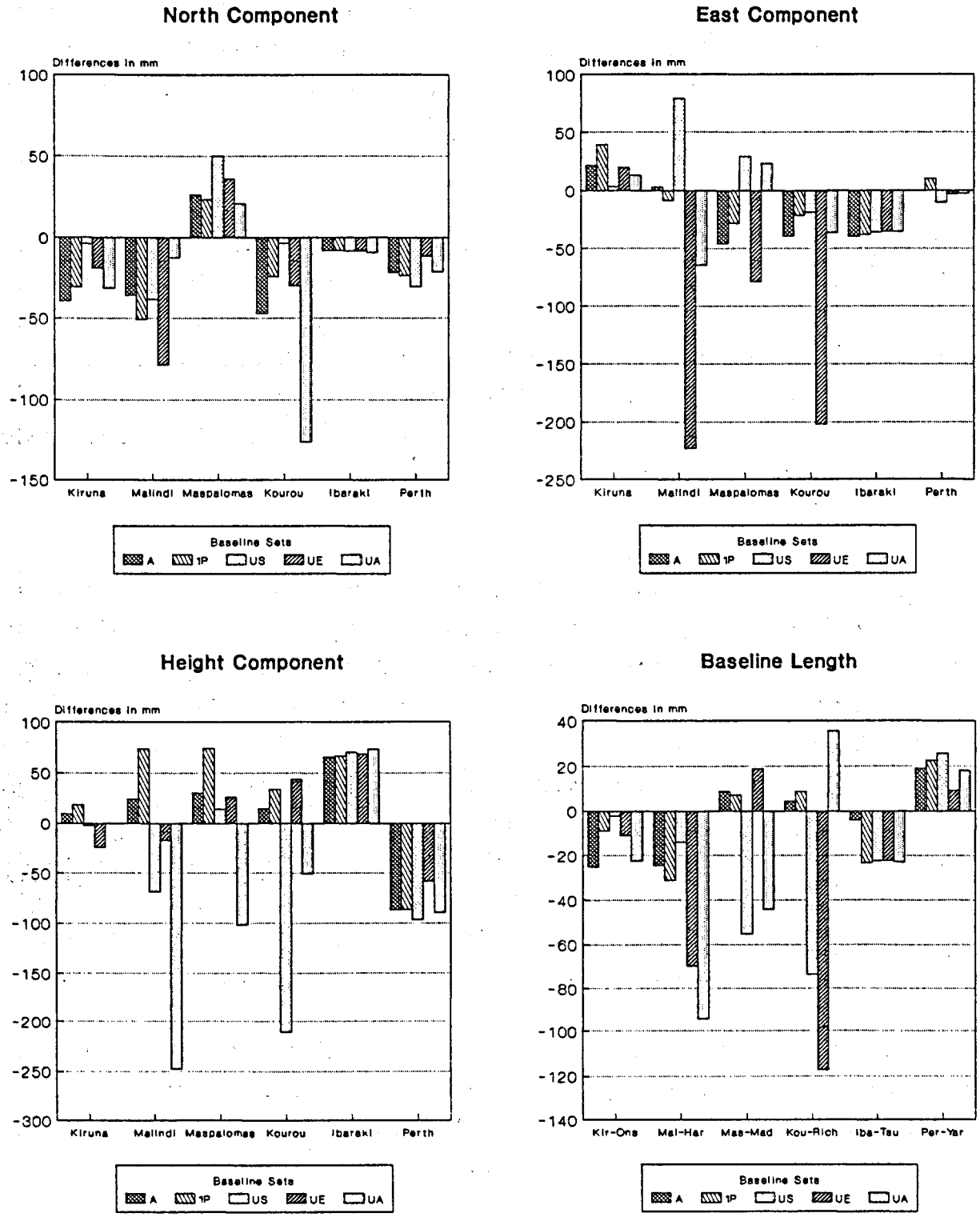

Figures 8.38, 8.39, 8.40, 8.41

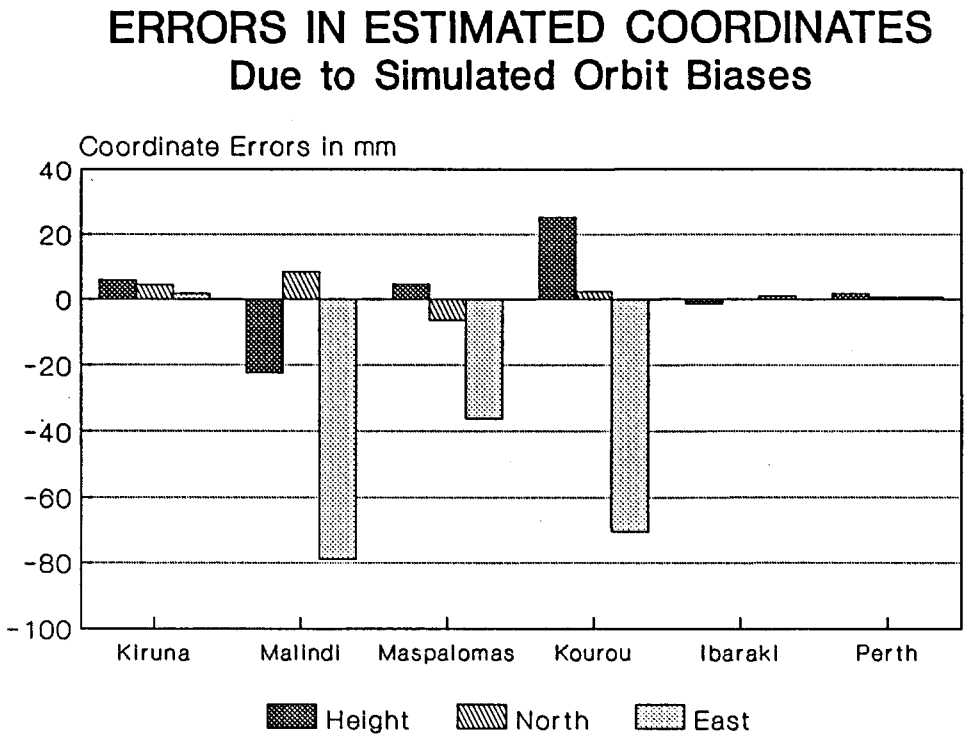

Figure 8.42

In summary we may say that even in the presence of troposphere and coordinate biases, it should be possible to determine site coordinates anywhere on the earth with an accuracy of below 10 cm using a set of about 20 globally distributed sites for orbit determination. It is clear that a considerable part of the coordinate errors due to the troposphere and coordinate biases might be removed by estimating troposphere parameters and by estimating also the fiducial site coordinates in the orbit determination step (using appropriate constraints on these coordinates).

9. EUROPEAN ESA GPS CAMPAIGN (ESA'91): REGIONAL ORBITS

The amazing strength of a satellite system like GPS for coordinate and orbit determination is only now becoming clear. This campaign has been included in this thesis to show the potential of continuous satellite tracking with the present, although still incomplete satellite constellation. Free network solutions and solutions using the fiducial point concept are presented.

9.1 Network and Campaign Description

9.1.1 The European ESA Tracking Sites and the Fiducial Sites

In December 1990 it was decided that, as a part of the ESA project outlined in section 8.1.1, the network consisting of the 6 European ESA tracking sites (Figure 9.1) should be determined in a separate campaign. The aimed at accuracy was 10 cm with respect to a well-defined reference frame (as e.g. the International Terrestrial Reference Frame (ITRF)). In addition to these 6 European ESA tracking sites 8 fiducial sites (see Figure 9.1) were selected to establish the reference frame and to enable orbit improvements according to the fiducial site concept: keep the fiducial sites fixed at positions accurately known from VLBI (Very Long Baseline Interferometry) or SLR (Satellite Laser Ranging) for the orbit determination.
The entire European network covers an area of about 2000 km × 5000 km.

9.1.2 The ESA'91 GPS Campaign

The GPS campaign to measure the European ESA tracking network was organized by the Institute of Physical Geodesy at the Technical University Darmstadt, Germany, and took place from May 1 to May 12, 1991.

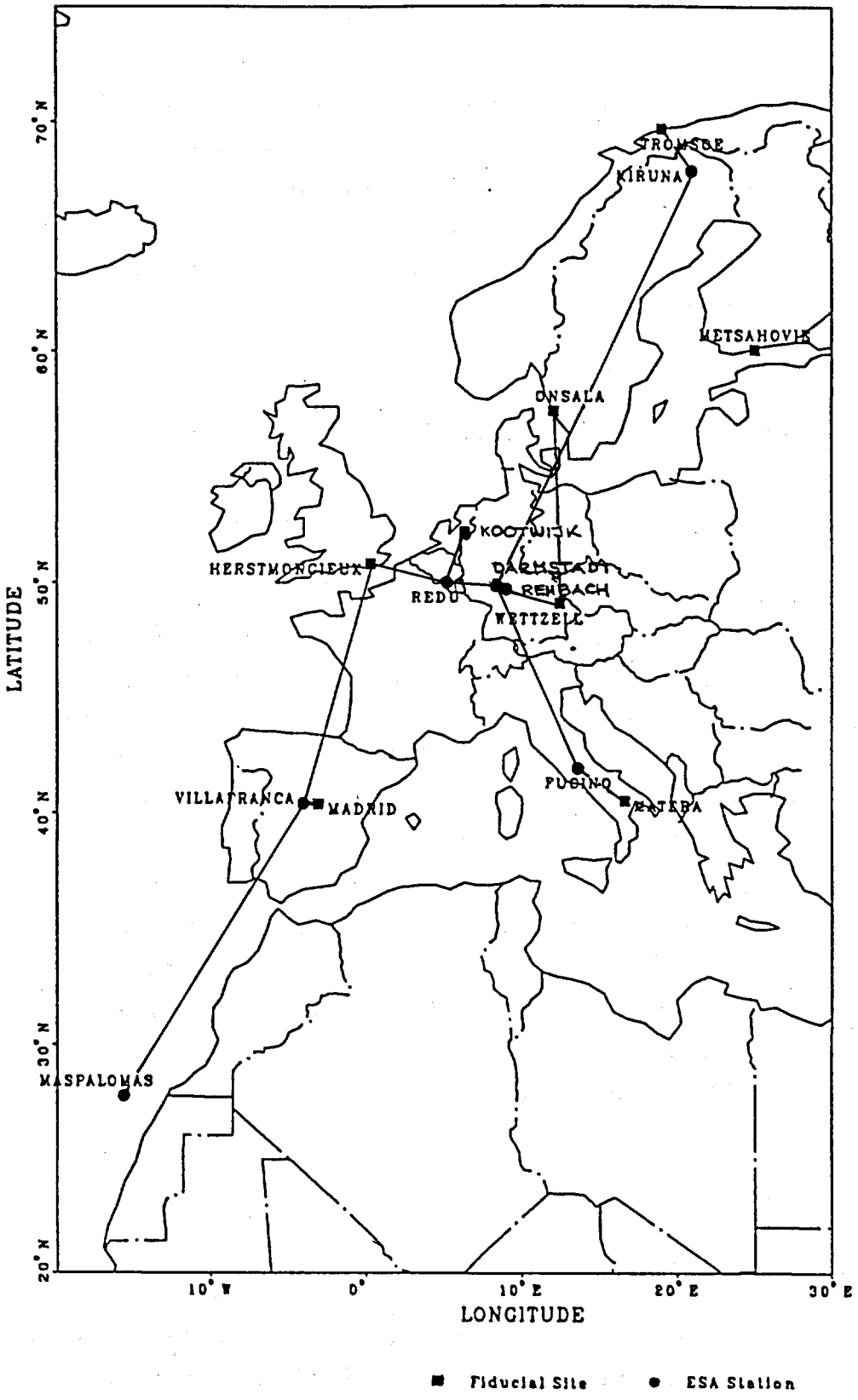

Figure 9.1

European ESA Tracking Sites and Fiducial Sites Occupied During the European ESA GPS Campaign, May 1991

As many of the ESA sites as possible were occupied by the same receiver type: New Trimble 4000SST receivers with P-code on L_2 were used at 5 ESA sites and at the fiducial sites Herstmonceux and Wettzell. Mas Palomas, the sixth ESA site, was equipped with a Trimble 4000STD receiver. The other fiducial sites were occupied by Rogue SNR-8 and Ashtech L-XII (at Onsala and Metsahovie) receivers (see Table 9.1).

Station Name	State	Receiver Type	Co-Location	Type
Fucino	Italy	Trimble SST	---	ESA
Kiruna	Sweden	Trimble SST	---	ESA
Mas Palomas	Spain	Trimble SST	---	ESA
Redu	Belgium	Trimble SST	---	ESA
Rehbach	Germany	Trimble SST	---	ESA
Villafranca	Spain	Trimble SST	---	ESA
Darmstadt	Germany	Trimble SST	---	THD
Herstmonceux	England	Trimble SST	SLR	FID
Kootwijk	Netherlands	Rogue	SLR	FID
Madrid	Spain	Rogue	VLBI	FID
Matera	Italy	Rogue	VLBI, SLR	FID
Metsahovie	Finland	Ashtech L-XII	VLBI, SLR	FID
Onsala	Sweden	Ashtech L-XII	VLBI	FID
Tromsoe	Norway	Rogue	VLBI	FID
Wettzell	Germany	Trimble SST	VLBI, SLR	FID

ESA: ESA Tracking Site FID: Fiducial Site
THD: Technische Hochschule Darmstadt

Table 9.1
List of ESA Tracking Sites and Fiducial Sites Occupied During the European ESA GPS Campaign, May 1991

To get the 2-dimensional coverage needed for navigation purposes the satellites have now been evenly distributed in space and may no longer be observed during daily time-windows of several hours. The number of satellites visible during the day varies between 3 and 4 for 80 % of the time (see Figure 9.2).

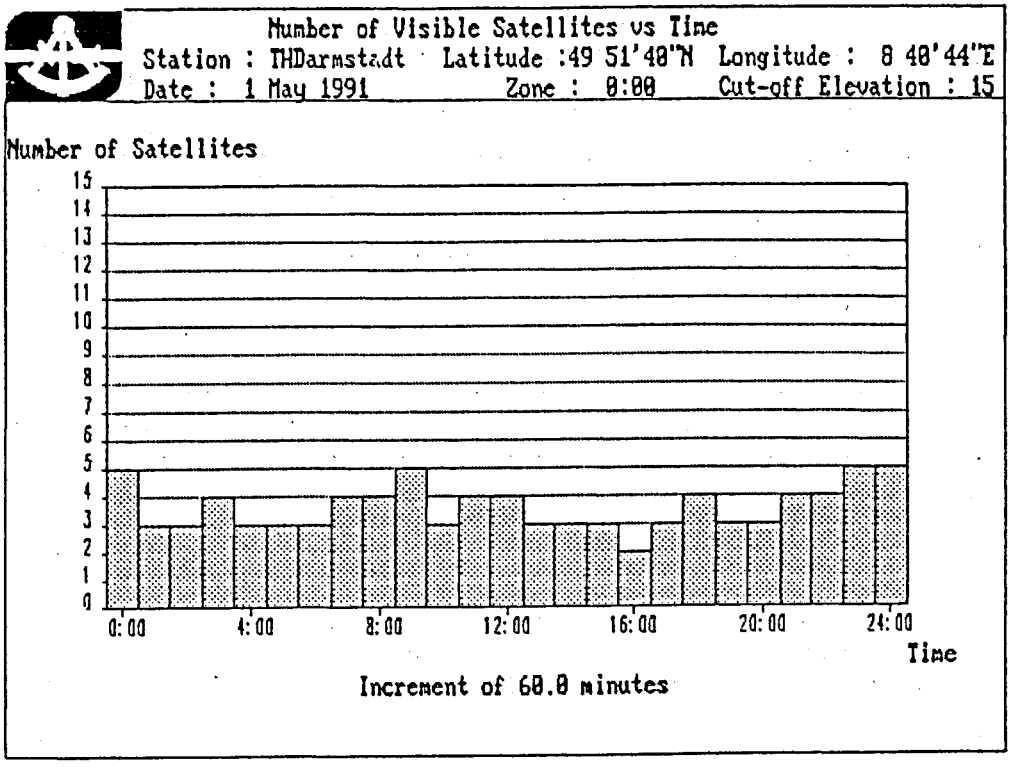

Figure 9.2
Satellite Visibility Plot for the ESA'91 GPS Campaign

Due to this circumstance we decided to track the GPS satellites for 24 hours a day. Two short breaks were necessary (at 4:00 and 16:00) to download the data. All the Trimble receivers were sampling data at a rate of 4 epochs per minute making the preprocessing of the observations (cycle slip repair) very easy even for baselines longer than 1000 km. Unfortunately it was not possible to have all the fiducial sites tracking at the same rate. Table 9.2 summarizes the campaign characteristics.

Time span covered	:	May 1 - May 12, 1991
Session definition	:	00:00 - 24:00
Number of Days (Sessions)	:	12 days
Session length	:	24 hours
Number of Sites	:	15
Number of Satellites	:	15
Data sampling rate	:	15, 30, and 120 seconds

Table 9.2
Characteristics of the ESA'91 GPS Campaign

9.2 Processing Strategies

In the European ESA Campaign three different receiver types were involved. Because combining different receiver types is critical (see e.g. [Gurtner et al., 1989a]) we formed baselines (the so-called single difference files (see section 3.1.4) are actually formed in the Bernese GPS Software) preferably between the same receiver types. In this way a pure Trimble-network was established and the other receivers were connected to the Trimble receivers by short baselines (see Figure 9.1). The antennae phase center offsets we introduced for the three receiver types are given in Figure 9.3.

```
PHASE CENTER ECCENTRICITIES FOR EUROPEAN ESA CAMPAIGN  (17-AUG-91)
-------------------------------------------------------------------

RECEIVER TYPE          ANTENNA S/N  FREQ  PHASE CENTER ECCENTR (M)
ANTENNA  TYPE          FROM    TO    L*    NORTH    EAST     UP
********************  ****** ******  *   **.**** **.**** **.****

ROGUE                       0 999999   1    0.0      0.0      0.0779
ROGUE                                  2    0.0      0.0      0.0964

TRIMBLE 4000STD             0 999999   1    0.0      0.0      0.0595
TRIMBLE 4000STD                        2    0.0      0.0      0.0580

TRIMBLE 4000SST             0 999999   1    0.0      0.0      0.0692
TRIMBLE 4000SST                        2    0.0      0.0      0.0677

ASHTECH LD-XII              0 999999   1    0.0      0.0      0.0640
ASHTECH LD-XII                         2    0.0      0.0      0.0640


ANTENNA PHASE CENTER OFFSETS MEASURED FROM BERNESE REFERENCE POINT
(BRP) TO L1/L2 PHASE CENTER.

        BERNESE REFERENCE POINTS:

        ROGUE           :  BOTTOM OF CHOKE RING
        TRIMBLE 4000STD :  BOTTOM OF ANTENNA PREAMPLIFIER
        TRIMBLE 4000SST :  BOTTOM OF ANTENNA PREAMPLIFIER
        ASHTECH LD-XII  :  BOTTOM OF ANTENNA PREAMPLIFIER
```

Figure 9.3
Antenna Phase Center Offset File Used for the Receivers Involved in the European ESA Campaign

Of the 12 days of data only a subset of 6 subsequent days was selected and processed, namely days 123-128 (May 3 - May 8, 1991).

The characteristics of the 1-day, 3-days, and 6-days solutions are listed in Table 9.3.

Solutions	#Days	Arc L. (days)	#Orbit Par./Sat.	#Trop.Par./ Base./Ses.	#Fiduc. Fixed
B1NT2323-2828	1	1	7	0	1
B3NT2325+2628	3	3	8	0	1
B3NT2328	6	3	8	0	1
B1TB2323-2828	1	1	7	1	1
B3TB2325+2628	3	3	8	1	1
B3TB2328	6	3	8	1	1
B1TM2323-2828	1	1	7	6	1
B3TM2325+2628	3	3	8	6	1
B3TM2328	6	3	8	6	1
F1NT2323-2828	1	1	7	0	3
F3NT2325+2628	3	3	8	0	3
F3NT2328	6	3	8	0	3
F1TB2323-2828	1	1	7	1	3
F3TB2325+2628	3	3	8	1	3
F3TB2328	6	3	8	1	3
F1TM2323-2828	1	1	7	6	3
F3TM2325+2628	3	3	8	6	3
F3TM2328	6	3	8	6	3
F1TN2323-2828	1	1	0	1	3
F1TN2325+2628	3	1	0	1	3
F1TN2328	6	1	0	1	3

Table 9.3
Solutions Computed for the ESA'91 Campaign

Every solution in Table 9.3 was computed using the data of all the sites (except Metsahovie, which was not included in the processing).

Whereas 1-day satellite arcs were used for the 1-day solutions, 3-days arcs were set up for 3-days and 6-days solutions, i.e. two sets of orbit parameters per satellite were estimated for the 6

days. For each satellite the 6 Keplerian elements (see Figure 4.1) and one (for 1-day arcs) or two (for 3-days arcs) radiation pressure parameters were determined (see section 4.2.1.4). No a priori constraints were used for the orbit parameters. We did not try to form longer arcs, because then our force model might not be sufficient (see section 4.1).

The solutions F1TNxxxx in Table 9.3 were obtained using 1-day arc standard orbits derived from the broadcast messages (see section 4.3, program DEFSTD).

In the "free" network solutions only one site, namely Wettzell, was fixed, in the fiducial point concept the three sites Herstmonceux (SLR), Wettzell (VLBI), and Tromsoe (VLBI) were fixed using ITRF values for the coordinates (see [Boucher & Altamini, 1989] and Table 9.4).

Station Name	Geocentric ITRF Coordinates in Meters X	Y	Z
HERSTMONCEUX	4033459.189	23626.249	4924303.096
KOOTWIJK	3899225.427	396731.704	5015078.257
ONSALA	3370702.540	711805.104	5349764.008
TROMSOE	2102940.527	721569.327	5958192.027
WETTZELL TR	4075579.451	931807.118	4801570.900

HERSTMONCEUX : Flush Bracket on Sollar Pillar (near SLR 7840)
KOOTWIJK : Point 339334-25
ONSALA : Point 401 Survey Marker
TROMSOE : GPSM Survey Marker
WETTZELL TR : Point 7598

Table 9.4
ITRF Fiducial Site Coordinates Used for the ESA'91 Processing

The selection of Madrid and Matera instead of Herstmonceux and Wettzell as fiducial sites would have covered a larger part of Europe, but the local ties between the VLBI and the GPS reference points for these two sites are not available yet. It is therefore clear that the three chosen sites in the northern part of Europe

will not constitute a good reference frame for the sites far in the south (especially for Mas Palomas).

Troposphere zenith delays were estimated as a constant over one day with an a priori constraint of 5 cm, or as a series of troposphere parameters (1 parameter per 4 hours) constrained with

$$\begin{aligned} \sigma_{abs} &= 5 \text{ cm} \\ \sigma_{rel} &= 2 \text{ cm} \quad \text{(in 4 hours)} \end{aligned} \tag{10.1}$$

(see section 5.2.1.1). Troposphere parameters were determined relative to Wettzell.

All the solutions were computed using L3 (the ionosphere free linear combination) and no attempt was made so far to resolve the initial carrier phase ambiguities.

9.3 Results

9.3.1 Orbit Results

9.3.1.1 Formal Errors of the Orbital Parameters

From Table 9.5 containing the formal errors of the orbital parameters (see section 4.2.1.4 and Figure 4.1) for 1-day and 3-days arcs we see that the semi-major axis, the eccentricity, and the direct radiation pressure parameter are better determined by about an order of magnitude when using 3-days arcs instead of 1-day arcs. For the angular elements the improvement is still about a factor of 3. The drastic change in the formal error of the semi-major axis is due to the fact, that the semi-major axis determines the mean motion of the satellite. An error in the mean motion causes an along track error growing linearly with time (see eqn. (7.3)).

Arc Length	a	e	i	Ω	ω	u_0	p_0
1 Day	0.18	$9.7 \cdot 10^{-9}$	0.09	0.11	3.19	0.68	$1.1 \cdot 10^{-9}$
3 Days	0.01	$1.9 \cdot 10^{-9}$	0.03	0.04	2.31	0.10	$4.3 \cdot 10^{-11}$

Table 9.5
Formal Errors of the Orbital Parameters for 1-Day and 3-Days Arcs

The errors in Table 9.5 for the 3-days arc let us expect formal errors in the satellite positions of about 3-5 meters (compare Table 7.1).

No big differences in the formal errors may be detected between the solutions with a different number of troposphere parameters estimated.

9.3.1.2 Comparison With Broadcast Orbits

A comparison of the broadcast orbits (see section 4.3) with the orbits we determined (solution F3TM2325) shows differences of the order of 3-8 m (see Figure 9.4). If we assume that our orbits are more accurate than the broadcast orbits (see coordinate results below as an indicator), these differences are in good agreement with the approximate quality of the broadcast orbits given in section 3.2.1.2, eqn. (3.37).

9.3.1.3 Comparisons of 1-Day, 3-Days, and 6-Days Orbit Solutions

Let us start with the comparison of orbits where no extrapolation is needed. In Figures 9.5 to 9.7 the orbit differences between the 3-days solution (F3TB2325) and the first 3-days arc of the 6-days solution (F3TB2328) are very small (10-30 cm). This is to be expected since the only difference between the two solutions is that in the 6-days solution all the 6 days contributed to the site coordinate estimates.

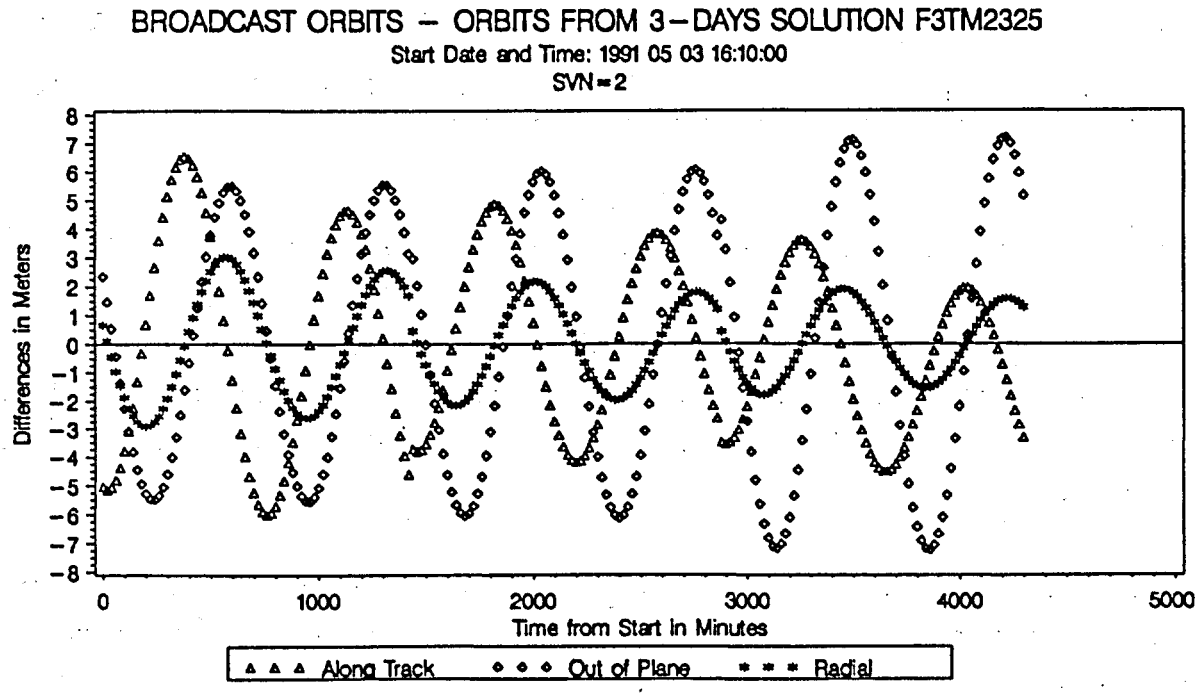

Figure 9.4
Differences Between a 1-Day Arc Derived From Broadcast Messages And a 3-Days Arc From Solution F3TM2325

The differences between the 1-day solutions (F1TBxxxx) and the 6-days solution (F3TB2328) amount to a maximum of 10 m in along track, 1-2 meters in the other directions. It seems that with a regional network of this type we may not expect to get 1-day orbits with a quality better than 1 m. We see, however, that the orbits are in much better agreement when satellite 2 is over Europe, indicated by the frames. The same is true for the positions of satellites 6, 16, and 19 relative to satellite 2 shown in Figure 9.8 (see also section 6.2.3 and 8.3.1.3) when all these four satellites are above Europe (indicated by the frames).

When we extrapolate the orbits from the first 3-days solution (F3TB2325) into the interval of the second 3-days solution (F3TB2628), we get another indication of orbit precision. Figure 9.9 shows the extrapolation over a time interval of 2 days. The differences remain almost constant over the 2 days of extrapolation. Only the along track component shows a small trend.

ORBITS FROM 1-DAY AND 3-DAYS SOLUTIONS COMPARED TO ORBITS FROM 6-DAYS SOLUTION
Start Date and Time: 1991 05 03 16:10:00

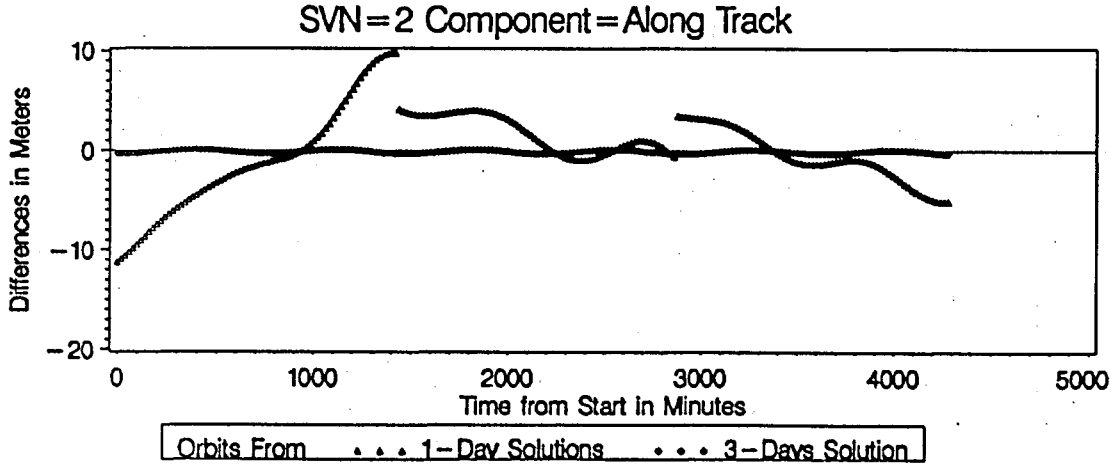

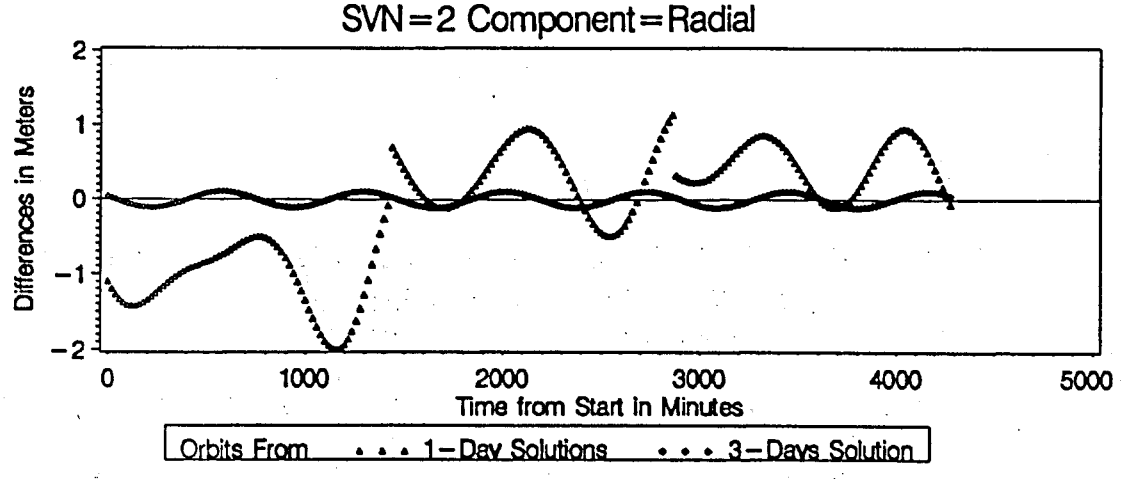

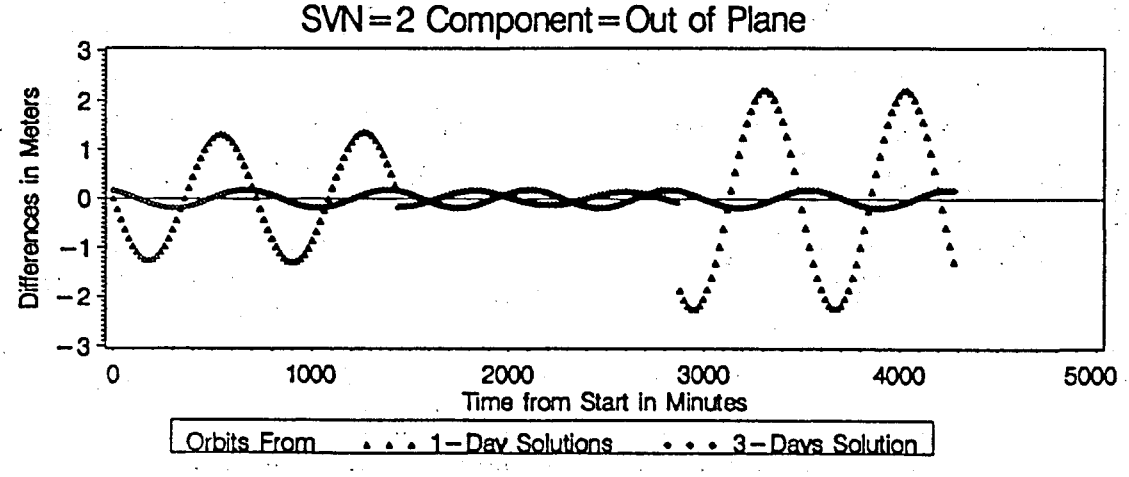

Figures 9.5, 9.6, 9.7

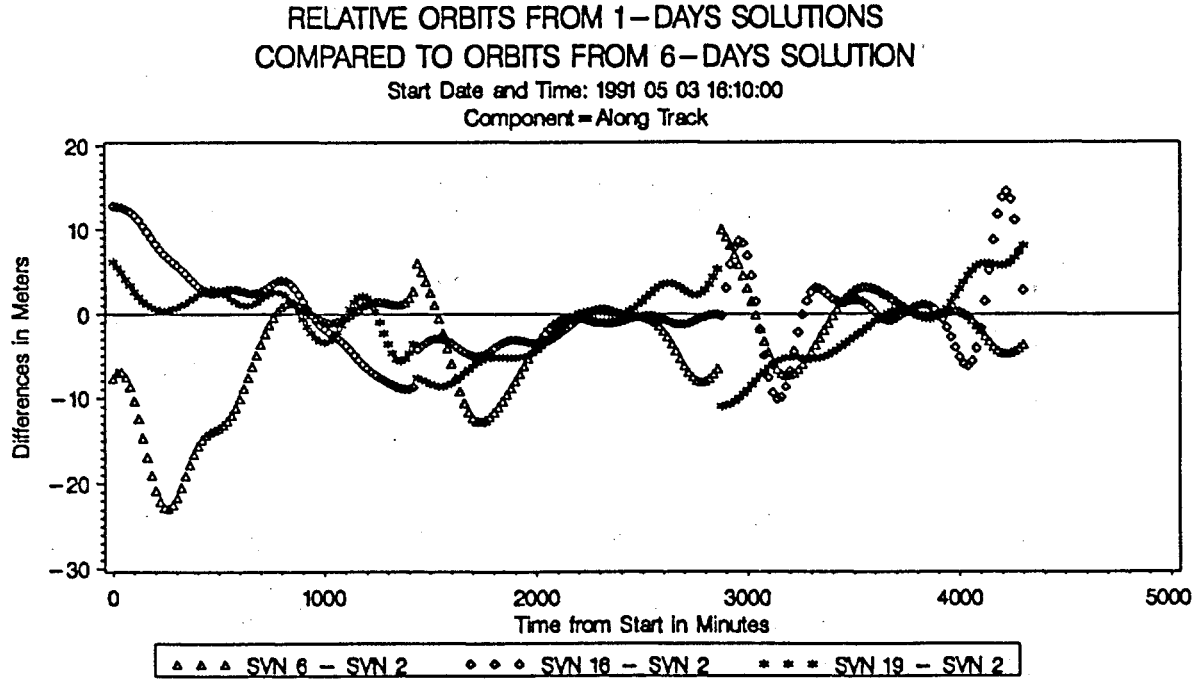

Figure 9.8

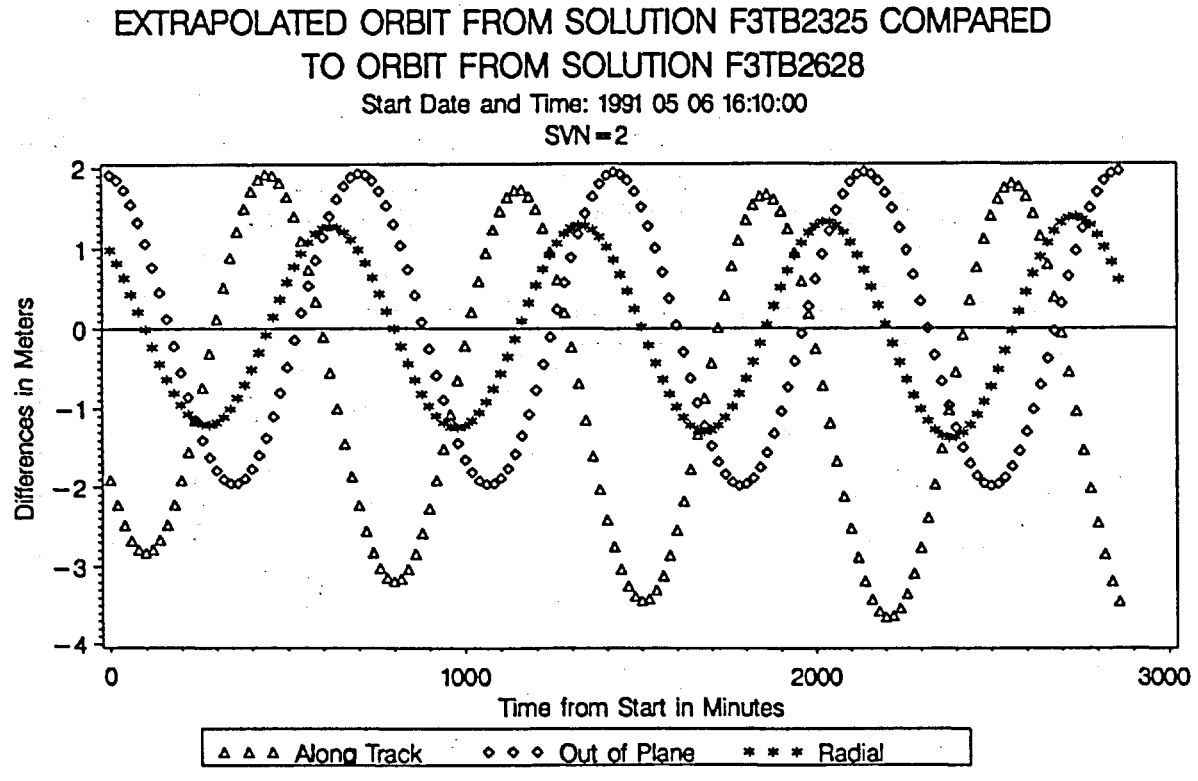

Figure 9.9

Figure 9.10 shows the differences between the extrapolation of the first arc of the 6-days solution F3TB2328 into the interval of the second arc and the second arc of solution F3TB2328. If we compare Figure 9.9 and Figure 9.10 we remark that they show almost identical variations. The fact that the estimated site coordinates are common to both arcs in the case of the 6-days solution, whereas the two 3-days solutions are independent of each other, does not have much impact on the orbit differences between the two arcs. This means that most of the differences between the orbits of the two arcs is due to the data available, the troposphere, and other influences, and not to the different estimates of site coordinates.

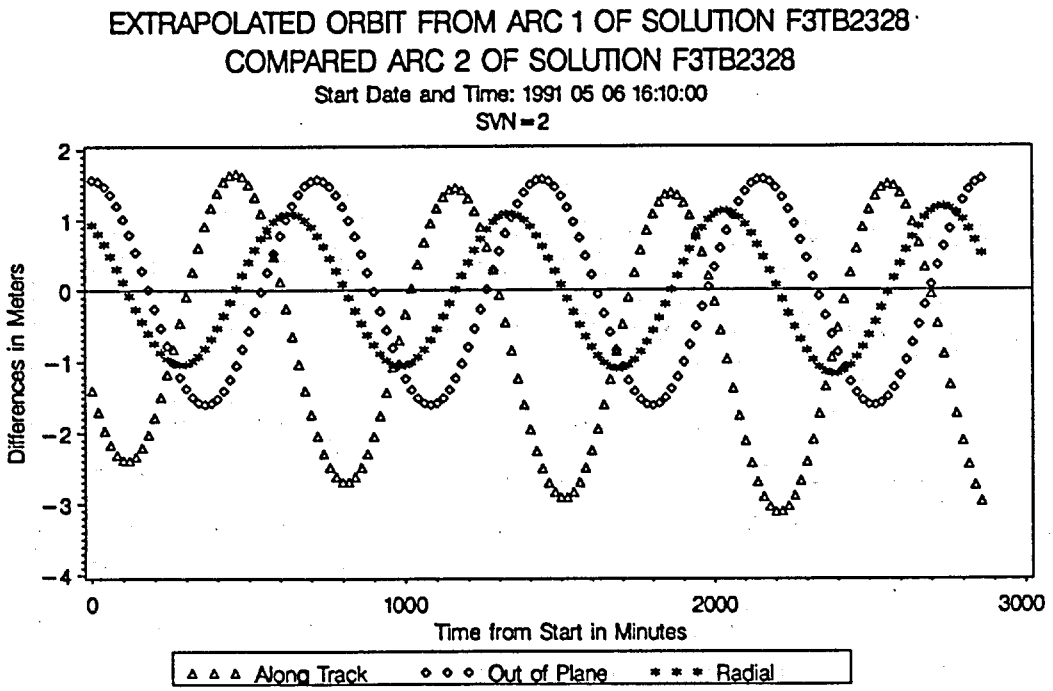

Figure 9.10

9.3.1.4 Orbits Using Different Troposphere Approaches

In Chapter 8 we have seen the influence of the simulated troposphere biases on the orbits by comparison with the true orbits (see Figures 8.23 to 8.25). The orbit biases due to the troposphere were of the order of 10-30 cm for the global GIG'91 net-

work (baseline set A) and about 3 times larger for a regional network (baseline set US).

Here we may compare the "fiducial" solutions with zero, one, or six troposphere parameters estimated per day and baseline. Figures 9.11 to 9.13 show the orbit comparison in along track, radial, and out of plane directions of the 3-days solutions F3NT2325 (no troposphere parameters) and F3TB2325 (1 trop. parameter per day) with solution F3TM2325. The differences in both cases are similar and below 1 m in along track, 20 cm in radial, and 50 cm in out of plane directions. They are consistent with the simulation results mentioned above and indicate that the effect of the tropospheric delays on the orbits, if carefully modeled, is below 1 m.

9.3.2 Coordinate Results

9.3.2.1 Free Network Solutions

Comparison of 1-Day and 3-Days Solutions:

Because only one point (Wettzell) was fixed in the free network solutions (allowing the network and the orbits to rotate around this point) we compare the daily GPS solutions B1TB2323-2828 using a 7-parameter Helmert transformation. The rotations and scale factors between the free daily solutions and the 6-days solution (B3TB2328) are given in Figure 9.14.

We see that the rotations are of the order of 10-20 masec and the scale factors of a few parts in 10^8. This means that the orientation and scale of the network is reproduced by GPS within a few parts in 10^8 from day to day just using one fiducial site and single-day arcs. The rotations are slightly larger if the daily solutions B1TMxxxx instead of B1TBxxxx are compared, probably due to the larger degree of freedom.

ORBIT FROM SOLUTIONS F3NT2325 AND F3TB2325 COMPARED TO ORBITS FROM SOLUTION F3TM2325
Start Date and Time: 1991 05 03 16:10:00

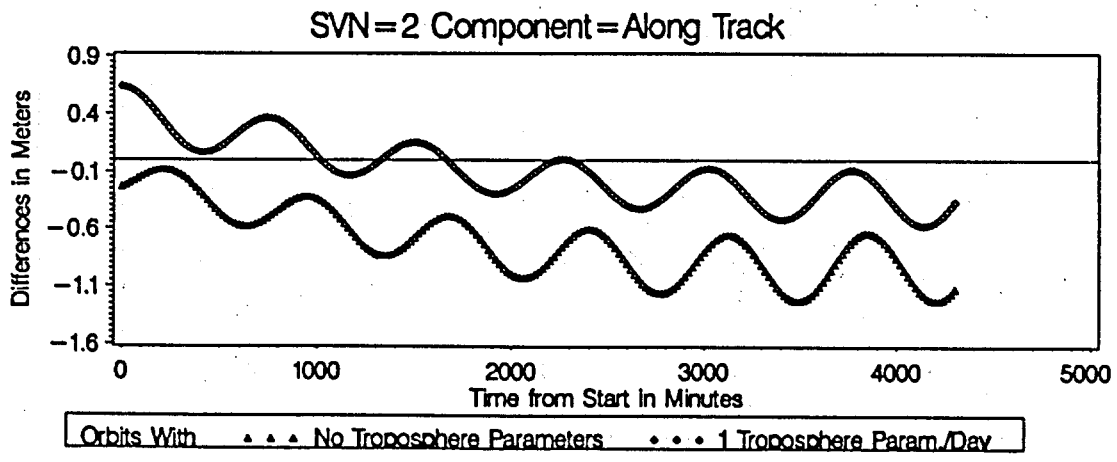

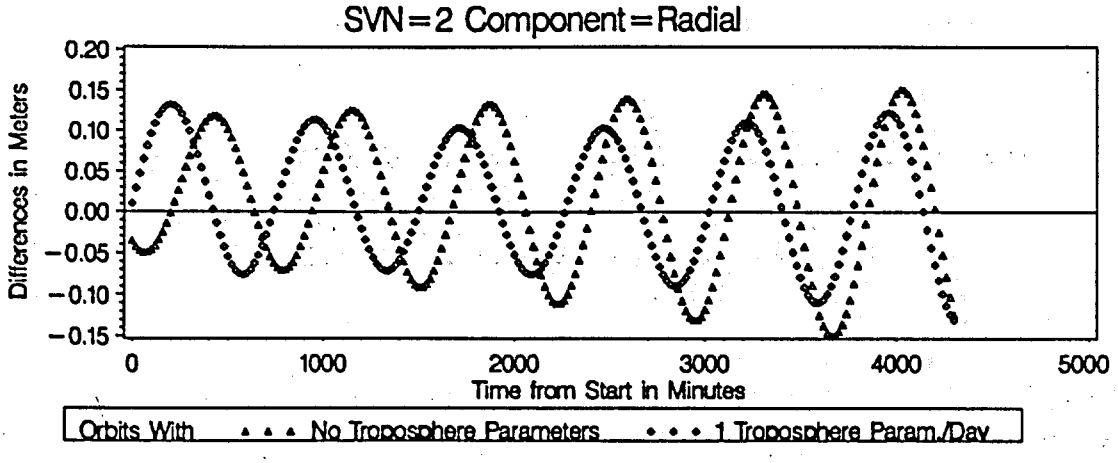

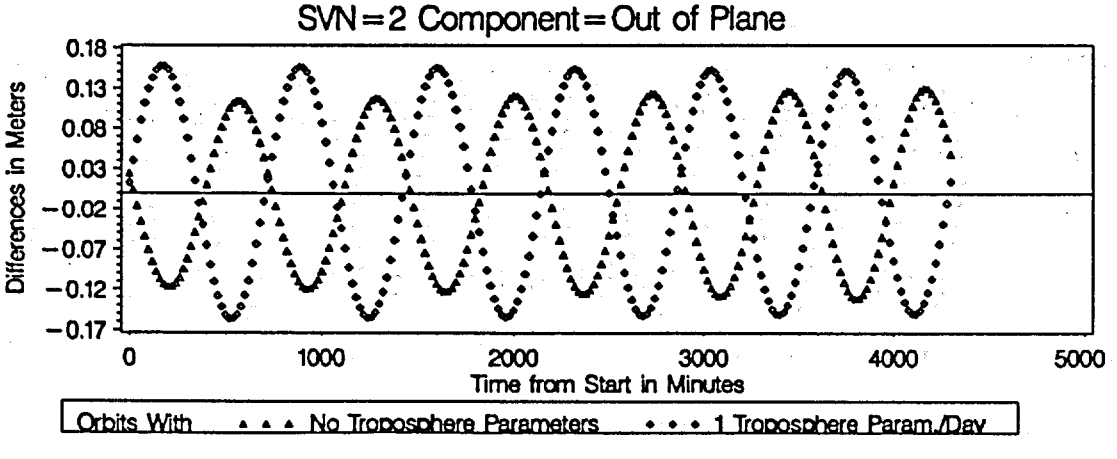

Figures 9.11, 9.12, 9.13

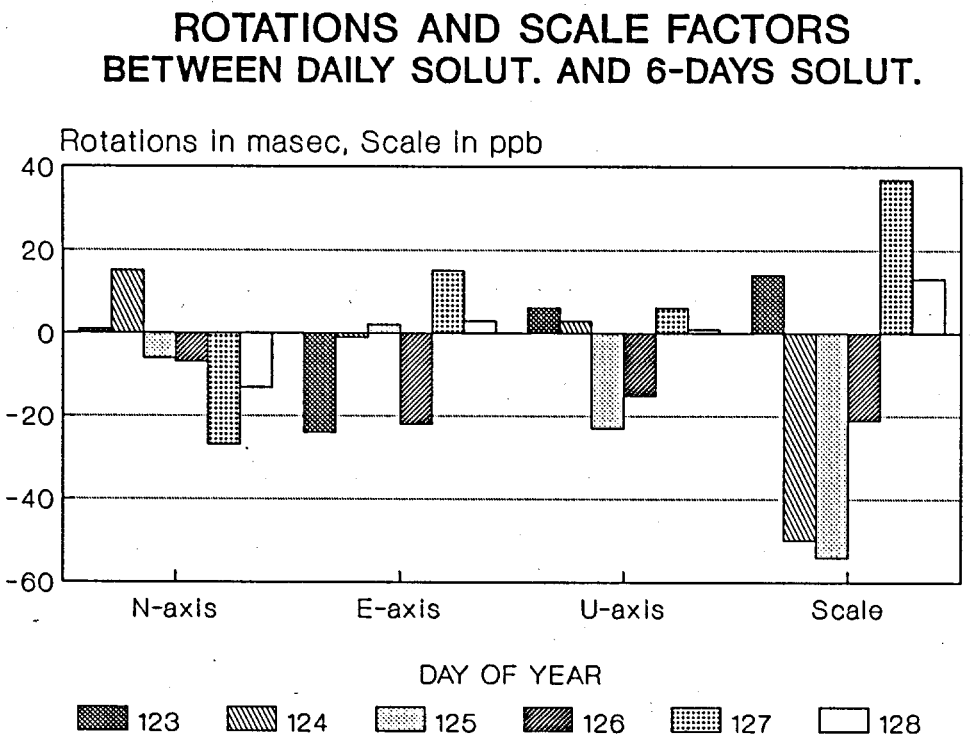

Figure 9.14
Reference Frame Comparisons Between Daily Solutions Using Single-Day Arcs (B1TB2323-2828) and the 6-Days Solution B3TB2328

An example of the transformation quality between two daily solutions, B1TM2525 and B1TM2626 (day 125 and 126, 6 troposphere parameters per day), is given in Table 9.6.

The largest residual is about 3.3 cm and most of the residuals are below 2 cm in all three components for this network of 2000 km × 5000 km.

Station Name	Residuals in a Local System (mm) North	East	Up
DARMSTADT	3.5	-15.8	-1.0
FUCINO	-8.8	-2.1	5.2
HERSTMONCEUX	17.5	-11.1	-12.6
KIRUNA	-16.8	16.9	0.9
KOOTWIJK	3.3	-12.2	4.8
MADRID	-3.9	17.8	-33.3
MAS PALOMAS	8.5	27.6	12.7
MATERA	-15.4	-12.9	26.4
ONSALA	2.3	8.6	-10.8
REDU	7.7	-15.7	1.0
TROMSOE	-3.3	32.6	14.2
VILLAFRANCA	9.9	-14.3	-3.0
WETTZELL TR	-4.6	-19.3	-4.3

Rms of Transformation: 16 mm

Table 9.6
Residuals of a 7-Parameter Transformation between the Solutions of Day 125 and Day 126 (B1TM2525 and B1TM2626)

The comparison between the two 3-days solutions (B3TM2325 and B3TM2628) is even better:

Rms of transformation : 14.8 mm

Rotation around north-axis: -0.004 +- 0.001 arcsec
Rotation around east-axis : -0.003 +- 0.001 arcsec
Rotation around up-axis : 0.002 +- 0.001 arcsec
Scale factor : -0.002 +- 0.003 ppm

From these results we can see the amazing strength that is given already now with 24-hour satellite tracking and the satellite constellation available today letting us figure out the potential of the full GPS configuration.

Figure 9.15 shows the rms errors of the Helmert transformations between two single day solutions (days 125 and 126) for different solution types (see Table 9.3) and also between two 3-days solutions.

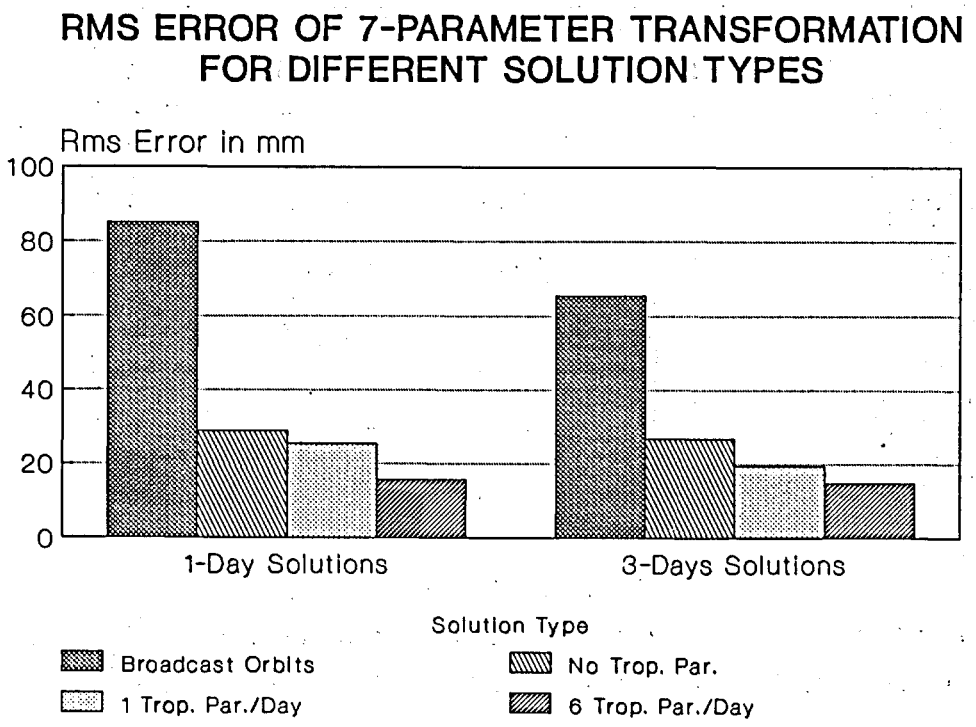

Figure 9.15

Rms Error of Helmert Transformations between 1-Day solutions (days 125 and 126) and between 3-Days solutions (days 123-125 and 126-128) for Different Solution Types

The relatively poor quality of the broadcast solutions shows that in fact an orbit improvement is most important. The consistency of the solutions increases clearly with the number of troposphere parameters estimated (0, 1, and 6 troposphere parameters per day and baseline).

Comparisons with VLBI and SLR:

Unfortunately at present we only have the local ties (between VLBI/SLR and GPS points) for 5 of the fiducial sites used during the ESA'91 campaign (Metsahovie has not been included in the processing yet). If we compare the 6-days free network solution B3TB2328 with the ITRF coordinates for these 5 fiducial sites,

the result is not comparable in quality to the internal GPS consistency (see Table 9.7).

Station Name	Residuals in a Local System (mm) North	East	Up
HERSTMONCEUX	21.0	-19.5	42.6
KOOTWIJK	16.4	-13.7	-63.1
ONSALA	0.6	89.8	6.2
TROMSOE	1.8	-20.2	2.7
WETTZELL TR	-39.8	-36.4	11.6

Rms of Transformation: 48 mm

Table 9.7
Residuals of a Helmert Transformation Between the 6-Days GPS Solution (B3TB2328) and the ITRF Coordinates

Two problems show up:

(1) The big residual of almost 9 cm in the east component of Onsala: In view of the GPS solutions presented above and the daily repeatabilities (see section 9.3.2.2), one is tempted to assume a problem in the local ties between the VLBI and the GPS point. Looking at the solutions using the fiducial point concept, the same discrepency between GPS and VLBI shows up, but even larger (no transformation): 13.1 cm for the east component of Onsala. The only problem that might reside in the GPS analysis is the combination of the Trimble receiver at Wettzell and the Ashtech receiver at Onsala (the only Ashtech involved) (see Figure 9.1).

(2) There might also be a problem in the height of the Kootwijk site. This is however difficult to confirm. The baseline Kootwijk-Redu is again a mixed baseline (Rogue-Trimble) and includes the problem of different phase center offsets.

It cannot be excluded even, that the problems are caused by another site. As soon as Matera and Madrid will be included in the comparison the situation will become clearer.

9.3.2.2 Solutions Using the Fiducial Point Concept

Baseline Repeatability:

In the case of the free network approach it is not reasonable to study daily repeatabilities, because each daily solution is given in a slightly different reference frame due to small rotations of the network (and the orbits) around the fixed site Wettzell (see Figure 9.14).

By fixing three sites we have established a reference frame common to all solutions. In Table 9.8 we show the daily repeatability of the solutions F1TM2323-F1TM2828 for the baseline Darmstadt-Wettzell which has a length of about 314 km.

Day	Deviation From the Mean Value in Millimeters				
	Latitude	Longitude	Height	Length	Length (ppm)
123	1.4	1.5	-6.1	-1.2	-0.004
124	0.3	-0.6	0.6	0.6	0.002
125	-0.6	-0.6	7.8	0.6	0.002
126	0.0	0.9	3.1	-0.8	-0.002
127	-1.3	-2.8	-0.4	2.3	0.007
128	0.3	1.6	-5.0	-1.6	-0.005
Rms	0.9	1.7	5.1	1.5	0.005

Table 9.8
Daily Repeatability of Baseline Darmstadt-Wettzell (314 km) Single-Day Arcs Estimated and 6 Troposphere Zenith Delays per Day (Solutions F1TM2323-F1TM2828)

All the results lie within a few millimeters of the mean value over the six days and therefore below $1 \cdot 10^{-8}$. It should be pointed out, that these results were not achieved with satellite arcs of several days, but with single-day arcs, i.e. each day was treated independently of the other days. It is clear that the repeatability inside the region of the three fiducial sites is especially good. The baseline Darmstadt-Fucino (954 km in length) which lies outside the triangle of fiducial sites, shows a repea-

tability of about $1 \cdot 10^{-8}$ in horizontal position, $2.5 \cdot 10^{-8}$ in height.

If no troposphere parameters are estimated (solutions F1NT2323-F1NT2828) the height repeatability is clearly degraded by about a factor 4 (see Table 9.9).

Day	Deviation From the Mean Value in Millimeters				
	Latitude	Longitude	Height	Length	Length (ppm)
123	1.7	3.4	-27.8	-3.5	-0.011
124	-0.5	-3.9	12.0	3.9	0.013
125	0.3	0.1	7.9	0.2	0.001
126	0.1	0.1	-17.3	-0.5	-0.002
127	-1.1	0.7	-2.3	-1.1	-0.003
128	-0.4	-0.4	27.3	0.9	0.003
Rms	0.9	2.3	20.1	2.5	0.008

Table 9.9
Daily Repeatability of Baseline Darmstadt-Wettzell (314 km)
Single-Day Arcs Estimated but no Troposphere Zenith Delays
(Solutions F1NT2323-F1NT2828)

Using the broadcast orbits (no orbit improvement) the daily repeatability of the baseline Darmstadt-Wettzell is of the order of 10 mm in latitude, 18 mm in height, and 50 mm or 0.15 ppm in baseline length (see Table 9.10). The longitude, with 50 mm, shows the lowest quality, which is typical for orbit biases (see simulation results in section 8.3.2.3).

Day	Deviation From the Mean Value in Millimeters				
	Latitude	Longitude	Height	Length	Length (ppm)
123	4.1	32.2	14.6	-29.9	-0.095
124	-5.0	-4.1	-8.2	2.4	0.008
125	10.6	53.1	8.1	-48.6	-0.155
126	-12.9	36.7	24.0	-38.9	-0.124
127	-5.2	-42.1	-22.9	39.1	0.124
128	8.4	-75.8	-15.7	75.9	0.241
Rms	9.2	50.5	18.4	49.1	0.156

Table 9.10
Daily Repeatability of Baseline Darmstadt-Wettzell (314 km)
Using Broadcast Orbits (Solutions F1TN2323-F1TN2828)

Comparison of 1-Day and 3-Days Solutions:

Table 9.11 gives the differences between solution F1TM2525 and F1TM2626 (allowing for a translation between the two sets).

Station Name	Residuals in a Local System (mm)		
	North	East	Up
DARMSTADT	2.2	-9.0	6.2
FUCINO	7.3	20.5	19.1
KIRUNA	-7.2	-21.5	-10.3
KOOTWIJK	-4.2	-10.0	12.9
MADRID	-17.0	24.0	-40.3
MAS PALOMAS	8.9	11.6	-18.7
MATERA	8.5	13.0	38.6
ONSALA	1.8	-2.0	-10.8
REDU	0.4	-9.7	11.5
VILLAFRANCA	-3.3	-6.7	-9.7
WETTZELL TR	2.6	-10.2	1.5

Rms of Translation: 16 mm

Table 9.11
Residuals After a Translation (3 Parameters)
Between the Solutions of Day 125 and Day 126
(F1TM2525 and F1TM2626)

The daily solutions agree with each other on the level of 2-3 cm over the entire network. A few years ago this quality, if at all, could only have been achieved by using at least 4-5 days of GPS data [Beutler et al., 1986].

The two 3-days solutions F3TM2325 and F3TM2628 are compared in Table 9.12.

Station Name	Residuals in a Local System (mm) North	East	Up
DARMSTADT	-2.3	-12.8	-19.0
FUCINO	-4.4	3.7	-3.4
KIRUNA	-8.2	-17.1	-35.7
KOOTWIJK	-4.9	-17.7	-17.4
MADRID	15.9	4.6	20.1
MAS PALOMAS	13.1	59.9	55.6
MATERA	-6.5	2.1	25.4
ONSALA	-0.8	4.6	-10.1
REDU	-2.9	-12.7	-15.1
VILLAFRANCA	4.1	-2.6	16.6
WETTZELL TR	-3.0	-12.1	-17.0

Rms of Translation: 20 mm

Table 9.12
Residuals After a Translation (3 Parameters) between the 3-Days Solutions F3TM2325 and F3TM2628

The results in this case are not as consistent as for the two daily solutions shown above. The main difference is given in the residuals of Mas Palomas. It is obvious, however, that with the three fiducial sites in the north (about 3000 km away from Mas Palomas) and with the estimation of troposphere parameters (allowing the network to rotate slightly) it is not possible to establish a reference frame for the sites far in the south of Europe. The picture will certainly change, if Madrid and Matera will be introduced as fiducial sites.

When allowing for a 7-parameter Helmert transformation (instead of a translation only) most of the resdiuals are below 1 cm and the rms drops to 11 mm. The estimated rotations are -2, -3, and 2

masec in the local north, east, and up directions plus minus 1 masec. The scale amounts to 0.003 ± 0.002 ppm.

We may conclude that with the present satellite constellation and 24-hour satellite tracking the quality of the coordinate results is better than $1 \cdot 10^{-8}$ and a network of the size of Europe may be determined to 1-3 cm centimeters.

9.3.2.3 Comparison of Free Network and Fiducial Point Concept

In this regional analysis the fiducial point concept still seems to give solutions that are more consistent than the free network solutions. Difficulties arise, however, outside the region of the fiducial sites (e.g. at Mas Palomas). To be really of help, the net of fiducial sites should cover the entire region of interest.

It is still a problem, however, whether the fiducial site coordinates in Europe are reliable (local ties, transformation between SLR and VLBI system). We have seen problems when comparing GPS solutions with VLBI/SLR coordinates (see section 9.3.2.1). In order to establish a high quality network in Europe the fiducials should be known to within 1-2 cm, else biases (distortions) will be introduced into the GPS solutions.

The constellation of the GPS is becoming more complete every year, and with every new satellite in orbit the strength of the GPS solutions increases, so that GPS becomes more and more independent of the other techniques. As we have seen above GPS already is capable to establish a local reference frame with a stability of a few parts in 10^8 by fixing one site only.

10. TURTMANN 1989 GPS CAMPAIGN: LOCAL TROPOSPHERE MODELING

We use this campaign to demonstrate the quality of local troposphere models and the value of troposphere parameter estimation in small networks.

10.1. Network and Campaign Description

10.1.1 The Turtmann 3D Test Network

The Turtmann 3D test network is situated in the central Valais, a large alpine valley in Switzerland. Figures 10.1 and 10.2 show the size and shape of the network. As stated in [Rothacher et al., 1986] the net was designed with the following objectives:

(1) Apply GPS techniques in the mountains

(2) Test, compare, and evaluate different receiver types

(3) Install a test net for other survey techniques such as inertial systems, EDM measurements, etc.

(4) Investigate recent crustal movements by repetition of the initial measurements after a long period of time (> 10 years).

The original network consists of 8 sites and spans both sides of the valley. Stations 7 and 8 define a 4.2 km long baseline at the bottom of the valley (620 and 670 meters in height). Stations 1 to 3 are situated on the northern slope between 1010 and 1530 meters, stations 4 to 6 on the southern slope between 1130 and 1480 meters. The stations were carefully selected to allow the precise determination of relative 3D positions using terrestrial methods. Station 9 (Emshorn) is located at a height of 2270 m and was added to the net in 1987. Thus the maximum height difference between stations is about 1650 m (Turtmann 7 to Emshorn 9).

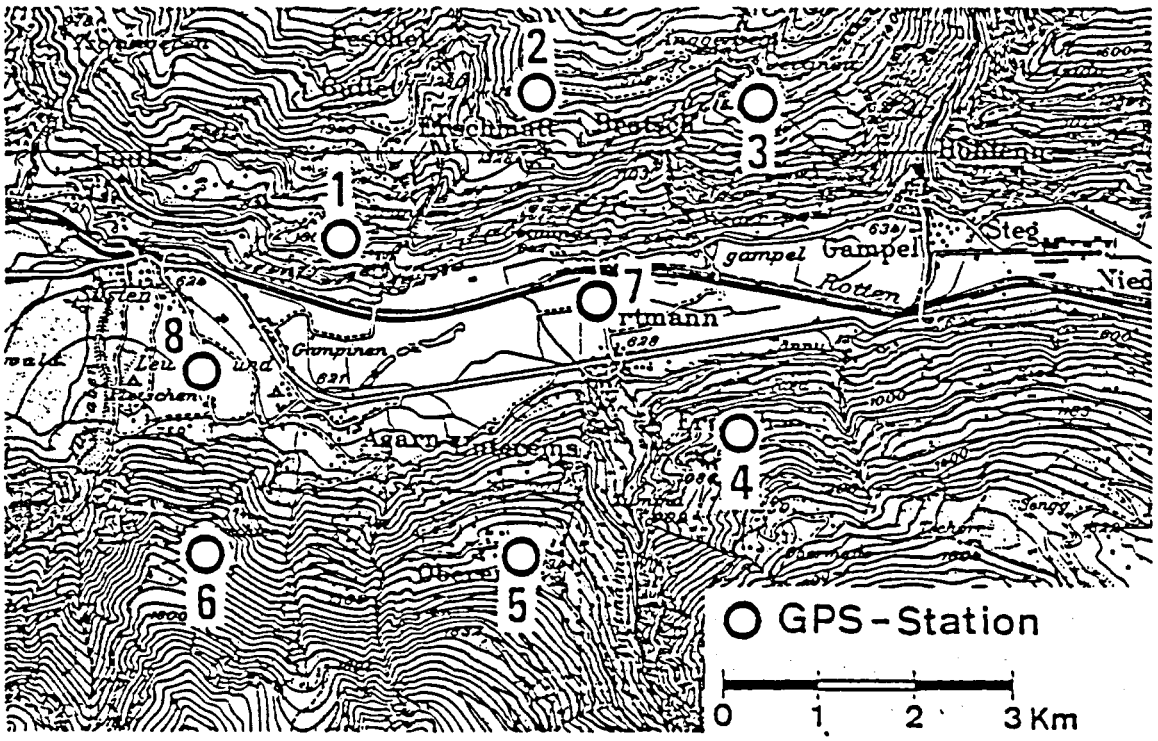

Figur 10.1
The Turtmann 3D Test Network

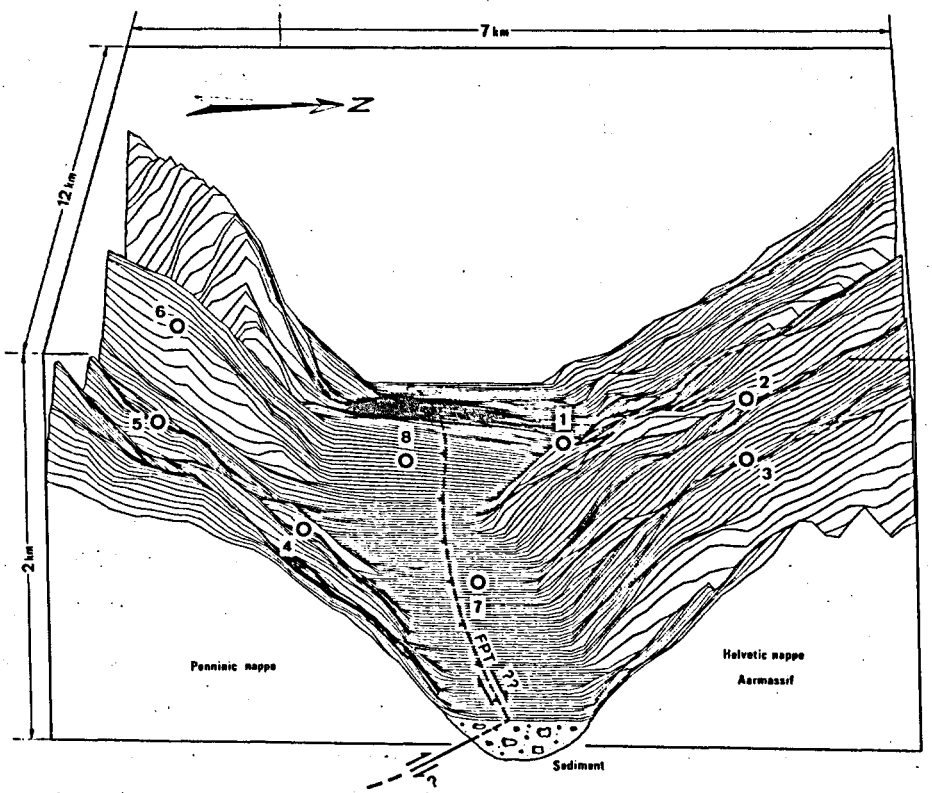

Figur 10.2
Perspective Drawing of the Turtmann Network

The various terrestrial measurements utilized to establish a high quality ground truth are described in detail in [Gurtner et al., 1989b]. The 3D adjustment with the three coordinates of station 7 fixed, yields results in the order of 1-2 mm in horizontal, 3-5 mm in vertical position. There exists no ground truth coordinates for station 9 (Emshorn).

Several GPS campaigns took place in Turtmann during the last few years with many different receiver types involved. Here we will only use the data of the Turtmann 1989 Campaign. Results obtained for other Turtmann campaigns may be found in [Rothacher et al., 1985] and [Gurtner et al., 1989b].

10.1.2 The Turtmann 1989 Campaign

During the 1989 campaign a total of 16 receivers were gathering data in the Turtmann network (10 WM-102, 1 Trimble 4000SL, 1 Trimble 4000SLD, and 3 Trimble 4000ST). In Table 10.1 the campaign schedule is listed.

Station	Height (m)	July 5	6	7
1 Brunnen	1010	WM	WM	TT
2 Braentschu	1508	WM	WM,TT	WM,TT
3 Jeizinen	1500	WM	WM,WM,TD	WM,WM,TS
4 Ergisch	1133	WM	WM	WM
5 Oberems	1387	WM	WM	WM
6 Agarn	1475	WM	TT	WM
7 Turtmann	624	WM,WM,TD	WM,WM,TS	WM,TD,
8 Susten	678	WM	WM,TT	WM,WM,TT
9 Emshorn	2271	WM	WM,TT	WM

WM: WM-102, TS: Trimble SL, TD: Trimble SLD, TT: Trimble ST

Table 10.1
Turtmann 1989 Observation Schedule

On many points more than one receiver was operated in parallel. The additional receivers were positioned on nearby points with known local ties. These very short baselines allow studies on the

combination of different receiver types. Such studies are not presented, however. Only the data of the WM-102 receivers were used to produce the results presented below.

The GPS measurements were taken during sessions of 4 hours on each day. Figure 10.3 shows the satellite distribution for Turtmann during the sessions.

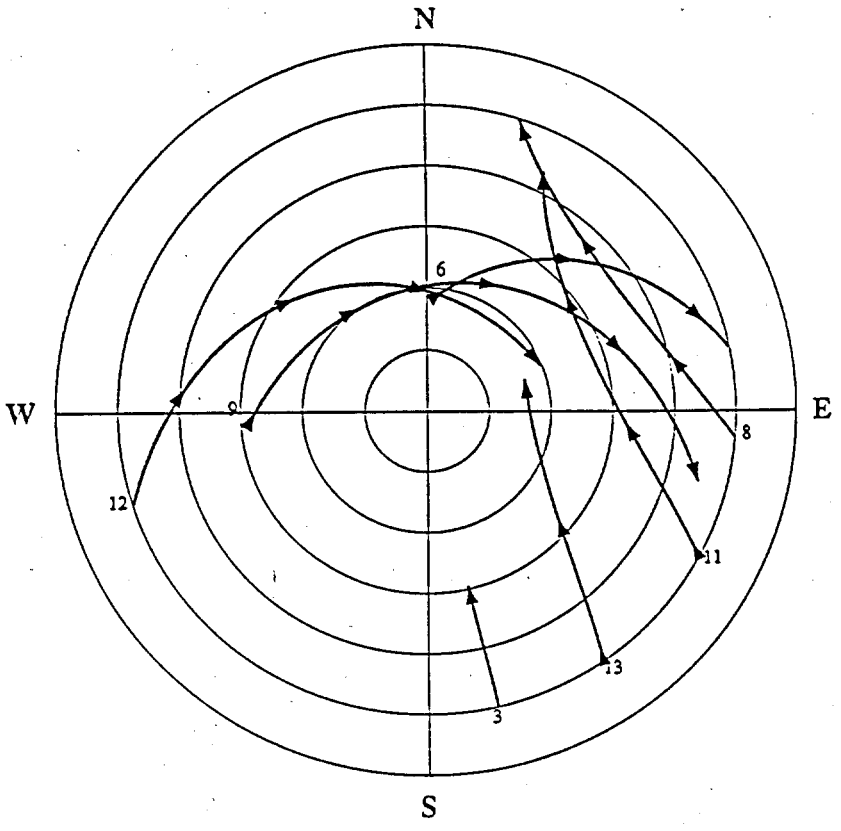

Figure 10.3
Satellite Distribution for Turtmann on July 5, 1989, 7^h-11^h UT

Surface met data (pressure, temperature, and humidity) were measured at each site at time intervals of 15 minutes. These data are the basic material for the computation of a local troposphere model as described in section 5.1.2.

10.2 Processing Strategies

10.2.1 L_1 Solutions and Ionosphere Modeling

In small networks (< 20 km) it may not be the best approach to process the ionosphere-free linear combination L_3 (see section 3.1.3) for the following reasons:

(1) The ionosphere-free linear combination L_3 has an observation noise which is about 3 times larger than the noise in L_1 (see Table 3.1). This implies that the estimated coordinates will be 3 times less accurately determined, if we disregard systematic errors.

(2) Antenna phase center offset errors in L_1 and L_2 will be increased in L_3 by a factor of 2.5 and 1.5 respectively. Since the accuracy aimed at in such a small network is of the order of a few millimeters, errors in the antenna phase centers of only a few millimeters will already show up in the results when processing L_3.

We therefore decided to use the L_1 observations only and to correct the scale introduced by the ionospheric refraction (see [Beutler et al., 1988] or [Santerre, 1991]) by using an ionosphere model computed from L_4 one-way phase observations (see section 3.1.3). All the solutions below have been obtained using the same ionosphere model. Details and results concerning the estimation of simple ionosphere models may be found in [Wild et al., 1989] and [Rothacher et al., 1990].

All the solutions have been computed using the data of the three days (complete solutions). An elevation cut-off angle of 20 degrees was used.

10.2.2 Local Troposphere Modeling

The most important features of this Turtmann network are its small size and its large height differences. The former makes im-

mediately clear that orbits are not of great importance (see eqn. (3.34)). The latter implies that the most challenging problem when processing the Turtmann 1989 Campaign lies, no doubt, in the modeling of the tropospheric refraction. All the different models and parameter estimation possibilities discussed in Chapter 5 have therefore been tested and will be compared. They are listed in Table 10.2.

Approach	Description
A	Use of a local troposphere model (section 5.1.2).
B	Estimation of one and more troposphere zenith delays per baseline and per session putting a priori constraints on the troposphere parameters and parameter differences (section 5.2.1.1).
C	Estimation of the tropospheric zenith delays as a polynomial in height for each session. Only one parameter per session was estimated, namely the height gradient of the tropospheric delay (section 5.2.1.2).
D	Estimation of one stochastic tropospheric zenith delay per baseline and per session (section 5.2.2).

Table 10.2
Trosposphere Modeling and Estimation Approaches for the Turtmann 1989 GPS Campaign

In approach A polynomials of degree 2 for the refractive index have been computed every 20 minutes. Values between the met sampling times are obtained by linear interpolation.

The parameters of model B and D have been estimated relative to the site TURT 7 (Turtmann) after having removed a plausible a priori model for tropospheric refraction (e.g. Saastamoinen).

The availability of a high precision ground truth will be a great advantage in the interpretation of the results.

10.3 Results

10.3.1 The Tropospheric Delays

The four major solution types listed in Table 10.2 give us detailed information on the variations of the tropospheric zenith delay with time and station height.

10.3.1.1 Tropospheric Delays of the Individual Models

Delays from a Local Troposphere Model (Approach A):

An example of the tropospheric delay as a function of height obtained by approach A has been included in section 5.1.2, Figure 5.2 . Relative to the standard model by Saastamoinen described in 5.1.2 the tropospheric delay is assumed to be a polynomial of degree 3 in height (integration of the refractivity (see eqn. (5.4)) represented as a polynomial of degree 2 relative to the standard model). The temporal changes of the delay are totally correlated between the sites as can be seen in Figure 10.4. The variations are of a few mm/hour up to more than 2 cm within 20 minutes early in the morning. Figure 10.5 shows that the variations relative to the site TURT 7 (Turtmann) are much smaller (about 1-2 mm/hour). An exception is the highest site EMSH 9 with a sudden change of the delay by 1 cm around 9:00 am. This feature is probably real, since it shows up in the results of all the different models (see Figure 10.12 below). Figure 10.5 also illustrates that the gradient in height of this local model is quite different from the one of the standard atmosphere. Between the lowest (TURT 7) and the highest site (EMSH 9) we have a difference of 5.5 cm or a gradient difference between the two models of about 3.3 mm per 100 m height difference.

Delays From Deterministic Estimation (Approach B):

If only one deterministic troposphere parameter is estimated per baseline and session, no information is available on the temporal changes.

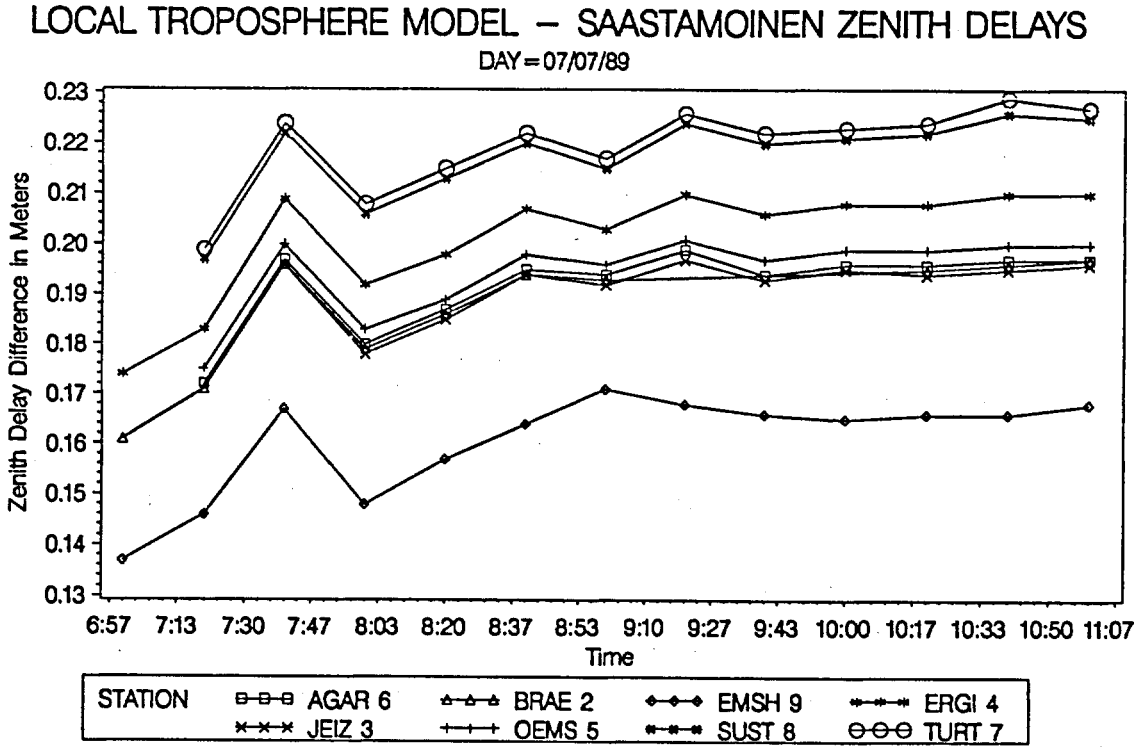

Figure 10.4

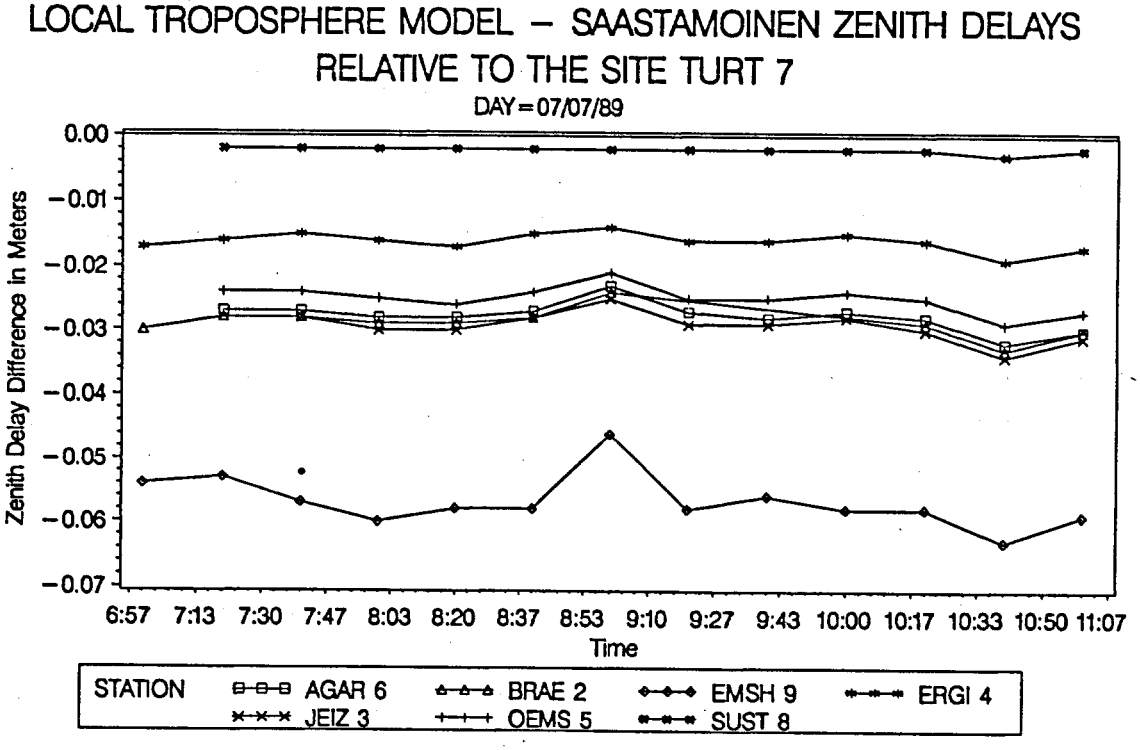

Figure 10.5

Figure 10.6 demonstrates what happens if we estimate 1, 3, 5, or 9 troposphere delay parameters per session corresponding to 1 parameter per 4 hours, per 1.5 hours, per 1 hour, and per 0.5 hours.

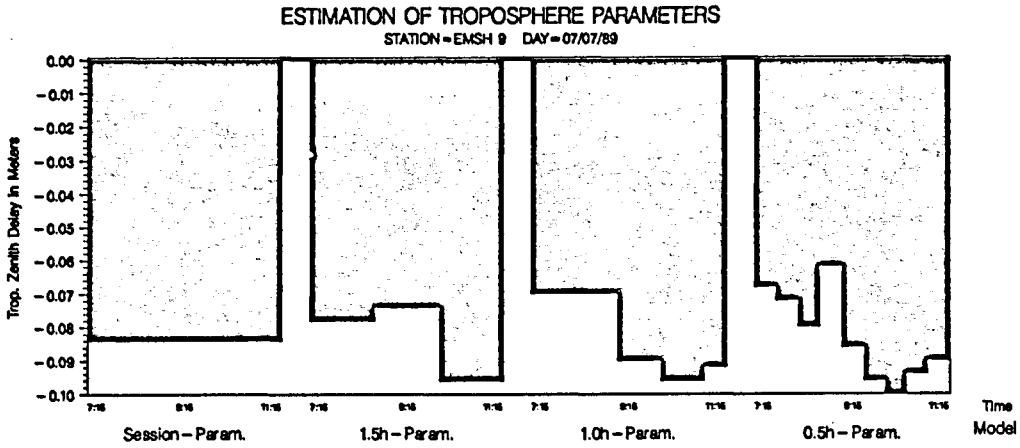

Figure 10.6
1, 3, 5, and 9 Tropospheric Zenith Delays Estimated per Session With A Priori Constraints Between Subsequent Parameters of 7.4 mm/1.5h, 6 mm/1h, and 4.2 mm/0.5h for 3, 5, and 9 Parameters Respectively

More and more details of the time variations become visible. By increasing and increasing the number of parameters per session we could go to the limit of estimating one troposphere zenith delay per observation epoch. This extreme case will give the same results as the stochastic estimation (approach D). The question is, however, whether the obtained variations of the tropospheric zenith delay are real. This may depend very much on the momentary strength of the satellite scenario.

To keep the variations in time within reasonable limits, we may use a priori constraints between subsequent parameters (see section 5.2.1.1). In Figure 10.7 we show the tropospheric zenith delays we get when small or large constraints are introduced.

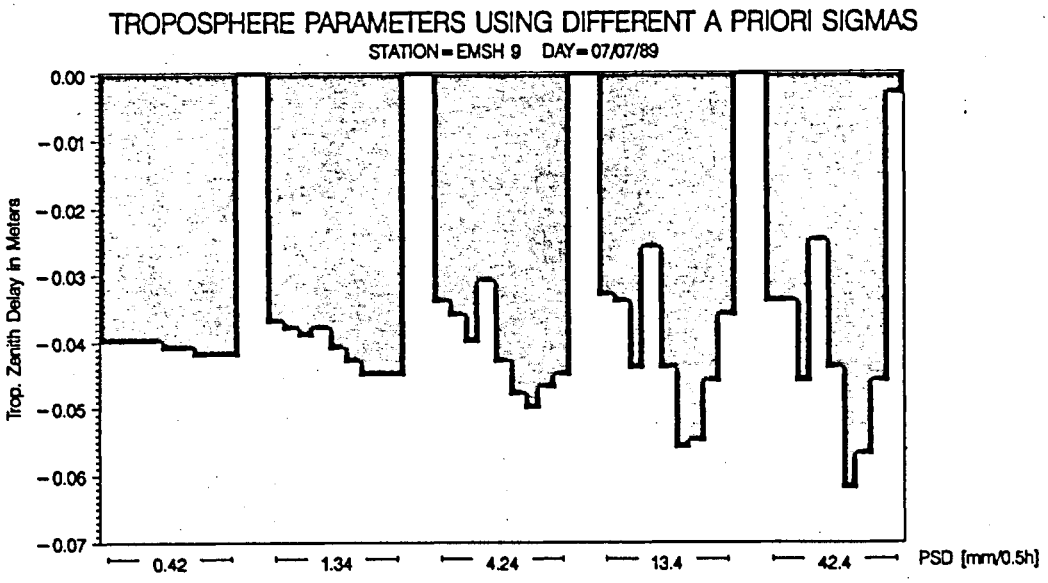

Figure 10.7

It is obvious that the tropospheric delays obtained with large a priori sigmas (e.g. 42.4 mm/0.5h) are unrealistic (changes of several centimeters within half an hour). A value of 4.2 mm/0.5h (corresponding to a power spectral density Φ of about 10^{-8} m^2/sec according to eqn. (5.31)) might be appropriate in view of the fact that we estimate **relative** troposphere parameters in a small network. The formal errors of the troposphere delay parameters vary between 0.8 and 3 mm depending on the size of the constraints and the number of parameters estimated per session.

The problem of finding reasonable a priori constraints in the deterministic case is analogous to the choice of reasonable values for the power spectral density in the stochastic estimation and will be further discussed below (approach D).

Delays from the Estimation of a Polynomial in Height (Approach C):

Since in this case one parameter (the linear change of the tropospheric delay with height) is estimated per session, we get information only on the change of the delay with height (relative to an applied standard model). The values obtained for the three

sessions are (in mm per 100 m of height difference) -0.0012 mm/100 m, -0.0020 mm/100 m, and -0.0027 mm/100 m with formal errors of 0.0001 mm/100 m.

Delays from Stochastic Estimation (Approach D):

Figure 10.8 shows an example of the tropospheric zenith delays obtained with stochastic estimation using different power spectral densities (PSD). The behaviour of the tropospheric zenith delays when changing the PSD is comparable to the one in the case of deterministic estimation when changing the a priori constraints (see Figure 10.7).

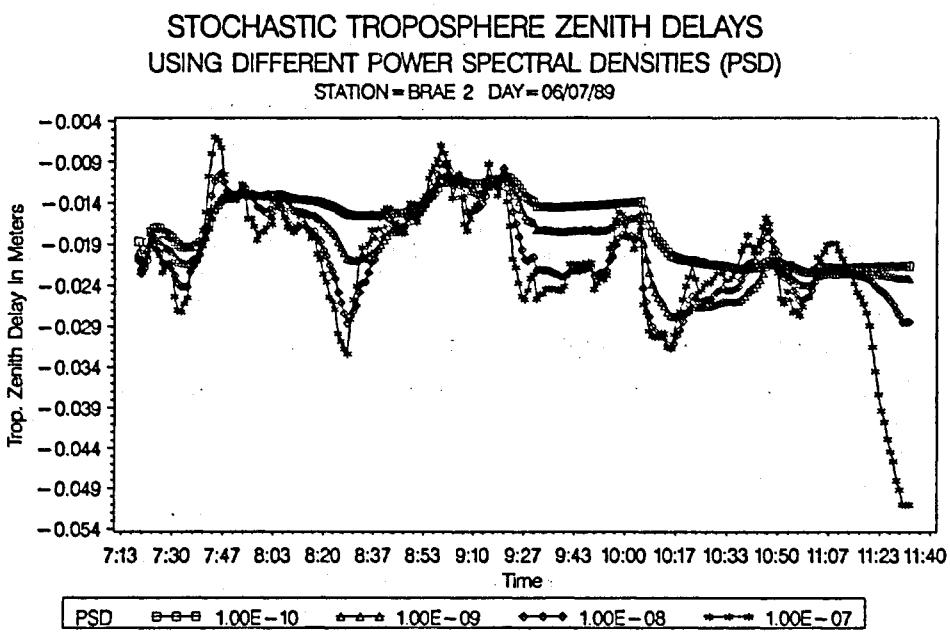

Figure 10.8

Although some of the characteristics of the variation in time may be real, an influence of the satellite scenario (see Figure 10.9 and Figure 10.3) on the estimation process can easily be recognized.

The power spectral density should therefore to be chosen to take into account not only the size of the network and the clues obtained from surface met data (e.g. the information in Figures

10.4 and 10.5), but also the satellite scenario: smaller PSD values should be used for a poor satellite geometry.

The formal errors of the stochastic delays are of the order of 0.8 mm for a PSD of 10^{-9} m^2/sec, 10 mm for a PSD of 10^{-7} m^2/sec.

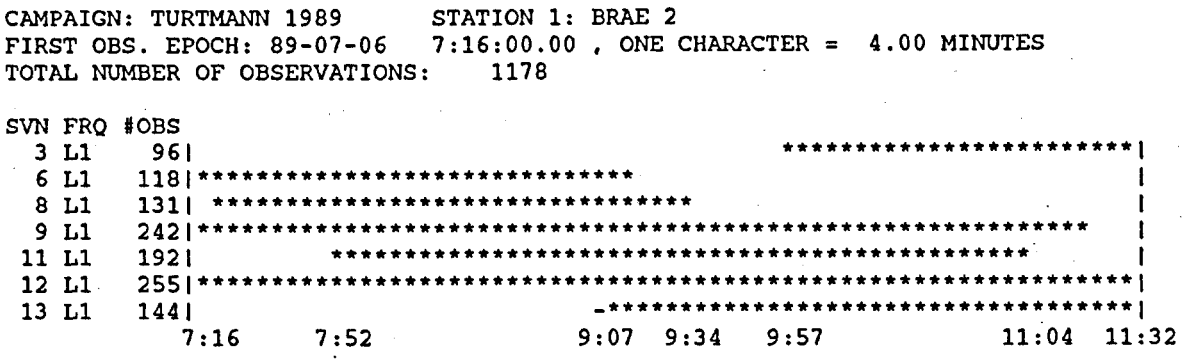

Figure 10.9
Satellite Tracking Scenario of July 6
for the Turtmann 1989 Campaign

10.3.1.2 Comparison of Tropospheric Delays

The different approaches may be compared with each other either as a function of height or as a function in time.

Comparison in Height:

All the four approaches of Table 10.2 give us the change of the tropospheric zenith delay with height. The comparison of these height gradients is presented in Figure 10.10 and demonstrates that all the four models are in close agreement. Especially the fact that the local troposphere model derived from surface met data only and, as a totally independent approach, the estimation of troposphere parameters from GPS observations give similar results, has to be emphasized.

Although the four models differ by only 1 cm over the entire height difference of 1650 m (corresponding to a gradient difference of 0.6 mm/100 m), there is a large discrepancy between the gradient of the standard troposphere model given by the zero line

in Figure 10.10 and the gradients of the four models. Obviously the standard troposphere model is not representative for the gradients actually present in the atmosphere. A wrong gradient, however, will cause a scale in the station heights.

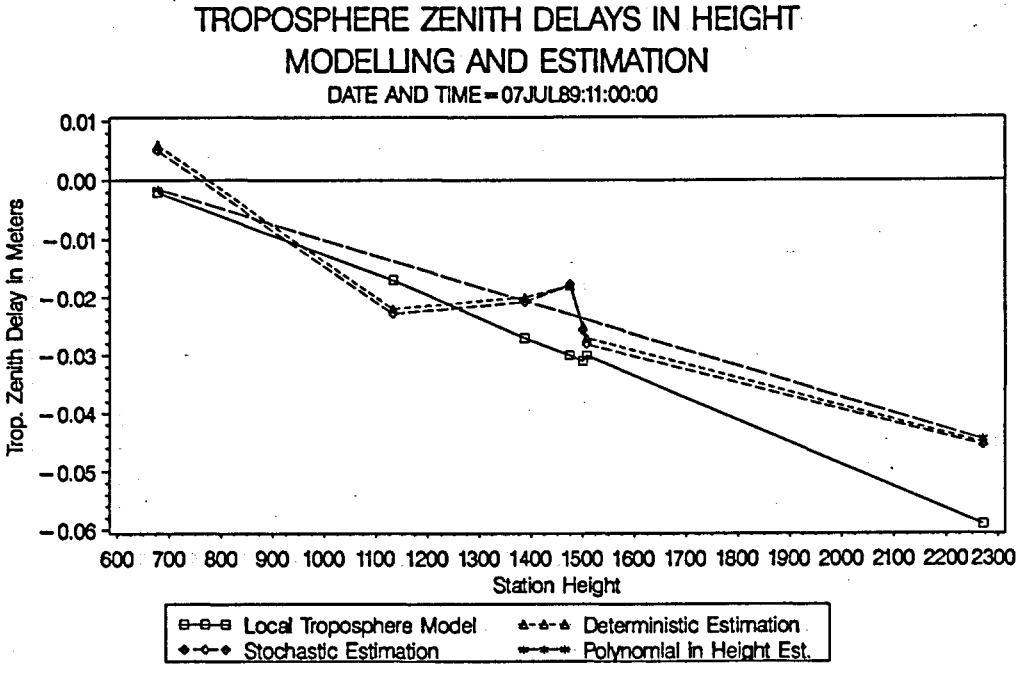

Figure 10.10

Comparison in Time:

Three of the four approaches listed in Table 10.2, namely A, B, and D, yield time variations of the tropospheric delay. We have to be careful, however, since the deterministic and stochastic estimates have been determined relative to a standard model of the tropospheric delays and relative to the delay at the TURT 7 site:

$$\Delta r^0_{Est,i}(t) = (\Delta r^0(t) - \Delta r^0_{Model})_{STATION\ i} - (\Delta r^0(t) - \Delta r^0_{Model})_{TURT\ 7} \qquad (11.1)$$

We have to subtract the same standard model from the tropospheric delays of the local troposphere model. The results for the site BRUN 1 on July 6 and for the site EMSH 9 on July 7 are given in Figures 10.11 and 10.12.

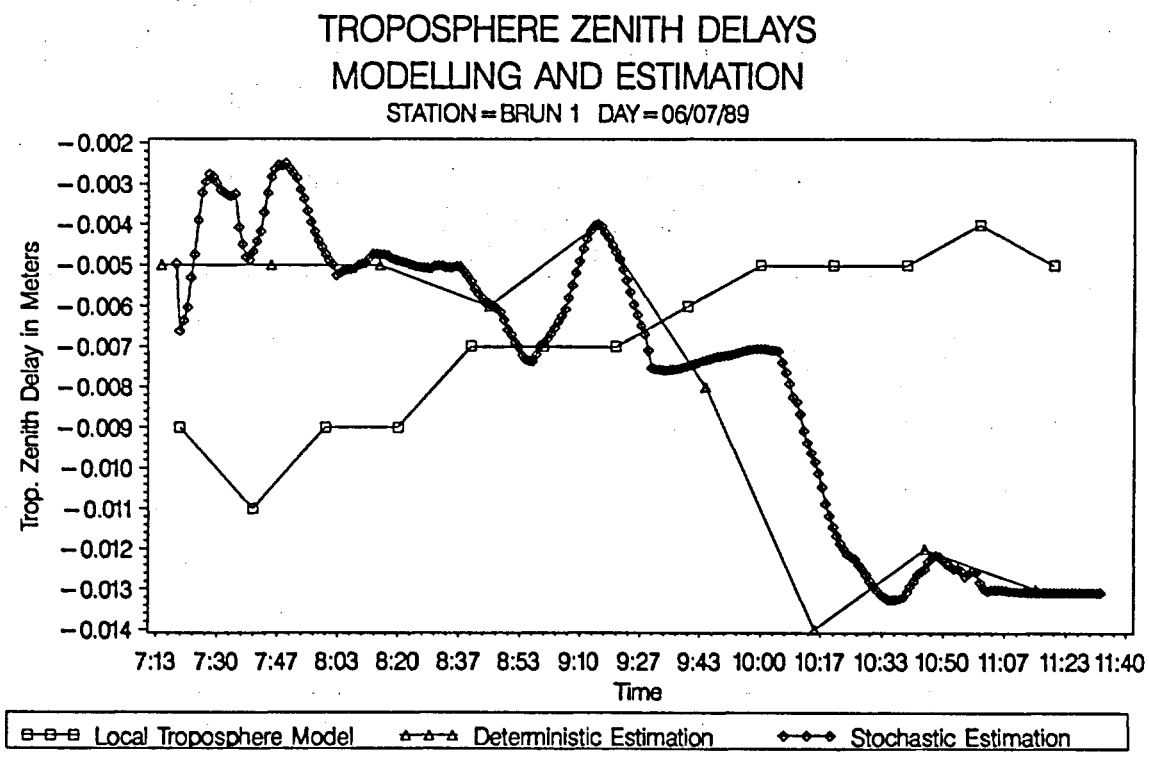

Figure 10.11

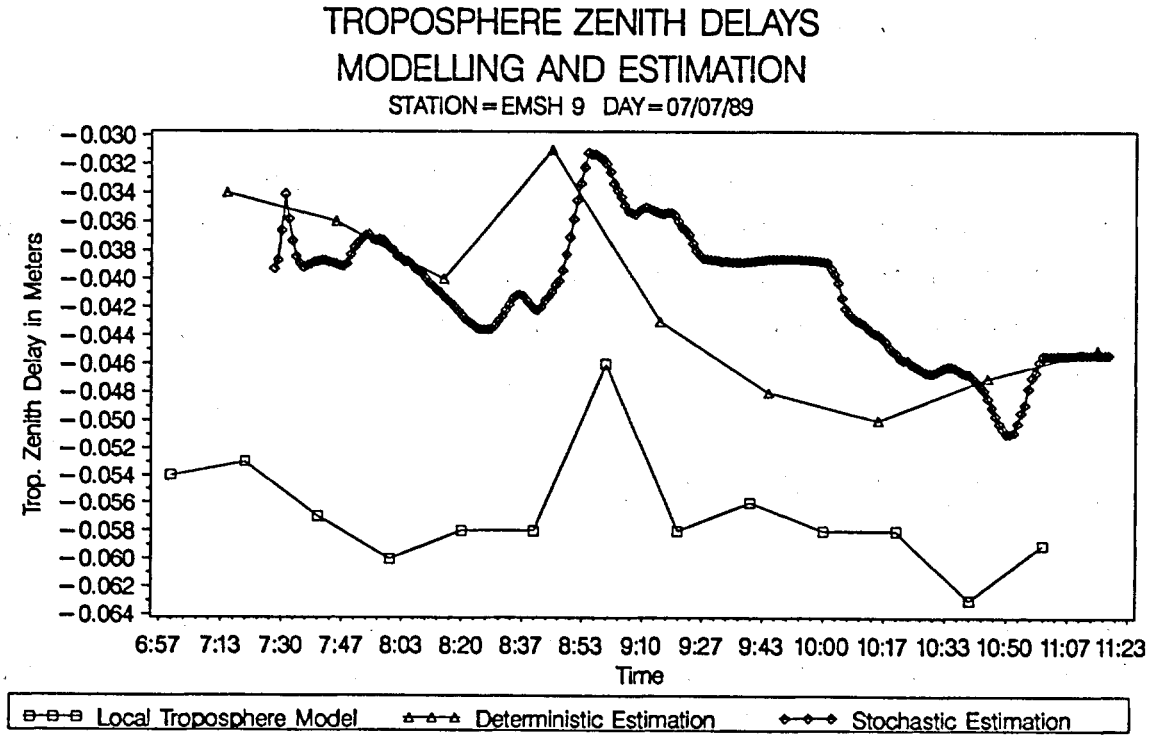

Figure 10.12

In both figures the deterministic and stochastic estimations are very similar. This is to be expected, because the same set of GPS observations was used in both estimation processes. But it also means, that a detailed modeling of the troposphere can be done using conventional least squares estimation techniques. If the same time resolution and corresponding values for the a priori constraints in the deterministic and the power spectral density in the stochastic case are used, the results should be identical within the formal errors. The results shown in Figures 10.11 and 10.12 have been computed using a priori constraints of σ_{rel} = 4.24 mm and σ_{abs} = 100 mm for the deterministic estimation (see eqns. (5.33) to (5.37)). A power spectral density of 10^{-10} m^2/sec and an a priori sigma of 100 mm were used in the stochastic case.

Whereas on July 6 (see Figure 10.11) no correlation at all can be detected between the local troposphere model and the estimated variations, there is a nice resemblance between the two on July 7, indicating that at least part of the variations are probably real. The systematic shift of about 1.5 cm between the local model and estimated values at the highest site EMSH 9 shows that a small gradient difference still exists between the two approaches. This is even more apparent in Figure 10.10.

10.3.2 The Site Coordinates

In this section the coordinate sets resulting from the four approaches (see Table 10.2) are compared with each other and with the terrestrial solution.

10.3.2.1 Comparison of GPS Solutions

Since troposphere biases and troposphere model differences propagate into the station heights (see section 3.2.2.1), we only compare the differences in the station heights. The changes in the horizontal coordinates between the four models are below 1 mm. In Figure 10.13 the height differences between the solu-

tions A, B, and D and the solution C (estimation of a troposphere gradient in heigth) are plotted as a function of station height. In the deterministic estimation B only 1 troposphere parameter per session (and baseline) was estimated. The stochastic solution was poduced with a power spectral density of 10^{-8} m^2/sec (a smaller value will give results similar to the solution B).

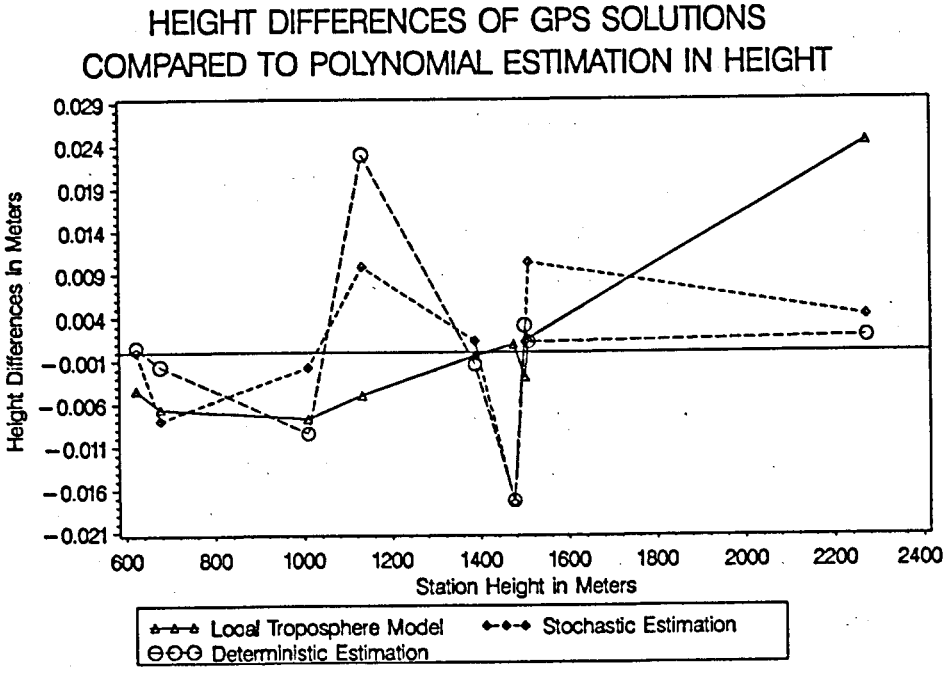

Figure 10.13

The trend we see in the height differences between the local troposphere model and the other models is caused by the difference in the troposphere gradient presented in the last section (see Figure 10.10). According to the magnification factor given in section 3.2.2.1 a difference of 1 cm in the tropospheric zenith delay between the highest and the lowest site produces a height difference of about 3 cm between these sites, in good agreement with what we see in Figure 10.13. The gradients in height of the other two solutions are very consistent with the gradient estimation (approach C).

The heights of the stochastic estimation remain closer to solution C compared to solution B. This might indicate that some of the time variations of the tropospheric delays visible in the stochastic estimation (see e.g. Figure 10.12) are real. There can

be no doubt that such time variations occur in the early morning hours.

10.3.2.2 Comparison with Terrestrial Solution

The comparison with the terrestrial solution has to be done through a Helmert transformation (similarity transformation), because the terrestrial solution is given in a different coordinate system. For the site EMSH 9 there is no ground truth available. Again we are interested only in the station heights, in this case the residuals in height after the transformation. These height residuals are given in Figure 10.14 for the solutions A to D.

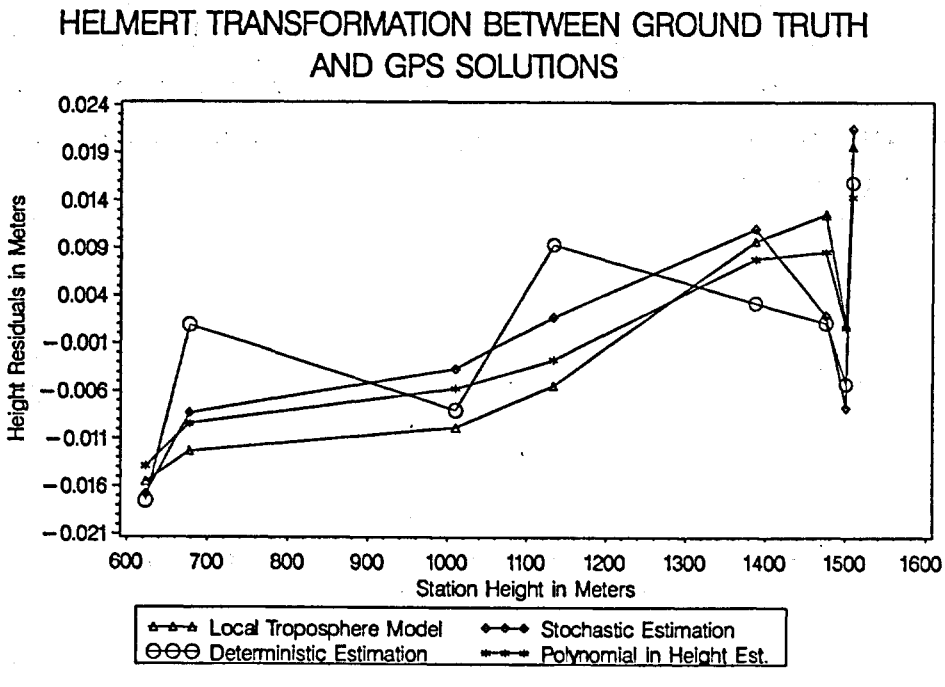

Figure 10.14

The four solutions exhibit a common slope in height compared to the ground truth. Because all the solution show the same trend, probably the ground "truth" is not correct (the terrestrial measurements are also affected by the troposphere). The strange downward peak at a height of about 1500 m (BRAE 2) might be explained by an incorrect antenna height. With the exception of solution B all the solutions agree with each other within 3-8 mm.

It should be pointed out that the difference between solution B and D is not due to the fact that in one case deterministic, in the other stochastic techniques have been applied. Both solutions could be obtained by either technique. The main difference is that only 1 troposphere parameter was estimated per session and baseline in the deterministic solution B (corresponding to a filter solution with a very small PSD). With the estimation of more parameters per session we can produce the same results as the ones using stochastic modeling. This has been demonstrated in section 10.3.1.2.

Figure 10.14 suggests that the GPS results have a quality of about 1 cm in height over a height difference of 1650 m. To assess the actual accuracy of the gradient in height given by the GPS solutions (which is quite different from the gradient in the terrestrial solution), however, the GPS data of the other Turtmann campaigns taking place under different meteorological conditions should be processed in the same way and compared with the results presented here.

A. APPENDIX

A.1 Transformation from Osculating Keplerian Elements to Position and Velocity

We start with the osculating Keplerian elements (see Figure 4.1) given at epoch t_0:

- a : Semi-major axis
- e : Eccentricity
- i : Inclination
- Ω : Right ascension of ascending node
- ω : Argument of perigee
- t_p : Perigee passing time

Instead of t_p also the argument of latitude $u_0=u(t_0)$ may be given.

With the gravity constant G and the mass M of the central body we then have:

Mean motion: $$n = \left(\frac{GM}{a^3} \right)^{1/2} \qquad (A.1)$$

Mean anomaly: $$M = n \cdot (t-t_p) \qquad (A.2)$$

Eccentric anomaly E from Keplers equation (to be solved iteratively):

$$E - e \cdot \sin E = M \qquad (A.3)$$

True anomaly ν from

$$\tan \frac{\nu}{2} = \sqrt{\frac{1+e}{1-e}} \cdot \tan \frac{E}{2} \qquad (A.4)$$

or from argument of latitude u:

$$\nu = u - \omega \tag{A.5}$$

Length of radius vector:

$$r = \frac{a\cdot(1-e^2)}{1 + e\cdot\cos\nu} = a\cdot(1 - e\cdot\cos E) \tag{A.6}$$

Position vector (components) in orbital plane:

$$\begin{aligned} x &= r\cdot\cos\nu \\ y &= r\cdot\sin\nu \\ z &= 0 \end{aligned} \tag{A.7}$$

Position vector in equatorial coordinate system:

$$\mathbf{r} = \mathbf{R}_3(-\Omega)\mathbf{R}_1(-i)\mathbf{R}_3(-\omega)\begin{pmatrix} x \\ y \\ z \end{pmatrix} \tag{A.8}$$

Velocity vector components in orbital plane:

$$\begin{aligned} \dot{x} &= -\sqrt{\frac{GM}{a\cdot(1-e^2)}}\cdot\sin\nu \\ \dot{y} &= \sqrt{\frac{GM}{a\cdot(1-e^2)}}\cdot(e + \cos\nu) \\ \dot{z} &= 0 \end{aligned} \tag{A.9}$$

Velocity vector in equatorial coordinate system:

$$\dot{\mathbf{r}} = \mathbf{R}_3(-\Omega)\mathbf{R}_1(-i)\mathbf{R}_3(-\omega)\begin{pmatrix} \dot{x} \\ \dot{y} \\ \dot{z} \end{pmatrix} \tag{A.10}$$

Rotation matrices:

$$R_3(-\omega) = \begin{pmatrix} \cos\omega & -\sin\omega & 0 \\ \sin\omega & \cos\omega & 0 \\ 0 & 0 & 1 \end{pmatrix} \tag{A.11}$$

$$R_1(-i) = \begin{pmatrix} 1 & 0 & 0 \\ 0 & \cos i & -\sin i \\ 0 & \sin i & \cos i \end{pmatrix} \tag{A.12}$$

$$R_3(-\Omega) = \begin{pmatrix} \cos\Omega & -\sin\Omega & 0 \\ \sin\Omega & \cos\Omega & 0 \\ 0 & 0 & 1 \end{pmatrix} \tag{A.13}$$

A.2 Transformation from Position and Velocity to Osculating Keplerian Elements

Calculate the two vectors

$$\mathbf{h} = \mathbf{r} \times \dot{\mathbf{r}} \qquad h = |\mathbf{h}| \tag{A.14}$$

$$\mathbf{q} = -\left(\mathbf{h}\times\dot{\mathbf{r}} + GM\,\frac{\mathbf{r}}{r} \right) \qquad q = |\mathbf{q}| \tag{A.15}$$

$\mathbf{h}$ is a vector normal to the orbital plane, giving the angles i and Ω:

$$\mathbf{h} = h \begin{pmatrix} \sin i \sin\Omega \\ -\sin i \cos\Omega \\ \cos i \end{pmatrix} \tag{A.16}$$

$$\tan\Omega = -\,h_1/h_2 \quad , \quad \mathbf{h}^T = (h_1, h_2, h_3) \tag{A.17}$$

$$\cos i = h_3/h \tag{A.18}$$

The vector $\mathbf{q}$ is inside the orbital plane and points to the perigee.

True anomaly:

$$\sin\nu = \frac{h}{q\cdot r}\ \mathbf{r}\cdot\dot{\mathbf{r}} \tag{A.19}$$

$$\cos \nu = \frac{h^2 - GMr}{q \cdot r} \tag{A.20}$$

Argument of latitude with:

$$\sin i \cdot \sin u = r_3/r \;,\quad \mathbf{r}^T = (r_1, r_2, r_3) \qquad \dot{\mathbf{r}}^T = (\dot{r}_1, \dot{r}_2, \dot{r}_3) \tag{A.21}$$

$$\sin i \cdot \cos u = \frac{1}{r \cdot h} \cdot (r_3 (\mathbf{r} \cdot \dot{\mathbf{r}}) - \dot{r}_3 \cdot r^2) \tag{A.22}$$

Argument of perigee:

$$\omega = u - \nu \tag{A.23}$$

Semi-major axis and eccentricity:

$$e = \frac{q}{GM} \tag{A.24}$$

$$a = \frac{h^2}{GM \cdot (1 - e^2)} \tag{A.25}$$

With mean motion n and eccentric anomaly E

$$n = \left(\frac{GM}{a^3} \right)^{1/2} \tag{A.26}$$

$$\tan \frac{E}{2} = \sqrt{\frac{1-e}{1+e}} \cdot \tan \frac{\nu}{2} \tag{A.27}$$

we obtain the perigee passing time

$$t_p = t - (E - e \cdot \sin E)/n \tag{A.28}$$

A.3 Partials of Position and Velocity With Respect to Osculating Keplerian Elements

Partials with respect to semi-major axis a:

$$\frac{\partial x}{\partial a} = \frac{x}{a} + \frac{3n}{2} \cdot \frac{\sin\nu}{\sqrt{1-e^2}} \cdot (t-t_p)$$

$$\frac{\partial y}{\partial a} = \frac{y}{a} - \frac{3n}{2} \cdot \frac{e+\cos\nu}{\sqrt{1-e^2}} \cdot (t-t_p)$$

$$\frac{\partial \dot{x}}{\partial a} = -\frac{\dot{x}}{2a} + \frac{3GM}{2r^3} \cdot \frac{x}{a} \cdot (t-t_p) \qquad \text{(A.29)}$$

$$\frac{\partial \dot{y}}{\partial a} = -\frac{\dot{y}}{2a} + \frac{3GM}{2r^3} \cdot \frac{y}{a} \cdot (t-t_p)$$

Partials with respect to eccentricity e:

$$\frac{\partial x}{\partial e} = -\frac{r}{1-e^2} \cdot (2 - \cos^2\nu + e\cdot\cos\nu)$$

$$\frac{\partial y}{\partial e} = \frac{y}{1-e^2} \cdot \cos\nu \qquad \text{(A.30)}$$

$$\frac{\partial \dot{x}}{\partial e} = -\frac{a\cdot n\cdot\sin\nu}{(1-e^2)^{3/2}} ((e + \cos\nu) + (1 + e\cdot\cos\nu)\cos\nu)$$

$$\frac{\partial \dot{y}}{\partial e} = -\frac{a\cdot n}{(1-e^2)^{3/2}} (1 - (2 + e\cdot\cos\nu)\cos^2\nu)$$

Partials with respect to perigee passing time t_p:

$$\frac{\partial x}{\partial t_p} = - \dot{x}$$

$$\frac{\partial y}{\partial t_p} = - \dot{y} \qquad \text{(A.31)}$$

$$\frac{\partial \dot{x}}{\partial t_p} = + \frac{GMx}{r^3}$$

$$\frac{\partial \dot{y}}{\partial t_p} = + \frac{GMy}{r^3}$$

Partials of rotation matrices:

$$\frac{\partial R_3}{\partial \omega}(-\omega) = \begin{pmatrix} -\sin\omega & -\cos\omega & 0 \\ \cos\omega & -\sin\omega & 0 \\ 0 & 0 & 0 \end{pmatrix} \qquad \text{(A.32)}$$

$$\frac{\partial R_1}{\partial i}(-i) = \begin{pmatrix} 0 & 0 & 0 \\ 0 & -\sin i & -\cos i \\ 0 & \cos i & -\sin i \end{pmatrix} \qquad \text{(A.33)}$$

$$\frac{\partial R_3}{\partial \Omega}(-\Omega) = \begin{pmatrix} -\sin\Omega & -\cos\Omega & 0 \\ \cos\Omega & -\sin\Omega & 0 \\ 0 & 0 & 0 \end{pmatrix} \qquad \text{(A.34)}$$

Derivatives with respect to argument of latitude u:

$$\frac{d}{du} r = \frac{r^2}{a^2 n \sqrt{1-e^2}} \dot{r}$$

$$\frac{d}{du} \dot{r} = - \frac{a \cdot n}{r \sqrt{1-e^2}} r \qquad \text{(A.35)}$$

REFERENCES

Abramson, R. (1982). "Technical Operating Report for NAVSTAR Block II Satellite, Volume IV, Solar Force Model." Rockwell International, SSD81-0164-4.

Ackroyd, N., R. Lorimer (1990). "Global Navigation. A GPS User's Guide." Lloyd's of London Press Ltd., London.

Anodina, T. (1988). "The GLONASS System Technical Characteristics and Performance." International Civil Aviation Organization Special, Committee on Future Air Navigation Systems (FANS), 4th Meeting, Montreal, May 2-20, FANS/4-WP/75.

Anodina, T., M. Prilepin (1989). "The GLONASS System." Proceedings of the Fifth International Geodetic Symposium on Satellite Positioning, Las Cruces, New Mexico, March 13-17, Vol. 1, pp. 13-18.

Bauersima, I. (1983). "Navstar/Global Positioning System (GPS) (II)." Mitteilungen der Satelliten-Beobachtungsstation Zimmerwald, University of Berne, No. 10.

Berg, H. (1948). "Allgemeine Meteorologie." Dümmler's Verlag, Bonn.

Bernstein, H. (1987). "Der Radar-Delay-Effekt in Entfernungsmessungen zu Satelliten." Zeitschrift für Vermessungswesen, Jg. 112, Nr. 2, S. 78-87, Stuttgart.

Beutler, G. (1982). "Lösung von Parameterbestimmungsproblemen in Himmelsmechanik und Satellitengeodäsie mit modernen Hilfsmittel." Astronomisch-goedätische Arbeiten der Schweiz, Schweizerische Geodätische Komission, Band 34.

Beutler, G., D.A. Davidson, R.B. Langley, R. Santerre, P. Vanicek, D.E. Wells (1984). "Some Theoretical and Practical Aspects of Geodetic Positioning Using Carrier Phase Difference

Observations of GPS Satellites." Mitteilungen der Satelliten-Beobachtungsstation Zimmerwald, Nr. 14, Druckerei der Universität Bern.

Beutler, G., W. Gurtner, I. Bauersima, R. Langley (1985). "Modelling and Estimation of Orbits of GPS Satellites." Proceedings of the First International Symposium on Precise Positioning with the Global Positioning System, Rockville, MD, April 15-19, Vol. 1, pp. 99-111.

Beutler, G., W. Gurtner, M. Rothacher, T. Schildknecht, I. Bauersima (1986). "Determination of GPS Orbits Using Double Difference Carrier Phase Observations From Regonal Networks." Bulletin Géodésique, Vol. 60, pp. 205-220.

Beutler, G., I. Bauersima, S. Botton, W. Gurtner, M. Rothacher, T. Schildknecht (1987a). "Accuracy and Biases in the Geodetic Application of the Global Positioning System." Paper presented at the XIX General Assembly of the International Union of Geodesy and Geophysics (IUGG), Vancouver, Canada.

Beutler, G., I. Bauersima, W. Gurtner, M. Rothacher, T. Schildknecht (1987b). "Evaluation of the 1984 Alaska Global Positioning System Campaign with the Bernese GPS Software." Journal of Geophysical Research, Vol. 92, No. B2, pp. 1295-1303.

Beutler, G., I. Bauersima, W. Gurtner, M. Rothacher, T. Schildknecht, A. Geiger (1988). "Atmospheric Refraction and Other Important Biases in GPS Carrier Phase Observations." Monograph 12, School of Surveying, University of New South Wales, Australia.

Beutler, G. (1990). "Numerische Integration gewöhnlicher Differentialgleichungssysteme: Prinzipien und Algorithmen." Mitteilungen der Satelliten-Beobachtungsstation Zimmerwald, Nr. 23, Druckerei der Universität Bern.

Beutler, G. (1992). "Himmelsmechanik II." Mitteilungen der Satelliten-Beobachtungsstation Zimmerwald, Druckerei der Universität Bern, in print.

Blewitt, G., R.W. King (1991). "Terrestrial Reference Frame Needs for the 1990's." Paper presented at the XXth General Assembly of the IUGG, August 11-24, Vienna, Austria.

Boucher, C., Z. Altamini (1989). "ITRF 89 and Other Realizations of the IERS Terrestrial Reference System for 1989." IERS Technical Note 6, Central Bureau of IERS, Observatoire de Paris, France.

Cappellari, J., C. Velez, A. Fuchs (1976). "Mathematical Theory of the Goddard Trajectory Determination System." Goddard Space Flight Center, X-582-76-77, Greenbelt, MD.

Carnebianca, C., G. Mastini, R. Rizzo (1985). "NAVSAT System Configuration Study." ITALSPAZIO, ITS-TR-011/85, ESA Contract No. 5754/84/F/RD(SC).

Chao, C.C. (1973). "A new Method to Predict Wet Zenith Range Corrections From Surface Measurements." Technical Report California Institute of Technology, Jet Propulsion Laboratory, 32-1256, XIV, pp. 33-41.

Colombo, O.L. (1986). "Ephemeris Errors of GPS Satellites." Bulletin Géodésique, Vol. 60, pp. 64-84.

Daly, P. (1988). "Aspects of the Soviet Union's Glonass Satellite Navigation System." The Journal of Navigation, Vol. 41, No. 2.

Davidson, D., D. Delikaraoglou, R. Langley, B. Nickerson, P. Vanicek, D. Wells (1983). "Global Positioning System Differential Positioning Simulations." Department of Surveying Engineering Technical Report, No. 90, University of New Brunswick, Fredericton, Canada.

Davis, J.L., T.A. Herring, I.I. Shapiro, A.E.E. Rogers, G. Elgered (1985). "Geodesy by Radio Interferometry: Effects of Atmospheric Modeling Errors on Estimated Baseline Length." Radio Sciences, Vol. 20, No. 6, pp. 1593-1607.

De Jong, C.D. (1991). "GPS-Satellite Orbits and Atmospheric Effects." Delft University of Technology, Reports of the Faculty of Geodetic Engineering, Mathematical and Physical Geodesy, No. 91.1, Delft.

Elgered, G., J.M. Johansson, B.O. Rönnäng (1990). "Characterizing Atmospheric Water Vapour Fluctuations Using Microwave Radiometry." Research Report No. 165, Department of Radio and Space Science With Onsala Space Observatory, Chalmers University of Technology, Göteborg, Sweden.

ESA Proposal (1990). Proposal to ESA Project "Study of the Location of ESA Tracking Sites by GPS." RFQ/3-6930/90/D/IM.

ESOC Contract (1990). "Study of the Location of ESA Tracking Sites by GPS." Contract No. 9166/90/D/IM(SC).

Euler, H., G. Hoefgen (1983). "GRANAS, A New Satellite-Based Navigation System." Presented at the 1st International Symposium Land Vehicle Navigation, Berlin Nov.23, 1984.

Feigl, K., R.W. King, T.A. Herring, M. Rothacher (1991). "A Scheme for Reducing the Effect of Selective Availability on Precise Geodetic Measurements From the Global Poistioning System." Geophysical Research Letters, Vol. 18, No. 7, Pages 1289-1292.

Feltens, J. (1988). "Several Aspects of Solar Radiation Pressure." Proceedings of the International GPS-Workshop in Darmstadt, April 10-13, 1988, published in Lecture Notes in Earth Sciences, GPS-Techniques Applied to Geodesy and Surveying, Springer Verlag, Berlin, pp. 487-502.

Flechtner, F., K. Kaniuth, Ch. Reigber, H. Wilmes (1990). "The Precise Range and Range Rate Equipment PRARE: Status Report on System Development, Preparation for ERS-1 and Future Plans." Proceedings of the Second International Symposium on Precise Positioning with the Global Positioning System, Ottawa, Canada, September 3-7, The Canadian Institute of Surveying and Mapping, pp. 111-123.

Fliegel, H.F., W.A. Feess, W.C. Layton, N.W. Rhodus (1985). "The GPS Radiation Force Model." Proceedings of the First International Symposium on Precise Positioning with the Global Positioning System, Rockville, MD, April 15-19, Vol. 1, pp. 113-119.

Fliegel, H.F., T.E. Gallini (1989). "Radiation Pressure Models for Block-II GPS Satellites." Proceedings of the Fifth International Geodetic Symposium on Satellite Positioning, Las Cruces, New Mexico, March 13-17, Vol. 2, pp. 789-798.

Frei, E., G. Beutler (1990). "Rapid Static Positioning Based on the Fast Ambiguity Resolution Approach: The Alternative to Kinematic Positioning." Proceedings of the Second International Symposium on Precise Positioning with the Global Positioning System, Ottawa, Canada, September 3-7, The Canadian Institute of Surveying and Mapping, pp. 1196-1216.

Gardner, C.S. (1976). "Effects of Horizontal Refractivity Gradients on the Accuracy of Laser Ranging to Satellites." Radio Sciences, Vol. 11, No. 12, pp. 1037-1044.

Geiger, A. (1987). "Simplified Error Estimation of Satellite Positioning." Paper presented at the GPS Technology Workshop, Jet Propulsion Laboratory, Pasadena, March 23.

Gelb, A. (1974). "Applied Optimal Estimation." MIT Press, Cambridge, Mass. .

Goad, C.C., L. Goodman (1974). "A Modified Hopfield Tropospheric Refraction Correction Model." Paper presented at the Fall An-

nual Meeting of the American Geophysical Union, San Francisco, California, December 12-17.

Goad, C.C., B.W. Remondi (1983). "Initial Relative Positioning Results Using Global Positioning System." Paper presented at the IUGG XVIII General Assembly, Hamburg.

Green, G.B., P.D. Massati, N.W. Rhodus (1989). "The GPS 21 Primary Satellite Constellation." Navigation: Journal of the Institute of Navigation, Washington, Vol. 36, No .1, pp. 9-24.

Gurtner, W., G.Beutler, M. Rothacher (1989a). "Combination of GPS Observations Made With Different Receiver Types." Proceedings of the Fifth International Geodetic Symposium on Satellite Positioning, Las Cruces, New Mexico, March 13-17, Vol. 1, pp. 362-374.

Gurtner, W., G. Beutler, S. Botton, M. Rothacher, A. Geiger, H.-G. Kahle, D. Schneider, A. Wiget (1989b). "The Use of the Global Positioning System in Mountainous Areas." Manuscripta Geodaetica, Vol. 14, pp. 53-60.

Gurtner, W., G.L. Mader (1990a). "Receiver Independent Exchange Format Version 2." GPS Bulletin of the Commission VIII of the International Coordinates of Space Techniques for Geodesy and Geodynamics (CSTG), Vol. 3, No. 3, September-October.

Gurtner, W., G.L. Mader (1990b). "The RINEX Format: Current Status, Fututre Developments." Proceedings of the Second International Symposium on Precise Positioning with the Global Positioning System, Ottawa, Canada, September 3-7, The Canadian Institute of Surveying and Mapping, pp. 977-992.

Hartl, Ph., Ch. Reigber (1985). "The Precise Range and Range Rate Equipment - PRARE." International Coordination of Space Techniques for Geodesy and Geodynamics (CSTG), Bulletin No. 8, Munich, pp. 124-134.

Herring, T.A., J.L. Davis, I.I. Shapiro (1990). "Geodesy by Radio Interferometry: The Application of Kalman Filtering to the Analysis of Very Long Baseline Interferometry Data." JGR, 95, pp. 12561-12581.

Hopfield, H.S. (1977). "Tropospheric Correction of Electromagnetic Ranging Signals to a Satellite: A Study of Parameters." Paper presented at Symposium on Electromagnetic Distance Measurements and the Influence of Atmospheric Refraction, International Association of Geodesy, Wageningen, The Netherlands, 23-28 May.

IAU Resolutions on Astronomical Constants, Time Scales, and the Fundamental Reference Frame (1981). U.S. Naval Observatory, Circular No. 163.

International Earth Rotation Service (IERS) (1989). "IERS Standards (1989)." D.D. McCarthy (ed.), November 1989, Observatoire de Paris.

International Earth Rotation Service (IERS) (1990). "The First GPS IERS and Geodynamics Experiment, January 22 - February 13, 1991." Newsletter #3, December 21, JPL, Pasadena, CA.

Kahman, H. (1978). "Elektronische Messverfahren in der Geodäsie." Wichmann, Karlsruhe.

King, R., E. Masters, C. Rizos, A. Stolz, J. Collins (1985). "Surveying with GPS." The University of New South Wales, School of Surveying, Monograph 9, Kensington, N.S.W.

King-Hele, D.G. (1964). "Theory of Satellite Orbits in an Atmosphere." Butterworths, London.

La Brune, Y., F. Nouel, C. Jayles (1986). "Precise Orbit Determination with DORIS System and the Associated ZOOM Software." Second International Symposium on Spacecraft Flight Dynamics, Darmstadt (RFA), ESA/SP No. 255.

Lambeck, K. (1974). "Study of the Earth as a Deformed Solid by Means of Space Methods." La Géodynamique Spatiale - Space Geodynamics, Centre National d'Etudes Spatiales, Toulouse, pp. 537-654.

Landau, H., D. Hagmaier (1986). "Analysis of the Required Force-Modelling for NAVSTAR/GPS Satellites." GPS Research 1985 at the Institute of Astronomical and Physical Geodesy, Schriftenreihe Universitärer Studiengang Vermessungswesen, Universität der Bundeswehr München, Heft 19, pp. 193-208, Neubiberg.

Landau, H. (1988). "Zur Nutzung des Global Positioning Systems in Geodäsie und Geodynamik: Modellbildung, Software-Entwicklung und Analyse." Ph.D. Thesis, Studiengang Vermessungswesen, Universität der Bundeswehr München, Neubiberg.

Lanyi, G.E. (1984). "Tropospheric Effects in Radio Interferometry." TDA Progress Report 42-78, pp. 152-159, Jet Propulsion Laboratory, Pasadena, California.

Lefebvre, M. (1989). "DORIS." International Coordination of Space Techniques for Geodesy and Geodynamics (CSTG), Bulletin No. 11, Munich, pp. 141-155.

Lerch, F., S. Klosko, G. Pratel (1983). "A Refined Gravity Model from Lageos (GEM-L2)." NASA Technical Memorandum No. 84986, Greenbelt, MD.

Lichten, S.M., J.S. Border (1987). "Strategies for High-Precision Global Positioning System Orbit Determination." Journal of Geophysical Research, Vol. 92, No. B12, pp. 12751-12762, November 10.

Lichten, S.M., W.I. Bertiger, U.J. Lindqwister (1989a). "The effect of Fiducial Network Strategy on High-Accuracy GPS Orbit and Baseline Determination." Proceedings of the Fifth International Geodetic Symposium on Satellite Positioning, Las Cruces, New Mexico, March 13-17, pp. 516-525.

Lichten, S.M., W.I. Bertiger (1989b). "Demonstration of Sub-Meter GPS Orbit Determination and 1.5 Parts in 10^8 Three-Dimensional Baseline Accuracy." Bulletin Géodésique, Vol. 63, pp. 167-189.

Liebelt, P.B. (1967). "An Introduction to Optimal Estimation." Addison-Wesley, Reading, Mass. .

Lindqwister, U.J., Y. Bock (1990). "Development of a Permanent GPS Geodetic Array in California for Continuous Monitoring of Crustal Motion." EOS Transactions, American Geophysical Union, 71, p. 858.

Melbourne, W.G. (1985). "The Case for Ranging in GPS Based Geodetic Systems." Proceedings of the First International Symposium on Precise Positioning with the Global Positioning System, Rockville, MD, April 15-19, Vol. 1, pp. 373-386.

Melchior, P. (1983). "The Tides of the Planet Earth." 2nd edition, Pergamon Press, New York.

Milani, A., A.M. Nobili, P. Farinella (1987). "Non-Gravitational Perturbations and Satellite Geodesy." Adam Hilger, Bristol.

Milliken, R.J., C.J. Zoller (1980). "Principle of Operation of NAVSTAR and System Characteristics." Global Positioning System. Papers published in Navigation, reprinted be the Institute of Navigation, Washington D.C., pp. 3-14.

Mueller, I.I., S. Zerbini (1989). "The Interdisciplinary Role of Space Geodesy." Lecture Notes in Earth Sciences, Vol. 22, Springer Verlag, Berlin.

Murray, M.H., R.W. King, P.J. Morgan (1990). "SV5: A Terrestrial Reference Frame for Monitoring Crustal Deformation with the Global Positioning System." EOS Transactions, AGU, Vol. 71, p. 1274.

Neilan, R., W.G. Melbourne, G. Mader (1990). "The Development of a GPS Tracking System in Support of Space and Ground-Based GPS

Programs." Global Positioning System: An Overview, Proc. IAG Symposium 102, Y.Bock and N.Leppard (eds.), Edinburgh, Scotland, August 7-8, Springer Verlag, pp. 165-178.

Porter, W. (1976). "Solar Force-Torque Model for the GPS Space Vehicle System." Rockwell International, Downey, CA.

Prescott, W.H., J.L. Davis, J.L. Svarc (1989). "Global Positioning System Measurements for Crustal Deformation: Precision and Accuracy." Science, Vol. 244, pp. 1337-1340.

Prilepin, M.T. (1986). "Determination of Ionospheric Correction by Group and Phase Velocity." Proceedings of the Fourth International Geodetic Symposium on Satellite Positioning, Austin, Texas, April 28 - May 2, Vol. I, pp. 615-629.

Reigber, Ch., Ph. Hartl, H. Grassl, H. Kohl, W. Markwitz, W. Schaefer, P. Schwintzer, J. Zschau (1988). "Precise Range and Range Rate Equipment PRARE - Extended Version - for Application on the European Polar Platform: PRAREE." Proposal to ESA.

Remondi, B.W. (1985). "Distribution of GPS Ephemerides by the National Geodetic Survey." Paper presented at the First Conference on Civil Applications of GPS, ION, Pennsilvania, September.

Remondi, B.W. (1989). "Extending the National Geodetic Survey Standard GPS Orbit Formats." NOAA Technical Report NOS 133 NGS 46, Rockville MD, November.

Remondi, B.W., B. Hofmann-Wellenhof (1990). "GPS Broadcast Orbits Versus Precise Orbits: A Comparison Study." Global Positioning System: An Overview, Proc. IAG Symposium 102, Y.Bock and N. Leppard (eds.), Edinburgh, Scotland, August 7-8, Springer Verlag, pp. 203-217.

Resch, G.M. (1984). "Water Vapour Radiometry in Geodetic Applications." Geodetic Refraction, edited by F.K. Brunner, pp. 53-84, Springer Verlag, New York.

Rizos, C., A. Stolz (1985). "Force Modelling for GPS Satellite Orbits." Proceedings of the First International Symposium on Precise Positioning with the Global Positioning System, Rockville, MD, April 15-19, Vol. 1, pp. 87-98.

Rosetti, C., P. Diederich (1988). "Trends in the Evolution of Global Satellite Navigation Systems." IEEE Symposium Satellite Communications and Positioning.

Rothacher, M., G. Beutler, W. Gurtner, A. Geiger, H.-G. Kahle, D. Schneider (1986). "The Swiss 1985 GPS Campaign." Proceedings of the Fourth International Geodetic Symposium on Satellite Positioning, Austin, Texas, April 28 - 2 May, Vol. 2, pp. 979-991.

Rothacher, M., G. Beutler, W. Gurtner, U. Wild, D. Schneider, A. Wiget, A. Geiger, H.-G. Kahle (1990). "The Role of the Atmosphere in Small GPS Networks." Proceedings of the Second International Symposium on Precise Positioning with the Global Positioning System, Ottawa, Canada, September 3-7, The Canadian Institute of Surveying and Mapping, pp. 581-598.

Rothacher, M., G. Beutler, W. Gurtner, T. Schildknecht, U. Wild (1991). "Bernese GPS Software Version 3.3. Documentation, May 1991." Astronomical Institute, University of Berne.

Saastamoinen, J. (1972). "Atmospheric Correction for the Troposphere and Stratosphere in Radio Ranging of Satellites." In: The Use of Artifical Satellites for Geodesy, Geophysical Monograph Series, Vol. 15, American Geophysical Union, Washington, D.C., pp. 247-251.

Santerre, R., G. Beutler, A. Geiger (1990). "GPS Error Analysis and Modelling." Proceedings of the Second International Symposium on Precise Positioning with the Global Positioning System, Ottawa, Canada, September 3-7, The Canadian Institute of Surveying and Mapping, pp. 356-372.

Santerre, R. (1991). "Impact of GPS Satellite Sky Distribution." Manuscripta Geodetica, Vol. 16, pp. 28-53.

Schildknecht, T. (1986). "Der Beitrag von GPS Pseudodistanzbeobachtungen für die Auswertung von Phasenmessungen." Lizentiatsarbeit. Astronomisches Institut, Druckerei Universität Bern.

Smith, E.K., Jr., S. Weintraub (1953). "The Constants in the Equation for Atmospheric Refractive Index at Radio Frequencies." Proceedings of the I.R.E, 41, pp. 1035-1057.

Sovers, O.J., J.S. Border (1987). "Observation Model and Parameter Partials for the JPL Geodetic GPS Modeling Software 'GPSOMC'." JPL Publication 87-21, Pasadena, CA.

Spilker, J. (1978). "GPS Signal Structure and Performance Characteristics." Navigation: The Journal of the Institute of Navigation, Washington, Vol. 25, No. 2, pp. 121-146.

Swift, E.R. (1985). "NSWC's GPS Orbit/Clock Determination System." Proceedings of the First International Symposium on Precise Positioning with the Global Positioning System. Rockville, MD, April 15-19, Vol. 1, pp. 51-62.

Swift, E., M. Gouldman (1987). "Preliminary Evaluation of GPS Orbit/Clock Determination Accuracy." Paper presented at the XIX General Assembly of the International Union of Geodesy and Geophysics (IUGG), Vancouver, Canada.

Swift, E., B. Hermann, P. Beveridge, W. Gouldman, M. Thomson, V. Curtis, L. Lynch, D. Weedon (1988). "NSWC Processing Summary." Paper presented to the GPS Performance Accuracy Working Group, January 20-21, Los Angeles, CA.

Swift, E. (1990). "Reducing the Effects of Eclipsing on the GPS Precise Ephemeris and Clock Quality." Proceedings of the Second International Symposium on Precise Positioning with the Global Positioning System, Ottawa, Canada, September 3-7, The Canadian Institute of Surveying and Mapping, pp. 298-313.

Thayer, G.D. (1974). "An Improved Equation for the Radio Refractive Index of Air." Radio Science, Vol. 9, No. 10, pp. 803-807.

Tralli, D.M., T.H. Dixon, S.A. Stephens (1988). "Effect of Wet Tropospheric Path Delays on Estimation of Geodetic Baselines in the Gulf of California Using the Global Positioning System." Journal of Geophysical Research, Vol. 93, No. B6, pp. 6545-6557, June 10.

Treuhaft, R.N., G.E. Lanyi (1987). "The effect of the Dynamic Wet Troposphere on Radio Interferometric Measurements." Radio Sciences, Vol. 22, No. 2, pp. 251-265.

Van Dierendonck, A., S. Russell, E.Kopitzke, M. Birnbaum (1978). "The GPS Navigation Message." Navigation: Journal of the Institute of Navigation, Washington, Vol. 25, No. 2, pp. 147-165.

Wakker, K.F., B.A.C. Ambrosius, L. Aardoom (1983). "Precise Orbit Determination for ERS-1." Delft University of Technology, Department of Aerospace Engineering, Section Orbital Mechanics, ESA Contract Report, pp. 84-85.

Weiffenbach, G.C. (1967). "Tropospheric and Ionospheric Propagation Effects of Satellite Radio Doppler Geodesy." Electromagnetic Distance Measurement, University of Toronto Press, Toronto.

Wells, D.E. (1974). "Doppler Satellite Control." Department of Surveying Engineering, University of New Brunswick, Fredericton, N.B.

Wells, D.E., N. Beck, D. Delikaraoglou, A. Kleusberg, E. Krakiwsky, G. Lachapelle, R. Langley, M. Nakiboglu, K.P. Schwarz, J. Transquilla, P. Vanicek (1986). "Guide to GPS Positioning." Canadian GPS Associates, Fredericton, N.B.

White, H. (1986). "The World Geodetic System 1984 Earth Gravitational Model." Proceedings of the Fourth International Geodetic Symposium on Satellite Positioning, Austin, Texas, April 28 - May 2, Vol. 1, pp. 289-302.

Wild, U., G. Beutler, W. Gurtner, M. Rothacher (1989). "Estimating the Ionosphere Using One or More Dual Frequency GPS Receivers." Proceedings of the Fifth International Geodetic Symposium on Satellite Positioning, Las Cruces, New Mexico, March 13-17, pp. 724-736.

Willis, P., C. Boucher, M. Kasser, R. Biancale, A. Cazenave, M. Dorrer, F. Nouël (1989). "The DORIS Satellite Radio Tracking System: Status and Plans." Global Positioning System: An Overview, proc. IAG Symposium 102, Y. Bock and N .Leppard (eds.), Edinburgh, Scotland, August 7-8, Springer Verlag, pp. 391-399.

Willis, P., C. Boucher, H. Fagard, M. Gavoret, G. Imbert, M. Kasser, G. Balmino, R. Biancale, A. Cazenave, M. Dorrer, F. Nouël, J.J. Valette (1990). "Positioning With the DORIS System: Present Status and First Results." Proceedings of the Second International Symposium on Precise Positioning with the Global Positioning System, Ottawa, Canada, September 3-7, The Canadian Institute of Surveying and Mapping, pp. 131-144.

Willson, R. (1978). "Accurate Solar 'Constant' Determinations by Cavity Pyrheliometers." Journal of Geophysical Research, Vol. 83, No. C8, pp. 4003-4007.

Wuebbena, G. (1985). "Software Developments for Geodetic Positioning with GPS Using TI-4100 Code and Carrier Measurements." First International Symposium on Precise Positioning with the Global Positioning System, Rockville, MD, USA.

Zhu, S.Y., E. Groten, R.S. Pan, H.J. Yan, Z.Y. Cheng, W.Y. Zhu, C. Huang, M. Yao (1987). "Motion of Satellite - the Choice of Reference Frames." Astrophysical Space Science Series, The Few Body Problem, D. Reidel.

Zhu, S., E. Groten (1988). "Relativistic Effects in GPS." Proceedings of the International GPS-Workshop in Darmstadt, April 10-13, published in Lecture Notes in Earth Sciences, GPS-Techniques Applied to Geodesy and Surveying, Springer Verlag, Berlin, pp. 41-46.

Zielinski, J.B. (1988). "Covariances in 3D Network Resulting From Orbital Errors." Proceedings of the International GPS-Workshop in Darmstadt, April 10-13, published in Lecture Notes in Earth Sciences, GPS-Techniques Applied to Geodesy and Surveying, Springer Verlag, Berlin, pp. 504-514.

"Geodätisch-geophysikalische Arbeiten in der Schweiz" (Fortsetzung der Publikationsreihe "Astronomisch-geodätische Arbeiten in der Schweiz") der Schweizerischen Geodätischen Kommission (ab Bd. 32):

32 1978 Das Geoid in der Schweiz. W. Gurtner. 103 Seiten.

33 1977 Integrale Auswertung von Satellitenbeobachtungen. G. Beutler. 114 Seiten.

34 1982 Lösung von Parameterbestimmungsproblemen in Himmelsmechanik und Satellitengeodäsie mit modernen Hilfsmitteln. G. Beutler. 257 Seiten.

35 1982 Schwere-Anomalien und isostatische Modelle in der Schweiz:
I. Zum Konzept der isostatischen Modelle in Gebirgen am Beispiel der Schweizer Alpen. E. Klingelé und E. Kissling.
II. Aufbau der Kruste und des oberen Mantels in der Schweiz. E. Kissling.
III. Gravimetrische Untersuchungen in der Kontaktzone Helvetikum/Aar-Massiv. P.J. Cagienard, H.-G. Kahle, St. Müller und E. Klingelé. 169 Seiten, 1 Karte.

36 1984 Ein gravimetrisches Krusten-Mantel-Modell für ein Profil im nördlichen Alpenvorland bis an die Ligurische Küste. H. Schwendener. 160 Seiten.

37 1986 Les levés aéromagnetiques de la Suisse. E. Klingelé. 69 Seiten.

38 1986 Lokale Schwerefeldbestimmung und gravimetrische Modellrechnungen im Satelliten (GPS)- Testnetz "Turtmann" (Wallis). I. Bernauer, A. Geiger. 106 Seiten.

39 1989 125 Jahre Schweizerische Geodätische Kommission
I. Bedeutung geodätischer Raumverfahren für Landesvermessung und Geodynamik. (R. Sigl)
II. Beitrag der Geodäsie zur Geodynamik. (H.-G. Kahle)
III. L'état actuel de la recherche sur les movements de l'écorce terrestre en Suisse. (F. Jeanrichard)
IV. Die Satellitengeodäsie im Dienste der globalen Geodynamik. (I. Bauersima)
V. Die Veranstaltungen zum 125 Jahr-Jubiläum der Schweizerischen Geodätischen Kommission. (W. Fischer). 62 Seiten.

40 1989 Integrale Schwerefeldbestimmung in der Ivrea- Zone und deren geophysikalische Interpretation. B. Bürki. 186 Seiten.

41 1990 ALGESTAR satellitengestützte Geoidbestimmung in der Schweiz. U. Marti. 61 Seiten plus Punktprotokolle.

42 1990 Höhensysteme, Schwerepotentiale und Niveauflächen: Systematische Untersuchungen zur zukünftigen terrestrischen und GPS-gestützten Höhenbestimmung in der Schweiz. B. Wirth. 204 Seiten.

43 1990 Gravimetrisches Geoid der Schweiz: Potentialtheoretische Untersuchungen zum Schwerefeld im Alpenraum. A. Geiger. 231 Seiten.

44 1991 Rapid Differential Positioning with the Global Positioning System (GPS). E. Frei. 178 Seiten.

45 1992 Dreidimensionales Testnetz Turtmann 1985-1990 Teil I. F. Jeanrichard (Hrsg.) Autoren: A.Geiger, H.-G. Kahle, R. Köchle, D. Meier, B. Neininger, D. Schneider, B. Wirth. 183 Seiten.